

Forschungsberichte aus dem
wbk Institut für Produktionstechnik
Karlsruher Institut für Technologie (KIT)

Daniel Kupzik

**Robotic Swing Folding of three-dimensional
UD-tape-based Reinforcement Structures**

Band 257

Research report from
wbk Institute of Production Science
Karlsruhe Institute of Technology (KIT)

Hrsg.: Prof. Dr.-Ing. Jürgen Fleischer
Prof. Dr.-Ing. Gisela Lanza
Prof. Dr.-Ing. habil. Volker Schulze

Daniel Kupzik

Robotic Swing Folding of three-dimensional UD- tape-based Reinforcement Structures

Volume 257

Robotic Swing Folding of three-dimensional UD-tape-based Reinforcement Structures

Zur Erlangung des akademischen Grades eines
DOKTORS DER INGENIEURWISSENSCHAFTEN (Dr.-Ing.)

von der KIT-Fakultät für Maschinenbau des
Karlsruher Instituts für Technologie (KIT)
angenommene

DISSERTATION
von

Daniel Kupzik, M.Sc.

Tag der mündlichen Prüfung: 15.06.2022
Hauptreferent: Prof. Dr.-Ing. Jürgen Fleischer
Korreferentin: Prof. Dr. Jill Urbanic

Bibliographic information published by the Deutsche Nationalbibliothek

The Deutsche Nationalbibliothek lists this publication in the Deutsche Nationalbibliografie; detailed bibliographic data are available in the internet at <http://dnb.d-nb.de>.

Zugl.: Karlsruhe, Karlsruher Institut für Technologie, Diss., 2022

Copyright Shaker Verlag 2022

All rights reserved. No part of this publication may be reproduced, stored in a retrieval system, or transmitted, in any form or by any means, electronic, mechanical, photocopying, recording or otherwise, without the prior permission of the publishers.

Printed in Germany.

ISBN 978-3-8440-8716-1
ISSN 0724-4967

Shaker Verlag GmbH • Am Langen Graben 15a • 52353 Düren
Phone: 0049/2421/99011-0 • Telefax: 0049/2421/99011-9
Internet: www.shaker.de • e-mail: info@shaker.de

Editor's Preface

In the context of economic globalization, the rapid and efficient implementation of innovative technologies is crucial for manufacturing companies. Universities can add a significant contribution to the competitiveness of industry as “value-adding partners” by developing scientific fundamentals, methods and technologies as well as actively supporting the transfer process into practical application.

This series of publications will report on current research results of the Institute of Production Science (wbk) at Karlsruhe Institute of Technology (KIT) which support this purpose. Our research work is aimed at both performance enhancement of additive and subtractive manufacturing processes, the production facilities, and process automation, as well as at the holistic consideration and optimization of production systems and networks. In all cases, technological as well as organizational aspects are considered.

Prof. Dr.-Ing. Jürgen Fleischer

Prof. Dr.-Ing. Gisela Lanza

Prof. Dr.-Ing. habil. Volker Schulze

Author's Preface

The thesis at hand was created during my work as a research associate at the wbk Institute of Production Science. The work was carried out in the DFG International Research Training Group GRK2078 *Integrated engineering of continuous-discontinuous long fiber reinforced polymer structures (CoDiCoFRP)* with which I was connected during my whole time at wbk.

I am grateful to Prof. Dr.-Ing Jürgen Fleischer for his guidance in my work at wbk and for scientifically supervising this thesis. I thank Prof. Dr. Jill Urbanic for co-supervising this thesis and especially for her valuable input regarding the shape optimization of the manufactured geometries. I thank Prof. Dr.-Ing. habil. Thomas Böhlke for his guidance during my years at KIT and for supervising my defense.

Furthermore, I want to thank all colleagues at wbk, especially from the research department Machines, Equipment and Process Automation (MAP) and the service centers. My special thank goes to the colleagues I shared an office with for their support and the positive mood they spread. I thank Sven Coutandin for the supervision and guidance he gave me as Chief Engineer especially during my first years at wbk. I want to emphasize the contribution my students made to the content of this thesis. Thank You! I want to thank Felix Mispagel for giving me insight into metalworking by explaining methods and small tricks in using tools and machine tools.

Karlsruhe, June 2022

Daniel Kupzik

Abstract

Hybrid fiber-reinforced components made of Long-Fiber-reinforced Thermoplastic (LFT) and unidirectional continuous fiber reinforced tapes (UD-tape) offer great opportunity to reduce weight while saving manufacturing cost compared to monolithic UD-tape components. In such a combination, the excellent formability of LFT is used for filling corners, ribs, and other geometrically complex areas of the component while the UD-tape increases strength and stiffness. Preforming continuous fiber materials, like UD-tape, is a costly step in manufacturing fiber-reinforced polymer (FRP) components. The effort for preforming should be minimized to further improve the competitiveness of the hybrid design. Current preforming processes do not fit the requirements of reinforcement structures. Therefore, they require additional handling steps for positioning the material and costly tooling for controlling the forming of the material. At the same time, the existing processes offer high capability for workpiece complexity, which is not needed as the complex areas in hybrid components are formed by LFT.

In this thesis, a process for the flexible preforming of linear reinforcements from UD-tape strips is designed, commissioned, and optimized. An algorithm for adjusting the preform shape to the preforming process restrictions while maintaining the general shape is presented. Using the novel preforming process, cost for component specific preforming tools can be avoided and deviations in subsequent process steps can be compensated for during running manufacturing.

After literature reviews, sequential swing folding of the tape was selected as forming mechanism. All preform geometries can be created by combining simple bends at different areas of the strip. This way, companies can avoid component-specific tooling and a component-specific parameter selection. Furthermore, preforming and handling are combined to create synergic effects.

For the implementation of the process, a manufacturing cell is designed and implemented. The cell consists of an industrial robot, an end effector that grips and heats the tape, and a supply unit that unreels and cuts the tape. With the help of this cell, parameters for the robot movement and the temperature control of the bending zone are derived. A kinematic movement model for linking the bending angle and the robot movement is developed. Heating parameters are selected based on the requirement to melt the bending zone before the movement, maintain its temperature during bending, and

cool it before its release. For the two investigated thermoplastic UD-tapes, suitable parameter sets were identified. Geometry analysis and evolutionary optimization are used to adapt the preform geometry to the process while maintaining a near-net-shape form. For the user-friendliness of the found method, a graphical toolbox is designed.

Kurzfassung

Hybridbauteile aus Langfaserverstärktem Thermoplast (LFT) und unidirektional endlosfaserverstärkten (UD-) Tapes bieten die Möglichkeit zur Gewichtseinsparung bei geringeren Fertigungskosten gegenüber reinen UD-Tape-Bauteilen. In hybriden Bauteilen wird die einfache Verarbeitung des LFT genutzt um Ecken, Rippen und weitere geometrisch anspruchsvolle Bauteilbereiche zu füllen, während Steifigkeit und Festigkeit durch das UD-Tape erhöht werden. Das Preforming ist der aufwändigste Schritt in der Verarbeitung des endlosfaserverstärkten UD-Tapes. Um die Wirtschaftlichkeit hybrider Bauteile zu erhöhen, muss dieser Aufwand minimiert werden. Bisherige Prozesse für das Preforming sind nicht an die Anforderungen von Verstärkungsstrukturen in hybriden Bauteilen angepasst und benötigen daher zusätzliche Handhabungsschritte um das Material bereit zu stellen, und teure, bauteilspezifische Werkzeuge, um das Material zu formen. Gleichzeitig bieten sie große Möglichkeiten bei der Bauteilkomplexität die nicht benötigt werden, da komplizierte Bauteilregionen in hybriden Bauteilen durch LFT abgebildet werden können.

In dieser Arbeit wird ein Prozess für das flexible Preforming linearer Verstärkungsstrukturen aus UD-Tape-Streifen entwickelt, in Betrieb genommen und optimiert. Zusätzlich wird ein Algorithmus vorgestellt, mit dem die Preformgeometrie an die Prozessrestriktionen angepasst wird. Durch den neuen Prozess können Kosten für bauteilspezifische Preformwerkzeuge vermieden werden und Abweichungen in folgenden Prozessschritten können in der laufenden Produktion bei folgenden Werkstücken kompensiert werden.

Basierend auf einer Literaturrecherche wurde das sequentielle Schwenkbiegen des Tapes für die Umformung ausgewählt. Alle Preformgeometrien können erzeugt werden, indem einfache Biegungen an den verschiedenen Stellen des Bauteils kombiniert werden. Auf diese Art werden bauteilspezifische Werkzeuge und eine komplizierte Parameterauswahl bei neuen Bauteiltypen vermieden. Weiterhin sind Handhabung und Preforming kombiniert, um Synergieeffekte zu nutzen.

Um den Prozess umzusetzen, wurde zuerst eine initiale Roboterzelle entworfen und aufgebaut. Diese besteht aus einem Industrieroboter, einem Endeffektor, welcher das Tape greift und temperiert, sowie einer Bereitstellungseinheit, die das Tape abrollt und zuschneidet. Mithilfe dieser Roboterzelle wurden Parameter für die Roboterbewegung und die Heizung der Biegezone untersucht. Für die Bewegung wurde ein kinematisches

Modell hergeleitet, welches Biegewinkel und Roboterbewegung in Verbindung setzt. Die Heizparameter wurden so gewählt, dass die Biegezone vor der Bewegung geschmolzen wird, während der Bewegung geschmolzen bleibt und vor dem Öffnen des Handhabungsgreifens wieder erkaltet. Für die beiden untersuchten Tapetypen konnten geeignete Parameter gefunden werden. Geometrieanalyse und evolutionäre Optimierung wurden genutzt, um die Preformgeometrie an den Prozess anzupassen und dabei eine endkonturnahe Geometrie beizubehalten. Für den einfachen Einsatz der Methode wurde eine grafische Nutzeroberfläche implementiert.

Table of Contents

Table of Contents	XIII
Abbreviations and Terms	XVII
1 Introduction	1
1.1 Motivation	1
1.2 Structure of the Thesis	3
2 Background and State of the Art	5
2.1 Manufacturing of Thermoplastic FRP Components	5
2.1.1 Characteristics of the Used Materials	5
2.1.2 Processing	8
2.1.3 Advantages and Manufacturing of Hybrid Components	10
2.2 Preforming Processes	12
2.2.1 Preforming of Thermoplastic Materials	13
2.2.2 Handling-Integrated Flexible Preforming	14
2.2.3 Conclusion of the Preforming Processes	21
2.3 Prerequisites and Requirements of the Novel Preforming Process	21
2.3.1 Available Forming Mechanisms	22
2.3.2 Process Route for UD-tape Reinforcement Structures	22
2.3.3 Process Selection	24
2.3.4 Process Development	26
2.4 Conclusion	27
3 Objective and Approach	28
3.1 Objective	28
3.2 Approach	30
3.2.1 Application of Bending for the Manufacturing of UD-tape Preforms	30
3.2.2 Process Behavior	31
3.2.3 Used Materials	32
3.2.4 Expected Influencing Parameters	33
3.2.5 Possible Preforming Geometries	34

3.3	Thesis Procedure: Work Packages and Interactions	34
4	Experimental Setup Development	36
4.1	Bending Movement	38
4.1.1	Kinematic System	38
4.1.2	Gripper	39
4.2	Heating the Bending Area	41
4.2.1	Induction and Direct Resistive Heating	42
4.2.2	Convective Heating	43
4.2.3	Radiation Heating	43
4.2.4	Contact Heating	48
4.2.5	Heating Method Selection	50
4.3	Supply of Tape Strips	52
4.3.1	Conveying	53
4.3.2	Cutting	53
4.3.3	Combined Supply Unit	54
4.4	Control System	54
4.5	Commissioning	56
5	Analysis of the Swing Folding Process	58
5.1	Bend Kinematic	59
5.2	Heating and Geometry Parameter Selection	65
5.3	Analysis of Swing Folding with Radiation Heating	68
5.3.1	Process Route	68
5.3.2	Observed Phenomena	69
5.3.3	Systematic Parameter Variation	72
5.4	Analysis of Swing Folding with Contact Heating	84
5.4.1	Process Route	85
5.4.2	Observed Phenomena	85
5.4.3	Systematic Parameter Variation	87
5.5	Processing of Further Types of UD-tape	101

5.6	Conclusion of the Process Parameter Variation	102
6	Finding Process Compliant Near-net-shape Geometries	104
6.1	Task	105
6.2	Systematic Optimization Methods	107
6.2.1	Gradient Descent Optimization	108
6.2.2	Evolutionary Optimization	108
6.3	Prerequisites for the Optimization	110
6.3.1	Optimization Loop	110
6.3.2	Kinematic Description of the Problem	111
6.3.3	Design of the Genome	114
6.3.4	Fitness Evaluation	115
6.3.5	Adaption	119
6.4	Analytical Preprocessor	120
6.4.1	Definition of the Situation	120
6.4.2	2D Preprocessor	122
6.4.3	3D Preprocessor	123
6.5	Evolutionary Optimization Approach	124
6.5.1	Genome Manipulation	124
6.5.2	Fitness Function	126
6.6	Gradient-Based Optimization Approach	130
6.6.1	Numerical Gradient Calculation	130
6.6.2	Adaption of the Evolutionary Algorithm	131
6.7	GUI and Example Workflow	133
6.8	Conclusion on Finding Process Compliant Near-net-shape Geometries	137
7	Summary and Outlook	138
7.1	Summary	138
7.2	Outlook	140
	References	I
	List of Figures	XXIII

Abbreviations and Terms

Term	Description	Unit
ANOVA	Analysis of Variance	
Co	Continuous (fiber-reinforced material)	
Co-molding	Combined molding of UD-tape and flowable component	
DiCo	Discontinuous (fiber-reinforced material)	
FRP	Fiber-reinforced Polymer	
GUI	Graphical User Interface	
LHS	Latin Hypercube Sampling	
LFT	Long-fiber-reinforced Thermoplastic	
LFT-D	Directly processed Long-fiber-reinforced Thermoplastic	
PA	Polyamide	
PEEK	Polyether Ether Ketone	
PP	Polypropylene	
TCP	Tool Center Point	
UD	Unidirectional (fiber-reinforced tape)	
a_1, a_2	Cutting gaps	mm
α	The skewness of the bend on a tape	°
β	Amount of bending in a bend	°
b_0	Set size of the bending zone in the longitudinal direction of the tape	mm
b_{0m}	Measured actual molten length available for b_0	mm
COS_{global}	Coordinate system of the .stl file	
COS_{prepoc}	Coordinate system which is oriented according to the component in the .stl file	
COS_{tape}	Coordinate System in the tape in the preprocessor	
D_{lt}	Distance from lamp to tape	mm
D_{lr}	Distance from lamp to reflector	mm
D_{ta}	Distance from tape to aperture	mm
$\Delta\alpha$	Error in α	°

$\Delta\beta$	Error in β	°
L_{aim}	The calculated optimum length for a tape in the Shape Optimization	mm
l_i	Length of a segment of the preform	mm
\vec{l}_i	Longitudinal vector of a segment of the preform	
MAE	Mean Absolute Error	°
m_{mat}	Matrix material type	
\vec{n}_i	Normal vector of a segment of the preform	
Ω	Blade rotation	°
P_{end}	The end point of the tape in the shape optimization	
$P_{end,def}$	Set end point for an optimal tape	
P_{start}	The start point of the tape in the shape optimization	
$P_{start,def}$	Set start point for an optimal tape	
PT	Pre-tensioning distance	mm
\vec{r}_1	Movement to the gripping position	
\vec{r}_2	Bending movement	
$R(t)$	Bending radius at the current $\beta(t)$	mm
$R_{\vec{n}_i}$	Rotation around \vec{n}_i	
$R_{\vec{v}_i}$	Rotation around \vec{v}_i	
s_0	Tape thickness	mm
t_0	TCP offset	mm
t_c	Cooling time	sec
t_{cph}	Preheating time with the contact heating	sec
T_{ch}	Contact heating temperature	°C
t_{rph}	Preheating time with the radiation heating	sec
t_{rh}	Heating time with the radiation heating	sec
$var_{px}, var_{py}, var_{pz}$	Variation of the start point in shape optimization	
$var_{r1}, var_{r2}, var_{\gamma}$	Variation of the start direction in shape optimization	
\vec{v}_i	Bending edge vector of a bend of the preform	
w	Tape width	mm
W_a	Aperture width	mm

1 Introduction

1.1 Motivation

Fiber-reinforced polymers (FRP) offer excellent opportunities to fulfill the global megatrend of efficient transportation (Ahmad & Markina et al. 2020). Light-weighting moved structures reduces energy consumption to overcome friction and inertia (Ministry of Natural Resources Canada 2014; Bandivadekar & Bodek et al. 2008). Therefore, the use of FRP in the automotive and aerospace sector is increasing (Holmes 2014).

The transition to electric mobility poses new challenges for the application of FRP. Firstly, the ability to recuperate a portion of the energy during deceleration decreases the influence of the vehicle weight on the acceleration effort in stop-and-go traffic. Secondly, the challenging economic situation of the automotive market increases demands for lower manufacturing costs. Automotive firms and research programs had to redirect their investments towards electric drive solutions, which decreases the funding for FRP solutions.

However, heavy battery systems and increasing safety requirements demand a more efficient material use in vehicle structures to prevent the vehicle weight from increasing. In electrically driven vehicles, the vehicle's weight influences the range. Studies showed that increased vehicle weight led to a significant decrease in range (Joost 2012). Furthermore, other studies illustrate that only 12.6% to 33.4% of the kinetic energy could be recuperated during braking in real-world driving (Sun & Wen et al. 2020; Björnsson & Karlsson 2016). Compensating the loss in range by adding battery capacity increases cost, causes emissions during manufacturing (Ellingsen & Singh et al. 2016), and further increases the vehicle weight leading into a vicious circle, making lightweight manufacturing equally important for electric vehicles. FRPs have the potential to reduce vehicle weight, however, cost still prevents them from being widely used in car body manufacturing (Heuss & Müller et al. 2012; Mascarin & Hannibal et al. 2016).

To overcome these challenges, cost efficiency in manufacturing FRP components must be improved. FRPs can be classified according to their fiber length. Fibers longer than 50 mm are called continuous fibers, while fibers below that threshold are called discontinuous fibers (Chawla 2019). Hybrid components from discontinuous fiber-reinforced (DiCo) material and high-performance continuous fiber-reinforced (Co) material have

the potential to be cheaper than Co-components while having weight advantages compared to purely DiCo-components (Wulfsberg & Herrmann et al. 2014). They can be made with either thermoset or thermoplastic matrix material. Thermoplastic materials offer better impact properties (Verrey & Wakeman et al. 2006) and cycle times than thermoset FPR. In this thesis, Long-fiber-reinforced Thermoplastic (LFT) is used as DiCo-material, and thermoplastic unidirectional tape (UD-tape) is used as Co-material. One reason for the significant difference in manufacturing cost is the preforming step. Co-materials must be carefully draped into shape during the preforming step to enable the molding process and maintain the optimal fiber direction. Studies showed that the preforming step of Co-components causes up to 50% of the manufacturing cost (Weiland & Weimer et al. 2013; Verrey & Wakeman et al. 2006). Preforming Co-material is especially challenging for corners and areas that are curved in multiple directions (Lightfoot & Wisnom et al. 2013). The cost of preforming is increased by tooling cost, commissioning cost, and the effort for non-value-adding handling steps (Fleischer & Teti et al. 2018; Kropka & Muehlbacher et al. 2017). DiCo-materials are easier and therefore cheaper to form compared to Co-materials. LFT material chunks are even able to flow into the final shape during molding. The properties of LFT depend on the fiber length (Morii & Jumonji 2009).

Multi-material approaches proved advantageous for metal constructions (Hirsch 2011) or metal-FRP-combinations (Fleischer 2021) to exploit the specific advantages of the materials. If wisely selected, the same exploitation of advantages is possible for FRP (Kropka & Muehlbacher et al. 2017). DiCo-material fills geometrically complex areas of the component, while the Co-material is placed along the component to transmit loads. This approach still requires the preparation of Co-reinforcements. However, these are less complex and have a simpler orientation layup compared to pure Co-components without DiCo-zones.

To fully exploit the cost reduction potential, a process for preforming the Co-material, adapted to the specific task of making reinforcements, has to be developed. During the development, tooling cost, commissioning effort, and the effort for non-value adding process steps will be regarded. Flexibility in the process can accelerate the adaption to new components or improve the quality during manufacturing by adjusting the reinforcement shape without significant interruptions. To avoid tooling costs, the process shall be designed to work without component-specific tooling. Therefore, the process shall

be designed to work flexibly without component-specific tooling. Most conventional preforming processes need an experience-based iterative adjustment or a systematic optimization before manufacturing new shapes (Coutandin & Brandt et al. 2018) to minimize defects (Kunze & Böhm et al. 2019). This effort could be avoided by exploiting the less complex shape of reinforcement geometries. A universal catalog of process parameters that suits all reinforcement preform geometries shall be found for this.

Furthermore, preforming requires additional handling steps for loading and unloading raw material in the preforming device. By combining the forming and handling devices, these additional steps could be minimized. A literature review for flexible, handling-integrated preforming methods showed that no process adapted to reinforcement structures of continuous unidirectional thermoplastic material exists. This thesis therefore aims to develop a process for the flexible preforming of UD-tape reinforcements with an adapted handling device.

1.2 Structure of the Thesis

This thesis describes the development of a procedure for the preforming of UD-tapes through sequential swing folding.

In Chapter 2, the literature review is presented. First, existing manufacturing processes and the used materials are described. Afterward, already existing methods for preforming are presented. The focus is set on methods that allow the flexible forming of the material to avoid tooling costs and additional process steps. From these methods, a deficit in the state of the art for preforming thermoplastic UD-tapes is derived. Based on a screening of available forming methods, bending is selected for preforming the reinforcement geometries. The requirements on the process are derived from the material properties and challenges with other preforming processes. Particularly significant factors are the handling of the tack of the molten material and proper temperature control. Available forming mechanisms are screened, and localized bending is selected as forming mechanism.

In Chapter 3, the bending-based preforming process is designed. Swing folding is selected as the most promising bending method. A way of combining bends to create complex shapes is developed. A study on the expected behavior of the process is briefly presented. Available materials for experimentation, expected influencing factors, bending and geometrical limitations of the workpieces are named.

In Chapter 4, the hardware for the experimental setup is designed. The test rig will serve as a prototypical model for later manufacturing stations and be used for parameter validation and optimization and the final validation of the process. The design process starts with analyzing the necessary functions based on a representation of the process. Afterward, units for the kinematics, force introduction, heating, tape supply, and control are designed. Finally, the commissioning and improvements during the testing are described.

In Chapter 5, the process parameter variation and process optimization are described. The domain in which parameters should be located is defined and optimizations in terms of process and hardware are implemented. Finally, the process limitations regarding accuracy are validated with a design of experiments.

In Chapter 6, the transformation method for a process-compliant geometry is developed. Its aim is to derive a process-compliant near-net-shape UD-tape preform geometry from the CAD data of the finished part. First, the task is set based on the necessities of the bending and subsequent molding step. Next, the optimization loop is introduced. A universal description of all process-compliant geometries, an evaluation function, and a module for target-oriented parameter adaption, are developed. For parameter adaption, both evolutionary and gradient descent-based methods are tested. Finally, the integration of the developed methods into a graphical program is described.

In Chapter 7, the development of the novel bending process is summarized and an outlook on the further processing is given.

2 Background and State of the Art

In the following section, the relevant background for this thesis and state-of-the-art in the field of this thesis are presented. Regarding the development of a new process chain and its steps, background on fiber-reinforced thermoplastics and their manufacturing processes is given.

2.1 Manufacturing of Thermoplastic FRP Components

In this section, the characteristics of unidirectionally reinforced tapes (UD-tape) and long-fiber-reinforced-thermoplastics (LFT), as well as the processes from raw material to a finished component are presented. A particular focus is set on the peculiarities of hybrid components consisting of LFT with local reinforcements from UD-tape.

2.1.1 Characteristics of the Used Materials

In the following section, the characteristics of the used materials are explained to generate a base for understanding this thesis. A thermoplastic matrix is used as it offers better impact properties, lower cycle times in manufacturing, and better recyclability than duroplastic materials (Verrey & Wakeman et al. 2006; Fleischer & Teti et al. 2018). However, thermal creep may occur, and strength and stiffness are generally lower. From the wide variety of thermoplastic semi-finished materials (Henning & Moeller 2011; Chawla 2019), LFT and UD-tape were selected for manufacturing hybrid components in this thesis project due to their adaption to the specific requirements of the DiCo and Co phase. The most common types of matrix and fiber materials are listed below together with the topologies used in this thesis (LFT and UD-tape).

2.1.1.1 Matrix Material

Most thermoplastic materials are available on the market for use as matrix material. Requirements for the matrix material are its price, processability, mechanical properties, and thermal stability. Most often, technical thermoplastics like polyamide (PA) are used. However, both high-performance polymers like polyether ether ketone (PEEK) for mechanical strength and standard polymers like Polypropylene (PP) for cost reasons can be applied in specific applications. (Neitzel & Mitschang et al. 2014).

2.1.1.2 Reinforcement Fibers

Fibers are applied to reinforce the matrix materials. The material and arrangement of the used fibers have a significant influence on the resulting mechanical properties of the composite. Strength and stiffness of the components are increased by conducting the load along the fiber reinforcement. However, the strength may be decreased normal to the fiber direction due to the interface strength being lower than the strength of the pure matrix material. In thermoplastic composites, the most common fiber types are glass fibers and carbon fibers. The fibers can be applied as continuous fibers or as discontinuous fibers of different lengths. Discontinuous fibers up to 10 mm length are referred to as short fibers, and fibers between 10 mm and 50 mm as long fibers. Above 50 mm length, fibers are called continuous. In addition, the arrangement of the fibers influences the performance of the components. The highest performance can be obtained by arranging the fibers unidirectionally and stacking layers of various orientations, if necessary. If the fibers are oriented more randomly, losses in performance occur due to the curvature of the fibers and the lower possible fiber volume fraction resulting from the less effective fiber packaging. (Chawla 2019)

2.1.1.3 Material Pairings

When designing a composite, fiber and a matrix material have to be selected. A trade-off between mechanical properties and cost has to be found. This trade-off leads to typical combinations in both reinforcement type (Co/DiCo) and material type (matrix/fiber). On the reinforcement type side, expensive materials are mostly combined with continuous fiber high-performance topologies like UD-tapes, while cheaper materials are often used for short or long-fiber-reinforced materials like LFT. On the material side, the same is valid as expensive high-performance matrix materials like PEEK are often combined with carbon fibers, while glass fiber composites often apply a cheaper matrix system. (Abts 2014; Neitzel & Mitschang et al. 2014; Moeller 2014)

2.1.1.4 LFT

LFT is a flowable molding compound consisting of long fibers embedded in a thermoplastic matrix. Its mechanical properties are superior to short fiber-reinforced materials resulting from the longer fibers (Morii & Jumonji 2009; Vaidya & Chawla 2008). Two process routes are common to manufacture the raw materials for the molding process. The first one is pellet-based LFT manufacturing. Here, fiber rovings are impregnated

with molten thermoplastic material by an extruder while being pulled through an impregnation chamber. After cooling down, the strand is cut into pellets of usually 10 mm or 1 inch (Figure 2-1 (a)). In the compression or injection molding facility, these pellets are molten in a heated extruder and injected or laid into the mold. In the melting extruder, the parallel orientation of the fibers is changed to a statistical distribution.

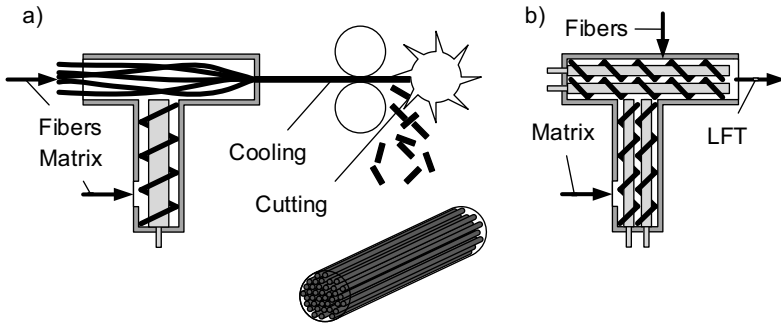


Figure 2-1: Manufacturing of LFT pellets and manufactured pellet (a) and direct LFT extrusion (b) (Neitzel & Mitschang et al. 2014)

The alternative way to process LFT is the direct LFT (LFT-D) process. Here, continuous fibers are fed into a plastification extruder (Neitzel & Mitschang et al. 2014) together with a thermoplastic matrix material. The screw movement will hereby break the continuous fibers into long fiber segments and impregnate them with the molten thermoplastic matrix material (Figure 2-1 (b)). The resulting material can be processed directly. LFT-D material is mostly used for compression molding processes. (Vaidya & Chawla 2008)

2.1.1.5 UD-tape

UD-tapes are flat tapes with a typical thickness between 0.1 mm and 0.35 mm and width between 6.35 mm and 1000 mm. The tapes consist of a matrix material with embedded parallel fibers. The raw material is manufactured by impregnating a strand of parallel fibers. A typical process for this impregnation is the powder-prepreg process, where the spread fibers are impregnated with a polymer suspension. Afterward, the liquid component is vaporized in an oven, and the polymer powder is molten to impregnate the fibers (Neitzel & Mitschang et al. 2014). Usually, continuous fibers are used to manufacture UD-tapes, but directed discontinuous long fibers can also be applied. The

discontinuous fibers can have advantages in forming complex structures and the impact behavior of the final components (Yu & Potter et al. 2014).

Background information on UD-tape manufacturing, processing, and properties is also presented in (Vaidya & Chawla 2008). In longitudinal direction (Chawla 2019), UD-tapes offer excellent mechanical strength and stiffness in the magnitude of high-performance metals at a much lower weight (Toray Advanced Composites 2020; EVONIK Industries 2017). In normal direction to the fibers, strength and stiffness are limited to much lower values by the interface strength between fiber and matrix and the matrix strength. The relation between load-angle and mechanical properties proves that UD-tapes are very suitable for reinforcing specific longitudinal load paths while they need to be stacked in different directions to endure complex loads. If a layer of LFT is combined with the UD-tape, this disadvantage can be minimized, as the LFT will transmit forces along the tape width. Combining both materials into a hybrid material in which the LFT is used for complex shapes and areas with undefined, complex loads, and the UD-tape is used along the main load-paths to conduct forces is therefore advantageous.

2.1.2 Processing

LFT is commonly processed via compression molding (Chawla 2019). After plasticizing the material, it is placed in the tempered compression mold by manual handling or a robot equipped with needle grippers (Mennig & Stoeckhert 2013). After the molding step, the LFT forms a solid part. The process is shown in Figure 2-2.

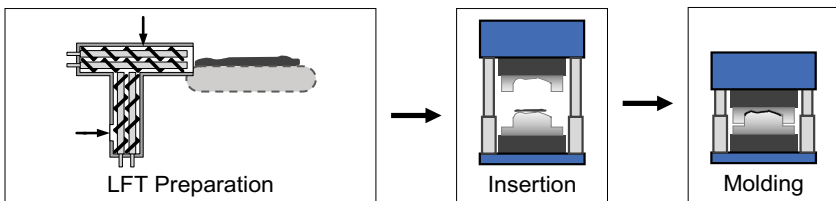


Figure 2-2: LFT is processed by directly molding the material

UD-tape can be processed with a variety of procedures. The procedures can be separated into two groups. In the first group, the first step is to generate a stack from single tapes and afterward form this stack. In the second group, three-dimensionally formed tapes are assembled to form a structure. An overview of standard manufacturing processes is given in (Fleischer & Teti et al. 2018).

A procedure used to manufacture components with sizes up to automotive dimensions is first to generate a flat stack of UD-tape and afterward to form this stack (see Figure 2-3). A typical representative is the route used by the fiberforge (Cramer & Beidleman et al. 2009; Evans & Mclard et al. 2014; Baumgärtner & John et al. 2016). In this process, a stack is manufactured by laying tape onto a moving table. The first layer of tape on the table is held by vacuum gripping. Subsequent layers are joined to the first layer using spot welding techniques. The resulting stack needs to be consolidated for optimum part quality (Habla & Kropka et al. 2019). An example possibility for this consolidation is to vacuum-consolidate the heated stack between two plates (Dieffenbacher 2018). Alternatively, a double belt press can be used for consolidation (Kropka & Muehlbacher et al. 2017). The forming of continuous fiber layups in one step may be challenging for complex component geometries as defects like wrinkling will occur (McGuinness & Brádaigh 1995; Boisse & Hamila et al. 2011). (Coutandin & Brandt et al. 2018) and (Joppich 2019) explain mechanisms for possible defects and a strategy for their avoidance in dry fiber materials. In (Schäferling 2019), folds and wrinkles could be identified as relevant defects in thermoset UD-tape. Often, a preforming step is necessary to avoid defects in the final forming step (Joppich & Doerr et al. 2016). Processes for preforming the stack are presented in Section 2.2.

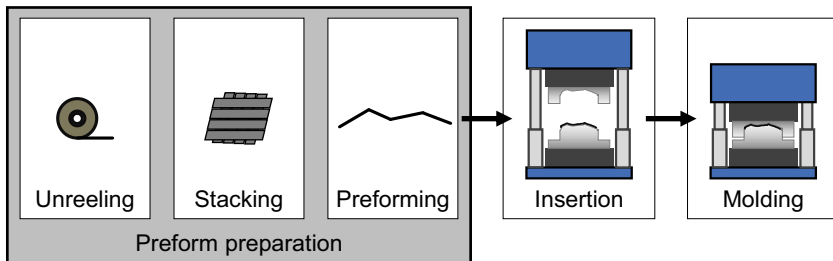


Figure 2-3: Manufacturing monolithic components from UD-tape requires the stacking of numerous material parts and the preforming of the stack for a reliable insertion and molding.

Alternatively, the structure can be assembled from already preformed tapes. Again, these tapes can be formed using the methods from Section 2.2. The advantage of this alternative is that forming single tapes, which will later form a subsection of the structure, is usually simpler than forming the whole structure as problems like wrinkling can mostly be avoided. Furthermore, resources can be saved (Fleischer & Albers et al.

2016). A larger degree of freedom regarding fiber orientations is available, as the finished structure does not need to be formable. (Kropka & Muehlbacher et al. 2017) present an applied example of this process route. An obvious disadvantage of this second process route is that a precise joining of single preforms is more difficult than joining flat tapes resulting from their shape. This is especially true if they have to be precisely joined in curved areas of the structure.

2.1.3 Advantages and Manufacturing of Hybrid Components

The presented process chains can be used individually to manufacture monolithic fiber-reinforced components or combined for the manufacturing of intrinsic (Fleischer 2021) hybrid structures. In this section, the combination of both material types is discussed.

An overview of the properties of LFT and UD-tape is given in Table 2-1. Both materials show their specific advantages and disadvantages. The most apparent advantage of LFT compared to continuously reinforced material is a cost-benefit resulting from processing advantages. The reason for this is the material's ability to flow into the final component shape in a single molding step. This way, the manufacturing effort is only slightly influenced by the geometric complexity of the component. In contrast to this, the geometric complexity of the components determines how difficult preforming is with Co-material. (Boylan & Castro 2003) showed that duroplastic flowable composite materials have increased strength if the length or amount of the embedded fibers is increased. However, it also shows that the closing force increases with longer fibers, indicating larger forces on the material and an increased risk of defects. In (Davis & Graham et al. 2003), it is shown that similar effects on the closing force exist in thermoplastic composites processing. The dependency of fiber length and mechanical properties is examined for natural fibers in (Takagi & Ichihara 2004).

The most obvious reasons for using continuous fiber materials are the superior strength and stiffness properties they offer. Both values can be up to 7 times higher in the fiber direction of a unidirectional material compared to a flowable discontinuous fiber composite. (Chawla 2019). The mechanical properties are dependent on the length of the fibers and their orientation relative to the load. (Henning & Moeller 2011) names a variation of approximately factor 10 for the tensile strength depending on the fiber orientation in UD-material. Due to this strong anisotropy, single-layer UD-materials should be avoided in component regions where loads from various directions can occur.

Table 2-1: Material Characteristics

	LFT	UD-tape
Mechanical properties	Isotropic behavior offers acceptable mechanical properties in all directions	Anisotropic behavior leads to excellent strength and stiffness along the fiber direction
Processing	Complex geometries can easily be manufactured as the material liquefies in the mold and fills the shape of the mold.	Complex geometries require costly preforming processes to avoid defects like wrinkling or folds.

The different component regions often fulfill specific tasks in situations where several functions are integrated into one component. Possible requirements for highly integrated components are structural or semi-structural, optical, or a tight seal to another component. As described in the previous sections, continuous UD-materials are most suitable for structural tasks. LFT can usually fulfill semi-structural tasks and the remaining functions at a much lower manufacturing effort.

To utilize the advantages of both material types, they can be combined into hybrid components. UD-tapes will be used in highly loaded areas of the component to exploit their superior mechanical properties in such a combination. For cost reasons, geometrically complex regions should be filled with LFT. UD-tape should be used for the force transmission between load-introduction regions. This will result in a structure of longish UD-tape strips. Of this structure, the single UD-reinforcements will only have to be preformed sufficiently to enable a subsequent hybridization step (e.g., co-molding) while the final shape can be reached in that hybridization step. The components are manufactured by first producing a reinforcement structure and afterward hybridizing this structure in a molding step. Both duroplastic (Wulfsberg & Herrmann et al. 2014) and thermoplastic (Joppich & Menrath et al. 2017) components can be made in such a hybrid way.

The goal of this thesis is to improve the manufacturing of hybrid components from a flowable thermoplastic component and UD-tapes (Figure 2-4) by a new preforming process. The core of this thesis is developing a novel way of preforming the reinforcement structure from UD-tape for reinforcing LFT components. For this, the tape must only be sufficiently preformed to enable the placement in the mold while the final shape can be obtained during molding.

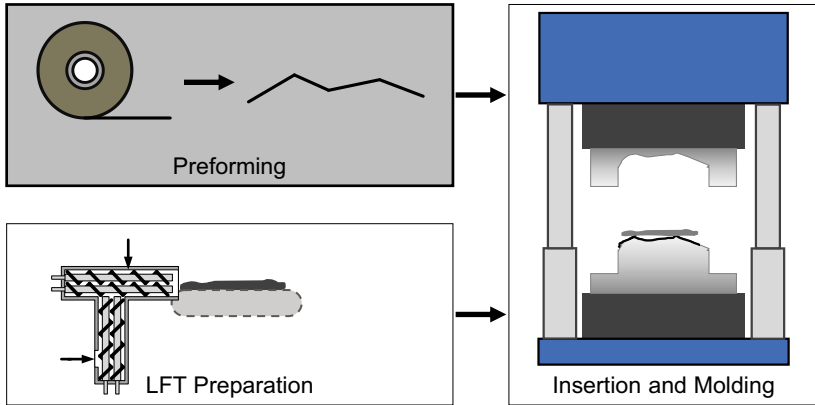


Figure 2-4: Process route for the manufacturing of hybrid LFT – UD-tape components. This thesis focuses on the preforming of the reinforcements.

2.2 Preforming Processes

Preforming is a step to form a raw material into an intermediate product that can produce the final component. The aim of preforming is to improve the reliability and quality of the molding, thus requiring a near-net-shape geometry of the preform with some final forming taking place during the molding step. The degree of remaining forming during molding is typically large for processes with pre-impregnated materials and lower for dry processes, like RTM (Henning & Moeller 2011). In the process chain mentioned above, the preforming step is connected to the previous and subsequent processing steps via handling devices. The effort for preforming and the connected handling is estimated to cause between 30% and 50% of the component cost (Weiland & Weimer et al. 2013; Verrey & Wakeman et al. 2006). Therefore, an improvement in efficiency in these steps is essential to increase the use of composite materials for lightweight manufacturing. Such an improvement can be obtained either by making the steps themselves more efficient or by advantageously combining them to create synergies.

During the development of the process, the properties of the material and process chain, as well as the typical design of reinforcements are regarded. The aim of the preforming is to enable the subsequent molding process to make good finished components at minimum preforming cost. Usually, preforming is necessary for controlling the fiber orientation in areas with a complex shape. A near-net-shape preform will often be

sufficient for good results in the molding process, making a net-shape preform unnecessary. The deviation to the net-shape can be used as a degree of freedom to minimize cost.

Overall preforming cost is increased by the forming tool cost and cost for the process adjustment during commissioning. The cost for the unique tooling is high as a component-specific draping device must be machined and auxiliary devices such as down-holders or closed-loop controlled limited-slip clamps are needed. When the tools are made, they need to be adjusted for the specific component. Examples for expensive adjustment tasks are finding correct values for down-holder and clamping forces (Kunze & Böhm et al. 2019) or selecting the sequence in stamp draping (Coutandin 2020; Coutandin & Brandt et al. 2018). These costs could be significantly reduced if a universal process was used, which can be applied to various components without expensive adaption.

The second possibility to optimize cost is to reduce the number of conducted process steps by combining handling and preforming. Such an approach is called integrated preforming and should avoid the handling before and after preforming. More complex geometries are possible with integrated preforming than without preforming (Bücheler 2017; Pangboonyanon & Zaiß et al. 2016) while the number of process steps is not increased (Behrens & Raatz et al. 2017).

In Section 2.2.1, the peculiarities of preimpregnated thermoplastic FRP in preforming are discussed. In Section 2.2.2, implementations of handling-integrated or flexible forming devices are presented. In Section 2.3, possible preforming mechanisms for the newly developed process are introduced and compared and local bending is selected as the most suitable forming mechanism for the preforming of UD-tape reinforcement structures.

2.2.1 Preforming of Thermoplastic Materials

In general, preforming is used where it is necessary to obtain appropriate behavior while placing the material and the mold and during the mold closure (Kühnel & Schuster et al. 2014). When complex 3D components are made, preforming shows advantages for the final components (Kropka & Muehlbacher et al. 2017). In contrast to dry textiles, thermoplastic preforms require additional measures for successful preforming. The material needs to be softened by heat for plastic deformation, and the matrix tack needs to be regarded.

Thermoplastic matrix materials are softened by increasing temperatures (Huang & Guo et al. 2020). After a deformation at a high temperature and a cooling step, the new shape will remain permanent after cooling the material. The fibers and the matrix material determine the shape of thermoplastic composites. The fibers show high stiffness in their longitudinal direction while they are easy to elastically bend due to their small diameter. Therefore, the shape of composite fiber material can be changed by heating, deforming, and cooling. When the matrix is softened, the fibers will rearrange and be frozen in the new arrangement as soon as the matrix hardens again (McGuinness & O Bradaigh 1997; Joppich 2019).

At higher temperatures, the matrix material also develops tack. This means that problems with tack like adhesion to and decontamination of tools can occur. It also means that higher temperatures can be applied to consolidate stacks (Baumgärtner & John et al. 2016).

2.2.2 Handling-Integrated Flexible Preforming

Handling-integrated preforming is applied in various approaches in the literature. The goal of this thesis is to find a shape flexible preforming method for thermoplastic reinforcements in automotive and similar structures. To obtain flexibility, component-specific tools should be avoided. To be able to process thermoplastic UD-tape, a heating mechanism must be integrated and large contact surfaces to the molten area should be avoided due to the tackiness of the material. The complex shape of the components requires preforms with narrow curvatures and a size in the typical automotive range.

In the following, the most relevant approaches are presented. They are categorized into three main functioning principles: soft grippers, which can drape the material on the target, component-specific deforming grippers, and flexibly deformable multi-axis grippers.

2.2.2.1 Soft Grippers

Compliant grippers can grasp the material in its flat state and deform together with the material when pressed down onto the target area of the handling process. In the handling of composite raw materials, this can be used for preforming. In the following, two approaches are briefly described.

2.2.2.1.1 Barrel End Effector

The Barrel End Effector (Angerer & Ehinger et al. 2011; Ehinger 2012) performs a combined translational-rotational movement to roll over a surface where it either grasps or places a piece of fabric. The fabric is gripped by suction through the end effector's surface. The effector is built up of deformable segments around a vacuum in the middle for the grasping effect (Figure 2-5). The surface of the elements can be heated electrically to activate the binder fleece on the outer surface of the textile.

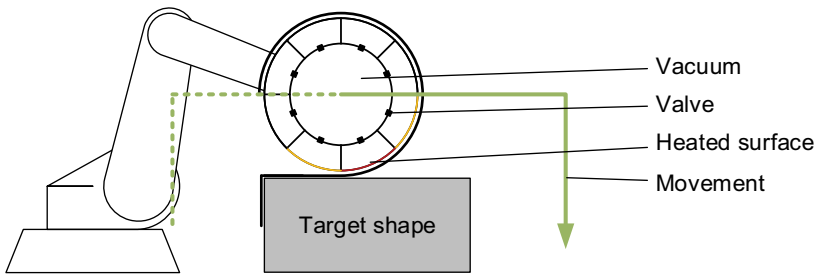


Figure 2-5: Barrel End Effector (based on (Ehinger 2012))

Using the end effector, tool-less, flexible preforming is possible if the compression mold can be used as target shape. Otherwise, a model of the shape has to be used. The segments are heated sequentially to avoid absorption of the binder by the textile. The device is optimized for handling dry textiles as the matrix material of thermoset or thermoplastic prepreg would cause tack between raw material and end effector. The shape complexity of the preform is limited, and the process was only shown for flat or convex target shapes.

2.2.2.1.2 Form Hand

The Form Hand (Löchte & Kunz et al. 2014; Kunz & Raatz et al. 2013) applies a similar function principle as the Barrel End Effector and can be used to drape dry textiles and for various grasping tasks. It consists of a rigid frame with a flexible cushion attached. The Form Hand is sketched in Figure 2-6. The cushion consists of a thin, flexible surface layer and a filling granulate (a). The surface layer is permeable for air to enable suction gripping on the surface. If vacuum is applied to the inner cushion side, the granule particles compact and stiffen compared to the ventilated state (b).

Like the Barrel End Effector, the form hand can grip a flat tape and form it when pressing it down. In contrast to the foam in the Barrel End Effector, the granule inside the Form Hand has a shape memory effect. This effect can be used to press the Form Hand onto a final shape model and transport the preformed textile to the final mold without deforming it. Resulting from the large contact area to the flexible cushion surface layer, processing of pre-impregnated materials is critical for the Form Hand. Forming can take place in multiple dimensions on convex surfaces. However, only a limited degree of deformation and precision is presented in the references.

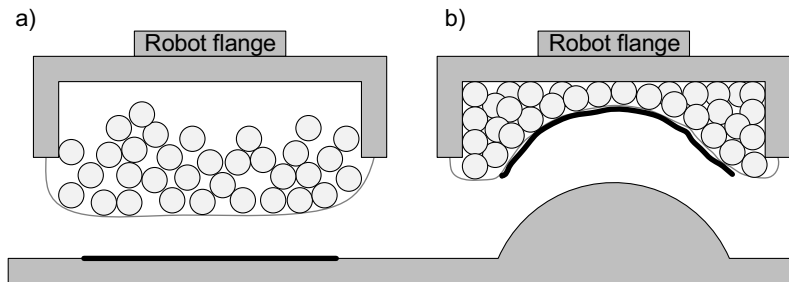


Figure 2-6: Working principle of the Form Hand (based on (Löchte & Kunz et al. 2014))

2.2.2.2 Deforming Grippers

The second approach to integrated preforming is used for simple geometries in literature. The applied principle is to have an end effector with one or more axes that move the individual gripper units along a path that brings the raw material to the target shape. The position and movement of the gripper units must be adapted to the components and individual end effectors have to be made for each manufactured workpiece or layer within the workpiece. Universal end effectors can only be applied to few geometries. However, the advantage of the approach is that the forming can take place during the handling operation without adding any steps.

2.2.2.2.1 MoPaHyb End Effector

The end effector developed by (Moll & Ohlberg et al. 2019) is targeted to preform thermoplastic UD-tapes and, therefore, directed at a similar task as this thesis. It is used as an example for a group of end effectors that are based on moving individual gripping unit groups along a predefined path. In the work, a π -shaped layup as presented in

Figure 2-7 is formed. Its core preforming mechanism features vacuum suction cups moved along two pneumatically driven axes. The position and movement of the suction cup are shown in Figure 2-7.

The suction grippers are attached to guiding axes that are moved by pneumatic cylinders. Infrared radiation tubes are used to maintain the preform temperature. The hardware is mounted to an aluminum profile frame. The work emphasizes that large contact areas have to be avoided to prevent heat loss and tack. The end effector forms all areas of the tape simultaneously and is therefore fast. However, it is optimized for only one workpiece and cannot be used for others. Furthermore, it can be assumed that the oxidation problem named in (Bruns & Raatz 2017) can also occur for this end effector. For high forming degrees, complex motions are needed, which increases the cost for such a gripper. Similar approaches were taken by (Graf & Richter et al. 2018) for thermoplastic materials and (Kordi & Hüsing et al. 2007) for textiles.

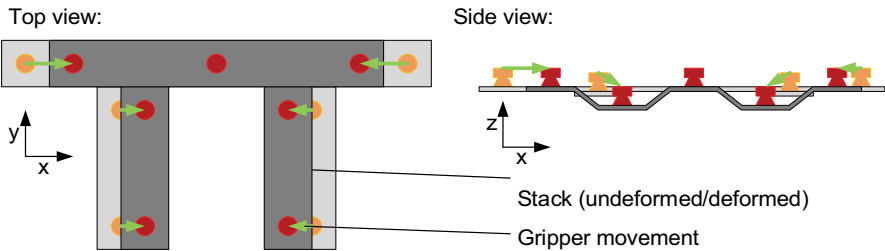


Figure 2-7: Movement of the gripping units (based on (Moll & Ohlberg et al. 2019))

2.2.2.2.2 Octopus End Effector

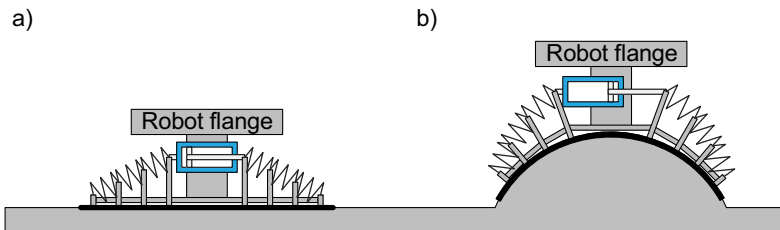


Figure 2-8: Function of the Octopus End Effector (based on (Brecher & Kukla et al. 2015))

The Octopus End Effector (Brecher & Emonts et al. 2013; Brecher & Kukla et al. 2015) is actuated by a single drive and adapts to the mold surface by compliance while holding the material with needle gripping units. It can be used to drape textiles onto simple one-dimensionally curved convex objects with a large curvature radius. The working principle is sketched in Figure 2-8. First, the flat textile is gripped (a). Afterward, the gripper is lifted. After placing the gripper on the mold, the cylinder lowers the arms. The final shape is determined by the mold as springs in each segment push the next segments as far as necessary to touch the surface (b).

With this system, draping happens during the placement on a tool that would be either an additional tool or the mold for the material. If the final mold is used, a longer idle time of the press becomes necessary, especially if more than one layer shall be preformed. In addition, only simple geometries can be processed. A heating system could extend the working principle for processing thermoplastics.

2.2.2.2.3 Vortex End Effector

The Vortex End Effector (Bruns & Raatz 2017) is easily adjustable to various components, which require only one bend for preforming. Its components are sketched in Figure 2-9. In the process, the end effector grasps a flat organo sheet using vortex gripper units. Vortex gripper units blow a vortex of air at the handling object and thereby create a normal force. In this case, the air can be heated for a combined heating and gripping effect. After the organo sheet is lifted and the relevant regions of the organo sheet are heated, the bending takes place. For this, the segments of the end effector are moved by motors integrated into the base unit.

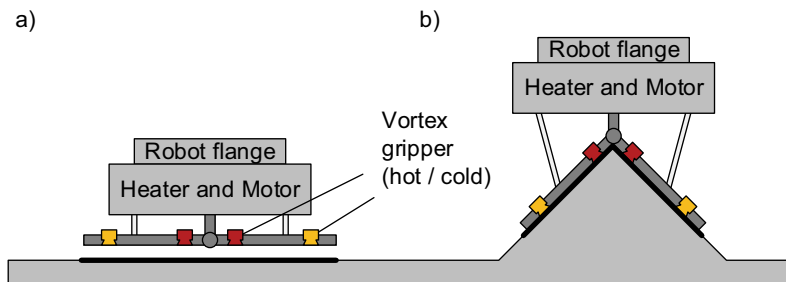


Figure 2-9: Grasping and placement of the organo sheet using the Vortex End Effector (based on (Bruns & Raatz 2017))

The Vortex End Effector is designed to preform thermoplastic composite raw materials and, therefore, close to the thesis at hand. Its advantages are an easy adaption to the geometry of the manufactured part and the preforming during the handling operation. However, the heating duration is defined to be above 40 seconds to avoid fiber breakages. The large heated area and heating time can also cause oxidation and degradation in the material. Furthermore, wrinkles occur because of the preforming kinematic. According to the reference, these wrinkles will be undone in the subsequent high-pressure stamp forming process.

2.2.2.3 Flexible Multi-axis and Sequential Draping

Multi-axis and sequential draping approaches use universal end effectors whose forming effect is determined by the motion control code. They have in common that a complex movement in multiple axes is possible.

2.2.2.3.1 Pixel End Effector

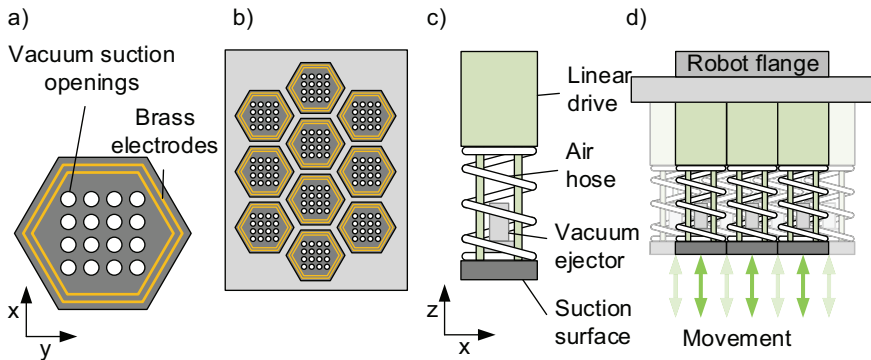


Figure 2-10: Function of the Pixel End Effector (based on (Förster & Ballier et al. 2017))

The target of developing the Pixel End Effector (Förster & Ballier et al. 2017) was to find a solution for the fully flexible forming of complex geometries from carbon fiber textile materials. It works by selectively moving individual gripper units on its pixels. Every hexagonal pixel has suction openings and brass electrodes on its contact surface (Figure 2-10 (a)). The units are arranged in a pattern with only small gaps (Figure 2-10 (b)). The suction surface is moved normally to the material surface by a linear drive (side view in Figure 2-10 (c)). The vacuum is generated by an ejector, which is supplied with

air through a spiraling air hose. Each pixel can be moved individually to follow the target shape (Figure 2-10 (d)).

The slippage of the textile along the suction surface can be determined by measuring the electrical resistance through the fibers between the two brass electrodes. By varying the supplied pressure to the vacuum ejectors, the slippage can be controlled. The end effector can instantaneously be adjusted to the target geometry. It does not need component-specific tools, and the preforming takes place during the movement from grasping to the placement of the textile. The possible degree of forming is limited by the borders between the pixels and the maximum possible height difference between them. The effector is built for dry textiles. Its adaption for thermoplastic materials is problematic, resulting from the large contact area and the necessity of an even slippage without pronounced stick-slip effects. Furthermore, a thermoplastic matrix would inhibit the electrical conduction between the electrode and the fibers.

2.2.2.3.2 Tape Laying

Tape Laying is a procedure where continuous stripes of tape are rolled onto a negative representation of the component and consolidated. The tape is unreeled from a spool, heated, and pressed onto a mold by a roller for placing the materials. Usually, the end effector, containing spool, heating, and roller, is moved along the mold surface. The procedure is called fiber placement if tows narrower than 0.5 inches are used and tape laying for wider tapes. Example applications are given in (Lamontia & Funck et al. 2003; Lukaszewicz & Ward et al. 2012). The procedure is well suited for thermoplastic components, however, all parts of the tape have to be heated sequentially and a mold is needed. The fiber orientation can be varied by adapting the end effector movement.

2.2.2.3.3 Sequential Draping

(Elkington & Ward et al. 2016; Elkington & Bloom et al. 2015) present a robotic approach to imitate the manual draping. A mat of thermoset prepreg is placed on a negative representation of the component and iteratively pushed down and modeled by a robotic end effector. Three different compliant interactors are available in the end effector: one point wedge and two rollers – cylindrical and profiled for corners. The process has been copied from human draping. Similar research has been conducted with collaborating robots (Malhan & Kabir et al. 2018). Both approaches allow complex shapes but require a negative of the component and deformation in large areas of the tape, which need to be heated for a long process time.

2.2.3 Conclusion of the Preforming Processes

The presented preforming methods highlight the need for flexibility and the advantage of integrating additional handling steps. None of the presented methods combine the ability to preform without component-specific tools, the ability to preform during handling, and the ability to process thermoplastic matrix materials. Furthermore, the degree of preforming and the possible preform size are limited for some methods. Barrel End Effector and Form Hand require a negative representation of the part for preforming and are challenged by processing tacky material. Grippers similar to the MoPaHyb End Effector can only preform one specific component. The Octopus End Effector only allows preforming cylindrical shapes, while the Vortex End Effector allows only a single bend in the preform. The Pixel end Effector has large contact areas prone to tack and only allows a vertical movement of the single units of approximately 30 mm. Tape Laying and Sequential Draping both require negatives of the component and are relatively slow. Furthermore, Sequential Draping is poorly suited to thermoplastic materials as high temperature is required in a large area for a long time. An overview of the methods is given in Table 2-2. The literature review showed, that a new preforming process is needed as none of the presented alternatives is suitable for the flexible preforming of thermoplastic UD-tape reinforcement structures.

Table 2-2: Comparison of Barrel End Effector (A), Form Hand (B), MoPaHyb End Effector (C), Octopus End Effector (D), Vortex End Effector (E), Pixel End Effector (F), Tape Laying (G), and Sequential Draping (H)

Requirement	A	B	C	D	E	F	G	H
Component flexible								
Heating of thermoplastics								
Processing of tacky materials								
Complex preforming shape								
Larger preform dimensions								

Fulfilled: ● Not Fulfilled: ○

2.3 Prerequisites and Requirements of the Novel Preforming Process

In this section, available forming mechanisms from (DIN 8582) are screened and evaluated. Furthermore, the requirements that the novel preforming process has to fulfill are analyzed. In the third step, bending is proposed and motivated as forming mechanism

for the novel process. Finally, necessary steps for implementing a bending process are derived.

2.3.1 Available Forming Mechanisms

According to (DIN 8582), forming can occur via:

- forming under pressure, tension, or a combination of both
- forming through shear
- forming through bending

The forming based on tension/compression often appears in combination with shear-based forming in other directions of the component and vice versa (Brannon 2003). Most fiber materials that are used in composite structures allow no plastic longitudinal deformation. Therefore, pressure- and tension-based forming mechanisms like in the deep drawing of metals cannot be used. Instead, preforming must be based on shear and bending.

For shear deformation, fibers glide along their neighboring fibers and thereby allow a plastic deformation in the dry textile or layup, uncured thermoset prepreg, or heated thermoplastic prepreg.

When using bending mechanisms, the fibers, which are not placed on the neutral axis, would have to change their length to allow for plastic deformation. As plastic deformation is not possible for the used fiber materials, other mechanisms need to apply. In textile-based raw materials, this can happen by deforming the woven structure to straighten the outer fibers and bulge the inner fibers. In dry or globally heated impregnated unidirectional materials, bending ideally causes global intra-ply shear (Sachs & Akkerman et al. 2014). In locally heated unidirectional materials, only the fiber buckling on the inner side of the bend can occur and the neutral axis will be pushed outwards by compacting the outer fibers.

2.3.2 Process Route for UD-tape Reinforcement Structures

Fiber orientation needs to be optimized concerning the load case and load introduction regions. Often, loads are carried through the component along load paths between those introduction regions. When preforming flat stacks of tape, restrictions in the fiber orientation in the stack before forming and in the final component occur.

Double-curvature forming of stacks generally requires some areas of the stack to allow longitudinal or shear deformation. As glass or carbon fibers do not allow plastic longitudinal deformation, the stack needs to be adapted to the deformation via shear. Shear is possible in unidirectional materials when the fibers within the layer slide along their neighbors. In bidirectional materials, the fibers in one direction will slide along each other and rotate relative to the fibers in the other orientation. The angle between the orientations in bidirectional materials should be larger than 45° to avoid shear locking (Coutandin & Wurba et al. 2019). In areas with three or more directions, significant slippage between the orientations is necessary as the length of a diagonal between two orientations, representing the third fiber direction in a quadrilateral of two fiber directions, changes its length with the shear angle. In Figure 2-11, the three situations are compared.

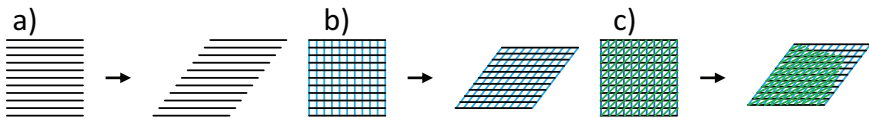


Figure 2-11: Representation of shear by lines of constant length: For parallel fibers, shear only leads to a longitudinal displacement of the fibers (simple-shear) (a). Two layers of fibers require a shear in at least two directions (pure shear) (b). Three directions of fibers require slippage between the fibers, or the shear is locked (c).

Fiber orientations in the preformed stack are dependent on the orientation before preforming and the shear deformation. Possibilities are especially limited close to sharp corners as large deformations are necessary here. In state-of-the-art, preforms can be assembled from subpreforms after forming to allow more complex shapes (Mühlbacher 2012; Coutandin & Wurba et al. 2019). If the subpreforms are formed separately, slippage and locking between the individual layers are avoided. It can be concluded, that multidirectional layups complicate the forming.

For practical and cost reasons, a highly available standard UD-tape from a spool is used as the raw material of the new process. In dry textile material, shear deformations work well as the fibers are relatively free to slide, and defects are avoided by the weaves' stabilizing effect on the material. If a viscous matrix is involved, deformation forces increase, which is challenging. For UD-materials, the risk of defects is further increased, as the coherence between the directions is weaker. This argument favors the assembly of finished preforms instead of preforming an assembled stack.

When choosing which of these two process routes should be taken, also the design of the finished component needs to be regarded. This thesis scope is the manufacturing of reinforcement structures for hybrid components in which the continuous fibers only cover a small share of the component's area. Often, these single reinforcement strips are not connected to another in the finished component. When a stack is preformed, forming has to take place at several positions simultaneously and the adhesion between the individual tapes restricts the component shape. When the assembly is done after preforming, the preforming step is simplified, and forming complex geometries will be vastly improved. This way, a great variety of reinforcement structures can be produced based on a standardized preforming process. Therefore, preforming before the assembly is a feasible process route.

2.3.3 Process Selection

As described in Section 2.3.1, forming can occur under pressure and/or tension, shear, and bending deformation. As the material properties of the applied fibers do not allow plastic longitudinal strain, only shear and bending remain as possible preforming mechanisms.

In most tool-based preforming processes, shear preforming is applied (Fleischer & Teti et al. 2018). Several solutions are available to control the movement of the material (Coutandin 2020; Coutandin & Brandt et al. 2018; Arnold & Sutcliffe et al. 2016; Chen & Boisse et al. 2011). To form thermoplastic UD-tape, the material must be heated in regions where plastic deformation is desired. For shear-based forming, the whole component must be heated. The temperature must be kept in a specific range for best forming results and to avoid degradation, which is challenging for large areas. This is especially true where the tape is held by grippers or placed on a surface as heat conduction will significantly influence the resulting temperature field. Another challenge in contact areas to the heated tape is the tack of the molten matrix. It may lead to matrix material sticking to the handling devices when releasing the tape. Thereby, the preform can be damaged (e.g., fiber pullout), and the handling device will be soiled. Thus, shear-based forming of thermoplastic prepreg is challenging to control and therefore not suitable for flexible, handling-integrated preforming.

Bending can strongly affect large part regions' position while the forming itself takes place locally in a small area of the part. In contrast to this, longitudinal and shear defor-

mation requires a larger deformation zone. If thermoplastic materials are used, the deformation zone determines what section of the part needs to be heated. The simplified tempering of the small bending zone compared to a much larger shear zone is an advantage for a bending-based preforming approach. Processes with a large heated deformation zone require the control of the deformation within this zone. For example, the pixel end effector (Section 2.2.2.3.1) applies numerous sensor-equipped linear actuated grippers for this task, which is complicated and time-consuming. Furthermore, bending is especially suitable for forming longish structures like tubes, beams, and tapes. Resulting from these advantages the novel preforming process shall be based on localized bending.

According to (DIN 8582; DIN 8586), free bending and die bending are possible alternatives for the forming. Die bending can be applied to form workpieces according to the shape of the die while the amount of bending is determined by the shape of the die. In free bending, a bending movement is continued until the target amount of bending plus the necessary over bending is reached. Within free bending, a linear or rotational bending movement can be applied for bending longish material strips. Swing folding is a variant of free bending using a rotational tool movement. It is suitable for flexible forming, as the rotation defines the amount of bending and could be integrated into handling as only a small area of the tape needs to be softened.

Processes that bend linear semi-finished materials are widely used to create complex structures. One industrial application is the manufacturing of tubular metal frames, where a typical process is the draw-bending around a tool (Strano 2005) which has also been adapted to composites (Engel & Manns et al. 2020). Resulting from the remaining elastic deformation during the plastic flow of the metal, springback is an issue for accuracy for many bending applications (Schmoeckel & Beth 1993; Strano 2005; Pourboghraat & Chu 1995). For forming thermoplastic matrix materials, springback is expected to be a less significant issue as only the elastic tension within the individual fibers remains after the stiffening of the matrix, and no tension over the tape's whole cross-section remains. The rate-dependent viscous properties of thermoplastic UD-materials have been analyzed in (Sachs & Akkerman et al. 2014). Depending on the shape of the raw material, further mechanisms like wrinkling, folding, splitting, or flattening may occur (Utsumi & Sakaki 2002). For applications with high requirements regarding the quality or complex deformation, special solutions were developed. An interesting approach for tool-less high-quality bending is laser tube bending (Zhang & Jones et al. 2005) or laser

sheet bending (Kant & Joshi et al. 2013), where laser-induced thermal stresses are used to create bends. Tubular frames can also be made in an integrated process chain (Both & Brüggemann et al. 2011) in which the profiles are bent during extrusion (Fleischer & Schulze et al. 2014). A similar process, where thermoplastic matrix composite material is fed through a heater and bent by rollers, was presented by (Gertner & Miller 1996). By bending flat materials, complex functional geometries can be obtained. Examples are the gravity-assisted laser bending of polymers (Mueller & Kruck et al. 2013), robotic 3D structures from paper (Wang & Plecnik et al. 2016), or the manufacturing of sheet metal housings (Fleischer 1989). These applications showed that a wide variety of products and geometries can be made by bending.

Due to its good controllability, flexibility, and ability to form a wide range of geometries, local bending is selected for forming the preforms.

2.3.4 Process Development

To apply new bending processes, suitable parameters have to be found for precise and error-free execution. Furthermore, methods for the planning need to be developed. In the following, examples of the development and commissioning of bending processes are given. Planning the bending is necessary, as all presented processes impose their specific restrictions on the possible workpiece shapes. Suitable tools (Strano 2005) or tool motions (Liao & Wang 2003) and sequences (Fleischer 1989; Gupta & Bourne et al. 1998) need to be selected. This selection should regard the whole process chain (Verlinden & Cattrysse et al. 2007). For some procedures, the bend pattern generation is also subject to research: (Nagabandi & Wang et al. 2016) plan bends to form 3D structures from stripes. (Lang 1989) has developed an approach to calculate bend lines for origami and (Andreozzi & Bessone et al. 2016) design bend patterns for architecture. In most work regarding origami folding, folds are regarded as sharp edges, but they may also be regarded as smooth transitions (Peraza Hernandez & Hartl et al. 2016).

To apply bending on thermoplastic UD-tapes, suitable parameters must be found on an experimental setup, and a method for finding a compromise between the deviation from the net-shape and preforming effort must be found. For the reinforcement of hybrid structures, long, thin tapes will be placed along the load paths. For a successful co-molding, they must be formed for stable placement in the mold. For this, suitable hardware and process parameters with low angular error are needed. As the local bending poses shape restrictions on the final part, a process-compliant preform shape close to

the final shape needs to be found. The preform will be brought to the final shape during the co-molding step. At the same time, the buckling in the bends will be reduced.

2.4 Conclusion

In this chapter, available composite materials with thermoplastic matrix and their manufacturing processes were presented. Directed continuous fiber materials and undirected discontinuous fiber materials have their specific advantages and disadvantages. Continuous fiber materials offer superb mechanical properties, while discontinuous fiber materials are cheaper to process. In hybrid components, the advantages of both material types can be exploited. The continuous fiber-reinforced reinforcement structure has to be preformed to manufacture such components. Preforming causes a large share of the cost for composite structures as expensive tooling as well as additional process steps are needed in most approaches.

Therefore, a handling-integrated preforming method that does not use component-specific tools shall be found to reduce or eliminate those expenses. The literature review showed no such method is available, although much research has been conducted in the field. One reason for missing a suitable method is that none of the available work was directed at the specifics of reinforcement structures, which typically consist of longish elements directed according to load paths. From the available forming mechanisms, localized bending was selected as the most suitable for preforming reinforcement structures from UD-tape.

This thesis is to develop a preforming process based on the bending of UD-tapes. To enable the process, an experimental setup must be found. Using this setup, process parameters have to be selected. To further improve the preforming cost, a method to find a compromise between preforming effort and deviation between preform shape and net-shape must be implemented.

3 Objective and Approach

In the following sections, the objective of this work, the approach, and the thesis procedure are presented.

3.1 Objective

In Chapter 2, significant advantages of hybrid structures for the cost at a given performance could be shown. With conventional preforming processes, a share of this advantage can be exploited, although unnecessary limitations in process conduction are accepted. The limitations arise as preforming processes are directly copied from monolithic components without regarding the peculiarities of reinforcements within hybrid parts. Therefore, these limitations can be avoided with a task-adapted forming process.

One example is the shape of the manufactured preform. For monolithic components from continuous fiber-reinforced materials, the formed stack will most often consist of several layers of fibers oriented in various directions depending on the component design. In that case, the fibers cover the whole component surface, making a rigorous control of the forming necessary due to internal forces from the various angles and the complex preform shape. In the case of reinforcement structures, however, most reinforcements are made of lattice-like UD-tape structures. As shown in Figure 3-1, more complex deformations occur if whole stacks are formed compared to the forming of UD-tape strips, which simplifies the preforming.

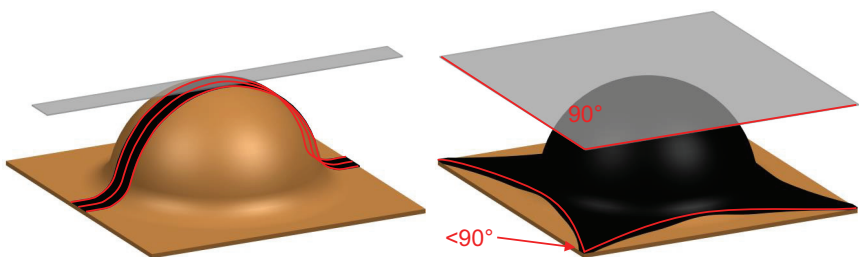


Figure 3-1: Single tape strips can be formed into complex geometries without changing the angle between its fibers. The forming of stacks as required for monolithic components causes angular changes between the fibers and a linked displacement of the outer contour.

Preforming is necessary to improve the positioning in the mold and ensure a wrinkle-free component quality. The material should be brought as close to the final shape as necessary for subsequent process steps but not any closer to avoid unnecessary preforming complexity. Localized bending was selected for this approximation of the final shape, as it offers flexibility without tooling cost, and good controllability for handling integration.

This work aims to apply bending for the flexible preforming of reinforcement elements from carbon fiber UD-tapes with a thermoplastic matrix. The objective is to exploit the advantages of locally reinforced hybrid components by specifically adapting the manufacturing steps to the demands of the components.

In the following section, a preforming process based on the bending of UD-tapes is developed. In Figure 3-2, the challenges are sketched beside the robotic cell which is selected for the experimental setup later in this thesis. To conduct the process, an experimental setup and parameters for its operation are necessary. Furthermore, process-specific shape restrictions and the requirements of the process chain must be taken into account. Following scientific problems have to be answered:

- Which hardware is suitable to conduct the process?
- Which parameters influence the process and how should they be set?
- How can a process and process chain compliant workpiece shape be derived?

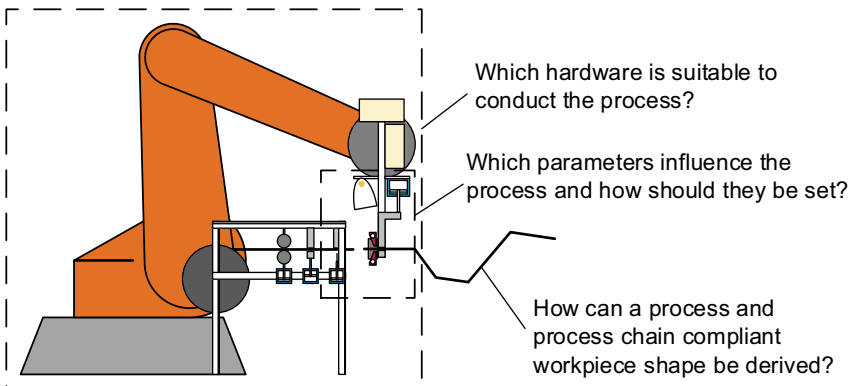


Figure 3-2: Derivation of the challenges for conducting the bending process.

3.2 Approach

In this section, the application of bending for the manufacturing of UD-tape preforms is discussed. First, requirements are analyzed. Afterward, the process is defined and described. Based on that, expected influencing parameters and possible preform geometries are described. Finally, an overview of the thesis procedure is given.

3.2.1 Application of Bending for the Manufacturing of UD-tape Preforms

Several localized bends can be combined to form the global shape of the preform. The core idea is presented in Figure 3-3. The reinforcing tape strip shall be bent in softened, heated zones while the solid segments between the molten regions are held by a kinematic.

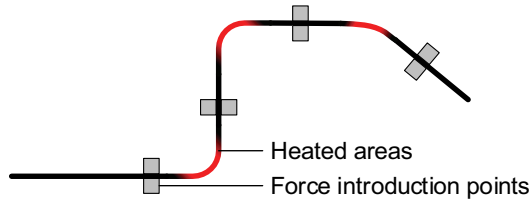


Figure 3-3: The tape strip can be brought into a complex shape with only local deformation

The main benefit of integrating into handling is that instead of simultaneous grasping and forming at multiple positions, the process can be conducted with only one heating device and two force introduction points. The process is sequentially repeated until the final shape is obtained for multiple-bend preforms. The sequential creation of the above-mentioned shape is sketched in Figure 3-4.

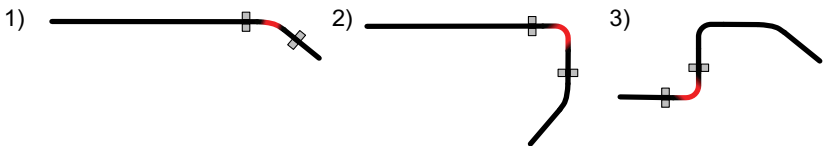


Figure 3-4: Sequential forming of a tape strip

If the tape is supplied into the sketch from the left, it can be held still in the supply while the free end is bent. Thus, the process requires only a tape unreeling device, a freely

movable force introduction device, and a small area heater. This way, complex structures similar to tubular frames can be created. In (DIN 8586), this is represented as swing folding process with the peculiarity of zero lateral forces in the bending zone due to the guided motion of the tape segments. The creation of a single bend is sketched in Figure 3-5. After the tape has been bent, it can be conveyed further (to the right in the figure) and bent at the next position.

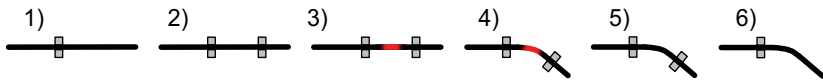


Figure 3-5: Steps of bending: Supplying a tape strip (1), gripping the free end (2), heating the bending area (3), bending (4), cooling (5), releasing (6)

3.2.2 Process Behavior

In the process, the tape can be regarded as two solid bodies connected by fibers in a viscous heated zone. The local behavior in the bending zone was examined in a qualitative finite element study (A_Penev 2019) to estimate the process possibilities. The simulation represents a tape strip that is locally heated along its transverse direction and bent in that heated zone. The cold areas beneath the bend were simulated as rigid blocks. The individual fibers in the heated zone were represented by a series of beam elements that interfere with one another with friction. The molten matrix was neglected, as its transmitted forces are only relevant above a specific deformation rate.

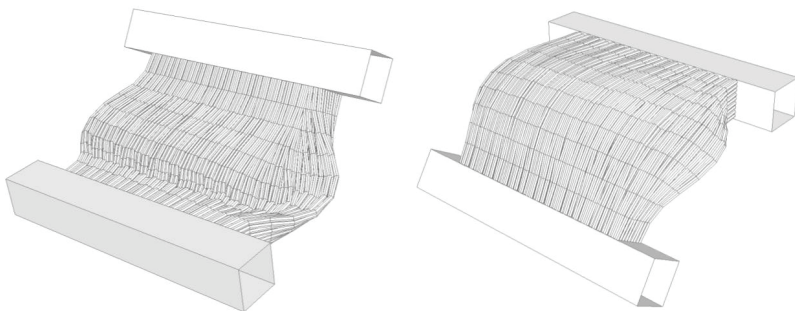


Figure 3-6: Fiber deformation on the inner and outer sides of the bend. (A_Penev 2019)

As presented in Figure 3-6, the bending mechanism in locally heated UD-tape differs from the elongation-based bending of metals. In UD-tapes, the neutral axis will be

pushed outwards, as fibers cannot plastically elongate, the outer fibers will be compacted towards the neutral axis, and the inner fibers will buckle to effectively decrease their length. The study showed that the degree of unwanted deformation (buckling, compression of the fibers) strongly depends on the ratio between tape thickness and bend radius. Further factors which obstructed the deformation are a high fiber content and stronger interactions between the fibers. As fibers buckle outwards at the two ends of the bend line, the tape strip's width has a minor influence. According to (Bruns & Raatz 2017), this buckling can be undone in the following compression molding step.

It also became apparent that the necessary bending momentum is much smaller than the momentum required for bending a cold tape. A tape was locally heated to validate the assumption of a low-force forming motion. With only gravitational forces, it easily bent downwards without significant elastic deformation outside the bending zone (Figure 3-7).



Figure 3-7: Bending of a heated area by gravitational forces

3.2.3 Used Materials

In this thesis, two types of UD-tape were used for experimentation. Both Polypropylene (PP) and Polyamide (PA) tape were selected to take into account different matrix systems. The material properties are described in Table 3-1, and their behavior is described in an experimental examination (Matsuo & Hojo et al. 2017). According to their matrix system, they are referred to as PP and PA tape.

Table 3-1: Material properties of the used UD-tapes

	Tencate Cetex TC910	Tencate Cetex TC960 carbon
Fiber	Carbon	Carbon
Matrix	Polyamide (PA6)	Polypropylene (PP)
Fiber weight content	60%	27%
Area weight	131 g/m ²	116 g/m ²
Thickness	0,16 mm	0,27 mm

In the development of a heating unit, also translucent and dyed glass-fiber-reinforced tapes of unknown specification were tested. These tests proved the dependency of radiation heating on the color of the tapes. Self-consolidated multi-layer tapes were used to give an outlook on thicker materials. They could only be used for qualitative analysis as their thickness and straightness varied.

3.2.4 Expected Influencing Parameters

The tape is locally heated, bent, and afterward cooled for preforming. Therefore, it can be expected that all parameters for these three actions and the hardware in the robotic cell influence the process. Expected parameters are given in an Ishikawa diagram in Figure 3-8. The research on finding parameters with a good resulting part quality and low process time is presented in Chapter 5,.

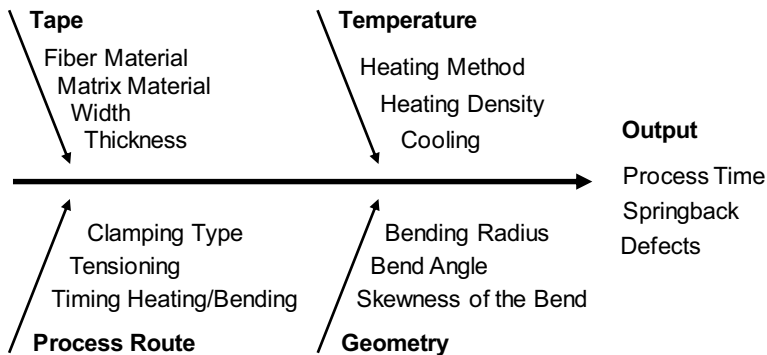


Figure 3-8: Ishikawa diagram of the expected influencing parameters

3.2.5 Possible Preforming Geometries

A bend in a tape can alter the direction of the tape's centerline along the tape. By placing the bend and adjusting the skewness of the bend line, any centerline direction in space can be obtained after a bend. However, the normal direction of the tape after the bend is also influenced by this selection. Therefore, limitations are set to possible geometries of a tape. A possible geometry is shown in Figure 3-9. With the approach, the net-shape can be approximated with a flexible number of bends (Figure 3-10). The number of bends on a tape should be as low as possible to minimize manufacturing effort. In Chapter 6, a toolbox for adapting a bent tape to the reinforcement geometry in a hybrid component is presented. In this thesis, the bending angles are called α (skewness of the bending line) and β (amount of bending). The tape segment length is called l .

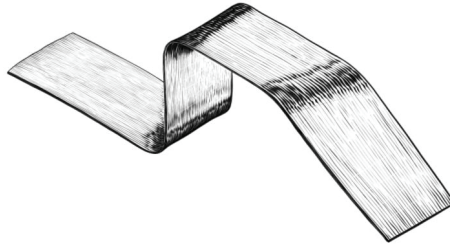


Figure 3-9: Possible preform geometry with straight and askew bends. (Figure by Alexej Bachtin)

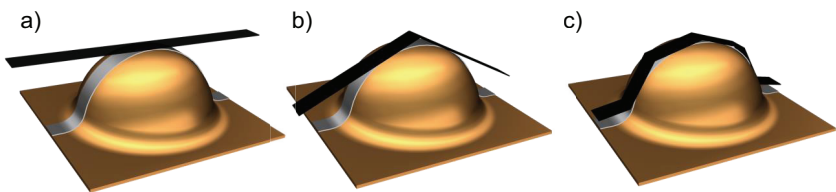


Figure 3-10: Approximation of a reinforcement shape without preforming (a), with one bend (b) or with three bends (c)

3.3 Thesis Procedure: Work Packages and Interactions

The research on the swing folding of UD-tapes is based on the three research questions:

- Which hardware is suitable to conduct the process?
- Which parameters influence the process and how should they be set?

- How can a process and process chain compliant workpiece shape be derived?

The work packages are designed according to these research questions. In Figure 3-11, work packages and their content are presented. The Experimental Setup Development (Chapter 4) is the first work package on the physical side of the project. A test rig for conducting the process is needed during the thesis and as a model for later series production cells. In the implementation of the test rig, the task is clarified, and modules are designed. After the experimental setup is built and commissioned, experimentation on the process can be conducted. The Analysis of the Swing Folding Process (Chapter 5) was started on this initial prototype, and experience in process conduction was reflected into the experimental setup through continuous improvement measures. The goal was to find high-quality parameters for the movement and heating of the tape, thereby increasing accuracy and speed. The Analysis of the Swing Folding Process is finished with a final Design of Experiments with no subsequent hardware changes to characterize and validate the process. The Finding of Process Compliant Near-net-shape Geometries (Chapter 6) is conducted in parallel to the physical research. The goal of this work package is a toolbox for finding a process-compliant representation of the reinforcements in the final part. Necessary steps in this development are a description of possible tape geometries, a method to evaluate a tape geometry's quality, and an algorithm for the adjustment of the geometry.

Experimental Setup Development (Chapter 4)		
Task Clarification	Unit Design	Improvement
Analysis of the Swing Folding Process (Chapter 5)		
Kinematics	Temperature Control	Validation
Finding Process Compliant Near-net-shape Geometries (Chapter 6)		
Description	Evaluation	Adjustment

Figure 3-11: Work packages within the thesis

4 Experimental Setup Development

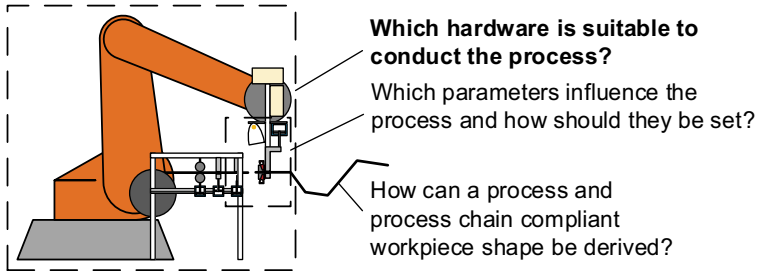


Figure 4-1: Research questions of this thesis

In this chapter, the first research question from Figure 4-1 is answered. For the experimental process analysis, an automated bending station has to be designed and implemented. An approach similar to (VDI 2221) is used in this thesis. Four main steps are conducted:

- Clarify the task and structure it into realizable modules
- Design the modules
- Commission the system and select operating parameters
- Validate

The task has been described in Section 3.2. In the next section, the steps for determining and structuring functions are described. The modules are designed in sections 4.1 to 4.4. In 4.5, the implementation is presented. Parameters for the operation of the station and the validation are described in Chapter 5.

During process conduction, the tape has to be supplied (unreeling, cutting off), heated and bent. A function chart according to (VDI 2860) is used to structure and identify the main process steps (Figure 4-2).

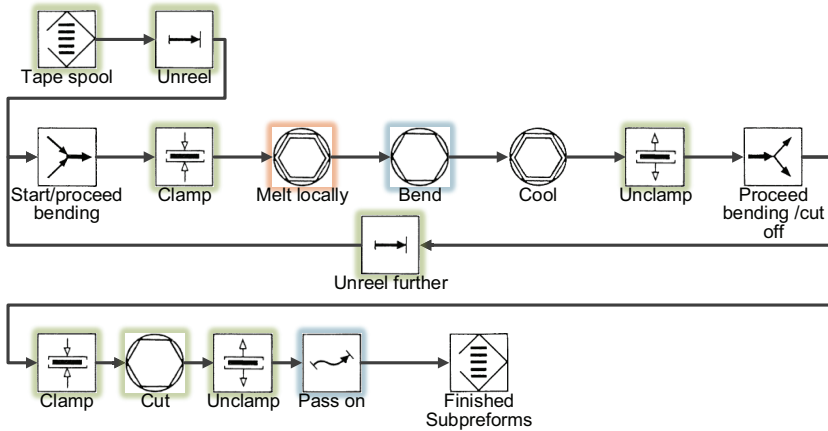


Figure 4-2: Function chart representation of the sequential bending process with tape supply in green, heating in red, and bending and movement of the specimen in blue

Next, the functions are allocated to functional units. With the help of this allocation, necessary function elements are identified and possible solutions generated. In this design process, both the different variants of grouping the functions and the selection of function elements are degrees of freedom. A preview of the possible combinations of identified function elements and combinations are presented in the morphological box in Table 4-1. The detailed description of the selection of the single elements is described in Sections 4.1 to 4.4.

Table 4-1: Morphological box of the function principles for the individual functions

Task	Solution principle			
Movement by...	Kinematic	Rolls	Robot	
Gripper type	Vacuum	Suction	Clamping	
Heating in...	Separate	Supply unit	End effector	
Heating	Hot air	IR	Conduction	Induction
Tape supply	Roller drive	Pull by robot		
Cutting by ...	Scissors cut	Free cut		
Cutting in...	Supply unit	End Effector		

For flexible experimentation and adaptability, the modules will be built using standardized aluminum profiles and connectors. For the function elements, purchased items will be used where possible, e.g. pneumatic cylinders for movements. For practicability and storage reasons, the footprint of the units shall be kept small.

4.1 Bending Movement

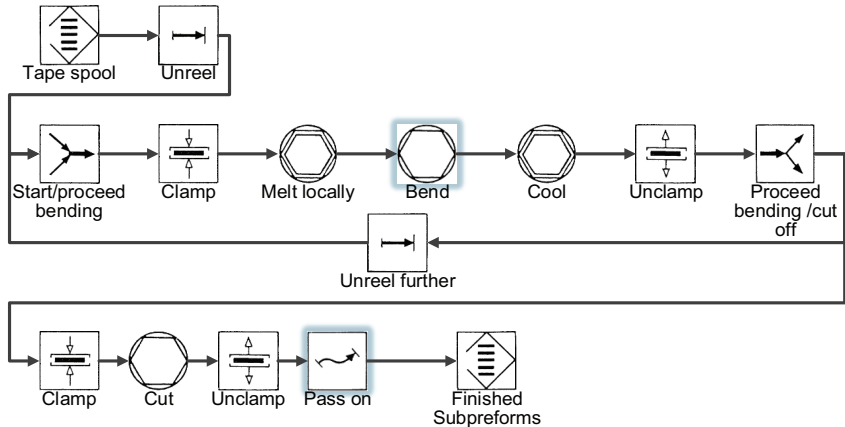


Figure 4-3: Function charts with highlighted bending and handling system

To induce a bending movement into the tape (Figure 4-3), both a gripping system and a kinematic for moving the gripping system are selected. The system must secure the tape while it is cold, move it as soon as the heating unit has softened the matrix, and then keep it in its final shape until the material has cooled again. For the movement, the kinematic system must enable the control of a sufficient number of independent degrees of freedom to set the three parameters of a bend (skewness of the bend α , amount of bending β , and tape segment length l). The requirement of the gripping process is to securely hold the tape while the maximum friction along the tape should be limited to certain boundaries to allow tensioning by sliding the gripper along the tape.

4.1.1 Kinematic System

The kinematic system needs to move the gripper to a position on the tape, along a bending trajectory, and back to the initial bending position for the next bend. After the cutting process, the gripper might also be used for storing the finished preform.

The following considerations are carried out to derive the number of necessary kinematic axes:

- The gripper should be placed close to the bending zone to avoid elastic deformation between gripper and bending zone.

- For the correct angular placement of the gripper to the bend (α), the kinematic system needs a rotational axis around the normal direction of the tape.
- One additional rotational axis is required to rotate the free end of the tape around the bend (β).
- Preliminary experimentation has shown that the bending movement cannot be represented by a pure rotation around a fixed axis. Two linear axes are required (see coordinate system “*b*” in Figure 5-5) to move the rotation axis to the suitable spot for the specific bend.

To summarize the considerations, at least two rotational and two translational axes are the minimum requirement for flexible process conduction. The functionality could be achieved by combining standardized electric axes while tight packaging to avoid collisions between the tape, supply unit, and gripper.

If the bending kinematics shall also pass on the finished preform into the storage, a large working volume is necessary. When longer axes are used, the packaging and collision avoidance within the system will become increasingly difficult. Therefore, the bending and handling kinematic should either be separate systems or a flexible system with a large working volume and a small collision silhouette. The most convenient option for avoiding collision problems and obtain high reliability is the use of an industrial robotic arm. The final selection was to use the available industrial robot (Kuka KR180) as a handling system and integrate the bending system into it. Its six degrees of freedom can freely position its end effector in space and therefore conduct the bending movement.

4.1.2 Gripper

The task of the gripper is to induce the bending and holding forces into the UD-tape. While doing so, the gripper should have a small interference contour close to the bend and be compact in the longitudinal direction of the tape to allow a small minimum distance between two bends. The gripper should securely hold the tape in the normal direction and the rotational degrees of freedom while allowing some slippage along the tape surface to allow for a tensioning of the tape by moving against the slippage.

Table 4-2 lists the available part handling gripping principles according to (Fantoni & Santochi et al. 2014). Further gripping principles are listed in (Alebooyeh & Wang et al. 2019).

Table 4-2: Available gripper types (Fantoni & Santochi et al. 2014)

Gripper Type	Short evaluation
Friction Gripper	Can be suitable
Jaw Gripper	Cannot be used as no shape fit can be obtained in longitudinal direction resulting from the tape's shape
Magnetic Gripper	Cannot be used for non-magnetic workpieces
Suction Gripper	Can be suitable
Needle Gripper	Cannot be used as no slippage is possible and cracks are generated
Electrostatic Gripper	Insufficient force per area in existing examples (Schaler & Ruffatto et al. 2018)
Van der Waals Gripper	Only suitable for low forces
Ice Gripper	Should not be used to avoid water in the process and interference with the heating
Acoustic Gripper	Not suitable for precise positioning
Laser	Only suitable on the micro scale
Bernoulli Gripper	Should not be used as the airstream will rapidly cool down the molten zone of the tape
Adhesive Gripper	Should not be used to avoid pollution of the tape

Of the presented types, friction and vacuum grippers are most suitable. The other gripper types are excluded due to the reason given in the short evaluation. Vacuum grippers differ in their suction cup arrangement and the shape and size and rigidity of the suction cups. An advantage of suction grippers would be that only one side of the tape needs to be accessible, reducing the interference contour. Low negative pressure and a supporting geometry of the suction cup need to be used to protect the thin tape from damages through the suction. The suction cup must be rigid in its activated state to induce a precise angular movement. The suction cup should not have a long sealing lip to induce forces into the tape as close to the heated area as possible. Therefore, and to allow slippage during the pre-tensioning, only solid low-pressure suction cups would be suitable. In preliminary experiments, it was shown that a relatively large suction surface is necessary for a reliable process, which would cause a large minimum distance between two bends. Furthermore, airstream caused by the vacuum leakage would permanently cool the tape and thereby influence the heating.

To overcome these disadvantages, a friction gripper can be used. It can have a minimum size in the longitudinal direction of the tape, and the force that is needed to make the tape slip through the gripper can be carefully adjusted. In (A_Vollmer 2018), a clamping gripper for the bending and handling tasks was designed and implemented. A concept with a static lower jaw was selected to support the tape in the initial position

of the gripper. A pneumatic cylinder pushes the upper gripper jaw against that static lower gripper jaw to clamp the tape. As the lower gripper jaw is fixed, it can be built very small, minimizing its interference contour. A pressure regulator for adjusting gripping and slipping force was added to the cylinder.

4.2 Heating the Bending Area

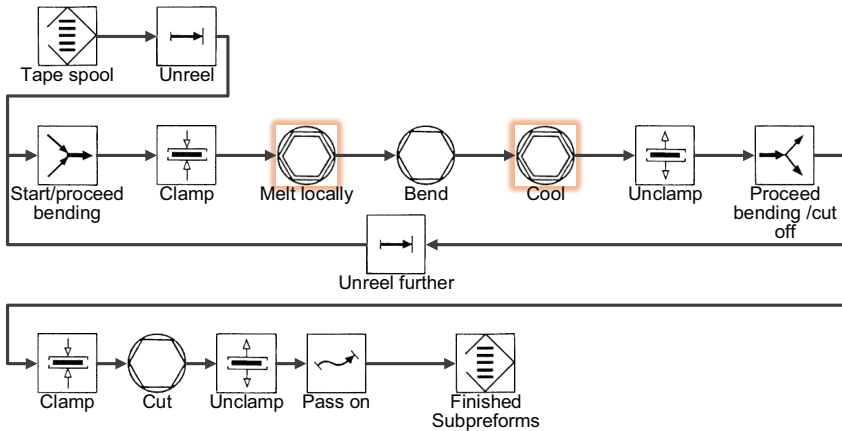


Figure 4-4: Function charts with highlighted heating and cooling

A heating unit was designed and built for the test rig (A_Vollmer 2018). The matrix in the area of the bending edge needs to be liquefied (Figure 4-4). Overheating must be avoided to prevent thermal degradation (Qin & Su et al. 2003; Lüderwald & Merz 1978; Bikiaris 2011; Wang & Tu et al. 2013). To avoid unwanted tape deformation, the molten area should be kept small. Therefore, the heating unit must be able to selectively melt a narrow area along the bending edge. To temper the tape, heat could either be generated in it or transferred into it. From a wide selection of heat generation (Blanke & Birden et al. 1960; Reese & Vorhof et al. 2020; Schmidt-Rohr 2015) and heat transfer (Lienhard & Lienhard 2020) possibilities, four were selected. Induction and direct resistive heating, convective heating, radiation heating, and contact heating were examined. Laser heating was excluded for lab safety reasons.

Either the heating unit must be correctly positioned on the tape or the area it is heating must be adjustable by external input for heating an adjustable narrow area. In the completed test rig, the bending edge and the heated area will need to be on the tape between the supply and the gripper. The position of the heated area can be kept constant

by keeping the gripper's position constant and adjusting the length of the tape segments by adjusting the tape conveying between two bends. This way, no linear movement/adjustment of the heating device is required. However, a rotation of the heated area on the tape will be necessary to allow the variation of the bending edge in α . For avoiding the additional rotation axes, the heating device is directly mounted to the robot end effector. This way, it will be positioned with a constant offset to the gripper, which is positioned by the robot relative to the bending edge.

In the following subsections, the heating principles are evaluated. Criteria for the selection are a compact integration into the end effector, a sensible heating control, reliable long-term use, low forces on the heated tape, and sufficient heating power.

4.2.1 Induction and Direct Resistive Heating

Inductive and direct resistive heating use electric current within the carbon fibers to heat the tape.

4.2.1.1 Induction Heating

Eddy current induced by an alternating magnetic field can be used to heat conductive material by joule losses. To fulfill the requirements, the currents can be guided in the heating zone by an adapted coil geometry. A prerequisite for inductive heating is the material's ability to conduct the currents while still creating joule losses. Although carbon fibers are generally sufficiently conductive for inductive heating, (Rudolf & Mitschang et al. 2000) indicate that unidirectional layups with a thermoplastic matrix cannot be heated as the single fibers are isolated from another. (Kim & Yarlagadda et al. 2002) describes that a limited amount of heating is possible in some cases when fibers have contact with another, especially if several unidirectional layers are stacked in 90° orientation. A test was set up to examine the heating of the used material in this thesis. For the experiment, a 6 winding round copper coil with a diameter of 70 mm and a length of 30 mm was fed with an alternating current from an induction generator. The resulting frequency of the oscillating circuit was 120 kHz. The input current into the induction generator was measured for evaluating the induction effect. In contrast to textile material or metal objects, no change in the input current could be measured when inserting the used UD-tapes into the coil. Therefore, inductive heating was excluded from further experimentation.

4.2.1.2 Direct Resistance Heating

The unidirectional character of the used tape also poses a challenge for the direct resistive heating of the tape. As for the eddy currents in inductive heating, the material's conductivity is only given along the fibers. It was shown that current could be fed into the material and along the fibers. A strong mechanical clamp had to be used to create initial contact. Heat distribution was uneven in such a way that the two introduction areas overheated before the area in between was relevantly warmed up. Furthermore, the heating characteristics were unstable, with decreasing electrical resistance during the heating. Perpendicular to the fiber direction, no current could be introduced using safe voltages. As the orientation of the bending edge in the final heating setup would be normal to the tape direction, no current could be fed along the bending edge to heat it evenly. Therefore, direct resistive heating was excluded.

4.2.2 Convective Heating

Preliminary experimentation on heating by a jet of hot air was conducted in (A_Vollmer 2018). For this, a Steinel HG 2420 controllable power hot air gun with a linear nozzle was directed at the free end of a clamped tape. With the stock nozzle, the shape of the molten area could not be adjusted to be linear. Due to the slow control of the hot air, the behavior of the molten area could not be controlled well. A custom hot air system would need to be implemented for improved controllability, causing considerable effort without promising good results. Furthermore, the impact of the jet of air induced an unwanted force into the tape. In future applications, this would cause a deformation of the molten area and potentially decrease the angular precision of the bends.

4.2.3 Radiation Heating

A widely used heating method in composite material manufacturing processes is infrared or visible radiation. Carbon fibers are well suited for radiation heating resulting from their high degree of absorbing visible and near-infrared radiation (Dombrovsky 2011). In multi-fiber situations, rays interfere in a more complex way than plain absorption/reflection as the reflected portion of the radiation can be directed towards another fiber, effectively increasing the absorption (Xu & Hu et al. 2015; Stokes-Griffin & Compston 2015). The optical properties of carbon fiber have only slight variations depending on the temperature and wavelength in the common scales. Therefore, a wide range of heaters can be applied for various tasks (Le Louët & Rousseau et al. 2017).

No commercially available radiation heating system could be applied to the end effector resulting from build volume limitations and interference contour requirements. In (A_Vollmer 2018), concepts for a radiation heating system were developed, examined, and compared. Such a system consists of a heat/light source and optical elements like reflectors and adjustable apertures. Reflectors can be used to focus the heat and thereby increase the heat density while reducing the size of the heated area. With the help of apertures, the heated area can be sharply limited while losing a large portion of the heating power.

A small interference contour and a large distance between heat source and tape are advantageous for maximum possible bending angles. A fast process requires a large heating power, and the heated zone should be limited to a small area around the bending edge to avoid unwanted deformation. Three concepts for radiation heating were compared regarding these requirements (Table 4-3).

Table 4-3: Concepts for limiting the heat-affected area using radiation heating

Aperture	Reflector	Reflector with aperture
-Lowest expected heating power	- Complex design and adjustment	- Complex design and adjustment and largest interference contour
+ Very compact	+ Best heating power	+ Best focus of the heating

As the later heated area will be linear, tubular tungsten lightbulbs (r7s; 118 mm; 500 W unless stated otherwise) were used for experimentation similar to commercially available line or longish area heaters use tubes¹. An experimental setup with an aluminum frame and adjustable mounts for lightbulb, aperture, reflector, and target/tape was used for easy geometry variation for the experimentation.

4.2.3.1 Aperture

Apertures are used to limit the area a radiation field can reach without specifically directing the radiation to the target. This way, the power of the cut-off radiation is lost. The distance between lightbulb and tape D_{lt} and tape and aperture D_{ta} and the aperture opening W_a were varied to examine the heating power of a light source shining through an aperture. The time until the first molten matrix was observed and the width of the

¹ <https://optron.de/index.php?id=13&lang=en> (last downloaded 28th June 2021)

molten matrix area 3 seconds after that were evaluated. The experiments were executed with the PA UD-tape. (A_Vollmer 2018)

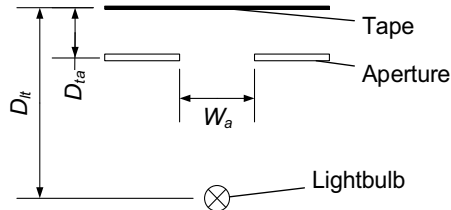


Figure 4-5: Parameters of the radiation heater with aperture

The experimental results are listed in Table 4-4. A small distance from the lamp to the tape decreases the heating time. With 30 mm distance and an aperture directly on the tape, melting could be rapidly initiated with the molten area increasing to the width of the aperture within the 30 seconds after initial melting. With 50 mm distance, the heating time increased. Furthermore, no sufficient melting was obtained with the 5 mm or 15 mm aperture. The 20 mm distance between tape and aperture was set to avoid heat conduction from the tape to the aperture. With it, no sufficient heating could be obtained within three seconds after initial melting with 5 mm or 15 mm aperture. Concluding, heating without an aperture leads to a fast increase in the area size, which would be difficult to control in later experimentation. Experiments with an aperture could only deliver decent results for the 30 mm distance, which is critical for the interference contour.

Table 4-4: Melting time and width depending on the geometric parameters

D_{it} / mm	D_{ta} / mm	W_a / mm	Time to initial melting / sec	Width of the molten area 3 seconds after initial melting / mm
30	0	50	5	50
		15	5	15
		5	9	0-1
50	0	50	12	50 with cold spots
		15	16	0-3 irregular
		5	Abort after 30	No melting
	20	15	12	0-3 irregular
		5	Abort after 30	No melting

4.2.3.2 Reflector

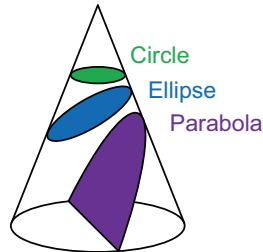


Figure 4-6: Circle, ellipse, and parabola are sections of a cone with the circle being normal to the symmetry axis of the cone and the parabola being parallel to a line on the cone surface. The ellipse is a stretched circle along one axis, and is between the circle and parabola shape.

The light from the rear side of the lamp can be directed towards the tape by a reflector to increase the heat flux. In commercial infrared heaters, spherical, parabolic, and elliptical reflectors are used. Parabolic reflectors reflect rays from their focus to a collimated beam to infinity. A spherical/cylindrical reflector focuses rays from its center back to the center. The later effect is used in some coatings on halogen light bulbs to reflect invisible radiation back to the tungsten filament (Bigio & Israel et al. 2005). For the sharp focusing of a ray from one point (in this case lightbulb) to another (in this case a thin area on the tape bending edge), elliptical reflectors can be used. The three named shapes can all be regarded as flat cuts from cones, with a circle being the limes of an ellipse with two very close focal points and a parabola being the limes of an ellipse with an infinite distance between the focal points (Figure 4-6).

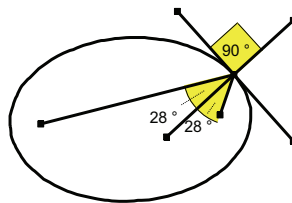


Figure 4-7: Reflection of a beam from one ellipse focus point to the other

The focusing properties of an ellipse and its derivatives circle and parabola are based on trigonometry. An ellipse is the group of points with the same sum of distances to its two focus points. Any ray emitted from one of the focus points will be reflected to the

other focus point at any point of the ellipse, as demonstrated in Figure 4-7. For the best effect, lightbulb and bending edge should be placed on the two focus points of the ellipse (Vorkov & Arola et al. 2018; Lee & Yang et al. 2014).

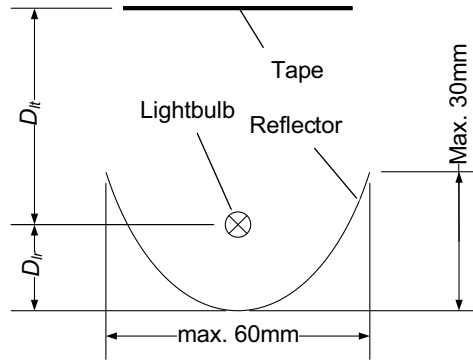


Figure 4-8: Reflector comparison setup

For the experimentation, reflectors were made by 3D printing the calculated shape and coating it with reflective aluminum foil. An initial comparison between elliptical, parabolic, and cylindrical reflectors of similar sizes proved that an elliptical reflector should be used. The width of the reflectors was limited to 60 mm, and the protrusion in front of the lamp was limited to 30 mm for an acceptable interference contour. The aim is to find a reflector that has a high heating density at a long distance. The setup is sketched in Figure 4-8. The problem cannot be regarded as an idealized ellipse as the tungsten filament of the lightbulb is coiled and therefore not a perfect point. Reflectors that have a small distance to the lightbulb D_{lr} are expected to be influenced more by this as the angular error of the filament's position is larger. However, reflectors with larger D_{lr} , have a smaller wrap angle of the reflector around the lamp as their front opening is wider. The distance from lamp to tape D_{lt} shall be as large as possible while maintaining sufficient heating density.

The parameters were varied according to Table 4-5. Additional to the already introduced parameters, the lamp's power was varied to enhance differences in the heating time. The times, which were necessary to create a sufficiently large heated area, are listed in Table 4-5.

Table 4-5: Heating time with various reflector geometries. An x indicates that the tape could not be molten.

D_{lr} / mm	5			10			20		
D_{lt} / mm	50	70	100	50	70	100	50	70	100
Lamp power / W	Heating time / sec								
100	4	5	x	6	7	x	8	x	x
230	1,5	3	5	2	3	6	3	x	x
300	1	1,5	4	2	3	4	2	x	x
500	0,5	1	3	1	1	3	1	x	x

As expected, larger D_{lt} increases the heating time. The fastest values for D_{lr} were 5 mm and 10 mm. A reflector design with $D_{lr} = 10$ mm and $D_{lt} = 100$ mm was selected as experiments showed slightly better evenness of the heat distribution along the bending edge, and better tolerance to slight geometrical deviations was expected resulting from the larger overall geometry.

4.2.3.3 Reflector combined with an aperture

To further sharpen the heated area, an aperture could be added to the design. For the experiment, the $D_{lr} = 10$ mm, $D_{lt} = 100$ mm reflector was used with a 500 W lightbulb and $D_{ta} = 3$ mm. The heating times with selected aperture widths are listed in Table 4-6.

Table 4-6: Heating time with a reflector and various aperture sizes

W_a / mm	open	5	4	3	2
Time for a sufficient molten area / sec	3	3	3.5	5	x

With moderate apertures, only a small loss in heating power became evident. The aperture opening should not be smaller than 4 mm to avoid an increase in heating time. However, the evenness of the molten area could be improved, which proves the benefit of an aperture for the bend quality.

The experiments indicate that the molten area can be restricted to a sharply limited region using an aperture if required. The disadvantage of an aperture is the increased interference contour of the heating unit.

4.2.4 Contact Heating

The last concept for heating the tape is contact with a heated object or clamping it between two heated objects. The tape in this work will be clamped between two jaws

of a gripper to avoid asymmetrical deformation. This concept promises a good control of the temperature, while a contamination of the jaws with matrix material might influence the reliability.

Temperature-dependent effects were examined in an experimental series (A_Vollmer 2018). Heatable jaws with 2 mm times 50 mm contact area were mounted to a pneumatic gripper to heat the tapes. The heaters were set to a specific voltage, and the temperature after a sufficient settling time was measured. Two experiments were conducted. The heat transfer in normal direction of the tape was evaluated by comparing the adhesion between two stacked tapes after 1.5 seconds of heating. The bendability was evaluated by heating a single tape for 1.5 seconds and bending it afterward. The results of these experiments are listed in Table 4-7. The adherence between the tapes rose rapidly at 165°C jaw temperature with no noticeable improvement for higher temperatures. The bends showed the best results around the same temperature range, with bending forces decreasing for higher temperatures.

Table 4-7: Effects of the contact heating depending on the jaw temperature

<i>Heating Voltage / V</i>	<i>Resulting jaw temperature / °C</i>	<i>Joining of two layers of tape</i>	<i>Description of the bend in a single tape after 1.5 seconds of heating</i>
5	84	no adhesion	mark visible
6	107	no adhesion	mark visible
7	140	no adhesion	bend
8	165	welded together	very narrow even bend
9	186	welded together	wider even bend
10	222	welded together	uneven bend

Bending trials with variable temperature and gravity-driven bending were conducted to evaluate bending forces. For this, the tapes were clamped between the jaws for a settling time and bent by gravity. It could be proven that higher temperatures lead to higher bending angles and, therefore, lower bending forces. The heated area outside the jaws was very small, which allows good control of the deformation. Especially for the lower temperatures, this might induce higher springback values caused by the smaller resulting bending radius and higher forces. The evenness and melting width of four PP samples are shown in Figure 4-9.

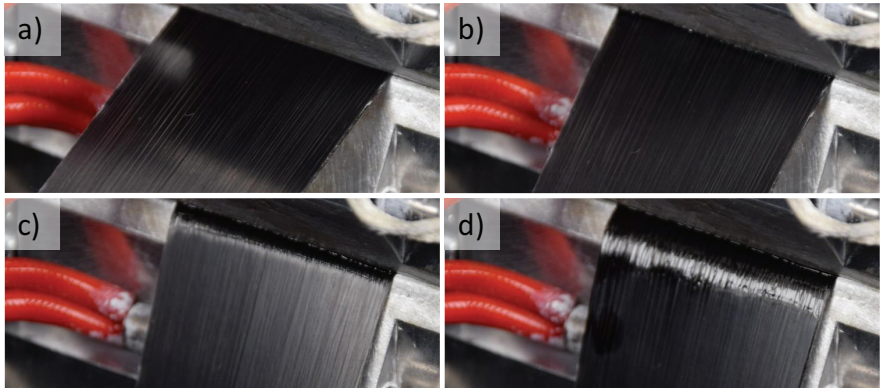


Figure 4-9: Forming of the molten area by gravity after a settling time at 140°C (a), 165°C (b), 186°C (c) and 222°C (d) jaw temperature. (Image: re-enacted experimentation on the final test rig)

4.2.5 Heating Method Selection

The heating unit will be mounted to the robot end effector to avoid additional axes. Resistive heating of the tape can be excluded as heating method as no electric conductivity along the bending edge is guaranteed. Convective heating is excluded, as it is difficult to control and influences the bending area by the impact of the air. The remaining methods, radiation and contact heating, are compared in Table 4-8. The contact heating promises short cycle times with a consistent heated area. It is not dependent on the black carbon fibers and works with transparent fibers. However, it might be critical in long-term use due to contamination with molten matrix material. Radiation heating will work without inducing forces into the tape and guarantees a contamination-free long-term use of the heater. The aperture caused increased interference contour on the process-adapted end effector. For a good compromise of heating power and focus, a mirror without an aperture should therefore be used. The maximum bending angle could not yet be evaluated before the final commissioning. As both methods show promising results in early experimentation and their specific advantages for certain applications, they are both implemented for the experimental process analysis. The final selection will be based on the results of the parameter selection (Section 5). (A_Vollmer 2018)

Table 4-8: Comparison of contact and radiation heating

Criterion	Contact	Radiation
Flexibility for other types of tape	0	-
Cycle time	+	0
Consistency	+	+
Pollution	-	+
Possible bending angles	not rated	not rated

The implemented end effector is presented in Figure 4-10. The components of the end effector are mounted to a changeable robot connector. For clamping the tape, a handling gripper with one linearly actuated swiveling jaw has been implemented. The radiation heater features a polished full aluminum mirror. For experimentation with contact heating, a parallel jaw gripper with closed-loop temperature control has been implemented. The contact heating can be dismantled from the effector to clear the area between the radiation heater and tape for experimentation with the radiation heating. The control for the two heating methods is mounted in separate boxes on top of the end effector.

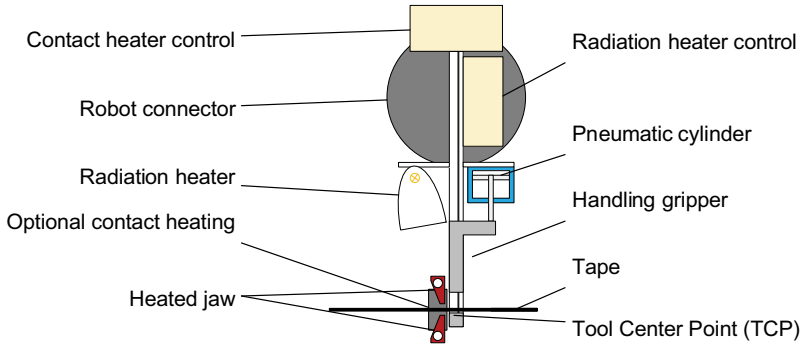


Figure 4-10: Bending end effector with both heating devices

The two heating units create molten areas of different sizes (Figure 4-11). The radiation heating melts an area of 3 mm – 10 mm at some distance from the handling gripper. The contact heating melts the tape between the heated jaws and at a small distance (approximately 1 mm) to the heated jaws. When bending, only the short area outside the heated jaws is bent. The smaller heated area of the contact heating is stiffer, increasing the bending forces (A_Penev 2019) and thereby the expected angular error.

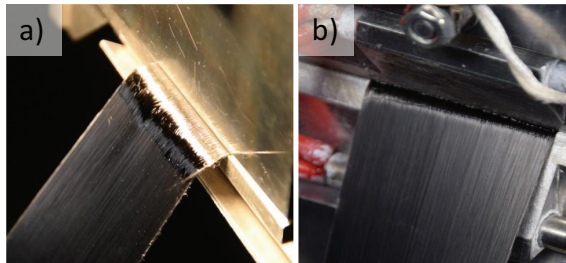


Figure 4-11: The radiation heating (a) melts a larger area of the tape than the contact heating (b) in the final implementation at the optimized heating settings.

4.3 Supply of Tape Strips

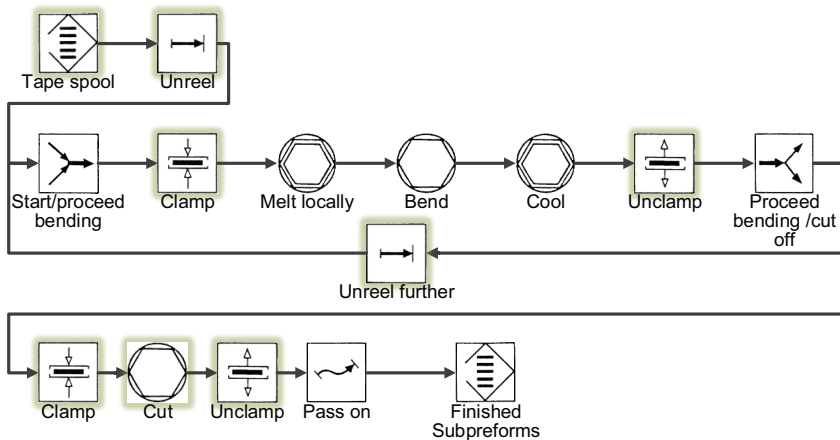


Figure 4-12: Function chart with highlighted process steps connected to the tape supply

The task of the supply unit is to place the tape strip in such a way that the robot can bend the free end and to cut the finished preform from the spool (Figure 4-12). The development of the supply unit is described in (A_Nguyen 2018). As the tape will be delivered on a spool, two conveyor rollers were selected for its unreeling. Shear cutting, water jet cutting, and laser cutting were considered for cutting the tape. Shear cutting was selected for reliability and simplicity as it showed satisfactory results for experimentation in the initial examination. The cutting unit was integrated into the supply unit to avoid a large interference contour at the robot end effector. Within the work, parameters

for conveying and cutting were examined, and the supply unit with its subunits was constructed and commissioned.

4.3.1 Conveying

The tape is conveyed between two rollers. For constant friction without damaging the tape, at least one roller must have a compliant mounting. Therefore, the free-rolling roller is mounted on a pneumatic cylinder. The contact pressure between the rollers and the tape can be adjusted using a pressure-regulating valve.

A Nanotec PD4-N5918X4204 stepper motor is used and controlled via CANopen by a PEAK PCAN-USB adapter to actuate the rollers. For conveying the tape, precise positioning is necessary while the needed conveying speed is negligible. To better fulfill these requirements, the motor drives the roller via a toothed belt drive with a 16/60 ratio (A_Mühlbeier 2019). A pneumatic clamp with flat jaws is added to the supply unit to secure the tape during bending and cutting.

4.3.2 Cutting

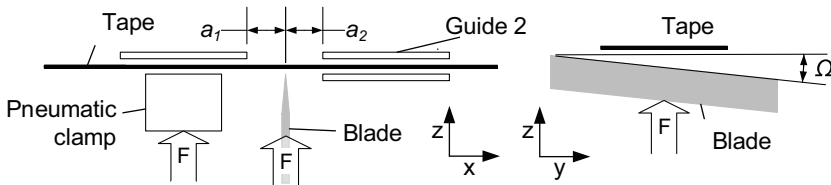


Figure 4-13: Cutting parameters

For the cutting, the cutting gaps a_1 , a_2 , and the rotation angle of the blade Ω were examined in an experimental design (A_Nguyen 2018). The parameters are shown in (Figure 4-13). The cutting gaps were varied in the three stages 1 mm, 3 mm, and 6 mm. Cutting with contact between blade and guide ($a_{1/2} = 0$ mm) was attempted but failed, as large forces were necessary. The blade rotation Ω was set to 0° , 10° or 30° . For the experimentation, a 0.5 mm wide blade was used, and the pressure of the actuating pneumatic cylinder was set to 4.2 bar (~ 4200 hPa).

Best results were achieved with $\Omega = 30^\circ$ and $a_1 = a_2 = 3$ mm. With a smaller rotation, forces would increase, and therefore more damage occurred. With wider values for the cutting gaps, the tape would deform before being cut, resulting in worse cutting-edge

quality. At $a_1 = a_2 = 1$ mm, some experiments showed a sharp bend close to the edge, which might cause difficulties conveying the tape afterward. Therefore, $\Omega = 30^\circ$ and $a_1 = a_2 = 3$ mm was selected for the cutting.

4.3.3 Combined Supply Unit

The supply unit was constructed using aluminum profiles. The lower roller, clamp, and blade are actuated by three pneumatic cylinders. The upper roller can be turned by a stepper motor via a belt drive. Figure 4-14 gives an overview of the implemented functions in the supply unit.

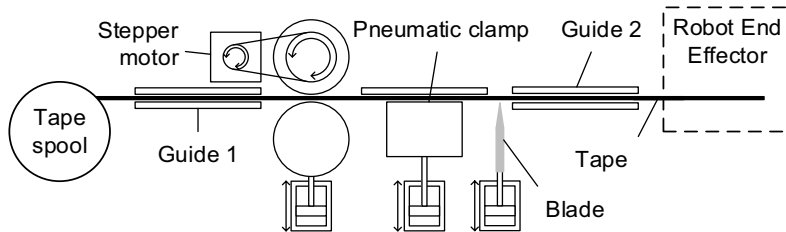


Figure 4-14: The tape is moving through the supply unit from left to right

4.4 Control System

The control system has to coordinate the robot movements, stepper motor, and I/O functions like pneumatic valves and switching the heating on and off.

For this task, a central control script was implemented in python on the control PC. This central script serves as a sequence control and calls services offered by the stepper motor and the robot. The robot program waits until it receives a command via the KUKA Ethernet XML interface, then executes it and falls back to waiting. The commands consist of a selection code for the action which shall be conducted and parameters for the adaption of this action. I/O functions are switched via the robot control connected to two Beckhoff Profinet I/O modules mounted to the robot arm and the supply unit. A system overview is given in Figure 4-15. (A_Mühlbeier 2019)

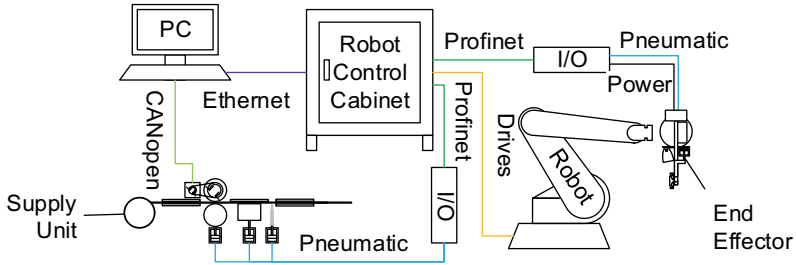


Figure 4-15: Control architecture of the experimental cell

The stepper motor offers speed or distance-controlled movements, which can both be used by the control. For the swing folding process, only distance-controlled movements at a constant maximum speed are used.

In the robot program, 16 functions were implemented. The most important functions are:

- Set and pulse digital outputs
- Wait
- Set tool, base, and velocity for movements
- Move absolute or relative in Axis or Cartesian coordinates along a Point to Point, Linear, or Circular path

The swing folding process is combined from a sequence of these functions. Experimentation to find the optimum sequence for accurate bending results is examined in Chapter 5.

For flexible experimentation and operation of the rig, the preform geometry and the necessary process parameters are read from two text files. In the geometry file, the overall preform length, the three parameters α , β , and l from Section 3.2.5 for each bend, and the tape width and material type are given. Based on this, the correct process parameter file is selected. The process parameter file contains heating and cooling times and material-specific kinematic parameters.

4.5 Commissioning

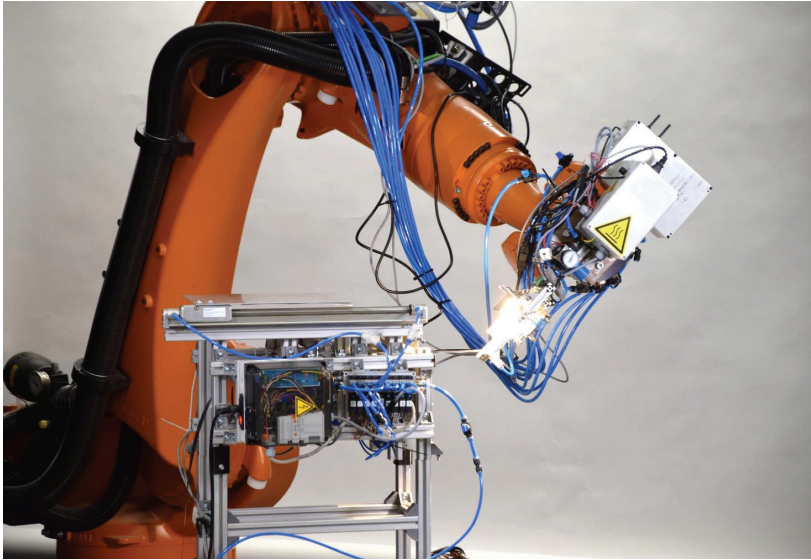


Figure 4-16: Frontal view of the bending setup

The setup is presented in Figure 4-16. The supply unit is visible in the foreground. The tape is moved through it from left to right. The position of the supply unit was selected to guarantee sufficient movement space of the end effector in the rotational axes around the bend and the translational axes for the handling of finished preforms (A_Mühlbeier 2019). On the right side of the supply unit, the robot can grip the tape with the end effector. The tape is heated between the supply unit and the end effector close to the end effector for each bend. Then the end effector is moved for the bending movement. For a faster process, a cooling nozzle was added to the end effector. After the last bend, the tape is gripped by the end effector and cut from the spool by the supply unit.

In the following paragraph, mechanical limitations in the bending angles are briefly discussed. Although the gripper was designed to be slim in the longitudinal direction of the tape, there still is a 15 mm minimum distance between two bends. α has to be in a certain range depending on the tape width to avoid collisions between the tape and the vertical beam of the end effector. With a 30 mm tape, α is limited to values between -30° and 60° . The limits of β depend on the distance from the end of the supply unit to the

bending edge. At the selected distance of 180 mm, β may be between 55° and -90° when using the radiation heating (A_Wi 2019) and $\pm 50^\circ$ when using the contact heating (A_Vollmer 2018). The two heating units are presented in Figure 4-17.

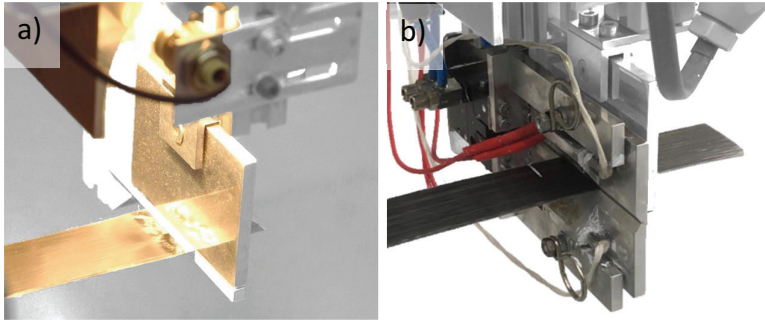


Figure 4-17: Radiation heater (a) and contact heater (b)

It became evident that full-power radiation heating during the bending movement could not be adjusted to function repeatable and gently. With full power heating, the tape would always be overheated in the first half of the movement and cool down during the second half. Therefore, a power control was added to the radiation heating with a low and high setting. The low setting was adjusted to obtain a narrow molten area after 30 seconds of heating and would therefore keep the tape at constant temperature once it was heated (A_Saur 2020). The high setting would heat the tape to the same molten area within a few seconds. In the final process, the high setting is used for preheating, and the low setting is used to keep the tape hot during the bending movement.

The cooling nozzle underwent constant improvement. A round nozzle was added to reduce the cycle time after the first experimentation (A_Wi 2019). After a deformation of the tape by the airstream became apparent (A_Saur 2020), the single nozzle was replaced by a tube with several openings, which was placed below the lower handling gripper jaw.

The described experimental bending cell was used for the process examination by parameter variation in Chapter 5.

5 Analysis of the Swing Folding Process

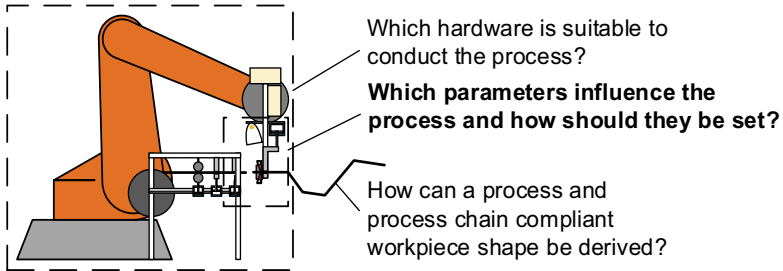


Figure 5-1: Research questions of this thesis

The controlled bending of the UD-tape shall deliver good results regarding angular accuracy in α and β , a correct length of the tape's sections, and avoid thermal damages in the bending zone. Therefore, parameters must be set correctly (Figure 5-1). For good angular precision, spring-back shall be minimized by bending in a zone of evenly molten matrix material. The molten zone shall be limited to the bend line to avoid deformation of the surrounding tape. Maximum temperatures in the heated zone shall not be higher than needed for the bending to minimize instant degradation. The process shall be fast for high productivity, which further emphasizes that heating the material for too long shall be avoided. Adhesion between the gripper and the tape shall not influence the process reliability.

In initial experiments, it could be shown that the movement of the gripper, the timing of the process, and the duration or temperature of the heating had a significant influence on the result. In this chapter, the influence of the process parameters and optimum values for the process parameters are examined based on a selection of the executed experiments. The goal is to identify which parameters influence the resulting bending angles and how they should be set.

In Section 5.1, a kinematic model of the swing folding process is derived. After initial experimentation with a purely rotational movement showed the error caused by tension or compression longitudinal to the tape, it was proven that the process does also have a translational movement component. The developed model is based on the assumption of an even bend between two solid tape ends.

In Section 5.2, the relevant influencing movement and heating parameters are listed.

In Sections 5.3 and 5.4 the process behavior is analyzed. First, the final process routes are presented. Afterward, qualitative phenomena are described. Fractional factorial design experiments are conducted and evaluated using the analysis of variance (ANOVA) method to determine the influence of parameters. When the most relevant parameters are identified, they are optimized in iterative experiments where they are individually varied. The process robustness regarding a factor is described by the variation of the result depending on that factor. Finally, the process is characterized using a multi-level design of experiments. In this thesis, the most relevant experimental series are presented. Further examinations can be found in the references.

The results of the parameters variation were examined using three measurement methods. The first was a mechanical angle gauge adapted to measure both bending angles in one measurement (A_Bachtin 2020). This is obtained by placing two planes of the meter on the tape while pushing the tape against a guide in the meter and reading from the two scales. The mechanical angle meter was the standard measurement device and used in all experiments unless specified otherwise. In experiments with alternative measurement methods, it was used for a regular check of the measurements. In (A_Ding 2020), a stereo camera measurement system was adapted to the swing folding process. The function principle of this device is presented in (Kupzik & Ding et al. 2020), and the system was further improved by (A_Steidle-Sailer 2021). It can be used to evaluate a bend automatically and is therefore suitable for experimental series with many parameter combinations. Unfortunately, the surface of the PA material did not show useable features, as the PP material did. For comparability between the materials, the stereo system was not used in the experiments documented in this thesis. Specimens with multiple bends were measured using a GOM ATOS system, where specified in the text.

5.1 Bend Kinematic

The bending movement of the robot has to induce a bend in the heated zone of the tape. The ideal geometry of this would be an even bend in the heated area and small to no deformations in the two solid regions next to the heated zone. A model for this deformation is presented in Figure 5-2.

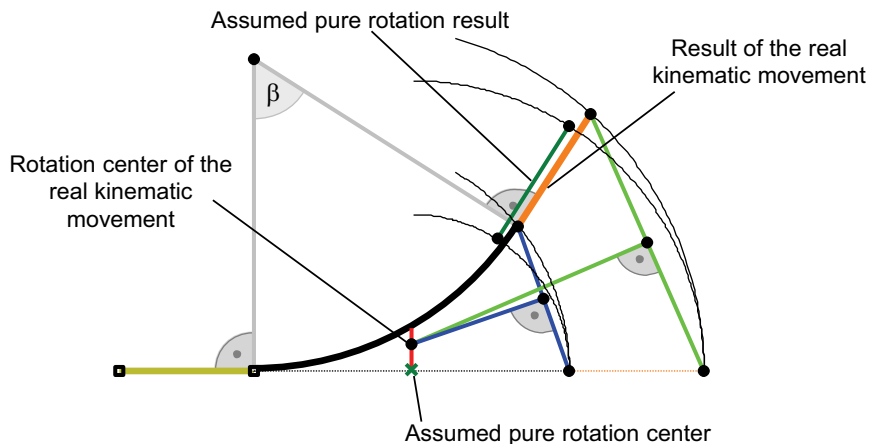


Figure 5-2: It can be proven that a rotation around a fixed TCP is not a sufficient description of the bending as the required rotational center of the real kinematic movement is moving along the red line depending on the angle β . The dark green line represents the result of a pure rotational around the dark green cross.

On the left side of the figure, the fixed tape end in the supply unit is shown in ocher. The heated and bent area is drawn as the adjacent black line. An even bend and a fixed length of the black line are assumed. The solid end of the tape, which is gripped by the end effector, is drawn in orange. The initial, undeformed tape is represented by the dotted line. By adding the connection lines between the ends of the orange sections and drawing their bisections (green and blue), the rotational center of the movement can be found at the crossing point of the two bisections. The red line represents the rotational centers for all β angles. The fact that the position of the rotation center moves proves that the bending cannot be simplified to a pure rotation around a fixed center. Therefore, the perfect robot movement cannot be a simple rotation around a fixed Tool Center Point (TCP) - axis.

The behavior of the swing folding process with a simple rotational kinematic was examined in experiments. The rotation center was placed in the supplied tape for this examination to secure equal conditions for positive and negative bends. The resulting position of the solid tape in the end effector after a rotation around the dark green cross is represented by a dark green line in Figure 5-2. To quantify the error depending on the angle, the position of the end points of the solid area is traced by the thin black lines for

the pure rotation and the correct kinematic approach. In the experiments, it could be proven that a pure rotation of the tape results in an error in β . The reason for this error is the deviation in the distance between the supply unit and the end effector at the end of the bending movement. The resulting difference between the necessary and the available length of the tape can introduce tension or compression into the tape. These forces will then alter the shape of the bend and thereby displace the bent area. As the heated area of the tape is not displaced, the result will be a partially elastic deformation in a cold area of the tape with a correspondingly large spring back. In Figure 5-3, a qualitative example is given.

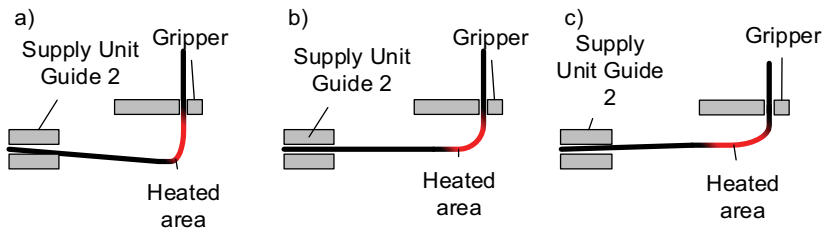


Figure 5-3: Qualitative example of the influence of tension. By moving the gripper horizontally, the position of the bent zone can be influenced: a) compression, b) correct length, and c) tension in the tape.

The effect of this error could be confirmed in an experimental series where the β error could be reduced by horizontally correcting the gripper position directly after a bending rotation (A_Wi 2019). The described deformations also became apparent in this experimental series (Figure 5-4), and the optimum correction distance was dependent on β , which is supported by the assumption that the rotation center is β dependent.

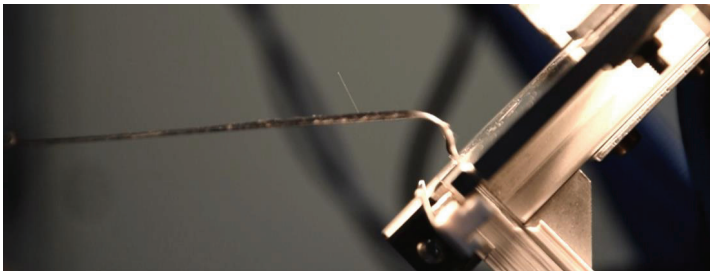


Figure 5-4: Deformation resulting from too much tape length between supply unit and end effector

A kinematic model with two stiff clamped tape segments, connected by a soft heated area, was developed and implemented in the robot control to maintain correct tape tension (Kupzik & Bachtin et al. 2021; A_Bachtin 2020).

In this model, the position of the coordinate system “*d*” is described in the fixed coordinate system “*a*” via a movement along “*b*” and “*c*” (Figure 5-5). For skew bending edges, the bending edge is first rotated around the “*a*₃” axis around the angle α into the new coordinate system “*b*”. Before bending, the end effector TCP is displaced from the rotated bending edge “*b*” to the gripping position “*c*” along the movement \vec{r}_1 . To execute the bend, the TCP is displaced and rotated from “*c*” to “*d*” along the movement \vec{r}_2 .

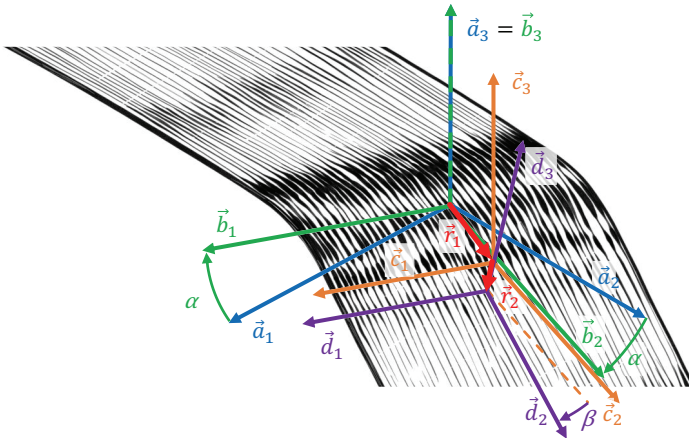


Figure 5-5: Definition of the coordinate systems *a* (position of the bend), *b* (system of the rotated bending edge), *c* (initial position of the gripper), and *d* (final position of the gripper) (Figure based on Alexej Bachtin)

Figure 5-6 shows the kinematics of a single bend in a two-dimensional representation. The assumptions for the selected description are that the tape consists of the three sections solid-molten-solid. The undeformed tape is shown in blue, the forming in yellow, and the final result in green. In the left of Figure 5-6, the solid end in the supply unit is kept at a constant position. Connected to the right end of this solid section is the molten section along b_0 . The length of the molten area is assumed constant as the carbon fibers will not extend or contract plastically. For securing an even bend quality without sharp redirections of the fibers, the molten area shall form a circular arc. On the right side of the molten area, the gripper holds the tape with a distance t_0 to the molten

area. The tape thickness is referred to as s_0 . With these assumptions, the position of the TCP coordinate system of the gripper can be transformed from its initial position “c” to the final position “a” via the intermediate positions $d(t)$ along the movement vector \vec{r}_2 . As the length of the idealized molten section is kept constant, the bending radius $R(t)$ changes with the bending angle β during the swing folding process until it becomes the final bending radius R_0 . From the constant length of the molten area, a relationship between the bending angle and the bending radius can be derived:

$$b_0 = R_0 \cdot \beta = R(t) \cdot \beta(t) = \text{const.} \tag{5-1}$$

$$R(t) = \frac{b_0}{\beta(t)}$$

$$R_0 = \frac{b_0}{\beta}$$

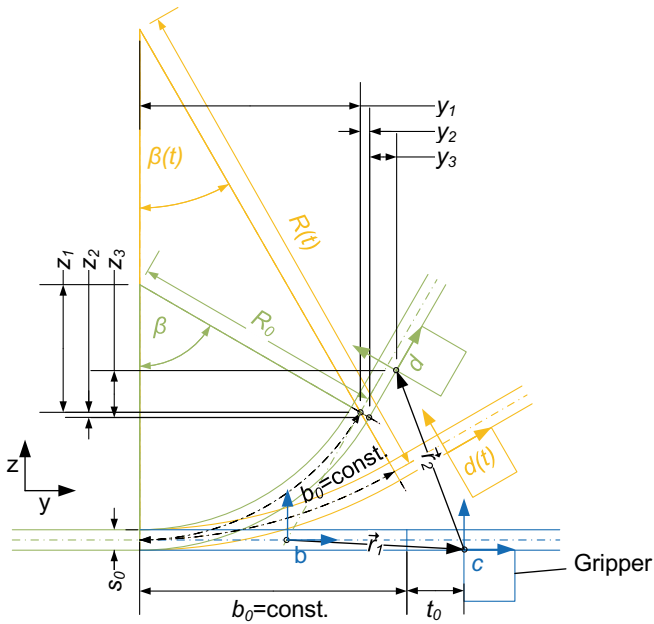


Figure 5-6: Kinematic description of a bending zone (figure based on (A_Bachtin 2020))

The position of the gripper relative to the center of the bending edge (\vec{r}_1) can be calculated as follows:

$$\vec{r}_1 = \begin{bmatrix} 0 \\ \Delta y(t) \\ \Delta z(t) \end{bmatrix}_{\{b\}} = \begin{bmatrix} 0 \\ \frac{b_0}{2} + t_0 \\ -\frac{s_0}{2} \end{bmatrix}_{\{b\}} \quad 5-2$$

For the calculation of \vec{r}_2 , several lengths are calculated:

$$y_1 = R_0 \cdot \sin(\beta) \quad 5-3$$

$$y_2 = \frac{s_0}{2} \cdot \sin(\beta) \quad 5-4$$

$$y_3 = t_0 \cdot \cos(\beta) \quad 5-5$$

$$z_1 = R_0 \cdot \cos(\beta) \quad 5-6$$

$$z_2(t) = \frac{s_0}{2} \cdot \cos(\beta) \quad 5-7$$

$$z_3(t) = t_0 \cdot \sin(\beta) \quad 5-8$$

The movement from b to c along \vec{r} can be described as follows:

$$\vec{r}_2 = \begin{bmatrix} 0 \\ \Delta y(t) \\ \Delta z(t) \end{bmatrix}_{\{b\}} = \begin{bmatrix} 0 \\ -t_0 - b_0 + y_1 + y_2 + y_3 \\ \frac{s_0}{2} + R_0 - z_1 - z_2 + z_3 \end{bmatrix}_{\{b\}} \quad 5-9$$

$$\vec{r}_2 = \begin{bmatrix} 0 \\ -t_0 - b_0 + \frac{b_0}{\beta} \cdot \sin(\beta) + \frac{s_0}{2} \cdot \sin(\beta) + t_0 \cdot \cos(\beta) \\ \frac{s_0}{2} + \frac{b_0}{\beta} - \frac{b_0}{\beta} \cos(\beta) - \frac{s_0}{2} \cdot \cos(\beta) + t_0 \cdot \sin(\beta) \end{bmatrix}_{\{b\}} \quad 5-10$$

With a special case for $\beta = 0$:

$$\vec{r}_2 = \begin{cases} \vec{0}, & \beta = 0 \\ \vec{r}_2, & \text{else} \end{cases}$$

This vector describes the motion from the gripping position into the final position of the bending movement for a bend with $\alpha = 0$. In the following section, the movement for other α angles is derived.

For bends with $\alpha \neq 0$, the coordinate system of the movement is rotated according to Figure 5-5. First, coordinate system “a” is rotated around α around its z axis into the coordinate system “b”. Afterward, “b” is translated along the vector \vec{r}_1 into “c”. In the coordinate system “c”, the gripper is moved along the previously defined movement \vec{r}_2 to form the bend. The coordinates of \vec{r}_1 and \vec{r}_2 can be transformed into the base coordinate system using rotational transformation matrices, or the movement can be executed in the TCP-coordinate system, which will move with the gripper during the operations.

5.2 Heating and Geometry Parameter Selection

The overall preforming process consists of the three main routines preparation, bending, and cutting, as sketched in Figure 5-7. After the start of the process, the robot cell is initiated for repeatable starting conditions. Afterward, UD-tape is supplied to the process and inserted into the end effector. In the main part of the process, the bending routine, the tape is gripped by the end effector, heated and bent. The bending routine is repeated until all bends are formed. After the last bend, the tape is cut and handed to the storage for further processing.

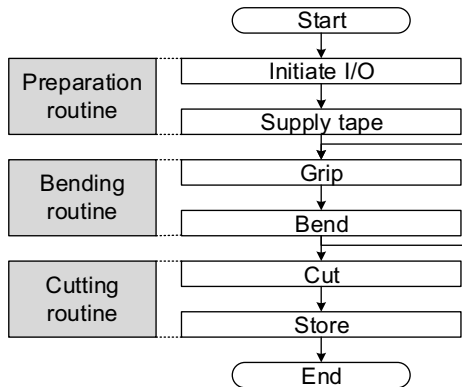


Figure 5-7: Overview over the swing folding process

The accuracy of the swing folding process is mainly influenced by parameters in the bending routine. The bending routine with its parameters is presented in Figure 5-8.

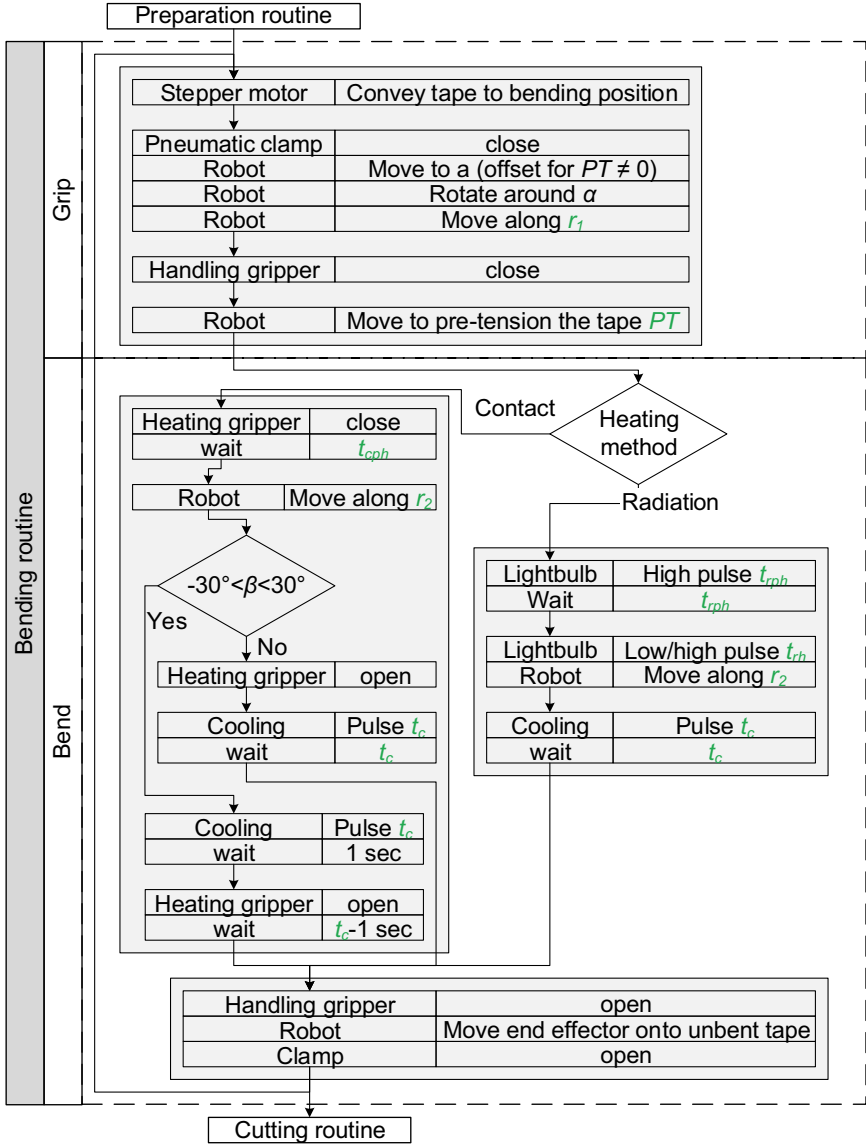


Figure 5-8: Detailed chart of the swing folding process

After conveying and clamping the tape, robot and end effector start the bending routine. To grip the tape, the robot is moved to the bending position “c” which is defined by rotating the coordinate system “a” by α and translating it along \vec{r}_1 . The handling gripper is closed and the gripper may be moved along the tape axis if pre-tensioning is active. During this moment, slack is taken out of the tape by tensioning it. When the slack is eliminated, the gripper starts sliding along the tape for which it is equipped with a gripping-force limiting pressure regulator.

The bending process itself differs between the two heating methods. For the radiation heating, the lightbulb is switched on at high power for the preheating time t_{rph} . After t_{rph} , the robot is moved along the vector \vec{r}_2 to bend the tape. During this movement, the lightbulb is switched to high or low power for the radiation heating time t_{rh} . In the final experimental setup, the t_{rh} is set to be the exact bending movement duration.

With the contact heating, the first step in the bending process is to close the heating gripper jaws that are heated to the contact heating temperature T_{ch} . After waiting for the contact preheating time t_{cph} , the end effector is moved along \vec{r}_2 to bend the tape. The opening sequence depends on the angle β . If β is within $\pm 30^\circ$, the cooling is switched on, and after one second, the heating gripper is opened. If the absolute value of β is larger than 30° , the heating gripper is opened immediately after the bending movement while switching on the cooling.

After the cooling has been active for the cooling time t_c , the handling gripper is opened and moved back to the unbent tape in a combined rotational/translational movement. Finally, the clamp is opened, and the next bend or the cutting can be prepared.

Based on this description, parameters that might influence the process are selected (Table 5-1). For the movement, the vectors \vec{r}_1 and \vec{r}_2 are calculated based on the kinematic model from Section 5.1. For calculating those, the bending zone size b_0 representing the length of bendable tape and the distance between the handling gripper and the bent zone t_0 are assumed. The bending radius $R(t)$ is calculated from the current bending angle $\beta(t)$. The tape thickness, which also influences the vectors, is taken from the tape datasheet. For the radiation heating, the preheating and heating time t_{rph} and t_{rh} influence the heated area and will be examined. The variable parameters for the contact heating are the jaw temperature T_{ch} as well as the preheating time t_{cph} . Both heating principles depend on the heating time t_c to be long enough to solidify the molten matrix.

For both heating methods, the following parameters are varied:

Table 5-1: Influence parameters of the swing folding process

Radiation	Contact	Varied to...
TCP offset t_0		... align the position of the heated and bending zone
Bending zone size b_0		... adjust the size of the heated and bending zone
Pre-tensioning PT		... examine the effect of slack in the tape
Radiation pre-heating time t_{rph}	Contact pre-heating time t_{cph}	... ensure an even molten area
Radiation heating time t_{rh}		... keep the tape molten during the whole bending
	Jaw temperature T_c	... optimize the molten area and stickiness / flow away
Cooling time t_c		... ensure solidification of the matrix

In the experiments, fluctuation in the bending angles α and β shall be identified and minimized. The parameter selection for the two process routes is described in two separate subsections.

5.3 Analysis of Swing Folding with Radiation Heating

In the experimentation with the radiation heating, the geometric parameters and the heating time are varied. By adjusting the geometric parameters in the kinematic model, the robot movement is optimized so that the behavior described in the model can be followed by the real tape. The heating parameters are adjusted to create an event molten zone. The process route is defined in 5.3.1. In Section 5.3.2, observations made during the experimentation are described qualitatively. In Section 5.3.3, parameters are varied systematically to improve and quantitatively describe the process behavior. The experimental series with the radiation heating are numbered R01 to R05.

5.3.1 Process Route

In (A_Wi 2019), the necessity of keeping the lightbulb at constant operating conditions was proven. If samples with several bends and a short heating time were manufactured, the correct bending angle β would not be obtained in the first bend, although later bends would have a correct β angle. This behavior could be avoided by switching the lightbulb on during the movement to the bending position to preheat it (A_Mühlbeier 2019).

The possible heating sequences were compared on an early version of the test rig. For the comparison, one specimen of each of the following angle combinations was made per parameter set in Table 5-1.

Table 5-2: Angle combinations per parameter set

α	0°	0°	0°	0°	60°	60°	60°	60°
β	30°	50°	-30°	-90°	30°	50°	-30°	-90°

High and low heating power were used, with low power being a dimmed setting of the lightbulb. The specimens were manufactured with low, high, or no preheating and low or high heating. For a fast process, heating variants with only the low heating power were omitted. (A_Wi 2019)

In all cases, the absolute value of β was smaller in the final measurements than in the set value. The best results could be obtained at settings where the lamp was initially switched to high power as the low setting would increase the time before the complete softening of the bending zone. The relation of the optimal heating time and the bending angle was researched. In that work, it is advised to keep the bending area molten until the bending movement is finished. Full power heating needs to be limited to a short time to avoid thermal degradation of the tape. Thus, a low-power setting should be used for this task. (A_Wi 2019)

The abovementioned experimentation was conducted with a rotational bending movement and subsequent linear correction movements. In experimentation using the corrected kinematics (Chapter 5.1), it became evident that the advantages of the corrected kinematics could only be used if no sliding movement between tape and gripper would occur in the initial moment of the bending motion. To avoid sliding, the tape should be molten in the whole bending zone before the bending movement for small forces.

Finally, a process route with high-power preheating and low-power heating during the bending was chosen. The final heating times and power settings are examined in the following sections.

5.3.2 Observed Phenomena

In the following section, peculiar phenomena without quantitative description are discussed.

5.3.2.1 Qualitative Effects of b_0

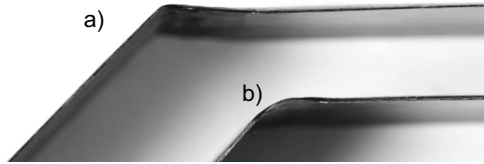


Figure 5-9: Sharpness of the bend for $b_0=1$ mm (a) and $b_0=5$ mm (b)

The effects of adjusting the position of the bending zone to the heated area became very apparent in the experimentation with the radiation heating as the size of the heated zone was larger compared to the contact heating, and the tape could move more freely as no displacements were enforced close to the bending zone. It proved possible to influence the shape of the bend by varying the value for the bending zone size b_0 in the kinematic model of the bend (Figure 5-9). (A_Bachtin 2020)

5.3.2.2 Effect of Insufficient Preheating

If the tape is not preheated sufficiently, it will bend elastic on a macro scale and not mainly plastic in the bending zone. If this happens excessively, the tape is tensioned too much and slides in the handling gripper whereby the length of material between supply unit and end effector is too long after the bending movement. This is not compliant with the kinematic model, and the robot movement and defects like warping occur. In Figure 5-10, the two situations are presented.

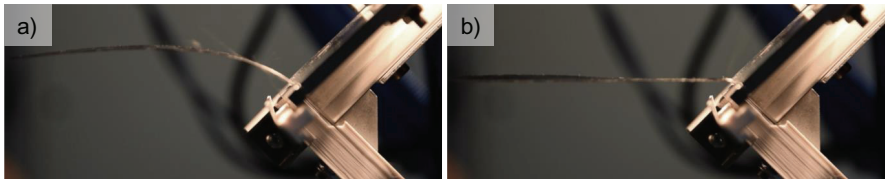


Figure 5-10: Bending motion of the tape without (a) and with sufficient (b) preheating. The created arc in (a) causes tension in the tape, which may pull more tape into the area between supply unit and end effector.

5.3.2.3 Effects of Extreme Cooling Duration and Airflow Induced Forces

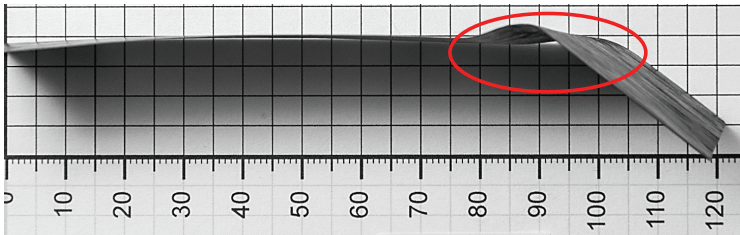


Figure 5-11: Airflow-induced deformation of the bend with the single nozzle cooling. The bending zone is bent in an S-shape instead of an even arc by the force that pushes the tape down. (Image source: (A_Bachtin 2020))

The effect of the cooling duration is limited to a sharp transition between sufficient cooling with good results and insufficient cooling with a large spring back after opening the gripper. Therefore, any value longer than the minimum cooling time will deliver comparable results. Furthermore, the cooling air induces a mechanical force into the tape, leading to unwanted deformations in the molten area if the airstream is too large. The deformation resulting from a too strong airflow is presented in Figure 5-11. Initially, a simple round 2 mm nozzle placed between the mirror and the handling gripper jaw was used to release the cooling air. This was replaced with a nozzle with multiple small openings which was mounted below the lower handling gripper jaw after experimental series R03/C04 (A_Saur 2020). This way, sharp jets are avoided.

5.3.2.4 Effect of a Fixed Heating Power Level

The forming movement of the robot takes up to 3 seconds depending on the set speed and β angle. The tape must be kept molten in the relevant area during this bending time to keep the bending force low. Relatively low heating power is necessary for keeping the tape molten as only heat losses must be compensated. The power of a constant heat source for rapidly melting the tape before the heating movement has to be set to a level significantly above the level that is necessary during the movement. If the same heating power is applied to both process steps, the tape temperature will constantly rise. If the time is chosen too long, this will damage the matrix material and require a prolonged cooling process. Therefore, a second, dimmable level of the radiation heating was commissioned after the experimental series R03. The level of this heat source is set by manually adjusting a potentiometer on the end effector. The power level is determined by switching on the low level of the heating and adjusting the width of the

molten area after 30 second settling time. To prevent the danger of overheating, the goal is to obtain a small molten area ($A_{\text{Saur 2020}}$). In Figure 5-12, the tape after the settling time is presented for three different levels of the low heating power. Figure 5-12 (b) shows the correct setting.

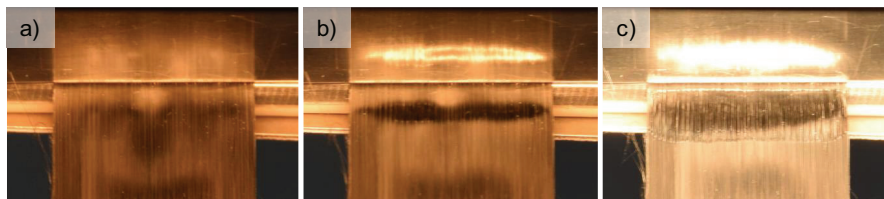


Figure 5-12: Adjustment of the low power level by comparing the size of the molten area after 30 seconds recognizable by the variation in surface reflectivity. Too weak heating power (a), small molten area (b), overheating and minor smoke development (c)

5.3.3 Systematic Parameter Variation

#	R01	R02	R03	R04	R05
Type	Fractional factorial design	Iterative parameter adaption	Full factorial design	Iterative parameter adaption	Latin Hypercube Sampling
Goal	Identification of relevant parameters	Selection of kinematic parameters	Process symmetry evaluation	Fine tuning of heating parameters	Process evaluation
Varied	$t_0, b_0, \alpha, \beta, t_c, t_{rph}, t_{rh}, m_{mat}$	t_0, b_0, α, β	α, β	t_{rph}, t_{rh}	$t_0, b_0, t_{rph}, \alpha, \beta$
Output	Main effects and significance	Kinematic parameters	Process improvement	Heating parameters + Accuracy	Validation of parameters and accuracy

Figure 5-13: Type, goal, varied parameters, and output of the experimental series with radiation heating

In the parameter variation, experimental plans were designed and executed to gain insight into the behavior of the process. As the process knowledge improved, the experimental plans could iteratively be adjusted to the task. An overview of the experimental series is given in Figure 5-13. First, the main effects and their significance were

analyzed. Afterward, kinematic parameters were adjusted. As the behavior seemed asymmetric in early experimentation, the symmetry was evaluated and improvements could be derived. Heating parameters were fine-tuned for good accuracy. Finally, the selected parameters and the accuracy were proved in a validation.

5.3.3.1 Experimental Series R01: Identification of Main Effects

A fractional factorial design of experiments with the resolution IV was conducted to identify the main effects (A_Bachtin 2020). The factors t_0 , b_0 , t_c , t_{rph} , t_{rh} , and matrix material m_{mat} were varied in two stages. Two different values for α and β were used as additional factors. For each experiment, one specimen was made. After each experiment, the response variables $\Delta\alpha$, $\Delta\beta$, and the actual molten length b_{0m} are measured. The low power setting of the heater can only be adjusted with an analog potentiometer making it difficult to set repeatably. Therefore, variation of the heating and its influence cannot be quantified and the low power setting was not used in early experimentation. The mean values of these experiments are listed in Table 5-3. A sign convention was defined that negative $\Delta\beta$ values correspond to too little bending and positive values for $\Delta\beta$ represent over bending independent of the sign of β . This convention applies to all experiments in this thesis and is used as many errors (e.g., poor heating or wrong bending movement) cause over or under bending in both bending directions simultaneously. This way, these errors are not canceled out if the average of results in both directions is calculated. In the lower area of Table 5-3, the influence of the factors on the response variables is quantified.

Table 5-3: Parameter set of experimental series R01

Exp.	t_0 / mm	b_0 / mm	α / °	β / °	t_c / s	t_{rph} / s	t_{rh} / s	m_{mat} -	$\Delta\alpha$ / °	$\Delta\beta$ / °	b_{0m} / mm
1	10	12	30	-25	8	4	4	PA	4.5	-3.7	12
2	0	3	30	-90	8	4	4	PP	0.7	-12.4	14
3	10	12	30	-90	4	2	4	PP	4.0	-6.8	12
4	0	12	0	-90	8	2	4	PA	2.5	-0.7	12
5	10	3	0	-25	8	2	4	PP	2.2	-1.8	10
6	10	3	0	-90	4	4	4	PA	2.0	0.0	15
7	10	12	0	-25	4	2	2	PA	10.8	-3.8	9
8	10	3	30	-25	4	4	2	PP	7.2	-3.3	12
9	0	3	0	-90	4	2	2	PP	2.8	-10.3	8
10	0	12	0	-25	4	4	4	PP	5.5	-8.8	12
11	0	3	30	-25	4	2	4	PA	4.8	-0.9	10

Exp.	t_0 / mm	b_0 / mm	α / °	β / °	t_c / s	t_{rph} / s	t_{rh} / s	m_{mat} -	$\Delta\alpha$ / °	$\Delta\beta$ / °	b_{0m} / mm
12	0	12	30	-90	4	4	2	PA	2.3	-7.2	12
13	0	12	30	-25	8	2	2	PP	-1.8	-4.0	10
14	0	3	0	-25	8	4	2	PA	4.0	-1.8	12
15	10	3	30	-90	8	2	2	PA	4.0	-4.6	9
16	10	12	0	-90	8	4	2	PP	1.7	-0.8	13
$\Delta\alpha$	1.9	0.2	-0.7	2.1	-2.7	-0.2	-0.6	1.6	Average Δ		
$\Delta\beta$	2.7	-0.1	-1.8	1.8	1.4	-0.6	0.1	3.2	3.6	-4.4	
b_{0m}	0.3	0.3	0.0	-1.0	0.3	2.8	1.5	0.0			

Resulting from the selection of a fractional factorial plan with Resolution IV, only main effects can be identified as two-factor effects are mixed.

In the experimental series, the two matrix materials are used as factor levels, complicating the presentation of results. For better visualization, the resulting β angles are separated in the two material groups in Figure 5-14 and Figure 5-15. In Figure 5-14, kinematic aspects of the series are compared. In both cases, the amount of bending is smaller than the set value, while the deviation and variation are smaller for PA (a). The TCP-Offset t_0 influenced the experiments with PP more than the ones with PA (b). For both materials, the deviation in β is larger for $\beta=90^\circ$ than for $\beta=25^\circ$ (c). In Figure 5-15, heating parameters are compared. For PP, results generally get worse if more heat is applied while the deviation of PA samples improves.

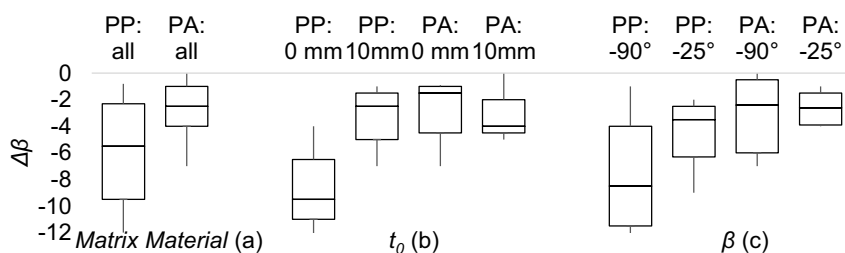


Figure 5-14: Results of the experimental series R01

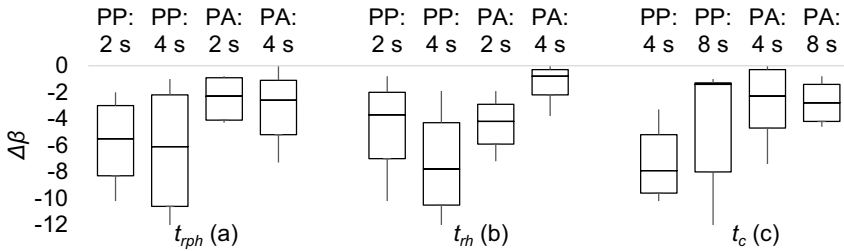


Figure 5-15: Results of the experimental series R01

To identify the relevance of the factors, a variance analysis was conducted, including all experiments of the series. In this analysis, the variance of the observations within the result of one factor on its plus or minus level is compared to the variance of the results of the whole experimental series and the deviation between the factor level groups. From this comparison, the F-Value is calculated and listed in Table 5-4. The F-Value threshold for a significance level of 95% is at 2.4 for the selected experimental design.

Table 5-4: Significance level of the effects

		Effect of							
		t_0	b_0	α	β	t_c	t_{rph}	t_{rh}	m_{mat}
σ	$\Delta\alpha$	1.6	0.2	0.6	1.7	2.2	0.2	0.5	1.3
	$\Delta\beta$	1.4	0.0	1.0	1.0	0.8	0.4	0.0	1.7
	b_{0m}	0.5	0.5	0.0	1.8	0.5	5.0	2.5	0.0

As presented in Table 5-4, the significance of most effects does not exceed the 2.4 threshold. For the deviation of α , only the cooling duration comes close to this threshold. None of the parameters changes influences β with more than 95% significance. The width of the molten area is influenced by the preheating time and the heating time. The influence of t_{rph} on b_{0m} is consistent as more heat is introduced in a longer heating period. The smaller effect of t_{rh} can be explained by the fact that the cooling is switched on immediately after the movement independent of the current state of the heating, effectively limiting the heating time to the duration of the movement.

In this experimental series, effects regarding the movement and heating conditions could be observed. The statistical significance of those observations is low. This can either result from the variation of the process itself or from selecting the factor levels

that might be too far or too near the optimum. Another possible influence is the mixing of the two materials in such a way that the two levels of a factor are good for one material each, resulting in no overall advantage for any level. The two materials are observed separately for further experimentation, and factor levels are selected iteratively instead of in an initial experimental design.

5.3.3.2 Experimental Series R02: Kinematic Parameters

This experimental series was conducted to obtain valid parameters for future examination without systematically identifying the effects (A_Bachtin 2020). In the previous experimental series, a deformation of the bending zone was observed for some parameter combinations. In this series, the kinematic parameters are adapted to minimize these deformations. In the beginning, t_{ph} , t_{rh} and t_c are selected in such a way that process reliability is improved by overheating the tape and cooling it down for a prolonged time. During the series, small alterations of the heating parameters are done according to observations (e.g., longer heating time after an observed insufficient heated area size) and to exclude influence by insufficient heating or spring back. To begin, t_0 was set to 10 mm, and b_0 was set to 3 mm following measurements at an unbent tape which was heated with the selected heating times. Only PP was used as matrix material to lower the number of experiments.



Figure 5-16: Variation of the bend shape depending on t_0 and b_0 . (Image source: (A_Bachtin 2020))

The evolution of the bending quality along the testing series is presented in Figure 5-16. On the left, the result of the initial set of parameters selected from the previous experimental series is presented with deformation at the bending zone. An overview of the used parameters is given in Table 5-5. From 1 to 7, heating parameters were varied to ensure a suitable heating parameter set and afterward kept constant. In experiment 6, the b_0 from experiment 4 was increased to 6 mm. Large qualitative improvement of the shape was reached from 6 to 7 when t_0 was decreased to 5 mm. In experiment 8, the

heating time was decreased, which shrunk the actual molten area and decreased the bending radius. Further adaptations of t_0 and b_0 in the experiments from 9 to 12 did not show major changes which indicates, that a good parameter region is found.

Table 5-5: Parameters used in the experimental series R02

Exp.	t_0 / mm	b_0 / mm	α / °	β / °	t_c / s	t_{rph} / s	t_{rh} / s	m_{mat} -	$\Delta\alpha$ / °	$\Delta\beta$ / °
1	10	3	0	-90	8	2	2	PP	1.0	0.0
2	10	3	0	-90	8	3	2	PP	1.0	2.0
3	10	3	0	-90	8	4	2	PP	2.0	2.0
4	10	3	0	-90	8	2	3	PP	2.0	1.0
5	10	3	0	-90	8	2	4	PP	1.0	3.0
6	10	6	0	-90	8	2	3	PP	2.0	1.0
7	5	6	0	-90	8	2	3	PP	3.0	1.0
8	5	6	0	-90	8	2	2	PP	1.0	1.0
9	3	6	0	-90	8	2	2	PP	1.0	1.0
10	3	3	0	-90	8	2	2	PP	2.0	1.0
11	5	3	0	-90	8	2	2	PP	2.0	0.0
12	5	3	0	-90	4	2	2	PP	1.0	0.0
13	5	3	-20	-90	6	2	2	PP	-1.0	0.0
14	5	3	-30	-90	6	2	2	PP	-2.0	-2.5
15	8	3	-30	-90	6	2	2	PP	-2.0	-3.0
16	8	3	30	-90	6	2	2	PP	3.0	-4.0
17	8	3	30	45	6	2	2	PP	2.0	0.0
18	8	3	-30	45	6	2	2	PP	0.0	-3.0
19	8	3	30	-45	6	2	2	PP	2.0	-5.0
20	8	3	-30	-45	6	2	2	PP	-2.0	-3.0
21	8	3	0	45	6	2	2	PP	1.0	-2.0
22	8	3	0	-45	6	2	2	PP	1.0	-1.5

From experiment 15 on, t_0 was set to 8 mm as this was the measured distance between the heated zone and the gripper and delivered good qualitative results. The other parameters were kept constant, and the range of bending angles was scanned to create a map of the deviations. In Figure 5-17, the resulting variations in α and β are presented. The overall deviation in the important β value seems to be larger than with $t_0 = 5$ mm, but the values seem to be close to a valid process.

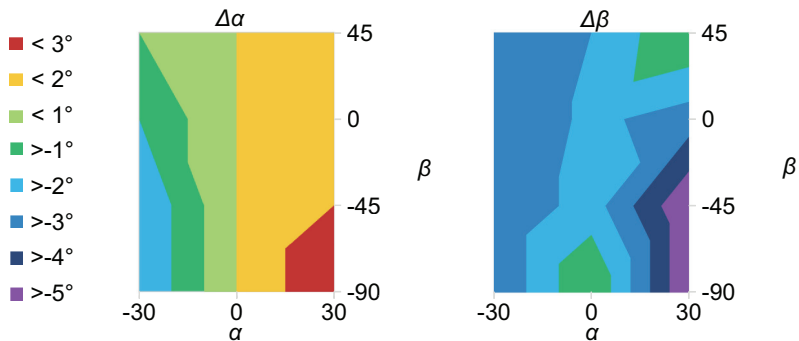


Figure 5-17: Angular deviations $\Delta\alpha$ and $\Delta\beta$ depending on α and β

5.3.3.3 Experimental Series R03: Effect of the Bending Direction

To examine subsequent bends' influence, longer strips with 6 bends each were manufactured (A_Bachtin 2020). The selected values were -25° , 0° , 25° for α and $\pm 45^\circ$ for β . For each material, two samples were manufactured with opposed direction of the β angles to identify systematic offset in the process. Resulting from the larger overall deviation of the experiments with $t_0 = 8$ mm, t_0 was set to 5 mm in this series. The angles were measured using a GOM ATOS System (Figure 5-18). As only four factors were varied, also their interactions can be evaluated using this 24-bend test. The experiments are presented in Table 5-6. The specimens PP1/PA1 start with positive β , and PP2/PA2 start with negative β values.

Table 5-6: Bends of the specimens

Sample	Bend	L / mm	α / $^\circ$	β / $^\circ$	m_{mat} -	t_0 / mm	b_0 / mm	t_c / s	t_{rph} / s	t_{rh} / s	$\Delta\alpha$ / $^\circ$	$\Delta\beta$ / $^\circ$
1/2/3/4	1	50	-25	+/- 45	PP/PA	5	8	2	2	6		
1/2/3/4	2	100	0	+/- 45	PP/PA							
1/2/3/4	3	150	25	+/- 45	PP/PA							
1/2/3/4	4	200	-25	-/+ 45	PP/PA							
1/2/3/4	5	250	0	-/+ 45	PP/PA							
1/2/3/4	6	300	25	-/+ 45	PP/PA							

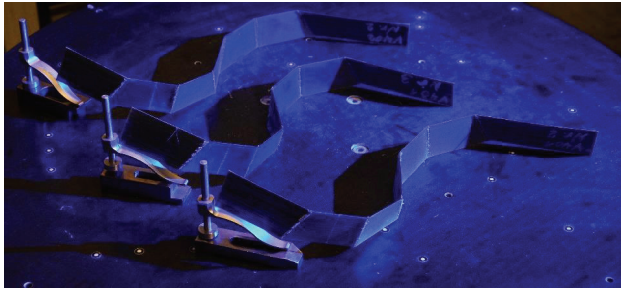


Figure 5-18: Measurement of the bending angles using the GOM System (Image source: (A_Bachtin 2020))

The influence of the length on $\Delta\alpha$ and $\Delta\beta$ is listed in Figure 5-19. No interdependency between the tape length and the angular error is recognizable. However, some asymmetric dependency is recognizable between β and $\Delta\beta$. The average measured value for $\beta = -45^\circ$ is $\beta_{measured} = -41.25$ while $\beta = +45^\circ$ leads to $\beta_{measured} = +44^\circ$. This behavior was even more pronounced for the contact heating where it was caused by the storage curvature of the tape. Experimental series R05 showed that also for the radiation heating, the angular symmetry can be improved by spooling the tape against its storage direction.

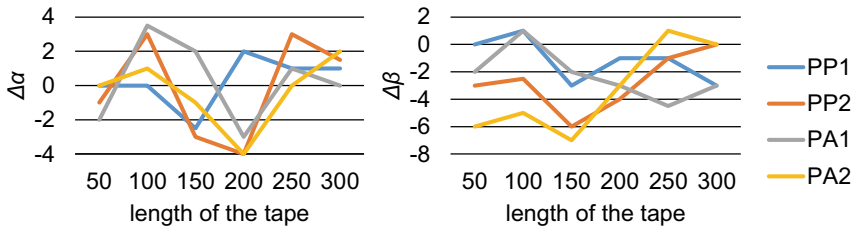


Figure 5-19: Angular error along the tape.

5.3.3.4 Experimental Series R04: Obtainable Angular Accuracy with Adjusted Heating

In this experimental series, hardware improvements that were identified during the earlier tests but postponed for comparability were included (A_Saur 2020). These Improvements were the adjustment of the radiation heating to a lower power during t_{th} and the improved cooling nozzle (Section 4.5). The goal of this experimental series is to select

heating parameters for the kinematic that was chosen in R02 and evaluate the resulting angular error $\Delta\alpha$ and $\Delta\beta$. The kinematic parameters were transferred from R02 ($t_0 = 8$ mm and $b_0 = 3$ mm), and a cooling time of $t_c = 8$ seconds was selected to avoid spring back. The low power setting of the radiation heater was first set according to Section 5.3.2.4. Afterward, t_{rph} and t_{rh} were iteratively adjusted depending on the results for the important $\Delta\beta$ value. For each parameter set, five samples with $\alpha = 10^\circ$ and $\beta = [-90^\circ, -30^\circ, -15^\circ, 15^\circ, 30^\circ]$ were manufactured from the PP tape and the mean absolute error $MAE = \frac{1}{5} * \sum |\Delta\beta_i|$ was calculated. The examined heating times and the resulting MAE are listed in Figure 5-20.

Based on the experimental results, it becomes evident that the angular error varies with the heating times. A sweet spot can be found at $t_{rph} = 2.75$ seconds and $t_{rh} = 4.5$ seconds, although the exact values vary with the environmental conditions. Based on this experimentation, the values for the final experimental series are chosen.

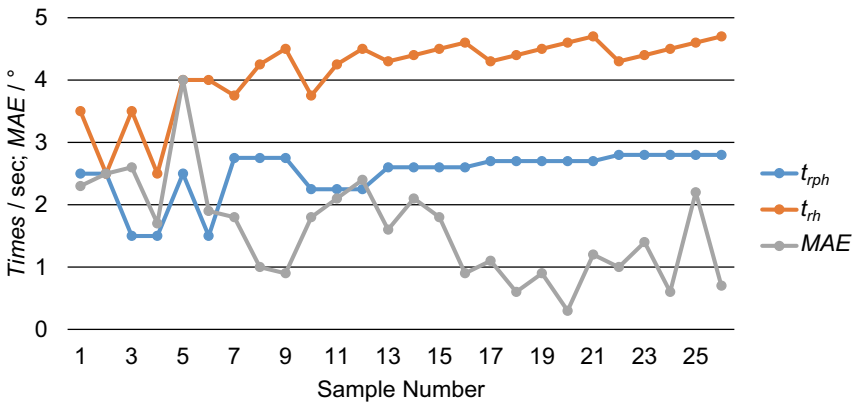


Figure 5-20: Mean Average Error in β and selected heating parameters

5.3.3.5 Experimental Series R05: Latin Hypercube Sampling

In the previously presented experiments, parameters were varied to identify their individual influence, or experiments were conducted according to two-level fractional factorial designs to examine interactions. However, the individual parameter variation and also the empirical variation in e.g., 5.3.3.4 showed that the process behaves nonlinear-

arly, which cannot be represented by two-level fractional factorial designs. Latin Hypercube Sampling (LHS) was applied to overcome this challenge while accepting a larger number of experiments (A_Steidle-Sailer 2021). In this method, numerous factors can be varied simultaneously in multiple levels. To generate an LHS design, first, the numbers of experiments and varied factors are determined. Each varied factor then is evenly distributed into as many levels as experiments are planned. Afterward, a table is generated, in which each experiment is assigned one level of each factor. In all experiments, each level of a specific factor is used exactly once. During the design of the table, algorithms are used to avoid correlation between the factors (Siebertz & van Beber et al. 2017). This type of design proved efficient for multi-level examination of multiple factors. (McKay & Beckman et al. 1979; Iman & Helton et al. 1981; Morris 1991; Park 1994)

Results of the experiments can be examined by using a regression model and then visualizing this regression. The statistical significance of the result limits the number of factors that can be examined in a certain number of experiments. More factors and more complex regression models generally require more experiments. In this thesis, quadratic regression is used to represent nonlinearity while limiting the number of required experiments. A selection of the executed experiments (A_Steidle-Sailer 2021) is listed in Table 5-7.

Table 5-7: Set of Experiments for the LHS

Material	Samples	Factor	Value/Range
PP	80	α	0°
		β	-45°
		b_0	[0 to 10] mm
		t_0	[0 to 10] mm
		t_{rph}	[0 to 4] seconds
		t_c	5 seconds
PP	60	α	0°
		β	-45°
		b_0	[0 to 10] mm
		t_0	[0 to 10] mm
		t_{rph}	2.7 seconds
		t_c	5 seconds
PP	80	α	[-45 to 45]°
		β	[-45 to 45]°
		b_0	5 mm
		t_0	3.4 mm
		t_{rph}	2.7 seconds
		t_c	5 seconds
PA	80	α	[-45 to 45]°
		β	[-45 to 45]°
		b_0	3.5 mm
		t_0	5 mm
		t_{rph}	3.2 seconds
		t_c	5 seconds

5.3.3.5.1 Geometric and Heating Parameters

Two LHS experiments were designed to determine t_{rph} , t_0 , and b_0 . The factor t_{rh} was not varied but set to the low power heating level and to last until the bending movement is finished. For the design, $\alpha = 0^\circ$ and $\beta = -45^\circ$ were used. In the first design, all three factors were varied. Resulting from the large influence of t_{rph} , the other two factors were additionally varied in a separate LHS, which confirmed the validity of the first. In the following, only results for PP are presented, as PA showed very similar behavior (A_Steidle-Sailer 2021). The results for PA were used for the angle variation in the same way as the results for PP. In Figure 5-21, the result of the three-factor variation is presented. The graphic shows three cuts through the quadratic regression along the axes of the parameters. It is apparent that t_{rph} has the largest influence and should be set to a value above 2.5 seconds. The same graphic for the two-factor experimentation is shown in Figure 5-22. In the chart, $t_0 = 2$ mm to 4 mm and $b_0 = 3$ mm to 6 mm were

identified as ideal values. This matches the results of R02, where it was identified that $t_0 = 5$ mm delivers better results than $t_0 = 8$ mm and $b_0 = 3$ mm was selected. Therefore, the selection of parameters could be validated, and further insight into the effect of the parameters was gained.

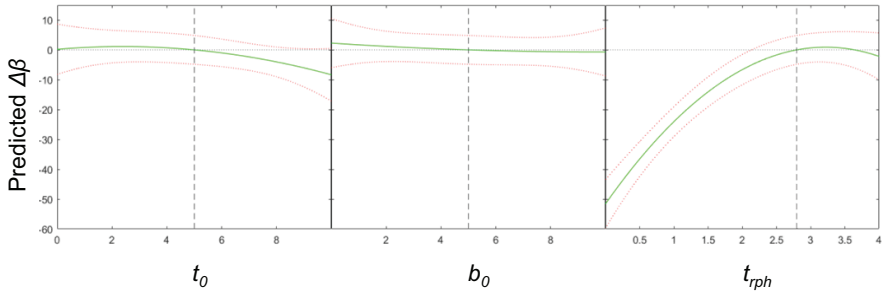


Figure 5-21: Regression for t_0 , b_0 and t_{rph} (translated figure from (A_Steidle-Sailer 2021))

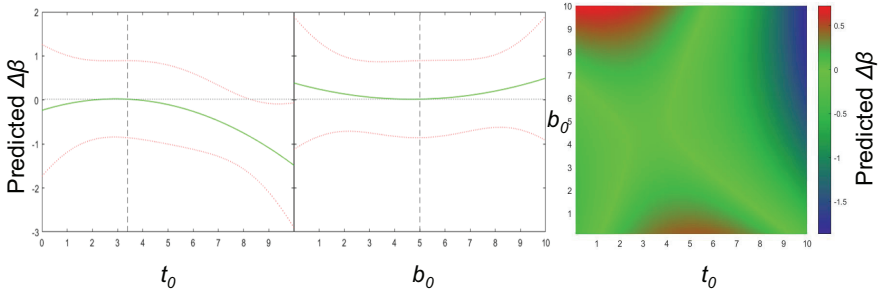


Figure 5-22: Regression for t_0 and b_0 (translated figure from (A_Steidle-Sailer 2021))

5.3.3.5.2 Angle Variation

An LHS with $\alpha = -20^\circ$ to 20° , and $\beta = -45^\circ$ to 45° was used to map the ability of the process (A_Steidle-Sailer 2021). Based on the previous experimentation, $t_0 = 3.4$ mm, $b_0 = 5$ mm and $t_{rph} = 2.7$ seconds were used. In Figure 5-23, the predicted angular error of the quadratic regression is shown. An accuracy of $\pm 2^\circ$ can be expected for a wide range of input geometries using the PP Material for both angles. Using PA ($t_{rph} = 3.2$ seconds), up to 2.5° of error is expected for larger bending angles (Figure 5-24) in the regression. For PP, a slight asymmetry in $\Delta\beta$ depending on β occurs. The asymmetric

behavior of $\Delta\alpha$ for PP is in the range of the measurement accuracy. The repeatability was evaluated using 5 selected angle combinations 10 times each (PP). The standard deviation between the bends was 0.9° for α and 0.6° for β . (A_Saur 2020)

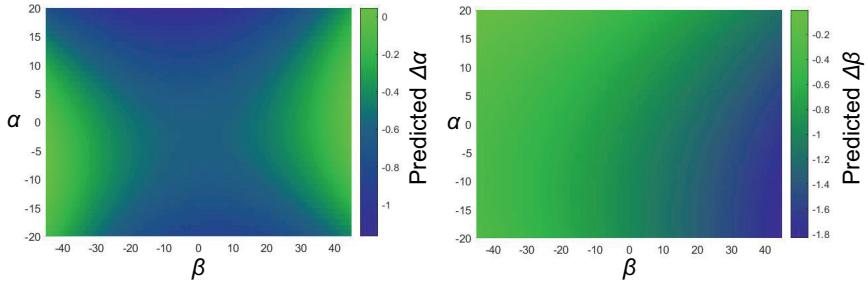


Figure 5-23: Heat Map of the predicted α and β error depending on the input angle (PP) (translated figure from (A_Steidle-Sailer 2021))

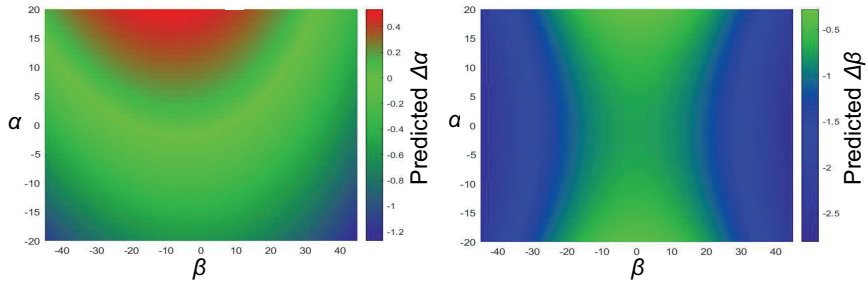


Figure 5-24: Heat Map of the predicted α and β error depending on the input angle (PA) (translated figure from (A_Steidle-Sailer 2021))

5.4 Analysis of Swing Folding with Contact Heating

For the contact heating, the geometric parameters, as well as the jaw temperature and the preheating time, are varied. The geometric parameters are varied to adjust the heated and bent zone. The preheating time needs to be long enough to melt the tape in the relevant area before the bending movement begins. The jaw temperature must be chosen to compromise large forming forces at low temperatures and adhesion be-

tween tape and gripper at high temperatures. In Section 5.4.2, observations made during the experimentation are described qualitatively. In Section 5.4.3, parameters are varied systematically to improve and quantitatively describe the process behavior. The experimental series with the contact heating are numbered C01 to C06.

5.4.1 Process Route

The tape temperature shall only be changed by opening and closing the heating gripper and not by altering the gripper jaw temperature to obtain fast cycle times with the contact heating. For the contact heating, the sequence was defined to be closing the heating gripper, bending, and switching on the cooling air. For the timing of the opening, two different process routes depending on β were implemented. For $-30^\circ < \beta < 30^\circ$, the heating gripper was opened after one second of cooling, else the gripper is opened simultaneously with the activation of the cooling air. This way, the tape could be partially hardened before opening the gripper to avoid re-deformation resulting from the adhesion to the gripper jaws at small angles β . At larger β values, the geometrical stiffness of the tape is larger so that these deformations do not occur, and the processing time can be minimized by the earlier opening of the heating gripper. In Section 5.4.3, the parameters jaw temperature and preheating time are examined.

5.4.2 Observed Phenomena

In the following section, peculiar phenomena without quantitative description are discussed.

5.4.2.1 Displacement of the Gripping Jaw Force Center

The jaws of both the handling gripper and the heating gripper are mounted rotatable to allow a flexible adaption to the tapes' real thickness and to avoid statically over determine positioning. When rotating the end effector around α , the two grippers may execute a horizontal movement relative to the tape centerline displacing the rotational center of the jaws from the tape centerline. In the case of the heating gripper, this leads to an uneven distribution of heat and deformation of the tape as the gripper force distribution depends on the gripping position. Compensation depending on the value t_0 is implemented in the position calculation to avoid this behavior. As indicated in Figure 5-25, the end effector is moved along the bending edge until the heating gripper is placed centrally on the tape. This movement can be in both directions depending on

the set distance between TCP and centerline (influenced by t_0 and b_0) (A_Bachtin 2020).

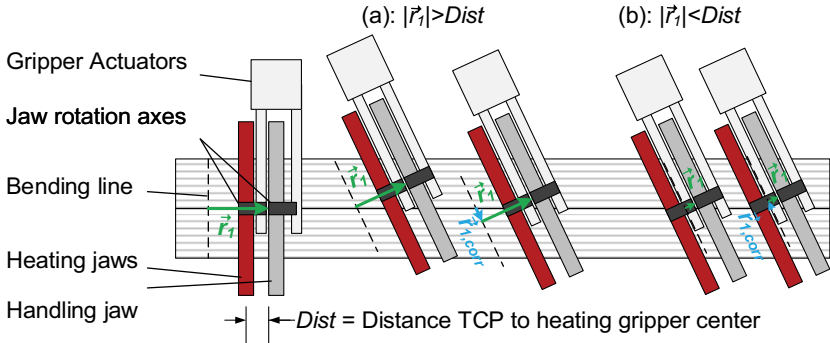


Figure 5-25: Correction gripper position to ensure even contact force between the heated jaws

5.4.2.2 Straightening Mechanism by a Set Bending Edge between Handling and Heating Gripper

The distance between TCP and the far end of the heating gripper jaws along the tape is 6 mm in the developed hardware. If the value t_0 is set smaller than this, the movement of the end effector lifts or lowers the tape between the supply unit and end effector depending on the bending direction (Figure 5-26). As it can be expected that the heated zone starts right at the heating jaws (the jaws introduce heat), the value t_0 should theoretically be set to 6 mm for the type of motion which was used with the radiation heating. In the experimentation with the contact heating, t_0 is set to either 6 mm to experiment with the described kinematics or to 0 mm to examine the effect of the tensioning induced into the tape by the motion in Figure 5-26. (A_Bachtin 2020)

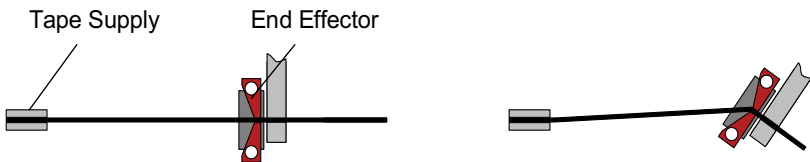


Figure 5-26: When setting $t_0=0$, overbending might occur due to the movement changing the tape orientation between supply and end effector

5.4.2.3 Adhesion between Heating Gripper and Tape

Depending on the heating temperature, adhesion between the tape and the heating gripper jaws occurs. The matrix material is pulled out of the tape in threads. This behavior has two disadvantages: the jaws become increasingly contaminated with matrix material, and a force is induced into the tape by the opening heating gripper. During the experimentation, no direct effect of the contamination became apparent as the material degraded at the jaws instead of accumulating preventing material build-up. In manufacturing, however, this might be an issue. Inducing forces into the tape deforms the used tapes after the actual swing folding process. As the matrix is still molten for a certain time, the unwanted deformation partially reverses for some parameter combinations. The result of adhering material is presented in Figure 5-27 (a).

5.4.2.4 Matrix Squeeze Out between the Heating Gripper Jaws

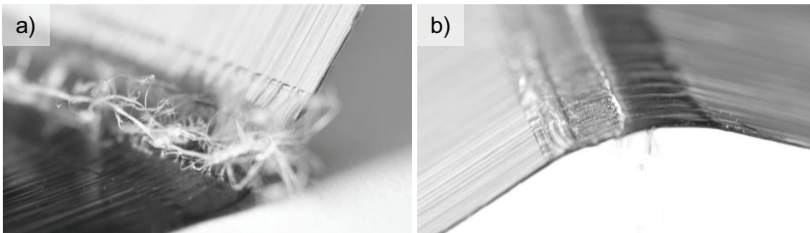


Figure 5-27: Pulling of threads resulting from the adhesion (a) and squeeze out of the matrix (b)

In the upper range of heating gripper jaw temperature, the matrix was increasingly squeezed out between the jaws by the gripping force (Figure 5-27 (b)). This led to smaller adhesion between the gripper and the tape, but subsequent process steps and the final part performance could be affected by the changes in properties. Therefore, the heating temperature should be kept low as long as this does not affect the angular accuracy. (A_Saur 2020)

5.4.3 Systematic Parameter Variation

As for the radiation heating, parameters were varied systematically for the contact heating. The plan is based on the experience from the radiation heating. An overview of the experimental series is given in Figure 5-28. Initially, the main effects and their signifi-

cance were analyzed. Afterward, kinematic parameters were adjusted. Heating parameter tuning led to no significant effect. As for the radiation heating, symmetry was evaluated. The possible accuracy was examined in a β variation. In the parameter and accuracy validation, the process proved to be less stable than with the radiation heating.

#	C01	C02	C03	C04	C05	C06
Type	Fractional factorial design	Full factorial design	Full factorial design	Full factorial design	One-factor experiment	Latin Hypercube Sampling
Goal	Identification of relevant parameters	Selection of kinematic parameters	Selection of heating parameters	Process symmetry evaluation	Evaluation of possible accuracy	Process evaluation
Varied	$t_0, b_0, \alpha, \beta, t_{cph}, t_c, Pt, T_{ch}$	t_0, Pt	t_{cph}, t_c	α, β	β	$t_0, b_0, t_{cph}, T_{ch}, \alpha, \beta$
Output	Main effects and significance	Kinematic parameters	none	Process improvement	Accuracy	Validation of parameters & accuracy

Figure 5-28: Type, goal, varied parameters, and output of the experimental series with contact heating

5.4.3.1 Experimental Series C01: Identification of Main Effects

The goal of this series is to identify relevant parameters for further experimentation. A fractional factorial design of experiments with the resolution IV similar to Series R01 was conducted to identify the main effects (A_Bachtin 2020). As for series R01, t_0, b_0, t_c, t_{cph} , and matrix material were varied in two stages and two different values for α and β were used as additional factors. For each experiment, one specimen was made. The heating time t_{ch} was omitted, as the heating gripper will be closed for the full bending movement. Additionally, the factors contact jaw temperature T_{ch} and pre-tension Pt are evaluated. Pt is selected as a factor for the contact heating as an interaction with the TCP Offset t_0 can be expected. To keep the resolution level IV, the number of factors was decreased by examining the matrix materials separately. Here, mainly the experimentation for PP is presented with the procedure for PA being the same unless stated otherwise. In the results, both material groups are described.

Table 5-8: Experimental plan of C01 PP

Exp.	t_0 / mm	b_0 / mm	α / °	β / °	t_c / s	t_{cph} / s	Pt / mm	T_{ch} / °C	$\Delta\alpha$ / °	$\Delta\beta$ / °
1	6	1	30	-45	4	2	3	150	2	-8
2	6	1	0	-15	4	2	0	160	1	3
3	6	1	0	-45	8	4	0	150	2	-13
4	6	0.2	30	-45	8	2	0	160	-1	-7
5	6	0.2	0	-45	4	4	3	160	2	-3
6	0	0.2	30	-15	4	2	3	160	-4	-4
7	0	1	0	-45	8	2	3	160	2	-4
8	0	0.2	0	-45	4	2	0	150	2	-7
9	0	1	30	-45	4	4	0	160	8	-11
10	3	0.6	15	-30	6	3	1.5	155	3	-3
11	6	0.2	30	-15	4	4	0	150	-1	-9
12	0	0.2	0	-15	8	4	0	160	2	-1
13	0	1	0	-15	4	4	3	150	1	-5
14	0	0.2	30	-45	8	4	3	150	3	-5
15	6	0.2	0	-15	8	2	3	150	3	-5
16	3	0.6	15	-30	6	3	1.5	155	-3	-3
17	0	1	30	-15	8	2	0	150	5	-7
18	6	1	30	-15	8	4	3	160	-3	-3
$\Delta\alpha$	-1.75	1.50	-0.75	-2.13	0.13	0.63	-1.50	-1.13	Average Δ	
$\Delta\beta$	-1.03	-1.43	-1.40	2.55	0.53	-0.73	2.60	2.90	1.31	-5.43

The 16 experiments listed in black in Table 5-8 were conducted to examine the main effects. The two experiments in blue are conducted with all factors set to their average setting to identify the degree of nonlinearity in the behavior. The results were evaluated using the ANOVA. The significance of the factors for α and β is listed in Table 5-9.

Table 5-9: Significance levels in C01 PP

		Effect of							
		t_0	b_0	α	β	t_c	t_{cph}	Pt	T_{ch}
or	$\Delta\alpha$	1.2	1.0	0.6	1.3	0.1	0.4	1.0	0.8
	$\Delta\beta$	1.0	1.2	1.2	2.2	0.5	0.7	2.2	2.5

The threshold value for 5% significance again is at a result of 2.4. For $\Delta\alpha$, none of the parameters exceeds the 95% significance threshold. For $\Delta\beta$, three parameters show a significance near the threshold with only T_{ch} being above the threshold. As in Experi-

mental series R01, the significance of the results is not excellent. Therefore, experimentation shall be limited to fewer parameters per series for the contact heating similar to the radiation heating. In Figure 5-29, the quantitative effects of the factors t_0 , b_0 , β , Pt , and T_{ch} are visualized as box plots. b_0 , β , Pt , and T_{ch} are the most significant factors. The factor t_0 is added as a comparison to the radiation heating, and α is omitted as it cannot be varied freely and does not have a significant effect.

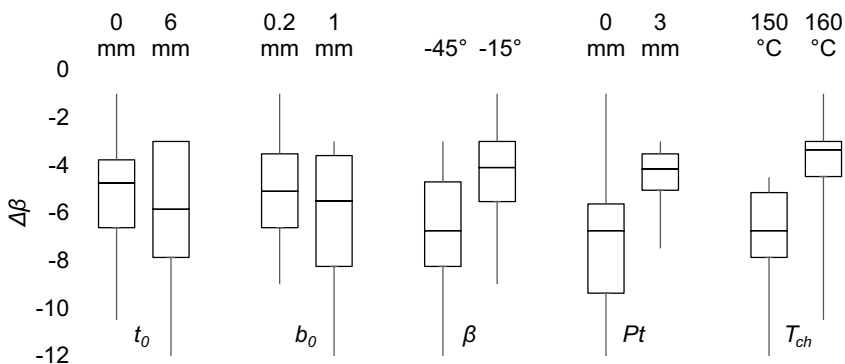


Figure 5-29: Results of C01 PP

For $\Delta\beta$, the center of the distribution does not seem to change between the two t_0 levels which goes hand in hand with the low significance. The spreading of the results however is smaller for $t_0=0$ mm. For b_0 , the situation is similar with only a small change to the mean value but a smaller spreading for $b_0=0.2$ mm. As predicted, β has an influence on $\Delta\beta$, with the error increasing with a larger bending angle. With the mean $\Delta\beta$ angle being -4.5° and -7.0° for $\beta=-15^\circ$ and $\beta=-45^\circ$, the relation does not seem to be linear. The value Pt improves the bending result for $Pt = 3$ mm by reducing both spreading and average error of the bending angle. Both levels of T_{ch} showed a relatively small spreading, although extreme outliers occurred, indicating that more experiments are necessary to evaluate the significance of the spreading results. The average bending error and spreading are better for the higher bending temperature $T_{ch} = 160^\circ\text{C}$.

The approach in experimental series C01 PA using PA is similar to series C01 PP. The input factors are the same, just the levels of T_{ch} were changed to 200°C and 210°C to react to the higher melting point of PA. The variance analysis (95% level at F-Value = 2.4) in Table 5-10 shows two main differences to C01 PP for $\Delta\beta$. The effect of T_{ch} is

less pronounced. This is probably caused by both levels of the factor being closer or symmetric to the optimum, while the optimum was probably above the higher level in C01 PP. The factor t_c is close to the threshold which is consistent with the experience with the radiation heating. Here, changes in the cooling time did hardly affect the result as long as the time was above a minimum value where the tape was solidified before the gripper opened and had a large effect for small changes below this minimum time. The sudden effect indicates that the minimum cooling time was below this limit for some experiments in C01 PA but not in C01 PP. The experience from this experimental series is that the significance of factors does not only depend on the process but also on the selection of the parameter levels. As the process behavior is not fully known before experimentation, the level selection in future experimentation will be iterative and experience-based.

Table 5-10: Significance levels in C01 PA

		Effect of							
		t_0	b_0	α	β	t_c	t_{cph}	Pt	T_{ch}
σ	$\Delta\alpha$	1.1	0.8	2.0	1.1	1.6	0.3	0.3	1.5
	$\Delta\beta$	2.0	0.5	1.1	1.6	2.3	0.8	1.4	1.6

Figure 5-30 represents the results of C01 PA. The temperature was omitted, and t_c was added compared to Figure 5-29. As for PP, $t_0 = 0$ mm leads to a narrower spreading of the result. Additionally, the median is improved for PA, indicating a positive effect of the tensioning (Section 5.4.3.2). The small effect of b_0 , however, is contrary in C01 PA compared to C01 PP. Larger values for β lead to larger deviations for PA as they do for PP. The minimization of the spreading through $Pt = 3$ mm is not as pronounced for PA as for PP and the improvement of the bending angle error is not as pronounced which may indicate an interaction with t_0 . The factor t_c affects PA, although it did not affect PP. The level $t_c = 8$ seconds leads to a smaller spreading and smaller angular error. This indicates that some samples were not fully solidified before the handling gripper opened and allowed the tape to spring back before solidifying. The overall error is smaller for PA than PP.

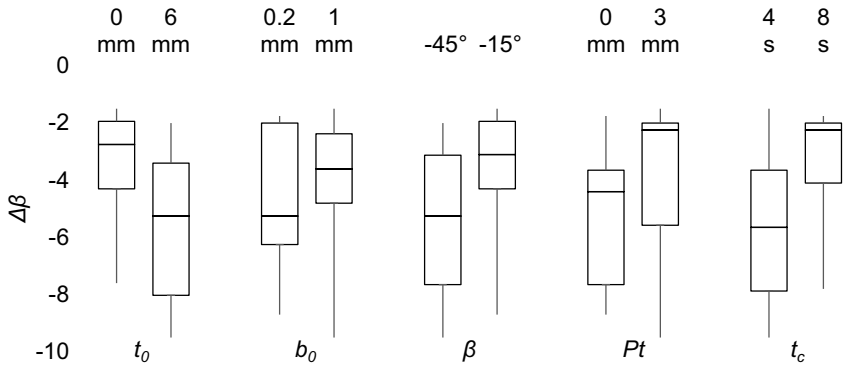


Figure 5-30: Results of C01 PA

5.4.3.2 Experimental Series C02: Kinematic Parameters

In this series, the interaction between the two tensing parameters Pt and t_0 is examined in a full factorial design (A_Bachtin 2020). For the evaluation, the same multi-bend specimens as the ones starting with negative β from series R03 were used and the error $\Delta\beta$ was evaluated by calculating the average $\Delta\beta$ from all bends of the specimen. The remaining process parameters are selected based on the experience from C01. The experimental setup and the results are presented in Table 5-11 and Figure 5-31:

Table 5-11: Used process parameters and average results of experimental series C02 PP and C02 PA

Exp.	t_0 / mm	Pt / mm	b_0 / mm	t_c / s	t_{cph} / s	T_{ch} / °C	C02 PP		C02 PA	
							$\Delta\alpha$ / °	$\Delta\beta$ / °	$\Delta\alpha$ / °	$\Delta\beta$ / °
1	0	0	0.6	4	2	PP: 155 PA: 205	2.2	-3.4	0.8	0.0
2	6	0					1.6	-6.9	1.6	-7.6
3	0	5					0.9	-1.2	0.0	-1.7
4	6	5					2.0	-7.6	0.8	-4.4

For both materials, dynamic tensing by $t_0 = 0$ mm seems to be advantageous. The pre-tensioning of 5 mm improves the mean value marginally, but the two results for $Pt = 5$ mm differ strongly for PP, hence no clear conclusion can be drawn. The interaction between t_0 and Pt also differs between the two matrix materials. To examine the results

in more detail, the results of the single bends of the specimens can be regarded. The individual results of C02 PP are presented in Table 5-12. It becomes evident that the average variation between the individual bends is smaller than the large 7° variation between the two samples with $Pt = 5$ mm, which underlines the validity of the test. The results of this experimental series will be used in a later evaluation of further effects and interactions.

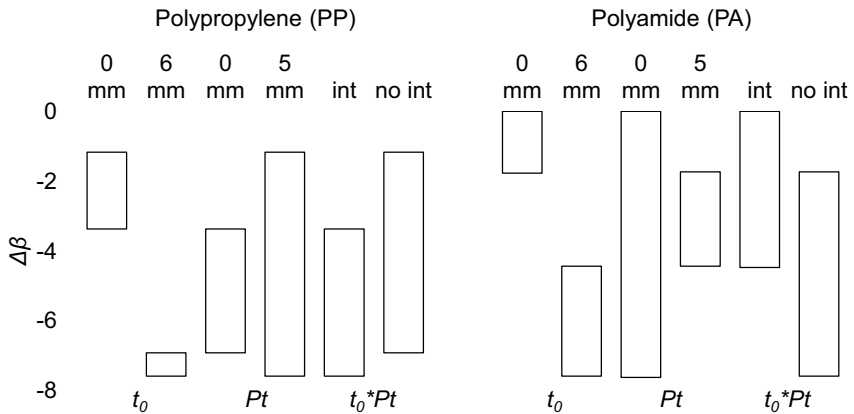


Figure 5-31: $\Delta\beta$ depending on the tensioning for PP and PA

Table 5-12: $\Delta\beta$ results of the experimental series C02 PP measured with GOM ATOS

L	300 mm	250 mm	200 mm	150 mm	100 mm	50 mm
$\Delta\beta$ Exp1	-1	-2	-4.7	-3.5	-7	-2
$\Delta\beta$ Exp2	-7	-9	-10	-3	-6.5	-6
$\Delta\beta$ Exp3	0.5	-1	0	-3.5	-1	-2
$\Delta\beta$ Exp4	-9	-8	-9	-8.5	-5	-6

5.4.3.3 Experimental Series C03: Temperature Control

Experimental series C03 is set up similarly to C02, with the two main examination factors being t_{cph} and t_c . They are varied full factorial according to Table 5-13. The same multiple bend specimens as in C02 are used. (A_Bachtin 2020)

No insights could be won from C03 alone apart from the similarity in the distribution of the angular error compared to C02. The large deviation in β for the PP tape could not

be repeated in later trials (Section 0), indicating that an unknown influence factor has affected this measurement's accuracy. The low average bending error for PA was not achieved by a good process accuracy but by errors canceling each other out (Table 5-15). For both materials, there seems to be a dependency of the angular error on the position of the bend on the tape or on the sign of β as the first or second halves of the tape represent negative or positive β angles (Table 5-14 and Table 5-15).

Table 5-13: Results of C03 depending on the length:

Exp.	t_{cph} / s	t_c / s	b_0 / mm	t_0 / mm	Pt / mm	T_{ch} / °C	C03 PP		C03 PA	
							$\Delta\alpha$ / °	$\Delta\beta$ / °	$\Delta\alpha$ / °	$\Delta\beta$ / °
1	2	2					1.7	-7.4	-0.3	-1.0
2	4	2	0.6	0	5	PP: 155 PA: 205	2.0	-9.1	0.8	-1.1
3	2	8					0.9	-6.9	0.3	-1.1
4	4	8					1.3	-6.7	0.3	-1.5

Table 5-14: Result of C03 PP measured with GOM ATOS

L	300 mm	250 mm	200 mm	150 mm	100 mm	50 mm
$\Delta\beta$ Exp1	0.6	-9.5	-13	-9	-6.5	-7
$\Delta\beta$ Exp2	-10	-11.5	-11.5	-9.5	-5.5	-6.5
$\Delta\beta$ Exp3	-5.5	-7.7	-10.5	-9	-5	-3.5
$\Delta\beta$ Exp4	-5	-7.5	-9.5	-9	-5.5	-3.8

Table 5-15: Result C03 PA measured with GOM ATOS

L	300 mm	250 mm	200 mm	150 mm	100 mm	50 mm
$\Delta\beta$ Exp1	-3.5	0.5	-6	0.5	1	1.5
$\Delta\beta$ Exp2	-2.5	-4	-7	1	1	5
$\Delta\beta$ Exp3	-3.5	-2.5	-6	0	1	4.3
$\Delta\beta$ Exp4	-4.5	-3	-6.5	0.5	2	2.5

5.4.3.4 Experimental Series C04: Effect of the Bending Direction

A finer variation of bending angles was conducted using polypropylene multiple bend specimens to examine the influence of the bending direction (A_Bachtin 2020). The beta angle was varied by 15° from bend to bend, starting and ending at either plus or minus 45° randomly selected. The α angle was either set to 0° or +/-25° for a whole specimen. The distance between the bends was set to 40 mm. 8 Specimens with 48

bends total were manufactured and measured. In Figure 5-32, the error $\Delta\beta$ is set into relation with either the tape length or the set value for β .

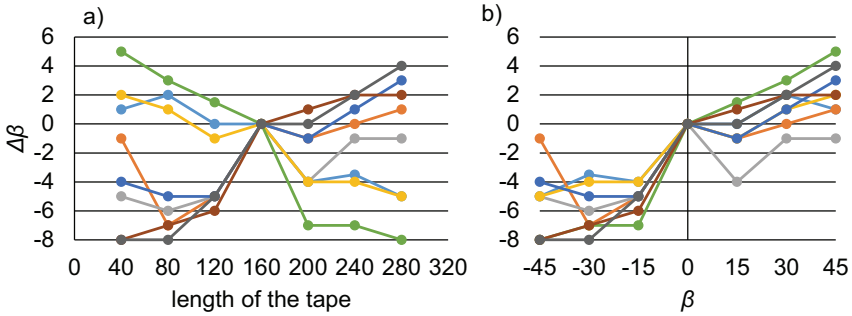


Figure 5-32: Comparison of the dependency between L and $\Delta\beta$ (a) and β and $\Delta\beta$ (b) with each specimen represented in a different color

No strong correlation is visible between L and $\Delta\beta$. The figure indicates that a closer correlation exists between β and $\Delta\beta$. The phenomena can be explained as an asymmetry in the bending result depending on the direction of the bend. If the robot bends the tape upwards, the amount of bend seems to be too large. In the case of downwards bending, spring back occurs.

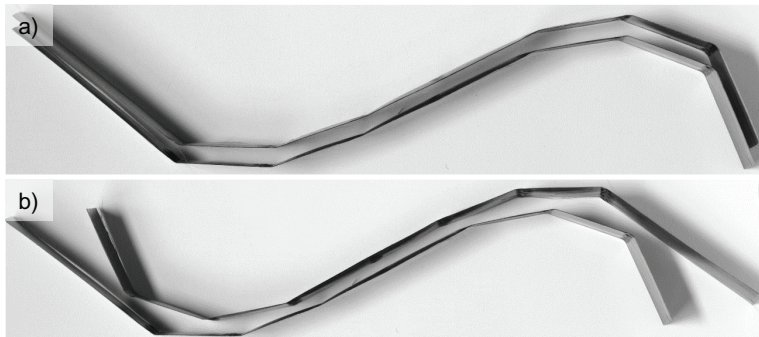


Figure 5-33: Placement of the same pair of tapes next to each other. The way they were manufactured (a) or one tape rotated (b)

The accuracy of the process can be visualized by placing two strips from this experimental series above another. This can be done either with both tapes beginning from

left to right or with one tape beginning from right to left, which leads to different amounts of shape deviation. In Figure 5-33 (a), the tapes are placed upon each other the way they were manufactured, proving the repeatability of the manufacturing. If one of the tapes is turned around to compare the negative angles to the positive angles, the systematic error becomes evident Figure 5-33 (b).

5.4.3.5 Experimental Series C05: Obtainable Angular Precision

This series was conducted to examine the asymmetry of the error $\Delta\beta$ in relation to β , which first showed up in R03 but seems to be far more relevant in experiments with contact heating (A_Saur 2020). First, possible asymmetries in the process were listed and evaluated. In contrast to the radiation heating, both sides of the tapes are heated equally with the contact heating. The handling gripper has an asymmetric working principle with one moving and one fixed jaw. However, it is only moving when the matrix is solid and should not influence the process. To ensure a symmetric effect of the handling gripper, the tolerances in the hinges were checked, and it was made sure that a symmetric situation existed after the pre-tensioning of the tape. Another possible reason for asymmetry could be in the tape itself delivered on 165 mm wide spools, slit, and re-spooled on the 30 mm wide spool in the supply unit. The tape was re-spooled in the same direction as it was on the initial spool in all experimentation. In small experiments, turning around the tape also turned the asymmetry of the bending result around. An approach for minimizing the error was to re-spool the tape the other way compared to its initial storage. As a second measure, the cooling nozzle was redesigned to have a wider, slower airflow as its previous jet of air caused a visible deflection of the tape (Section 4.5 and (A_Saur 2020)). An experimental plan was conducted to evaluate this approach: Ten single bend samples were manufactured per angle combination. An overview of the parameters and results is given in Table 5-16 and the individual results are plotted in Figure 5-34. The mean values of β and $\Delta\beta$ in Table 5-16 indicate that the measures could reduce both the error and the process variation. The individual results in Figure 5-34 emphasize this. Only one outlier has a β error larger than 3° .

Table 5-16: Examination of the bending error with the improved cooling nozzle

Exp.	A	B	C	D	E	F	G	H	mean α	mean $ \Delta\alpha $	mean β	mean $ \Delta\beta $
	t_0 / mm	b_0 / mm	α / °	β / °	t_c / s	t_{cph} / s	Pt / mm	T_{ch} / °C	/ °	/ °	/ °	/ °
1				-45					10.3	0.3	-44.8	1.2
2				-30					10.8	0.9	-29.2	0.8
3			10	-15	8	2	3	165	10.8	0.8	-14.7	0.3
4	0	0.6		15					10.4	0.4	13.8	1.2
5				30					10.1	0.3	29.1	0.9
6				45					omitted			

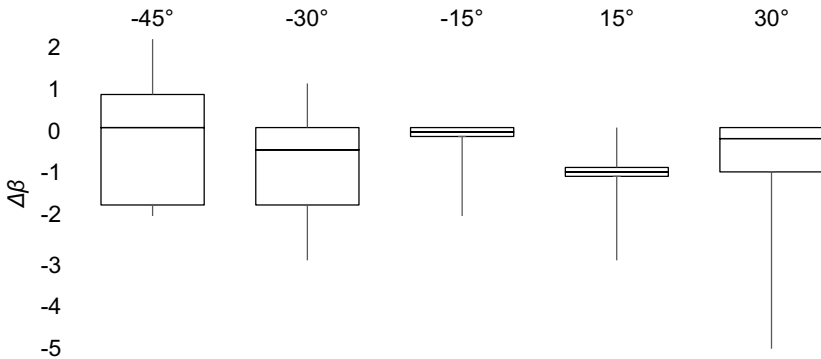


Figure 5-34: Remaining bending error after improving the used cooling nozzle

5.4.3.6 Experimental Series C06: Latin Hypercube Sampling

In this series, the Latin Hypercube Sampling method (LHS) was used. The advantages of this method are explained in 5.3.3.5. A selection of the executed experiments (A_Steidle-Sailer 2021) is listed in Table 5-17.

Table 5-17: Set of Experiments for the LHS

Material	Samples	Factor	Value/Range
PP	30	α	0°
		β	-45°
		b_0	[0 to 2] mm
		t_0	[0 to 3.6] mm
		t_c	4 seconds
		T_{cph}	2 seconds
		T_{ch}	160°C
PP	80	α	0°
		β	-45°
		b_0	0.6 mm
		t_0	0 mm
		t_c	[2 to 7] seconds
		t_{cph}	[0 to 4] seconds
		T_{ch}	[140 180]°C
PP	80	α	[-20 to 20]°
		β	[-45 to 45]°
		b_0	0.6 mm
		t_0	0 mm
		t_c	4 seconds
		t_{cph}	2 seconds
		T_{ch}	155°C
PA	80	α	[-20 to 20]°
		β	[-45 to 45]°
		b_0	0.6 mm
		t_0	0 mm
		t_c	4 seconds
		t_{cph}	2 seconds
		T^{ch}	218°C

5.4.3.6.1 Geometric Parameters

Also for the contact heating, the values for t_0 (0 mm) and b_0 (0.6 mm) from earlier experimentation could be confirmed for $\beta = -45^\circ$. In Figure 5-35, the plot and Heat Map for PP and $T = 160^\circ\text{C}$, $t_{cph} = 2$ seconds are shown. Larger values for t_0 cause under bending, and b_0 has minor influence on β . For PA, $t_0 = 0$ mm and $b_0 = 1.4$ mm were identified as ideal value.

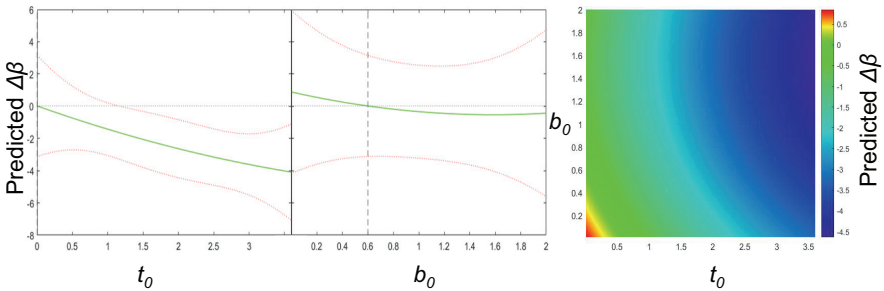


Figure 5-35: Regression for b_0 and t_0 (translated figure from (A_Steidle-Sailer 2021))

5.4.3.6.2 Heating Parameters

T , t_{cph} , and t_c were varied for validation. T showed most influence with a general improvement towards higher temperature. Larger values of t_{cph} also improved the result slightly. For PP, $T > 155^\circ$ was confirmed as jaw temperature. The resulting regression of the experiment is shown in Figure 5-36. When interpreting the result, it must be considered that the quadratic regression cannot properly represent the behavior of the $T - \Delta\beta$ curve, which becomes flat above a certain temperature.

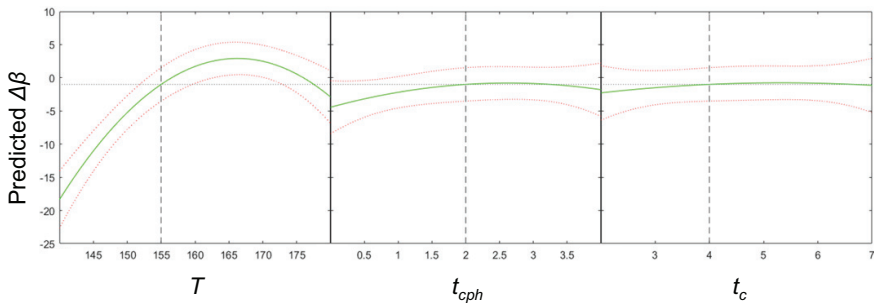


Figure 5-36: Regression for T , t_{cph} , and t_c (translated figure from (A_Steidle-Sailer 2021))

Also for PA, the identified $T > 205^\circ$ with only minor influence of t_{cph} and t_c complies to the previous experiments.

5.4.3.6.3 Angle Variation

Both PP and PA showed large angular errors with the contact heating. The higher springback, which was also shown in earlier experiments, can be explained by the significantly smaller heated zone, increasing the bending area's stiffness. The expected β error could be determined to be $< 11^\circ$ for both materials. The results are shown in Figure 5-37 and Figure 5-38. The results do not comply with the better accuracy result from experimental series C05 and the evaluation of geometric parameters in C06 indicating problems with the process stability of the contact heating. The repeatability of the process was evaluated using 5 selected angle combinations 10 times each (PP). The standard deviation between bends was 0.6° for α and 1.1° for β . (A_Saur 2020)

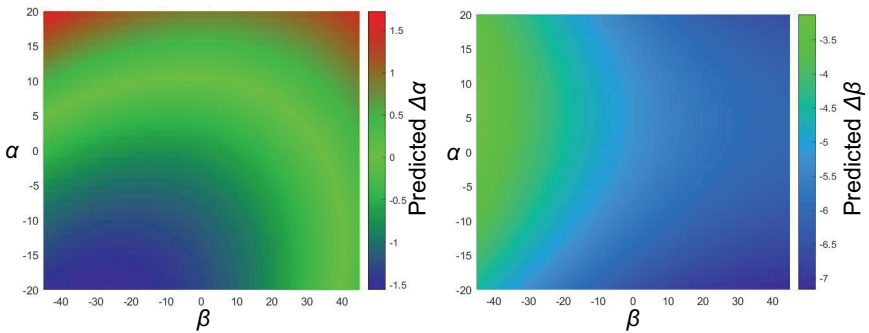


Figure 5-37: Heat Map of the predicted α and β error depending on the input angle (PP) (translated figure from (A_Steidle-Sailer 2021))

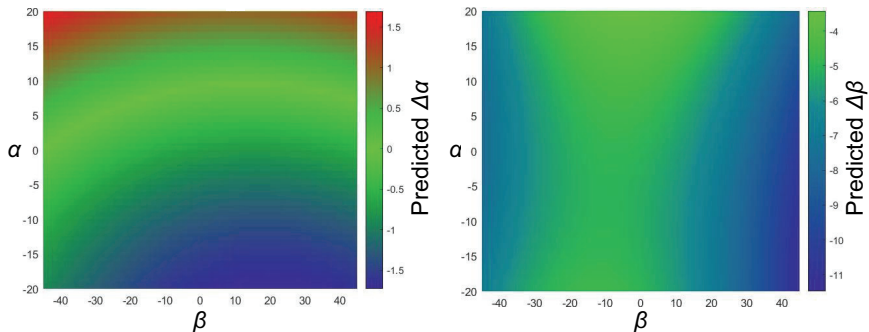


Figure 5-38: Heat Map of the predicted α and β error depending on the input angle (PA) (translated figure from (A_Steidle-Sailer 2021))

5.5 Processing of Further Types of UD-tape

The two types of tapes which were used for the parameter examination had a thickness per layer of 0.16 mm (PA) and 0.27 mm (PP). This is a common thickness for tapes, with thicker tapes rarely available. The thicker raw material would be advantageous for a larger reinforcement effect without stacking preforms. Thus either custom-made thick tapes or extruded profiles could be used.

The transfer of the process to further raw materials could be proven in additional experimentation. The goal was to examine further materials and tape dimensions. For this, a glass fiber-reinforced UD-tape was used and the two already described types of PP and PA tapes were stacked and consolidated to thicker tapes. The glass fiber tape was used along the whole development of the test rig to examine the heating behavior of transparent material. No quantitative experimentation was conducted using the glass fiber tape as it showed similar qualitative behavior to the carbon fiber tapes.

The consolidated multi-layer tape was used to evaluate the limitations of the swing folding process regarding the tape thickness. Self-consolidated multi-layer tape with a thermoplastic matrix up to 1.2 mm could be processed using both radiation and contact heating. Systematic measurements could not be conducted as the self-consolidated tapes showed some waviness after manual consolidation, inhibiting systematic experimentation. With the radiation heating, a longer preheating time was necessary to melt the matrix sufficiently. The fiber deformation is larger with thicker tapes as the difference in elongation between the inner and outer sides of the tape is longer. In the experiments, it became evident that, also for thicker tapes, the resulting real bending radius can be influenced by the set value for the width of the bending area b_0 . Therefore, b_0 should be larger for larger tape thickness to compensate by distributing the difference over a longer bend. With the contact heating, double-layer tapes were also successfully processed. For this, the jaw temperature was slightly increased and the pre-heating duration was extended. The thicker tape improved the process conduction for the contact heating as the stiffness was larger than with single-layer tape minimizing the influence of the adhesion to the heated jaws. An accuracy on $|\Delta\beta| < 3^\circ$ was obtained. (A_Bachtin 2020)

In Figure 5-39, single-layer tapes with radiation heating (a) and contact heating (b) are compared to a radiation heated double-layer tape (c). The outside of the bend is shown in the figures with small letters and the inside is numbered with capital letters. Especially

in the comparison between (A) and (C), the difference in fiber displacement between single- and double-layer tapes is evident. In this thesis, it could be proven, that the process can be applied to various types of tape. A systematic examination of possible material types and thicknesses should be done before attempting manufacturing from hugely different raw materials.

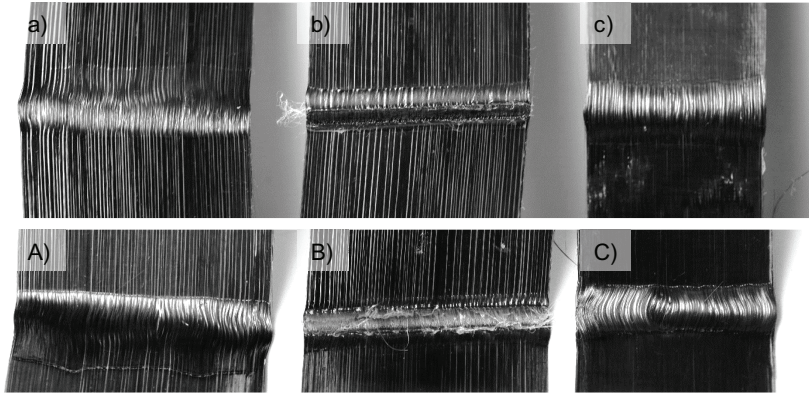


Figure 5-39: Comparison between single-layer radiation (a), single-layer contact (b), and double-layer radiation (c) from outside (small letters) and inside (capital letters) the bend.

5.6 Conclusion of the Process Parameter Variation

In this chapter, suitable process parameters for the preforming of UD-tapes by robotic swing folding were found. For both heating principles, the experimentation is started with a fractional factorial experimental plan to identify the main effects of the parameters. Afterward, the parameters of the kinematic movement model are adjusted in an iterative approach or a full factorial plan. It was possible to use a full factorial plan for the contact heating as the expected value range could be estimated based on the experience from the iterative approach with the radiation heating. For the contact heating, also a full factorial plan on the heating parameters was conducted with no relevant results. Next, the process behavior for opposite bending directions was compared. Here, an asymmetric behavior was identified which was caused by the cooling air and tensions in the raw material. This far, experimentation showed that the contact heating had larger error and variation in its results than the radiation heating. In the next step, the accuracy with ideal heating parameters was evaluated. With the radiation heating, these

parameters were selected during the accuracy analysis while preselected parameters were used for the contact heating. Both heating methods showed good angle accuracy in this experimental series. In the final validation, the parameter selection was confirmed for both heating methods. The good accuracy ($-2^\circ < \Delta\beta < 2^\circ$) could only be repeated for the radiation heating. The reason for this is the sensitivity of the contact heating to variation in its adjustment of the two grippers relative to each other and tape tensions (smaller heated area). A second challenge with the contact heating for the long-term run will be the contamination of the end effector with molten matrix. During the whole time, the radiation heating showed stable results and easy adjustability. In conclusion, radiation heating is the more promising heating method for the industrialization of the process and is selected as the final heating method.

6 Finding Process Compliant Near-net-shape Geometries

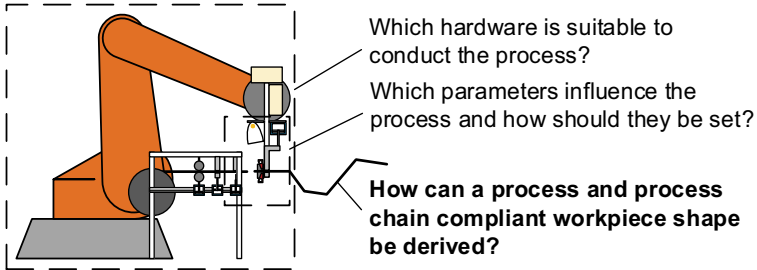


Figure 6-1: Research questions of this thesis

In this chapter, the last topic from Figure 6-1, the derivation of process compliant shapes, is described. The swing folding process that was developed in this thesis, produces bent UD-tape strips that are composed of planar UD-tape sections following certain limitations regarding positioning relative to another. The reinforced shell components do not follow these shape restrictions. Instead, they can have curved areas, inclines of angles independent of neighboring areas, and local curvatures in more than one direction along the surface. The full complexity of the components cannot be transferred to the swing folding process. Thus, a mechanism for deriving a useful tape design is necessary.

The tape strips will be integrated into the components by co-molding with the surrounding thermoplastic material. Placing the reinforcement reliably is a challenge when co-molding reinforcements from unidirectional materials with a flowable counterpart. In (Pangboonyanon & Zaiß et al. 2016), the positive influence of even low degrees of preforming before the molding step is presented. As with most other preforming processes, the goal of the swing folding process is to enable the reliable conduction of the subsequent steps by increasing the accuracy of the positioning and preventing defects. The final shape of the material can be obtained during the co-molding (Bruns & Raatz 2017).

Obtaining the final shape of the reinforcement already during the preforming process is not necessary in most process chains. In the hybridization of thermoplastic UD-tapes with a flowable thermoplastic mass, the tapes will be heated for the co-molding step to assure a good bond. Resulting from this heating, the reinforcement can both be hybridized and brought to its final shape in this step. A high degree of preforming will help the co-molding step. However, cost increases with a higher preforming degree. In classical

preforming processes, the fit to the final shape can e.g., be reached by processing the tape in complex tools. In the swing folding process, the fit can be improved by increasing the number of bends in the component. The desired fit needs to be set according to the requirements of the task and the co-molding process.

If the swing folding process is applied to utilize the flexibility of the process for prototypic applications, only interference between the bends limits the number of bends. If serial production is targeted, preforming costs shall be reduced. As the processing time increases almost linearly with the number of bends, a compromise between preforming degree and the number of bends should be found.

In this chapter, an approach to finding process-compliant tape designs for the given component shape is described. As the approach shall be applied to various component geometries, it needs to be independent of the geometry. (Kupzik & Biergans et al. 2019)

In Section 6.1, the task is described.

In Section 6.2, the two applied optimization methods are introduced.

In Section 6.3, prerequisites for an optimization toolbox are deduced. For the optimization loop, an adequate description of possible geometries and their coding, evaluation, and adaption is needed.

In Section 6.4, a group of analytical methods for finding process-compliant geometries is presented. It is suitable for limiting the initial parameter range in starting solutions as it delivers acceptable results with very low computational effort.

In Sections 6.5 and 6.6, evolutionary optimization and gradient-based optimization for adjusting random or analytically derived geometries are presented.

In Section 6.7, the workflow for optimization is summarized and the implemented Graphical User Interface is presented.

6.1 Task

Within the task of Input Shape Optimization, a process-compliant tape design needs to be found, which comes close to the component's shape. A specific area of the shell component's surface shall be used to define a design space in which the tape can be positioned. An .stl file of its upper, middle, or lower surface is used to define the component's geometry. As additional information, a start and end point of the tape shall be

passed to the optimization. As a further variable, the tape width will be taken into account. From this information, a tape design has to be calculated and the shape defining parameters $\alpha_{1..i}$, $\beta_{1..i}$ and $l_{1..i+1}$ need to be derived for the i bends. Two example geometries that will be used for explanations in this thesis are shown in Figure 6-2.

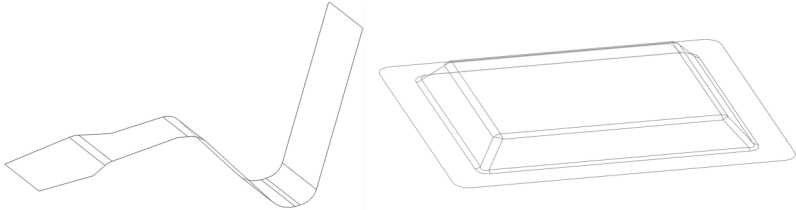


Figure 6-2: These component geometries will be used to explain the algorithm in this thesis.

Following requirements have to be fulfilled by the optimization:

Flexibility:

The approach shall be able to process shell geometries that follow the design guidelines for compression molding shell parts for manufacturing without sliders in the mold.

Process compliance:

Limitations in the possible bending angle of the test rig, the minimum distance between two bends, and the maximum rotations of the bend lines shall be regarded. For the subsequent co-molding process, it is important to be able to place the reinforcement on the lower mold. Therefore, it must be possible to define which of the two sides of the component the tape may not penetrate to avoid overlapping between the reinforcement and the mold. In addition, this condition needs to be regarded by the optimization result. For changes in the hardware, the limits need to be easily adjustable in the optimization code.

Computing time:

For the problem of finding a tape design for the reinforcement of a certain component, a vast high-dimensional solution space is available. The solution space is limited by the swing folding process compliance, which can be kinematically described (Figure 3-9). This way, the solution space can be limited to three parameters per bend. Additionally, 6 parameters for the start point and direction need to be set. Assuming (very coarse) 20 levels per parameter, this leads to $20^6 * 20^{4*3} = 2.6 * 10^{23}$ solutions for fully scanning

the solution space for preforming 4 bends. Experiments with the evaluation of solution sets showed that approximately 100 solutions can be evaluated per second on a standard computer. The needed time for evaluating all the parameter combinations of the abovementioned preform would therefore require approximately 10^{14} years. Therefore, a systematic optimization approach is needed.

A fast analytical preprocessor that identifies a favorable initial solution is combined with an optimization toolbox featuring genetic and gradient-based optimization in this approach. The analytical solution is limited to tapes with a planar middle axis ($\alpha_{1..i} = 0$) to simplify the solution of the problem. The genetic optimization can then be used to optimize the results using the whole solution space, including $\alpha \neq 0$. The gradient-based optimizer can be used for the fast approach to the next local optimum.

6.2 Systematic Optimization Methods

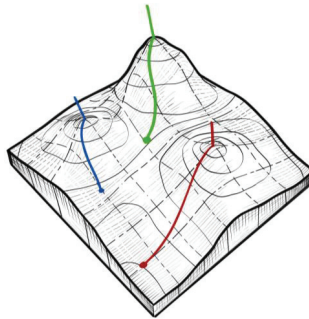


Figure 6-3: Optimization methods are used for the finding of maxima or minima of a function. One challenge is that the method can converge to local optima close to the starting point instead of the globally best point. (Figure by Alexej Bachtin)

In the following sections, the functional basics of the applicable optimization algorithms are given. Optimization aims to find the best solution by minimizing the penalty function or maximizing a fitness function (Grimme & Bossek 2018; Steinbuch & Gekeler 2016; Schröder 2010). In Figure 6-3, an example is given. The goal is to find the highest point of the hill, which represents the value of a fitness function depending on x and y . This example is strongly simplified compared to the multi-dimensional fitness function of the UD-tape. A straightforward analogy for the applied algorithms can be “always go uphill!”

for the gradient-based optimizer and “jump around randomly and repeat from the highest reached points of the previous iteration” for the evolutionary approach. When selecting an optimization approach, a Nelder Mead simplex approach (Luersen & Le Riche 2004) was regarded but discarded as it finds local optima like the Gradient Descent method. To optimize the preform shape, the preform will be represented by a fitness function based on its kinematic description and the target geometry.

6.2.1 Gradient Descent Optimization

A gradient-based optimizer adapts the parameter set so that it is continually guided along the steepest path. The main requirement is the availability of a gradient in the proximity of the current parameter set. If the function to be optimized is differentiable, the gradient can easily be calculated analytically. Numerical gradient calculation becomes necessary in other cases. If the gradient is calculated by varying each of n individual function parameters, $2n+1$ evaluations are necessary per optimization step. The steepest descent can be calculated from the gradient, and a preselected step size is gone along the direction of the steepest descent. Usually, the next optimum can be found within a small number of steps if the search starts close to this optimum. If the function is not shaped nicely for this type of optimization or the number of parameters is large, an extended numerical effort may be required until finding the local optimum (Steinbuch & Gekeler 2016). For complex problems, heuristic approaches are often preferred to purely gradient-based approaches (Eiliat & Urbanic 2019). Despite its numerical efficiency, gradient-based optimization tends to find local optima unless it allows temporary worsening of the fitness. In this thesis, its implementation was mainly used for fine-tuning the result of a coarse pre-optimization.

6.2.2 Evolutionary Optimization

Evolutionary optimization imitates the propagation of behavior and features from parent to child in natural populations. The natural species optimizes its genome to adapt to the environment. In nature, better-fit individuals have higher survival rates. Random mutations during reproduction drive the adaption in the genome. Information between different individuals can be exchanged by pairing/crossover, giving lucky children the best features from mother and father. In this random process, the far overwhelming number of children is worse or equally well fit to the environment as their parents. Only a few lucky ones have a better fit, but better fitness allows them to have more offspring than

worse fit individuals. This way, the average fitness of the offspring can increase based on random changes. (AL-Salami 2009; Bäck 1996)

The technical adaption of this process is the evolutionary optimization algorithm. It starts with an initial population, a set of *population size* individuals. Each individual is characterized by all of its parameters. The parameters are encoded as genes in the chromosome of the individuals. The difference between evolutionary and genetic algorithms is the valuation of the genes (Vikhar 2016). In this thesis, an evolutionary approach with a nearly continuous value-specter as presented in Table 6-1 is used instead of the binary genetic distribution.

Table 6-1: Example for the chromosome of three individuals with five genes each

Individual	Gene 1	Gene 2	Gene 3	Gene 4	Gene 5
#1	4	1	7	2	4
#2	3	5	1	2	9
#3	7	9	4	9	4

The individuals undergo a cycle of selection, crossover, and mutation for many generations until a stop criterion is met (Grimme & Bossek 2018). The cycle is presented in Figure 6-4. Further background information is available in (Eiben & Smith 2015; Steinbuch & Gekeler 2016). With this process, problems with a complex dependency of the solution quality on the parameters and with many parameters can be solved (Eiliat & Urbanic 2014).

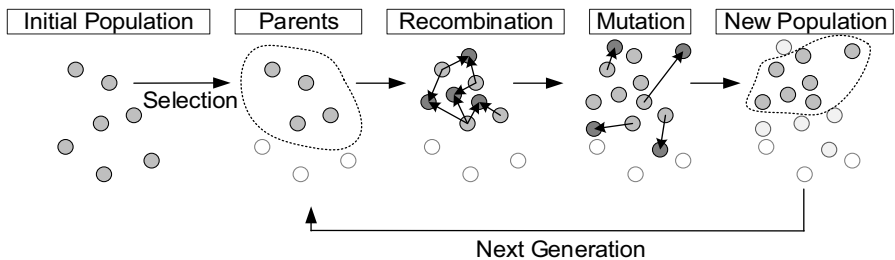


Figure 6-4: The steps of an evolutionary generation. Own representation based on (Grimme & Bossek 2018; Steinbuch & Gekeler 2016)

Definitions in this thesis are used according to (Steinbuch & Gekeler 2016):

Individual: An individual is a single representation of a solution for the problem. Its quality can be evaluated by the fitness function.

Generation: A generation contains a set of individuals. From each generation to the next, the individuals are altered by parent selection, crossover, mutation, and selection.

Parent selection: From the Generation, individuals are selected, which form the group of parents for the next generation.

Crossover: The individual genes of the parents are combined to form a child. One-Point crossover, where either all genes are selected from one parent or the beginning and end of the child's chromosome are combined from the two parents, proved most successful in this thesis.

Mutation: In the mutation step, the genes of the individuals may be randomly varied in one of many possible ways to increase gene variation.

Selection: From the remaining individuals, the best fit are selected to form the next generation. Adaptions, like an automatic discarding of double individuals, can be made to improve the optimization behavior.

The implementation in the toolbox is described in Section 6.5.

6.3 Prerequisites for the Optimization

For optimizing shapes, they must be represented in a suitable parametrization and adjusted in an optimization loop. In this section, the optimization loop is described. A kinematic description of multi-bend preforms is defined and a suitable genome for its representation is presented. A function for the evaluation of the solution's fitness and adaptation possibilities according to the genome are presented.

6.3.1 Optimization Loop

The optimization loop is represented in Figure 6-5. First, an initial solution is found. This can be done either randomly or with the help of the analytic preprocessor (Section 6.4). This initial solution is the first representation of the situation in a model. It represents tapes in the optimization loop by one or more parametrized instances of the kinematic description (Section 6.3.2). For a systematic optimization, this representation of the tape (Section 6.3.3) needs to be evaluated (Section 6.3.4). Based on the current tape geometry or geometries and knowledge gained about it in the evaluation, the model's parameters are adjusted (6.3.5 and 6.5 to 6.6). This is repeated until a certain threshold or number of iterations is reached. Finally, the result is displayed.

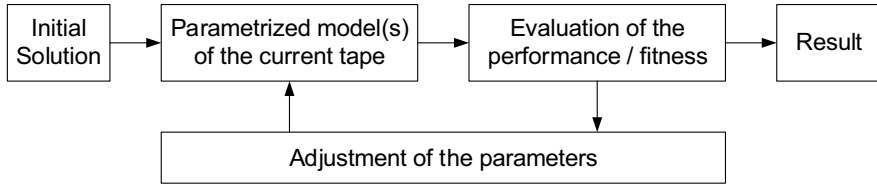


Figure 6-5: Steps of iterative optimization

6.3.2 Kinematic Description of the Problem

The possible solutions are described in a three-dimensional description of the tape deduced from the real process kinematics. This way, the search space of the optimization includes all kinematically possible solutions (A_Biergans 2018). Advantages are that few parameters are used, and solutions that cannot be manufactured can be excluded by later filtering. The shape of a single bend can be described by the two bending angles α and β as well as the distance l before the bend. The bends are assumed to be sharp at the bending edges. This simplification can be taken as no significant influence of the bend area on the fitness value of a tape is expected. The robot control system corrects the length error resulting from real, rounded edges during manufacturing.

The kinematic of the tape is represented by a vector-based description in which the longitudinal and normal vectors of the single elements are calculated by rotating around the bending edges. The tape is initially defined via its longitudinal centerline, as represented in Figure 6-6 (a). The first section of the tape is defined by a longitudinal vector \vec{l}_1 , a normal vector \vec{n}_1 , and a start point with adjustable values P_{start} . The bending edge vector \vec{v}_1 can be calculated by rotating \vec{l}_1 around \vec{n}_1 using the angle $(\alpha_i - 0.5\pi)$ (Figure 6-6 (b)). The second section of the tape begins in the center of the first bend and extends along \vec{l}_2 . \vec{l}_2 and \vec{n}_2 are calculated by rotating \vec{l}_1 and \vec{n}_1 around the first bending edge \vec{v}_1 by the angle β (Figure 6-7 (a)). The left and right borders of the tape are calculated by a modified version of this approach. First, the respective start points are calculated from the start point by translating it along the normal of \vec{l}_1 and \vec{n}_1 for half of the tape width. Afterward the borders are calculated by the same algorithm as the centerline. In this calculation, the length of the segment are calculated depending on the tape width and the α angle before and after the segment (Figure 6-7 (b)). (Kupzik & Biergans et al. 2019; A_Biergans 2018)

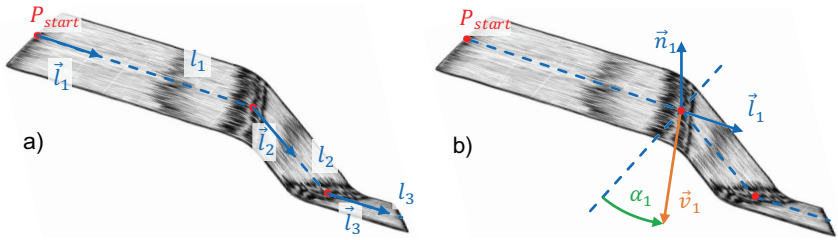


Figure 6-6: The tape centerline is described by its longitudinal vectors (a). The bend line can be described depending on those vectors, the normal vectors, and the bending angle α (b). (Figure based on Alexej Bachtin)

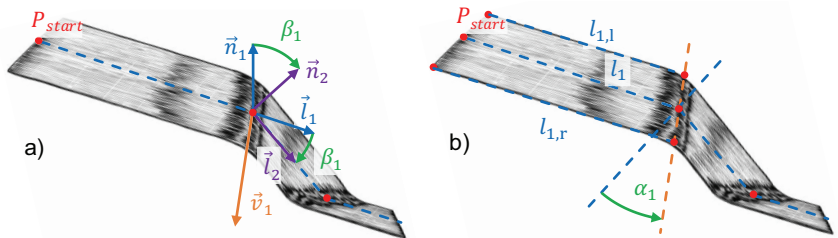


Figure 6-7: The longitudinal and normal vector of the next segment can be calculated by rotation around the bend line (a). For the calculation of the tape's sides, the length values are adjusted according to the width w and α (b) (Figure based on Alexej Bachtin)

For the implementation, the following equations are used. The position $x(l)$ of a point after a certain overall length l on the tape centerline is calculated using Equation 6-1.

$$x(l) = \begin{cases} P_{start} + l \cdot \vec{l}_1; & \text{for } l \leq l_1 \\ P_{start} + l_1 \cdot \vec{l}_1 + (l - l_1) \cdot \vec{l}_2; & \text{for } l_1 < l \leq l_1 + l_2 \\ P_{start} + l_1 \cdot \vec{l}_1 + \dots + (l - \sum_{i=1}^{n-1} l_i) \cdot \vec{l}_n; & \text{for } l_1 + \dots + l_{n-1} < l \leq l_1 + \dots + l_n \end{cases} \quad 6-1$$

The bending edge vector \vec{v}_i (Figure 6-6) is calculated by rotating the longitudinal vector \vec{l}_i around the normal vector \vec{n}_i :

$$\vec{v}_i = R_{\vec{n}_i}(\alpha_i - \frac{\pi}{2}) \cdot \vec{r}_i \quad 6-2$$

In the next step, the new longitudinal \vec{l}_{i+1} and normal \vec{n}_{i+1} vectors are calculated (Figure 6-7 (a)):

$$\vec{l}_{i+1} = R_{\vec{v}_i}(\beta_i) \cdot \vec{l}_i \quad 6-3$$

$$\vec{n}_{i+1} = R_{\vec{v}_i}(\beta_i) \cdot \vec{n}_i \quad 6-4$$

Finally, the sides of the tape can be calculated analog, using an adapted version of Equation 6-1 in which the length values of the tape at the respective side and the moved start points are put in. The calculation of the length (Figure 6-7 (b)) is demonstrated for the right border using the following equation by subtracting the length change of the previous bend and adding the length change of the next bend:

$$l_{i,r} = l_i + \Delta l_{i,r} - \Delta l_{(i-1),r} \quad 6-5$$

The length variations caused by the individual bends are calculated using the tape width w and α_i angle. The initial length variation is defined to be zero:

$$\Delta l_{i,r} = l_i + \frac{w}{2} \cdot \tan(\alpha_i) \quad 6-6$$

$$\Delta l_{0,r} = 0 \quad 6-7$$

Each individual tape can now be represented in a chromosome (= individual parameter set) of its defining parameters. For a tape with n bends, $3n + 7$ genes (= parameters in the chromosome) are needed. $3n$ genes are used to describe α , β , and l of the n bends. Additionally, 1 gene is needed for the free end length, 3 genes are needed for variation of the start point, 2 for the first longitudinal vector, and 1 gene is needed for the rotation of the normal vector around the first longitudinal vector.

For the fitness determination, the tape is evaluated on discrete points on its surface. These points are defined on the centerline and the sides of the tape. Three points are placed on each bending edge, and a number of points can be placed along the centerline and the sides between the bends. The two approaches of a constant number of points (Figure 6-8 (a)) and equidistant points (Figure 6-8 (b)) were implemented. In case of the "constant number of points" method, the same number of points is placed on each segment line (left, right, or center between two bends). For the equidistant method,

the number of points on a segment line (left, right, or center between two bends) depends on the length of the line.

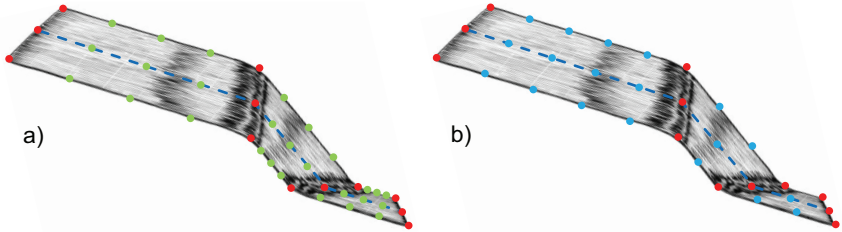


Figure 6-8: Constant number of evaluation points per segment (a) vs. Equidistant evaluation points (b) (Figure based on Alexej Bachtin)

6.3.3 Design of the Genome

The kinematic description from one end to the other, as previously described, was compared with a split description from the middle of the preform (A_Biergans 2018; A_Brenner 2020). The two approaches are presented in Figure 6-9.

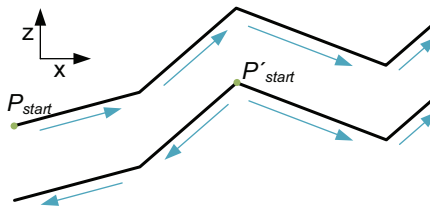


Figure 6-9: The tape can be represented symmetrically by moving P_{start} to P'_{start} and describing the two halves with two separate kinematic descriptions.

The approach of describing the tape from its middle was developed to avoid an asymmetric behavior where the start point P_{start} only depends on its coordinates while the end point P_{end} depends on all chromosomes although the physical problem is symmetric as start and end point are randomly assigned to the tape's ends. Expected advantages of the symmetric implementation are similar behavior for both physical tape ends and faster convergence as the tapes are shorter.

The results showed that the overall improvement of the geometry was slowed down by the symmetric approach as fewer new mutations were improving over the old ones (A_Brenner 2020). Resulting, more generations or larger populations were needed for a similar result. The explanation for the observed behavior is that the movement of the start point is more limited in the symmetric description compared to the asymmetric description.

The position of each element is defined by its predecessors and the start point. To displace the start point for a relevant share of the individuals, the individuals with the displaced start point must have better fitness values. To maintain a good fitness of the remote segments despite a displaced start point, a second random mutation needs to adjust the shape of the intermediate segments to correct the remote section’s position. The probability of having a meaningful random displacement of the start point and meaningful random compensation for remote areas at the same time is low for a tape. For the symmetric approach, the probability is even lower, as both free ends of the tape need to be meaningfully corrected at the same moment the start point is altered. Therefore, the asymmetric approach was selected.

An exemplary genome is presented in Table 6-2. The genes from index 0 to 2 encode the start point while 3 and 4 define the starting direction of the tape. Gene 5 is describing the rotation of the tape around its first longitudinal vector.. The genes 6 to $3i + 5$ are used to describe the bend parameters of the tape. In $3i + 6$, the length of the free end of the tape is encoded.

Table 6-2: Coding of the tape geometry in the genome

Gene index	0	1	2	3	4	5	6
Content	var_{px}	var_{pz}	var_{py}	var_{r1}	var_{r2}	var_{γ}	l_1
Gene index	7	8	...	$3i + 3$	$3i + 4$	$3i + 5$	$3i + 6$
Content	α_1	β_1	...	l_i	α_i	β_i	l_{i+1}

6.3.4 Fitness Evaluation

The term fitness is widely used for the quality of an individual in an evolutionary optimization approach. In this thesis, the term is used for all evaluating functions. It is used to compare previous and new solutions in evolutionary optimization and is used to calculate the direction of improvement in gradient-based optimization. In this thesis, the fitness is first calculated and then altered depending on the solution’s compliance to the hardware.

6.3.4.1 Fitness

To compare individuals, a quality measure is needed. The following criteria for this quality were derived from the requirements on a real-world tape reinforcement and implemented:

- It should start and end at the correct points (Start/End Subfitness)
- It should follow the contour closely (Distance Subfitness)
- It should have the correct length (Length Subfitness)

An overview is given in Figure 6-10. The real geometry is represented in green and the tape in blue. The Start/End Subfitness represents the distance between the start and end points of the lines. The Distance Subfitness describes the distance of the red evaluation points from the green .stl surface. The Length Subfitness compares the difference in length between the green and blue line.

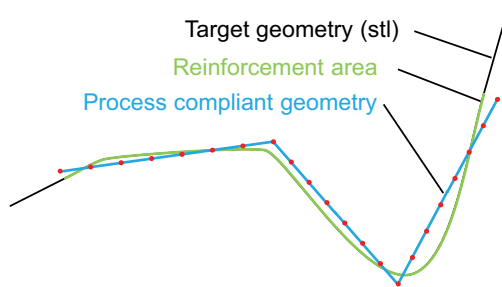


Figure 6-10: Overview of the comparison between real component and kinematic description of the tape.

From these requirements, subfitness measures were derived (A_Biergans 2018):

Start/End Subfitness

For searching the solution space, the start point P_{Start} must be movable by parameters in the chromosome of the individuals. It can therefore vary from the predefined start point $P_{Start,def}$. The end point P_{end} of the tape is defined by calculating $x(l_1 + \dots + l_n)$ in Equation 6-1. It can, therefore, also differ from the defined end point $P_{end,def}$. The start/end subfitness is calculated using the distance between the set points and the actual value of the individual (Equation 6-8). The distance is divided by the approximated optimum length (L_{aim} – see Section 6.4.2) to make the value independent of the component scale. The constant $k_{s/e}$ is used to normalize the range of the subfitness

values relative to another. The distance between the defined and the obtained points should be minimized.

$$fitness_{start/end} = -k_{s/e} \cdot f_1 \left(\left| \frac{P_{start/end} - P_{start/end,def}}{L_{aim}} \right| \right) \quad 6-8$$

Distance Subfitness

The tape should fit closely to the mold before co-molding. With the distance subfitness, deviations between the surface of the mold and tape are evaluated. The subfitness is calculated as a function of the sum of a function of the distance from each evaluation point to the surface of the .stl of the component (d_i) (Equation 6-9). The individual distances should be divided by the approximated optimum length (L_{aim}) to make the value independent of the component scale. The constant k_d is used to normalize the range of the subfitness values relative to another. The distance should be minimized for a large fitness.

$$fitness_{distance} = -k_d \cdot f_1 \left(\frac{1}{n} \sum_{i=1}^n f_2 \left(\frac{d_i}{L_{aim}} \right) \right) \quad 6-9$$

Length Subfitness

The length subfitness (Equation 6-10) is an important measure for controlling the population's behavior. By demanding a correct length of the tape and a correct start and end point, the tape is placed in a feasible region of the solution space. Not allowing superfluous length avoids solutions, in which the tape follows prolonged curves or multiple 180° folds in flat regions of the part to improve the average distance. Depending on the component geometry, altering the length subfitness in a non-linear and non-symmetric way can be advantageous. This way, a steeper penalty for all the length exceeding the approximated optimum value can be implemented without a large influence close to or below the optimum value. To force the tape to cut corners, the approximated optimum value L_{aim} can be multiplied by a factor to reduce it for the comparison. An advantageous pre-tensioning effect during the co-molding step could result from such a "too short" tape. The length is divided by the approximated optimum length (L_{aim})

to make the value independent of the component scale. The constant k_l is used to normalize the range of the subfitness values relative to another.

$$fitness_{length} = -k_l \cdot f_1 \left(\frac{L - L_{aim}}{L_{aim}} \right) \quad 6-10$$

Overall Fitness

In the overall fitness, the individual subfitness functions are added in a weighted sum. The overall fitness takes negative values, with 0 being the best obtainable value:

$$fitness = \gamma_d \cdot fitness_{distance} + \gamma_l \cdot fitness_{length} + \gamma_p \cdot fitness_{start} + \gamma_p \cdot fitness_{end} \quad 6-11$$

The weighting coefficients γ are used to distribute the importance of the individual subfitness measures. As the individual subfitness measures' importance may vary along the optimization process, a mechanism to alter γ was implemented. An important property of a fitness function for optimization is whether it can be derived. In this case, no analytical derivative is available and numerical derivation has to be used if necessary.

6.3.4.2 Manufacturing Constraint Penalties

The fitness functions bring the solution close to the component's surface and the correct start and end point. This way, a good fit to the component can be achieved, but the solution only complies with the kinematic description's restrictions, not the hardware implementation of a bending machine. The penalty criteria were derived by an analysis of the differences between the ideal and the implemented process (A_Wenzel 2020). The fitness is divided by the overall penalty to allow a large influence for the penalty:

$$fitness_{penalty} = \frac{fitness}{penalty_{overall}} \quad 6-12$$

The following implemented penalties can be switched on or off during the optimization run:

Minimum section length penalty

In the manufacturing of a subsequent bend, the handling gripper may not grip the tape in the previous bending zone. Therefore, the distance between two bends must be at least the width of the handling gripper jaw plus the TCP offset t_0 and the bending zone width b_0 . If contact heating is used, the actual size of the hardware must be used in the

penalty calculation. Further attention is required if $\alpha \neq 0$ as the minimum distance must also be regarded at the tape's left and right border. If the minimum section length is underrun in one or more sections, the minimum section length penalty is lowered.

α penalty

The robot workspace and the length of the handling gripper and heated area limit the applicable α angle range. In the test rig, the value is limited to $-30^\circ < \alpha < 60^\circ$ (A_Wi 2019). If one or more α angles lie outside this interval, the α penalty is lowered.

β penalty

The robot workspace and the collision contour of the end effector limit the applicable β angle range. In the hardware implementation, the value is limited to $-90^\circ < \beta < 55^\circ$ for the radiation heating (A_Wi 2019) and $-50^\circ < \beta < 50^\circ$ for the contact heating (A_Vollmer 2018). If one or more β angles lie outside this interval, the β penalty is lowered.

Mold intersection penalty

The .stl file represents one side of the shell component. The represented surface is not only the component's surface but also the surface of one of the used mold halves. When positioning the reinforcement for co-molding, the tape will be placed on this surface of the mold. Therefore, no intersection between the reinforcement and the mold should occur. To ensure this, the mold intersection penalty was added. The value is calculated depending on the number of evaluation points that are positioned on the wrong side of the .stl surface.

Overall fitness with penalty

The individual penalties follow a falling exponential function depending on their individual influence factors. To avoid overwhelming influence of single penalties, a constant is added to the individual values before they are multiplied to calculate the overall penalty. The overall penalty is used to influence the fitness of the individuals (Equation 6-12).

6.3.5 Adaption

For the adjustment of the parameters in the kinematic description, an optimization algorithm is used. An analytical preprocessor is applied in this thesis to find starting solutions close to the final solution (Section 6.4). With evolutionary optimization, this initial solution or a random initial solution can be optimized in a wide range of the solution

space (Section 6.5). A gradient-based optimization approach was implemented to further approximate local optima that the evolutionary optimization has found (Section 6.6).

6.4 Analytical Preprocessor

Early experimentation with the evolutionary optimization algorithm showed that sometimes a vast number of generations is necessary to optimize a randomly initiated set of individuals until the first tapes are close to the target surface. An analytic approach for the generation of an initial solution set can be used to minimize the numerical effort. The elements of this approach are described in Section 6.4.1 to 6.4.3. As presented in Figure 6-11, the results could be significantly improved by using a preprocessor while maintaining the computational effort. In this thesis, both a 2D preprocessor which leads to a flat solution with all $\alpha = 0$ and an edge detecting 3D preprocessor have been implemented. In general, the 2D preprocessor delivers good results with high reliability, while the 3D preprocessor can even predict α values for geometries with clearly visible edges.

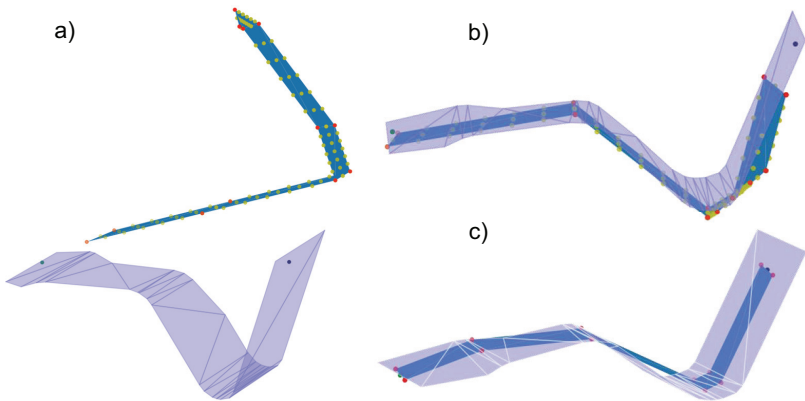


Figure 6-11: Randomly initialized solution (a), after 300 generations with 300 individuals of optimization (b) and 2D preprocessor solution (c)

6.4.1 Definition of the Situation

The component is loaded into the algorithm as .stl file, representing the surface as a list of triangles. The following description is based on Figure 6-12. The triangles are defined using their center and corner points in the file's global coordinate system (COS_{global}) in

the following sections. As the orientation of the component relative to the global coordinate system may vary depending on the designer's guidelines or the orientation of the component in an assembly, further coordinate systems are used. The preprocessor coordinate system ($COS_{preproc}$) is positioned relative to the component. The origin of the preprocessor coordinate system is defined by the weighted average of the triangle center points. The x-axis of the preprocessor coordinate system is calculated by least-square fitting a line to the triangle center points pointing in the positive x-direction of the global coordinate system (Trendline). The z-axis is placed in the plane that contains the x-axis and the weighted average vector of the normal vectors of the triangles. In this coordinate system, a large variety of components can be placed flat, with the main orientation of the shell being in the horizontal x-y-plane and the normal direction of the component being along the z-axis. (A_Biergens 2018)

A contour plot (Figure 6-21) in the preprocessor coordinate system is used for the selection of the start and end point of the reinforcement. This contour plot is generated by interpolating the component surface and plotting the points in the preprocessor x-y-plane with a color depending on their height along the z-axis (Figure 6-21). Start and end point can be flexibly selected by clicking this contour map of the component. Next, the tape coordinate system (COS_{tape}) is defined. The z-direction is copied from the preprocessor coordinate system and the x-direction is defined by the connection line between the projections of the two selected points onto the preprocessor coordinate systems x-y-plane. The origin is placed on the connection line between the two selected points and on the y-z-plane of the preprocessor coordinate system. (A_Wenzel 2020)

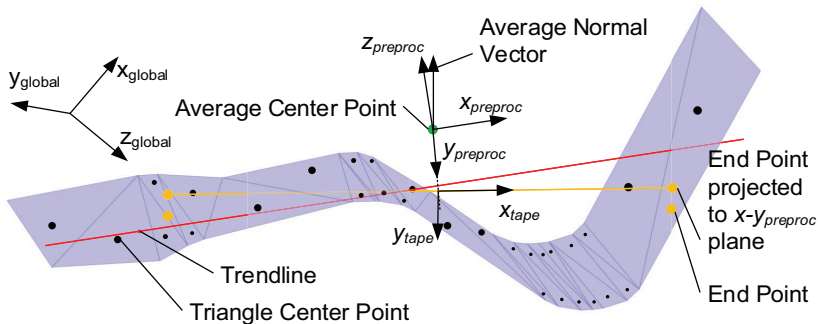


Figure 6-12: Coordinate System placement

6.4.2 2D Preprocessor

The initial solution will be placed in space in such a way that it connects the two selected points (start and end point) and follows the surface closely. For this, the intersection line between the shell surface (as interpolated according to Figure 6-21) and the tape coordinate systems x-z-plane is calculated. The resulting flat height profile of the component in the tape x-z-plane is approximated by linear segments (Figure 6-13(a)).

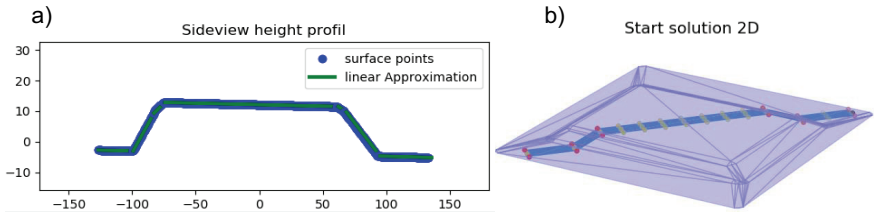


Figure 6-13: Height profile (a) and resulting 2D solution (b)

For the initial tape solution, the values $l_{1..i+1}$ are defined by the length of the linear segments. L_{aim} is calculated by adding $l_{1..i+1}$. From the angle between the linear segments, $\beta_{1..i}$ can be calculated. All α values are set to zero, and the starting direction is defined by the first segment's direction (Figure 6-13(b)). L_{aim} is calculated by closely following the length of the height profile. (A_Biergens 2018)

It could be shown that the evolutionary optimization could provide satisfactory results even if the local orientation of the tape did not fit the z-axis well (A_Biergens 2018). In this optimization process, the starting point, direction, and rotation were adjusted and α was applied to fit the component geometry better. In Figure 6-14, two solutions are compared after preprocessing and an optimization run. In Figure 6-14 (a), the normal of the tape does not align well with the surface normal. In Figure 6-14 (b), the tape is adapted to the surface by altering α and adjusting the other parameters accordingly.

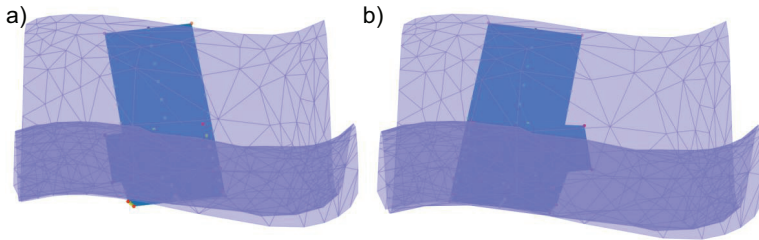


Figure 6-14: Adaption to a skew surface by the evolutionary optimization. 2D preprocessor solution (a) and 100 generations with 100 individuals of evolutionary optimization (b)

6.4.3 3D Preprocessor

The 2D preprocessor creates solutions that are placed in one plane, not using the ability to create askew bend lines. An edge detection algorithm was implemented to overcome this disadvantage (A_Wenzel 2020). By creating two additional 2D solutions with an offset along the COS_{tape} y-axis and comparing the found bend points, edges can be detected for geometries with sharp edges. The approach is presented in Figure 6-15. From the edges, α values can be calculated and inserted into the 2D solution which is then called 2D edge detection (2DE) solution. By adding the α values, the shape of the 2D solution is altered, which results in deviations at the end point position. This deviation is often insignificant if α is small, while deviations can be crucial in other cases.

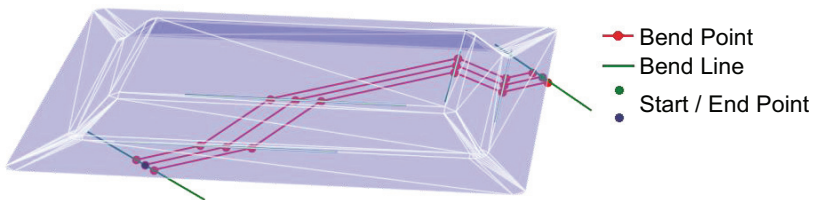


Figure 6-15: 2D Edge detection on a geometry with clear edges (translated figure from (A_Wenzel 2020))

An alternative for reducing the error at the end point is to iteratively calculate solutions from each actually reached bend point to the end point. This approach is called 3D preprocessor in this thesis. In the 3D preprocessor, the 2DE preprocessor is first started

between start and end point in the direction of the newly created tape segment. Afterward, the same 2DE preprocessor is started between the first bend of the initial iteration and a new end point. All following iterations are conducted similarly until no new bend points are found in one iteration. The parameters for the tape are calculated as for the 2D and 2DE preprocessors. However, the angle between the 2DE iterations can lead to slight deviations from process compliance which, again, lead to an offset between P_{End} and $P_{End,def}$.

Both presented edge detection preprocessors only function on geometries with sharp edges, while the 2D preprocessor works reliably for most geometries (A_Wenzel 2020). The fitness value of the 2DE and 3D preprocessor solutions is typically lower than the 2D value because of the deviation from the end point. However, the edge detection solutions have better potential to rapidly converge to better values than the 2D preprocessor. This is because the error is caused by errors in individual parameters (α , β or l) while the 2D preprocessor often needs pair-wise improvement of α , which is less probable (Section 6.6).

6.5 Evolutionary Optimization Approach

In this section, the genome manipulation by evolutionary optimization and by additionally implemented manual interaction and the influence of the fitness function shape on the optimization process are described.

6.5.1 Genome Manipulation

In the evolutionary algorithm, the genome of the individuals is manipulated by crossover and mutation. Furthermore, tools for adding and removing bends have been implemented based on the Galileo module².

6.5.1.1 Crossover

In this thesis, an arithmetic crossover and one-point crossover are compared. With an initial, less structured genome design, arithmetic crossover (calculating the new gene value as the average of the two parent genes) showed reasonable results (A_Biergans 2018). With the final genome design presented in Section 6.3.3, one-point crossover (the first genes of one parent are combined with the later genes of the other parent)

² <https://github.com/DEGoodmanWilson/Galileo> [last downloaded 06th July 2021]

proved advantageous. Here crossover at one point is the equivalent to combining two tapes by cutting them at a specific point and combining the two halves (A_Wenzel 2020). One-point crossover was set as the default setting for the optimization toolbox.

6.5.1.2 Mutation

During mutation, the value of each gene is randomly varied with a set probability called mutation rate. The gene can either be reset randomly in its whole range of values without regard to its previous value or in proximity to its previous value. Later proved useful for optimizing an existing solution as a single randomly reset gene would probably worsen the solution so that it becomes unfit and will be removed from the population. For finding the first solution, the random reset enables a global search in the whole solution space. The standard setting for the optimization is set to a uniform distribution around the previous value. The possible distance to the current value can be adjusted with the parameter mutation range. In this case, for example, a previous β value of 30° and a mutation range of 3° leads to a random β value between 27° and 33° . (A_Biergans 2018)

Parameters can be adjusted before the optimization or during the run (Eiben & Smit 2011). An adaption of the mutation rate based on the genetic variety was implemented in (A_Brenner 2020).

6.5.1.3 Adding and Removing Bends

The optimization of tapes is a compromise between a good fit and low manufacturing time. As the time increases with the number of bends, as few bends as possible should be used. The potential fitness of a tape, however, increases with the number of bends. The number of bends is initially determined by the preprocessor and its parameters. To enable later adjustments, modules for adding and removing bends are included in the optimization toolbox. The function of adding bends to solutions is also needed to combine individuals from different preprocessors with different numbers of bends.

To add bends, a tape section can simply be split at a certain position. The new α and β are set to zero, and the length from the previous generation is distributed to the two new length values according to the set position of the new bend. The removal of bends requires more effort to avoid large deflections at the tape end. For bend numbering before the removal, i is used in the following section, and for bend numbering without the removed bend, j is used. If bend number i is removed, the surrounding segments i

and $i + 1$ are also removed and replaced by a new segment connecting the bend $i - 1 / j - 1$ with the former bend $i + 1$ which is now bend j . If the first or last bend is removed, the same method is applied with the start or end point instead of $j - 1$ respective j . The parameters for the resulting tape have to be approximated. Resulting from the kinematic limitations of a bent tape, not both the rotation and the position of the tape end can be kept constant in all situations. In an empiric comparison, three methods for finding new bending parameters were compared. The length of the new segment was always defined by the distance between the two adjacent bend points of the removed bend. In the first method, α and β of the bends $j - 1$ and j were calculated in such a way to keep the longitudinal vector of the first following segment the same. This approach influenced the normal vector of the following segment. In the second method, all following α and β were adjusted to maintain the former longitudinal directions of the tape. The third method was to maintain the normal directions of the new and the following segment by placing a plane in the gap that resulted from removing the two tape segments. The normal direction of the new segment was calculated by calculating the average of the normals of the planes through the middle point of bend $j - 1$ and the side points of bend j and vice versa. The bend lines were placed in such a way that the normal of $j + 1$ was maintained. This way, variation in the longitudinal vector after j occurred. (A_Wenzel 2020)

An empirical comparison of the three methods showed that the third method delivered the best results as the position and angular error of the free tape end could rapidly be corrected in a few iterations. The approach of maintaining the longitudinal direction caused larger angular deviations of the following segments (method 1) and heavy misalignments of the normal direction along the tape (method 2), which took the evolutionary algorithm longer to correct. (A_Wenzel 2020)

6.5.2 Fitness Function

In the following section, the effect of both various fitness function shapes, as well as their relative weighting, is described.

6.5.2.1 Shape of the Subfitness Functions

The fitness function greatly influences the convergence of the optimization. In a study, quadratic, linear, and Gaussian functions were compared as f_1 in Equations 6-8, 6-9, and 6-10. (A_Brenner 2020). The goal was to weigh the influence of deviations in the

near and far range from the optimum differently. The basic shape of the functions is presented in Figure 6-16. The steepness of these three functions can be altered using the γ parameters and the constants defining the functions.

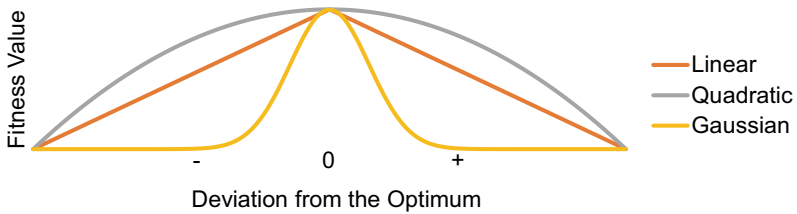


Figure 6-16: Fitness value depending on the distance from the optimum with the examined functions.

Changes have the greatest effect on a single subfunction, if the tape moves in the steepest area of its curve. The quadratic function gets steeper the further away the tape is from the optimum. The linear function is constantly steep, and the Gaussian function is steepest close to the optimum. The goal of the examination was to find out how the shape of the fitness function influences the behavior. As a test setup, randomly initiated tape strips were optimized, and the result was manually evaluated. 100 individuals were optimized for 50 generations using whole arithmetic crossover and empirically selected parameters for mutation and weights.

6.5.2.2 Effect of the Shape in Different Situations

In the trials, both the quadratic and the linear fitness showed converging behavior. The Gaussian fitness function showed no comparable convergence from the random start point. For the Gaussian functions, the individual subfitnesses of the randomly initiated solutions were either in the very flat outer area or in the steeper inner region of the function. That way, the subfitnesses in the inner regions would have fluctuations large enough to make the changes in subfitnesses in the outer regions insignificant. That way, the dominant subfitness function effectively renders all other subfitness functions useless. This is critical for the Gaussian function as the already optimized fitness function becomes dominant. Therefore, the randomly initiated tapes with Gaussian subfitness functions were optimized in one subfitness function and afterward drifted around randomly. This behavior can be improved by adjusting the width of the bell curve, but it stays an inherent deficit of this class of fitness functions.

The same effect of a predominance of a single subfitness function occurs for the Quadratic functions. However, in this case, the worst fitness function will become dominant. In the experimentation, quadratic fitness functions showed good convergence behavior. Large errors were effectively eliminated. The behavior close to the final shape was very flexible as the fitness functions close to their optimum did not have relevant influence allowing fluctuation and avoiding premature convergence. However, the individual weight parameter adjustments depended on how close the corresponding fitness subfunction could come to its optimum for the particular geometry, making it a manual process. (A_Brenner 2020)

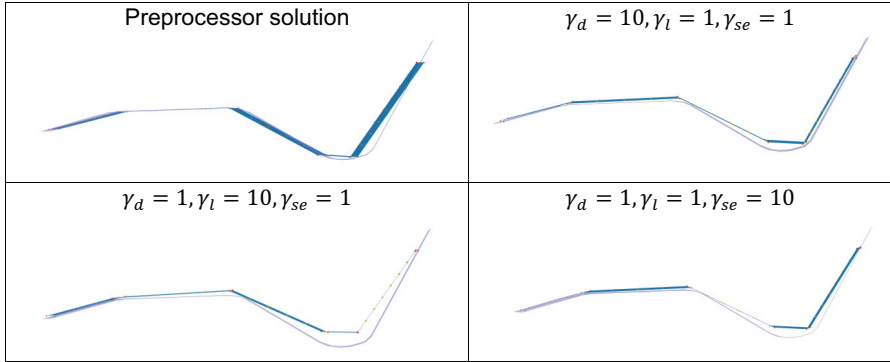
The convergence of the models using linear fitness functions was slightly slower than with quadratic functions. The quality of the results was comparable. An advantage was the lower manual effort required to adjust the weights of the individual subfitnesses.

Of the three types of subfitness functions, Gaussian functions showed the worst behavior. Quadratic functions converged best as long as they were far from the final shape and comparable to the linear functions close to the final shape. However, the selection of weight parameters required significantly less effort for linear functions, which also showed good convergence. As a preprocessor will be used in the future, the convergence behavior close to the final shape is most important. Therefore, linear subfitness functions will be used in general. In the length fitness, a distinction of cases is included to avoid penalizing tapes shorter than L_{aim} . This is the case to avoid buckling resulting from unnecessary tape length and as too short tapes are already penalized by their decreasing distance fitness and start/end subfitness values.

6.5.2.3 Balance between the Fitness Values

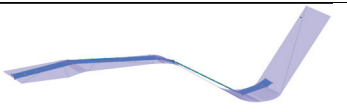
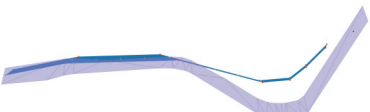
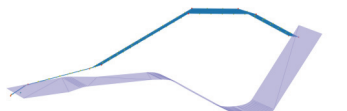
The behavior of the algorithm can be changed by adjusting the balance between the fitness values. Adjustments of the values in a limited range alter the importance of the goals, which is evident in the result of the algorithm. In Table 6-3 three possible distributions of fitness weights are compared to the preprocessor solution. The most visible effect is the smaller distance between tape and component if the distance subfitness weight is increased.

Table 6-3: Comparison of the behavior of different weight combinations after an optimization run with 30 Generations of 50 Individuals



If the weight of the subfitness functions varies largely, one subfitness function might become predominant, resulting in useless results. The effect is demonstrated in Table 6-4 for strongly increased weightings of distance fitness, length fitness, and start/end fitness. The extreme selection of weight values can make the optimization result useless.

Table 6-4: Extreme weighting of a certain subfitness function can cause small changes in this function to override important improvement in other functions and thereby optimize only for the one goal.

Predominant Subfitness	Effect	Example
Distance	The tape will either become very short to limit variations or fold double in flat areas of the component	
Length	Corners can be cut if the calculated optimum is wrong, which is not as severe as the other effects	
Start/End	The tape will form a clew/wad with the ends at the correct position	

6.5.2.4 Situation-adapted Weight Adjustment

The weight of the fitness functions can be altered along with the generations. This is especially useful for randomly initiated tapes. A successful strategy for the approach can be first to find a tape that meets both start and end point by weighting those respective fitness functions. Afterward, the tape can be tensioned by gradually increasing the importance of the length. Finally, the tape can be placed on the surface by gradually increasing the importance of the distance. As the preprocessor replaced the approach from random solutions, no systematic examination of the weight adjustment was conducted.

6.6 Gradient-Based Optimization Approach

Gradient-based optimization can be used for the computationally efficient optimization of suitable problems. In the following section, the application of classical gradient-based optimization and its limits as well as an adaption of the evolutionary optimization for similar functionality are described.

6.6.1 Numerical Gradient Calculation

Gradient-based optimizing offers a possibility to find the next local optimum rapidly. It requires, however, that the function to be optimized can be derived in the region of the optimization. For the fitness function in this thesis, no analytic derivative could be found. Therefore, numeric derivatives must be found to acquire some optimization functionality. A derivative can be found by sequentially altering the parameters by a small amount and recording the changes in the fitness function. An approach where this is applied was implemented in the optimization toolbox. In the implementation, the parameter that causes the biggest improvement for a defined step size would be set to its improved level in each iteration. This approach would set multiple parameters to new levels in many applications, and a fast overall improvement would occur after several iterations.

The challenge with the fitness function of the tape is its strong interdependence of the parameters, which can be regarded as dimensions in the optimization space. Therefore, improvement can often only be achieved for a combined variation of two or more parameters. In Figure 6-17, an example is given. For simplification, it is assumed that only the distance fitness is regarded and only the β angles and length values can be varied in this example. The original tape geometry is shown in black and the target mold is hatched. The start point and bend point 1, 2, and 3 are marked with green and orange

dots. Changing any single bend always increases the average distance between the tape and the target surface as large displacements occur in the area in the right of Figure 6-17. Example tapes with one changed angle are shown in purple, blue, and yellow for the three bends. The average distance improves only if more than one bend is changed. In the example in Figure 6-17, an improvement can be made by increasing the angle in bend 2 and compensating this by decreasing bends 1 and 3. In this situation, the fitness function has a saddle point with no improvement along any parameter axis.

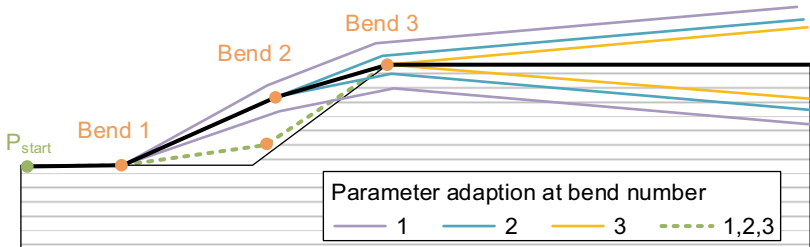


Figure 6-17: No change in only a single bend does improve the fitness although combined changes of multiple bends can improve the fitness.

This behavior makes iterative gradient-based optimization along a single parameter direction difficult. When varying the function along all of its parameters separately, it may falsely appear that no improvement is possible. To solve this problem, multiple parameters have to be adjusted in the right proportion. All combinations of parameter alterations with various degrees of altering should be evaluated to gain information about the shape of the fitness function. Due to the high number of parameters, this requires a high computational effort, making the method unattractive. Furthermore, no way of setting the degree of variation is known.

6.6.2 Adaption of the Evolutionary Algorithm

To overcome the challenge, the behavior of evolutionary optimization can be used. A random alteration of all parameters can be obtained by setting the mutation rate to 100%. To avoid big changes in the solution, the mutation range must be set to small values, e.g., 0.1% of the genome's range. A Gaussian mutation can be used to concentrate the offspring to the parents more densely. To ensure alterations in the population, only the offspring of the last generation should be transferred to the next generation. The population size influences the survival chances of low fitness individuals and

thereby affects the search. The convergence speed and the degree of change in which the solutions vary can be adapted by adjusting the mutation range and population size. In Figure 6-18, an example of the adaption of a tape to a geometry with sharp edges is given. In this example, mostly the α angles are varied. In Figure 6-18 (a), the 2D starting solution is presented. In Figure 6-18 (b), the fitness plot of the seemingly converged conventional evolutionary solution (Figure 6-18 (c)) is shown. Only the α angles in the end of the tape could be optimized to the geometry due to the low probability of positive advantageous variations at the tape's beginning. Figure 6-18 (d) shows the result of optimization by adapted evolutionary optimization as described above. In this result, all

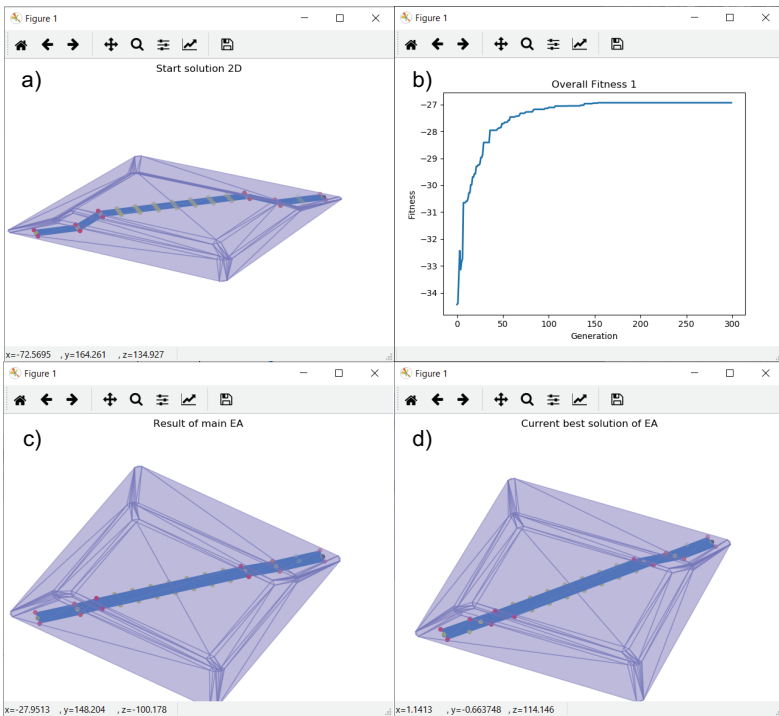


Figure 6-18: Comparison of the evolutionary algorithm and the pseudo-gradient approach. Initial solution (a), fitness graph of the evolutionary optimization (300 Generations, 300 Individuals (b), result of the evolutionary optimization (c), result of the adapted pseudo-gradient evolutionary optimization (d)

α values are adapted to the geometry. The same result could be obtained by the evolutionary approach at a much larger computational effort.

6.7 GUI and Example Workflow

During the development of the Input Shape Optimization, it became apparent that a graphical user interface (GUI) is needed for the interaction with the algorithm. In the following section, the implemented GUI (A_Biergans 2018; A_Brenner 2020; A_Wenzel 2020) and its usage are briefly described. An Overview of the workflow is given in Figure 6-19.

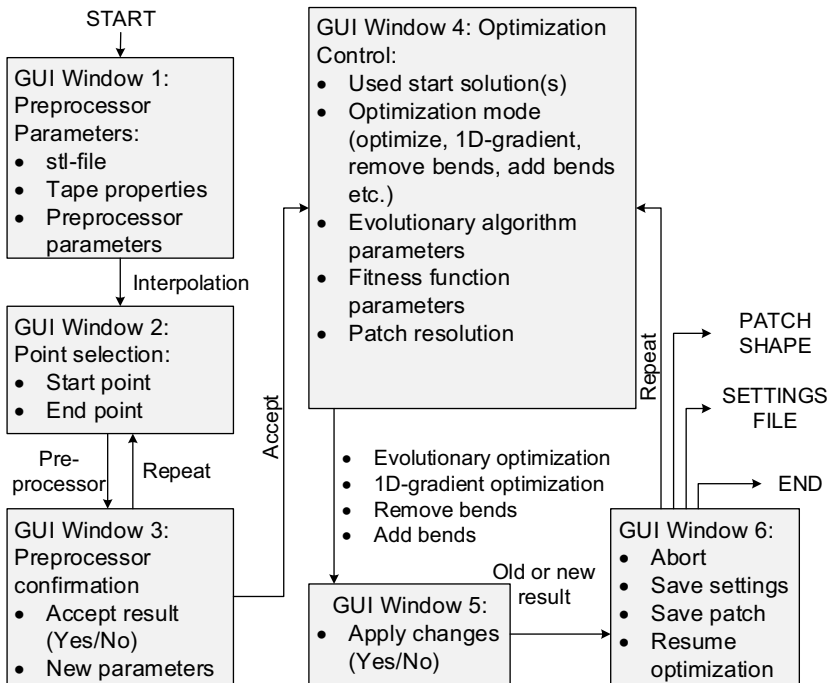


Figure 6-19: Optimization Workflow

In GUI Window 1, an .stl file and the preprocessors can be selected and parameterized (Figure 6-20). After the input file, the used tape is selected. The type is needed for writing bending parameters in the machine instruction. The tape width is needed for the correct kinematic modeling of the tape edges. The preprocessor(s) to be used are

ticked. Next, the resolution for the interpolation can be adjusted with only minor changes in both accuracy and computing time for resolutions above 1000 (points per coordinate direction). The center points of the triangles can be selected additionally to the corners as input for the interpolation. With the parameter “Width for edge-detection”, the distance between the planes in the 3D preprocessor solution can be adjusted. In the next field, the maximum allowed distance between the .stl file and the preprocessor solutions is given.

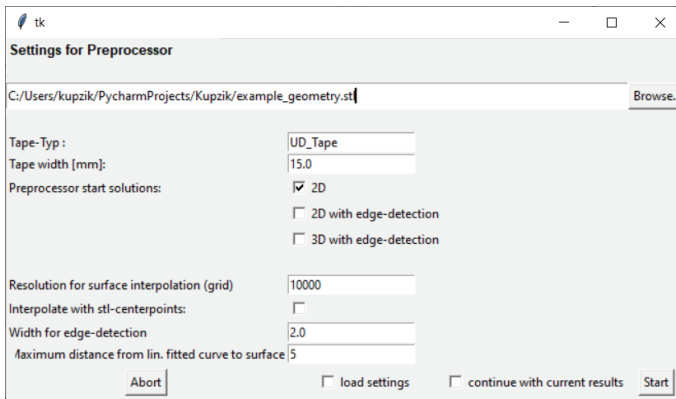


Figure 6-20: Preprocessor parameters in GUI Window 1

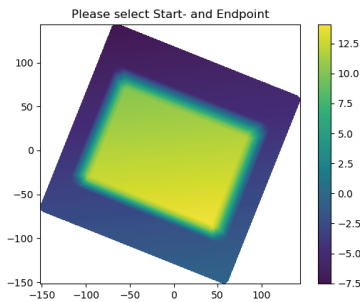


Figure 6-21: Presentation of the geometry in GUI Window 2

In GUI Window 2, the interpolated geometry is visualized to the user and the start and end point can be selected (Figure 6-21). The window shows a top view of the interpolation. Start and end point are selected by clicking on the interpolation surface.

Next, the preprocessor solutions are calculated. In informative windows, the centerlines of the selected solutions and their height profiles are shown (Figure 6-13). Afterward, the preprocessor solutions are shown in 3D plots. In GUI Window 3 (Figure 6-22), parameters can be adjusted by ticking “Try different setting”, or the optimization can be initiated by “Start”.

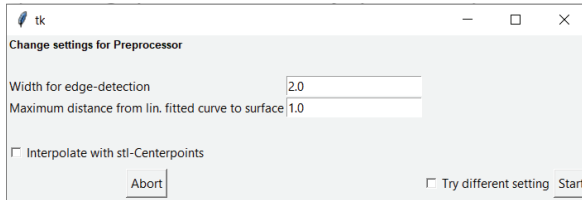


Figure 6-22: GUI Window 3: Confirmation of the preprocessor results

The optimization is controlled by the main GUI Window 4 (Figure 6-23). In the first section, the preprocessor solutions to be used are selected. The start solutions are optimized and overwritten individually, if any of the individual optimization functions is selected. They can either be optimized using evolutionary or simplified gradient optimization or manipulated by removing or adding bends. If none of the boxes in the individual optimization is ticked, the population of the optimization is initiated from all ticked preprocessor solutions, and the result is stored in the current best chromosome, which can then again be used for optimization. In the next section, the evolutionary algorithm (EA) parameters are defined, and production restrictions (de-)activated. Four sets of fitness weights and the transition generations between them can be defined. Finally, the type and number of evaluation points for the kinematic model are set.

After each manipulation or optimization run, the fitness development over the optimization time and the result are presented in a 3D visualization (Figure 6-18 (b), (c)). If bends with $\beta < 5^\circ$ occur in a solution, an alternative with those bends removed is proposed. The result can either be saved to the current best chromosome, discarded, or exported to machine instructions (Figure 6-24).

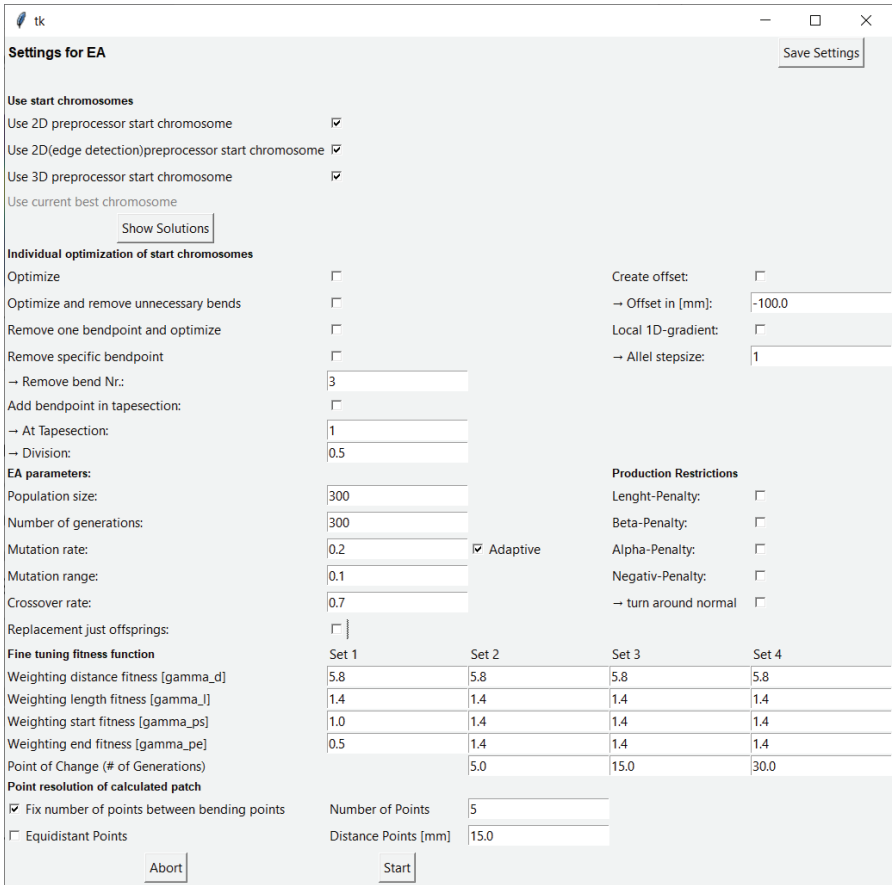


Figure 6-23: Optimization control in GUI Window 4

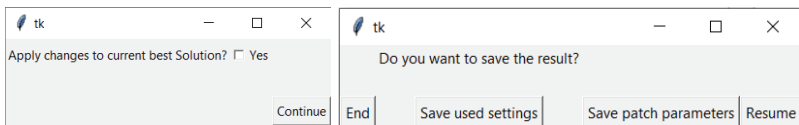


Figure 6-24: GUI Window 5 and 6: Confirmation and Export of a solution

6.8 Conclusion on Finding Process Compliant Near-net-shape Geometries

The Input Shape Optimization toolbox was developed and tested using various self-generated .stl files and the demonstrator geometries from the DFG GRK2078 project. All used geometries had a shell shape as can be expected for automotive LFT components. Four exemplary input geometries with optimization results are presented in Figure 6-25. With all tested geometries, the approach effectively supported the derivation of suitable bending machine code. In the visualization, it could be manually ensured that the preform shape is well suited to the CAD input file. The validation of the molding process following preforming, however, could not yet be executed, as the molding trials are scheduled to a later phase of the project.

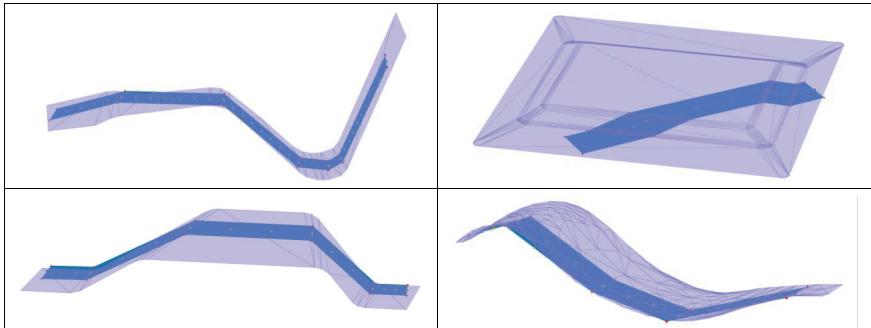


Figure 6-25: Results for four example geometries

The found shape optimization approach is suitable for structures that are bent from tape-shaped raw material. It cannot be used for optimizing other preforming processes like stamp draping. Future improvement can be obtained by integrating the approach into a loop with molding simulations. In such a loop, the quality of a preform would be evaluated based on their final position and shape after molding. This way, imperfections in the molding process could be compensated by an adapted shape and lay-in position of the preform.

7 Summary and Outlook

In this chapter, a summary of the research work in this thesis is given. In the outlook, measures of improvement for a series application and planned future work are presented.

7.1 Summary

Hybrid thermoplastic components combine the low cost of injection- or compression molded components with improved mechanical properties. They are made from a flowable component and continuous fiber reinforcements. Long-fiber-reinforced thermoplastics (LFT) are used as flowable component in this research project. UD-tapes are used for the reinforcement structure. In the preparation of the reinforcement structure, UD-tape is separated from a raw material supply, usually a spool, and preformed. The hybrid component is created in the co-molding step in which the reinforcement structure is embedded in the surrounding flowable material during solidification.

The literature review showed that a great share of the component cost is allocated to preparing the reinforcement structure. Additional process steps cause high costs. Furthermore, tooling cost increases the part price, especially for smaller batches. Methods for preforming unidirectional materials were screened and evaluated regarding their adaptability to various component shapes, their ability to preform thermoplastic materials, and the possibility to form complex shapes. None of the methods in state-of-the-art is able to flexibly form thermoplastic UD-tapes without specific tools.

This thesis aims to develop and commission a process that can preform UD-tapes for reinforcement structures in hybrid components without component-specific tooling. Therefore, a process development was started. The forming mechanisms drawing, bending, and shearing from (DIN 8582) were compared, and bending was selected as the most suitable for UD-reinforced thermoplastic tape for a well-controllable deformation and easy tempering. For flexibility, the motion is controlled via robotic swing folding. To avoid material degradation and avoid unwanted deformations, a small heated area and therefore a local bend is desired. The process behavior was examined in a finite element model to identify the influence of fiber content, tape thickness, tape width, and bend radius. To form complex shapes, a tape strip can be bent at several positions.

Three main tasks had to be solved to apply the novel process. Firstly, suitable hardware for supplying, heating, bending, and cutting the tape strips had to be designed in dependence on the process requirements. Secondly, parameters had to be found with which the hardware could be run for accurate bending. Thirdly, the process-dependent shape restrictions had to be regarded, and a way of adapting the bent shape to the set component shape had to be found.

Developing the hardware was the first started task during the research in this thesis. The design process was guided by (VDI 2221). To get an overview of the process' functions, it was analyzed in a functional chart according to (VDI 2860). It was identified that systems for the supply, movement, gripping, heating, and cutting of the tape are necessary. The tape is supplied from a spool by rollers that feed it through a guide. For additional stability, a clamp was added towards the exit of the guide. For the free movement of the end effector, a six-axis industrial robot was selected as kinematic system. It positions both the gripper as well as the heating unit on the tape. This way, the heating unit does not need its own axes for the placement of bends at a variable tape position or at a variable angle. A clamping gripper was selected for the force introduction. For the heating, resistive heating with direct contact or induction, convective heating, radiation heating, and contact heating were considered. After a ranking of prototypical heating units, radiation heating and contact heating were implemented. For the cutting, a pneumatically actuated blade was integrated into the supply unit. During the parameter examination, gained insights were constantly transferred into hardware improvements. One example is the evolution of a cooling nozzle at the gripper, which speeds up the manufacturing process.

To identify suitable process parameters, the swing folding process was systematically analyzed. A kinematic description of a bend was developed after a pure rotation of the end effector proved insufficient. It describes the movement of the end effector depending on the width of the softened tape area and the distance of the gripper to this area. The effects that were observed while experimentally varying the kinematic parameters correspond well with the finite element model of the process. The parameters for contact and radiation heating were analyzed separately from another. The heating yaw temperature and the waiting time between activating the heating and bending were varied for the contact heating. The waiting time between activating the heating and bending and the heating time during bending were examined for the radiation heating. The in-

fluence of the cooling time was analyzed for both heating methods. In a final experimental series, it could be shown that the correct selection of the kinematic parameters was essential for high-quality results. The tape needed to be molten before bending and re-solidified before opening the gripper. More than sufficient increases in heating or cooling showed little effect on the process result. The radiation heating showed better accuracy and a better chance of reliable long-term use compared to the contact heating.

For the industrial application of the process, a description of possible geometries and design methods are needed. Therefore, an input shape optimization toolbox was implemented, which can translate the component net shape into a similar, process-compliant preform shape. The toolbox can be operated via a graphical user interface (GUI). The two main functions are analytical preprocessing into tape segments for the generation of an approximate solution and an evolutionary optimization for the final geometry adjustment. This separation is beneficial as analytical solutions offer short computing times while an evolutionary optimization enables the adjustment to complex fitness criteria. For the analytical preprocessing, the distance evaluation between net shape surface and process compliant surface as well as edge detection methods are used. The evolutionary fitness function considers the average and maximum distance between net shape and process compliant geometry, the correct tape length, the correct positioning in the mold, and hardware-dependent limitations like maximum bending angles. In the GUI, all relevant settings for the shape optimization can be set and the progress can be monitored. Manual adjustment of the bend number and the evolutionary parameters can be made after each optimization run.

Finally, a summary and an outlook on the further processing of the bent UD-tapes are given. One possibility is the direct processing of the tapes in a mold. Alternatively, a more complex reinforcement structure can be assembled from the tape to simplify handling operations during the molding. To fully exploit the potential process flexibility, it can be combined with additive manufacturing.

7.2 Outlook

In the research connected to this thesis, a novel swing folding process for the flexible preforming of thermoplastic UD-tapes was successfully developed. For this process, hardware was developed, parameters were derived, and a shape optimization toolbox

was implemented. The hardware for the test setup was designed with simple adjustments and flexibility for research in mind. The used materials were selected based on availability on the market.

For serial production, aspects like wear-free guides and bearings should be considered. In the supply unit, the cutting unit could be redesigned to obtain a smaller distance between the unit's outlet and the blade, thus allowing shorter tape ends after the last bend. The largest potential for further improvement lies in the heating unit for softening the tape. During the experimentation, the contact heating showed some pollution with matrix, which degraded over time. This did not show any influence in the experimentation, but for series production, anti-stick coatings on the aluminum should be taken into account. For the radiation heating unit, more powerful units with better interference contour are commercially available if the budget for the devices and safety is set accordingly. If the safety concept allows the application of laser heating, it could be used due to its good controllability and power. A heating device that became available during the research work is the Heraeus humm3. It is based on a xenon flashbulb and guides the radiation to the heated zone in a quartz light guide prism (Lascelles & Brown et al. 2020). Resulting from the xenon flash bulb, rapid activation and deactivation and precise control of the power level should be possible (Monnot & Williams et al. 2018). This, and the high maximum output power, can be used to heat the tape rapidly and control its temperature during bending. The cooling process of the tape could also be accelerated as the heat can be rapidly deactivated, and the amount of residual heat in the hardware could be reduced. Furthermore, the smaller interference contour, resulting from the quartz guide, can widen the range of possible β angles as this was limited by the collision between heating unit and tape.

For industrial manufacturing of reinforcements, thicker raw materials should be used to increase the reinforcement effect. It could be shown that the process can be used for consolidated multi-layer tapes (Section 5.5). If the production volume is large enough for buying suitable raw material, either thicker tapes or pultruded profiles should be used. The commissioning of the process for this new material can be simplified by the experience gained during this thesis. A pragmatic approach would be to first examine the correct kinematic parameters on an overheated tape and later minimize heating until springback effects become noticeable. For the industrial use of any kind of material, tolerances of the process must be determined. This can be done by executing a

statistically relevant number of repetitions and calculating the process capability for various tolerance field widths.

The process functionality could be extended by forming a wider heated zone. For further flexibility, the width could be varied. The prerequisite for this would be a targeted laser beam heating with precise modeling of the heat demand, or a closed control loop to create and maintain the heated zone. To form the tape, the kinematic model should be extended with regard to lateral forces within the tape instead of the assumption of a constant bending momentum along the tape length. This way, the bending radius can be variable along the bend and geometric freedom is increased. To control this heating and movement, advanced modeling is needed. The connection between part shape and robot movement could for example be created by adding a vision system to generate data for machine learning during the robot movement. The data would have to include the shape of the tape and the position of the robot for each time step. Using this approach, the robot movement could be adjusted in real time during the bending process. Springback influence cannot be corrected during a single bending process, as it only becomes visible once the gripper releases the tape. Here the existing approach of measuring after the bend and correcting the next bends (Kupzik & Ding et al. 2020) could be extended using machine learning to overcome stability issues of the control.

The focus of this thesis was on the manufacturing of preforms for the local reinforcement of thermoplastic components. The assembly to reinforcement structures and the co-molding with thermoplastic hotmelt were demonstrated in a simplified setting. The assembly can take place in a spot welding station as shown in Figure 7-1 (A_Gerweck 2020). The already existing robotic arm can execute the handling tasks which are necessary for assembly.

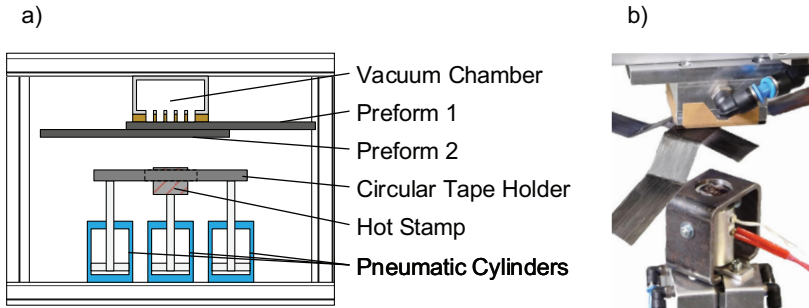


Figure 7-1: Outline (a) and implementation (b) of the assembly station

The molding step could be demonstrated rudimentary as the tooling for processing LFT was not yet accessible. A manual process using thermoplastic hotmelt as surrounding component material was set up (A_Mai 2020). This way, investigations with single and multiple layers of tape, and pre-consolidated tape preforms could be processed (Figure 7-2).

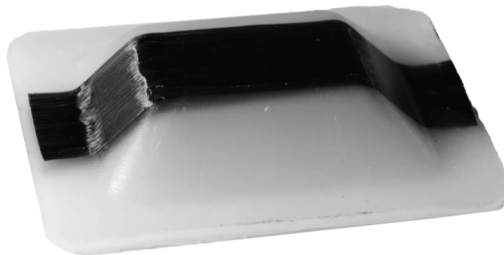


Figure 7-2: UD-reinforced specimen

The goal of future work is the industrial manufacturing of high-performance components from assembled reinforcement structures and LFT. The applicability of the process for tapes and thicker raw materials was shown. Single preforms were successfully joined to form reinforcement structures. However, the setting in demonstrating the co-molding was strongly simplified. The hot melt requires far less force for flowing compared to LFT. Therefore, thorough research on the co-molding of the preformed UD-tape strips is scheduled for the following generation of the research training group.

References

(A_Bachtin 2020)

Bachtin, A. (2020) MAP 1024, *Commissioning and experimental parameter analysis of different heating methods for a novel preform process*. Master's Thesis, Karlsruhe Institute of Technology, Karlsruhe, Germany, wbk Institute of Production Science. Guidance by: Kupzik, D.

(A_Biergans 2018)

Biergans, L. (2018) MAP 0879, *Development of a geometry optimization algorithm for automatic, flexible preforming of CFRP reinforcement structures*. Master's Thesis, Karlsruhe Institute of Technology, Karlsruhe, Germany, wbk Institute of Production Science. Guidance by: Kupzik, D.

(A_Brenner 2020)

Brenner, D. (2020) MAP 1158, *Investigation of the Behavior of a Modified Genetic Algorithm for the Shape Optimization of UD Tape Preforms*. Bachelor's Thesis, Karlsruhe Institute of Technology, Karlsruhe, Germany, wbk Institute of Production Science. Guidance by: Kupzik, D.

(A_Ding 2020)

Ding, J. (2020) MAP 1053, *Development and commissioning of a stereo vision unit for measurements and process control in a robot cell*. Master's Thesis, Karlsruhe Institute of Technology, Karlsruhe, Germany, wbk Institute of Production Science. Guidance by: Kupzik, D.

(A_Gerweck 2020)

Gerweck, M. (2020) MAP 1135, *Design and Validation of Concepts for Aligning and Joining UD-Tape Preforms*. Bachelor's Thesis, Karlsruhe Institute of Technology, Karlsruhe, Germany, wbk Institute of Production Science. Guidance by: Kupzik, D.

(A_Mai 2020)

Mai, D. (2020) MAP 1298, *Validation of a Preform Method through Statistical Analysis of the Preform Shape and Demonstration of Downstream Process Steps*. Bachelor's Thesis, Karlsruhe Institute of Technology, Karlsruhe, Germany, wbk Institute of Production Science. Guidance by: Kupzik, D.

(A_Mühlbeier 2019)

Mühlbeier, E. (2019) MAP 0944, *Development of a control system for a flexible forming cell for manufacturing unidirectional fiber reinforced structures*. Master's Thesis, Karlsruhe Institute of Technology, Karlsruhe, Germany, wbk Institute of Production Science. Guidance by: Kupzik, D.

(A_Nguyen 2018)

Nguyen, H. T. (2018) MAP 0788, *Conceptual design and implementation of a tape supply unit for a tool-free UD tape forming process*. Bachelor's Thesis, Karlsruhe Institute of Technology, Karlsruhe, Germany, wbk Institute of Production Science. Guidance by: Kupzik, D.

(A_Penev 2019)

Penev, P. (2019) MAP 0905, *Simulation of the bending zone in locally heated thermoplastic UD tapes during the forming process*. Master's Thesis, Karlsruhe Institute of Technology, Karlsruhe, Germany, wbk Institute of Production Science. Guidance by: Kupzik, D.

(A_Saur 2020)

Saur, L. (2020) MAP 1177, *Process parameter selection and process validation in a novel bending process for the preforming of UD tapes*. Bachelor's Thesis, Karlsruhe Institute of Technology, Karlsruhe, Germany, wbk Institute of Production Science. Guidance by: Kupzik, D.

(A_Steidle-Sailer 2021)

Steidle-Sailer, C. (2021) MAP 1346, *Development of a stereo optical measurement system for monitoring a robot cell manufacturing process*. Master's Thesis, Karlsruhe Institute of Technology, Karlsruhe, Germany, wbk Institute of Production Science. Guidance by: Kupzik, D.

(A_Vollmer 2018)

Vollmer, P. (2018) MAP 0789, *Development of a robot-based, variant flexible forming unit for preforming thermoplastic UD tapes*. Master's Thesis, Karlsruhe Institute of Technology, Karlsruhe, Germany, wbk Institute of Production Science. Guidance by: Kupzik, D.

(A_Wenzel 2020)

Wenzel, M. (2020) MAP 1250, *Shape Optimization of a CFRP component through geometry analysis and evolutionary algorithm*. Master's Thesis, Karlsruhe Institute

of Technology, Karlsruhe, Germany, wbk Institute of Production Science. Guidance by: Kupzik, D.

(A_Wi 2019)

Wi, S.-M. (2019) MAP 0887, *Experimental investigation of a novel, robot-based forming process for thermoplastic UD tapes*. Bachelor's Thesis, Karlsruhe Institute of Technology, Karlsruhe, Germany, wbk Institute of Production Science. Guidance by: Kupzik, D.

(Abts 2014)

Abts, G. (2014), *Kunststoff-Wissen für Einsteiger*, Hanser, München (Germany). <http://www.hanser-elibrary.com/action/showBook?doi=10.3139/9783446439290>. ISBN: 978-3-446-43925-2.

(Ahmad & Markina et al. 2020)

Ahmad, H.; Markina, A. A.; Porotnikov, M. V. & Ahmad, F. (2020), „A review of carbon fiber materials in automotive industry“, *IOP Conference Series: Materials Science and Engineering*, 971 , p. 32011, DOI:10.1088/1757-899X/971/3/032011.

(Alebooyeh & Wang et al. 2019)

Alebooyeh, M.; Wang, B.; Urbanic, R. J.; Djuric, A. & Kalami, H. (2019), „Investigating Collaborative Robot Gripper Configurations for Simple Fabric Pick and Place Tasks“, SAE International, Warrendale, PA, USA, DOI:10.4271/2019-01-0699.

(AL-Salami 2009)

AL-Salami, N. M.A. (2009), „Evolutionary Algorithm Definition“, *American Journal of Engineering and Applied Sciences*, 2 (4), p. 789–795, DOI:10.3844/ajeassp.2009.789.795.

(Andreozzi & Bessone et al. 2016)

Andreozzi, S.; Bessone, G. I.; Poala, M. B.; Bovo, M.; Amador, Silvia Fernandez De Alaiza; Giargia, E.; Niccolai, A.; Papetti, V. & Mariani, S. (2016), „Self-adaptive Multi-purpose Modular Origami Structure“, *Procedia Engineering*, 161 , p. 1423–1427, DOI:10.1016/j.proeng.2016.08.604.

(Angerer & Ehinger et al. 2011)

Angerer, A.; Ehinger, C.; Hoffman, A.; Reif, W. & Reihart, G. (2011), „Design of an Automation System for Preforming Processes in Aerospace Industries“. *2011 IEEE*

International Conference on Science and Engineering. Trieste, Italy. ISBN: 978-1-4577-1730-7, DOI:10.1109/CASE.2011.6042411.

(Arnold & Sutcliffe et al. 2016)

Arnold, S. E.; Sutcliffe, M.P.F. & Oram, W.L.A. (2016), „Experimental measurement of wrinkle formation during draping of non-crimp fabric“, *Composites Part A: Applied Science and Manufacturing*, 82 , p. 159–169, DOI:10.1016/j.compositesa.2015.12.011.

(Bäck 1996)

Bäck, T. (1996), *Evolutionary algorithms in theory and practice. Evolution strategies, evolutionary programming, genetic algorithms*, Oxford University Press, New York. ISBN: 9780195356700.

(Bandivadekar & Bodek et al. 2008)

Bandivadekar, A.; Bodek, K.; Cheah, L.; Evans, C.; Groode, T.; Heywood, J.; Kasseris, E.; Kromer, M. & Weiss, M. (2008), *On the road in 2035. Reducing transportation's petroleum consumption and GHG emissions*, Massachusetts Institute of Technology, Cambridge, MA, USA.

(Baumgärtner & John et al. 2016)

Baumgärtner, S.; John, J.; Henning, F.; Huber, T. & Hangs, B. (2016), „The Efficient Route to Tailored Organo Sheets. Producing CFRP Efficiently in a Vacuum Using Infrared Radiation“, *Kunststoffe international*, 2016 (10), p. 123–127.

(Behrens & Raatz et al. 2017)

Behrens, B.-A.; Raatz, A.; Hübner, S.; Bonk, C.; Bohne, F.; Bruns, C. & Micke-Camuz, M. (2017), „Automated Stamp Forming of Continuous Fiber Reinforced Thermoplastics for Complex Shell Geometries“, *Procedia CIRP*, 66 , p. 113–118.

(Bigio & Israel et al. 2005)

Bigio, L.; Israel, R.; Chowdhury, A. & Lieszkovsky, L., *IR-COATED HALOGEN LAMP USING REFLECTIVE END COATS* (2005), USA US 6,967,443 B2.

(Bikiaris 2011)

Bikiaris, D. (2011), „Can nanoparticles really enhance thermal stability of polymers? Part II: An overview on thermal decomposition of polycondensation polymers“, *Thermochimica Acta*, 523 (1-2), p. 25–45, DOI:10.1016/j.tca.2011.06.012.

(Björnsson & Karlsson 2016)

Björnsson, L.-H. & Karlsson, S. (2016), „The potential for brake energy regeneration under Swedish conditions“, *Applied Energy*, 168 (1), p. 75–84, DOI:10.1016/j.apenergy.2016.01.051.

(Blanke & Birden et al. 1960)

Blanke, B. C.; Birden, J. H.; Jordan, K. C. & Murphy, E. L. (1960), *NUCLEAR BATTERY-THERMOCOUPLE TYPE SUMMARY REPORT*, Monsanto Research Corporation, DC, USA.

(Boisse & Hamila et al. 2011)

Boisse, P.; Hamila, N.; Vidal-Sallé, E. & Dumont, F. (2011), „Simulation of wrinkling during textile composite reinforcement forming. Influence of tensile, in-plane shear and bending stiffnesses“, *Composites Science and Technology*, 71 (5), p. 683–692, DOI:10.1016/j.compscitech.2011.01.011.

(Both & Brüggemann et al. 2011)

Both, J.; Brüggemann, T.; Dosch, S.; Elser, J.; Kronthaler, M.; Morasch, A.; Otter, M.; Pietzka, D.; Selvaggio, A.; Weddeling, C.; Wehrle, E.; Wirth, F.; Baier, H.; Biermann, D.; Brosius, A.; Fleischer, J.; Lanza, G.; Schulze, V.; Tekkaya, A. & Zäh, M. (2011), „Advanced manufacturing and design techniques for lightweight structures“, *International Aluminium Journal*, 87 , p. 60–64.

(Boylan & Castro 2003)

Boylan, S. & Castro, J. M. (2003), „Effect of reinforcement type and length on physical properties, surface quality, and cycle time for sheet molding compound (SMC) compression molded parts“, *Journal of Applied Polymer Science*, 90 , p. 2557–2571, DOI:10.1002/app.12726.

(Brannon 2003)

Brannon, R. (2003), *Mohr's Circle and more circles*, University of Utah. <https://csm.mech.utah.edu/content/wp-content/uploads/2011/03/GoBagMohrsCircle.pdf>.

(Brecher & Kukla et al. 2015)

Brecher, C.; Kukla, C.; Schars, R. & Emonts, M. (2015), „FORM-ADAPTIVE GRIPPING SYSTEM FOR LIGHT-WEIGHT PRODUCTIONS“. *20th International Conference on Composite Materials*. Copenhagen, Denmark. <https://iccm-central.org/Proceedings/ICCM20proceedings/>.

(Brecher & Emonts et al. 2013)

Brecher, C.; Emonts, M.; Ozolin, B. & Schares, R. (2013), „Handling of Preforms and Prepregs for Mass Production of Composites“. *The 19th international conference on composite materials*. Montreal, Canada. <https://iccm-central.org/Proceedings/ICCM19proceedings/>.

(Bruns & Raatz 2017)

Bruns, C. & Raatz, A. (2017), „Simultaneous Grasping and Heating Technology for Automated Handling and Preforming of Continuous Fiber Reinforced Thermoplastics“, *Procedia CIRP*, 66 , p. 119–124, DOI:10.1016/j.procir.2017.03.286.

(Bücheler 2017)

Bücheler, D. (2017), *Locally Continuous-fiber Reinforced Sheet Molding Compound*. Doctoral Dissertation, Karlsruhe Institute of Technology, Karlsruhe, Germany.

(Chawla 2019)

Chawla, K. K. (2019), *Composite Materials*, Springer International Publishing, Cham, Switzerland. ISBN: 978-3-030-28982-9.

(Chen & Boisse et al. 2011)

Chen, Q.; Boisse, P.; Park, C. H.; Saouab, A. & Bréard, J. (2011), „Intra/inter-ply shear behaviors of continuous fiber reinforced thermoplastic composites in thermoforming processes“, *Composite Structures*, 93 (7), p. 1692–1703, DOI:10.1016/j.compstruct.2011.01.002.

(Coutandin 2020)

Coutandin, S. (2020), *Prozessstrategien für das automatisierte Preforming von bebinderten textilen Halbzeugen mit einem segmentierten Werkzeugsystem*. Doctoral Dissertation, Shaker, Düren, Germany. ISBN: 978-3-8440-7413-0.

(Coutandin & Brandt et al. 2018)

Coutandin, S.; Brandt, D.; Heinemann, P.; Ruhland, P. & Fleischer, J. (2018), „Influence of punch sequence and prediction of wrinkling in textile forming with a multi-punch tool“, *Production Engineering*, 12 (6), p. 779–788, DOI:10.1007/s11740-018-0845-9.

(Coutandin & Wurba et al. 2019)

Coutandin, S.; Wurba, A.; Luft, A.; Schmidt, F.; Dackweiler, M. & Fleischer, J.

(2019), „Mechanical characterisation of the shear, bending and friction behaviour of bindered woven fabrics during the forming process“, *Materialwissenschaft und Werkstofftechnik*, 50 (12), p. 1573–1587, DOI:10.1002/mawe.201900074.

(Cramer & Beidleman et al. 2009)

Cramer, D. R.; Beidleman, N. J.; Chapman, C. R.; Evans, D. O.; Passmore, M. K. & Skinner, M. L., *System and method for the rapid, automated creation of advanced composite tailored blanks* (2009), US8168029 B2.

(Davis & Graham et al. 2003)

Davis, B.; Graham, P.; Osswald, T. A. & Rios, A. (2003), *Compression molding*, Hanser, Munich, Germany. ISBN: 978-3-446-22166-6.

(Dieffenbacher 2018)

Dieffenbacher (2018), *Dieffenbacher: Effiziente Großserienfertigung von Composite-Bauteilen | K-AKTUELL.de*, Kunststoff Web [16.06.2020]. <https://www.k-aktuell.de/dieffenbacher-effiziente-grossserienfertigung-von-composite-bauteilen-57001/>.

(DIN 8582)

Deutsches Institut für Normen 8582 (2003), *Fertigungsverfahren Umformen*.

(DIN 8586)

Deutsches Institut für Normen 8586 (2003), *Fertigungsverfahren Biegeumformen*.

(Dombrovsky 2011)

Dombrovsky, L. A. (2011), *Infrared properties of carbon fibers* [23.09.2021]. <http://thermopedia.com/content/155/>.

(Ehinger 2012)

Ehinger, C. A. (2012), *Automatisierte Montage von Faserverbund-Vorformlingen*. Doctoral Dissertation, TU München, Munich, Germany, Lehrstuhl für Betriebswissenschaften und Montagetechnik.

(Eiben & Smit 2011)

Eiben, A. E. & Smit, S. K. (2011), „Parameter tuning for configuring and analyzing evolutionary algorithms“, *Swarm and Evolutionary Computation*, 1 (1), p. 19–31, DOI:10.1016/j.swevo.2011.02.001.

(Eiben & Smith 2015)

Eiben, A. E. & Smith, J. E. (2015), *Introduction to evolutionary computing*,

Springer, Berlin, Germany. <http://dx.doi.org/10.1007/978-3-662-44874-8>. ISBN: 978-3-662-44873-1.

(Eiliat & Urbanic 2014)

Eiliat, H. & Urbanic, R. J. (2014), „Using Genetic Algorithms to Optimize the Build Orientation for Fused Deposition Modeled Components Containing Internal Reinforcement Structures“. *Proceedings of the ASME 2014 International Mechanical Engineering Congress and Exposition*. Montreal, Quebec, Canada, American Society of Mechanical Engineers. ISBN: 978-0-7918-4644-5, DOI:10.1115/IMECE2014-37683.

(Eiliat & Urbanic 2019)

Eiliat, H. & Urbanic, J. (2019), „Determining the relationships between the build orientation, process parameters and voids in additive manufacturing material extrusion processes“, *The International Journal of Advanced Manufacturing Technology*, 100 (1-4), p. 683–705, DOI:10.1007/s00170-018-2540-6.

(Elkington & Bloom et al. 2015)

Elkington, M.; Bloom, D.; Ward, C.; Chatzimichali, A. & Potter, K. (2015), „Hand layup: understanding the manual process“, *Advanced Manufacturing: Polymer & Composites Science*, 1 (3), p. 138–151. <https://youtu.be/eJ1YvKxgb4M>, DOI:10.1080/20550340.2015.1114801.

(Elkington & Ward et al. 2016)

Elkington, M.; Ward, C. & Potter, K. (2016), „Automated layup of sheet prepregs on complex molds“, *Journal of Advanced Materials*, 3 , p. 70–84. [https://research-information.bristol.ac.uk/en/publications/automated-layup-of-sheet-prepregs-on-complex-moulds\(3e22f0d2-0b29-498c-a2d4-d05d95c978ad\).html](https://research-information.bristol.ac.uk/en/publications/automated-layup-of-sheet-prepregs-on-complex-moulds(3e22f0d2-0b29-498c-a2d4-d05d95c978ad).html).

(Ellingsen & Singh et al. 2016)

Ellingsen, L. A.-W.; Singh, B. & Strømman, A. H. (2016), „The size and range effect: lifecycle greenhouse gas emissions of electric vehicles“, *Environmental Research Letters*, 11 (5), p. 54010, DOI:10.1088/1748-9326/11/5/054010.

(Engel & Manns et al. 2020)

Engel, B.; Manns, M.; Tuli, T. B. & Reuter, J. (2020), „Roboterunterstütztes Biegen von Verbundrohren“, *VDI-Z*, 162 (12), p. 49–51, DOI:10.37544/0042-1766-2020-12-49.

(Evans & Mclard et al. 2014)

Evans, D. O.; Mclard, C.; Weinman, D.; Beachy, W. & Borgmann, R., *Method and System for Producing Composite Components at an increased Laying Rate* (2014), WO 2014/140145 A1.

(EVONIK Industries 2017)

EVONIK Industries (2017), *VESTAPE Uni-directional tapes for structural light-weight design. Datasheet* [23.09.2021]. <https://tp-composites.com/wp-content/uploads/sites/3/2017/04/VESTAPE-2-2017.pdf>.

(Fantoni & Santochi et al. 2014)

Fantoni, G.; Santochi, M.; Dini, G.; Tracht, K.; Scholz-Reiter, B.; Fleischer, J.; Kristoffer Lien, T.; Seliger, G.; Reinhart, G.; Franke, J.; Nørgaard Hansen, H. & Verl, A. (2014), „Grasping devices and methods in automated production processes“, *CIRP Annals*, 63 (2), p. 679–701, DOI:10.1016/j.cirp.2014.05.006.

(Fleischer 1989)

Fleischer, J. (1989), *Rechnerunterstützte Technologieplanung für die flexibel automatisierte Fertigung von Abkantteilen*. Doctoral Dissertation, Universität Karlsruhe (TH), Karlsruhe, Germany, Institut für Werkzeugmaschinen und Betriebstechnik.

(Fleischer 2021)

Editor: Fleischer, J. (2021), *Intrinsische Hybridverbunde für Leichtbautragstrukturen. Grundlagen der Fertigung, Charakterisierung und Auslegung*, Springer Vieweg, Berlin, Germany, Heidelberg, Germany. ISBN: 978-3-662-62833-1.

(Fleischer & Schulze et al. 2014)

Fleischer, J.; Schulze, V.; Burtcher, J. & Dosch, S. (2014), „Robot-based Guiding of Extrusion Profiles-increase of Guiding Accuracy by Considering the Temperature-dependent Effects“, *Procedia CIRP*, 18 , p. 21–26, DOI:10.1016/j.procir.2014.06.101.

(Fleischer & Albers et al. 2016)

Fleischer, J.; Albers, A.; Coutandin, S. & Spadinger, M. (2016), „Materialeffizienz im Resin-Transfer-Moulding-Prozess. Ganzheitliche Subpreforming-Strategie erlaubt Reduktion des Faserverschnitts“, *VDI-Z*, 158 (1/2), p. 82–84.

(Fleischer & Teti et al. 2018)

Fleischer, J.; Teti, R.; Lanza, G.; Mativenga, P.; Möhring, H.-C. & Caggiano, A.

(2018), „Composite materials parts manufacturing“, *CIRP Annals*, 67 (2), p. 603–626, DOI:10.1016/j.cirp.2018.05.005.

(Förster & Ballier et al. 2017)

Förster, F.; Ballier, F.; Coutandin, S.; Defranceski, A. & Fleischer, J. (2017), „Manufacturing of Textile Preforms with an Intelligent Draping and Gripping System“, *Procedia CIRP*, 66 , p. 39–44, DOI:10.1016/j.procir.2017.03.370.

(Gertner & Miller 1996)

Gertner, Y. & Miller, A. K. (1996), „Die-Less Forming of Large and Variable-Radii of Curvature in Continuous-Fiber Thermoplastic-Matrix Composite Materials“, *Journal of Thermoplastic Composite Materials*, 9 , p. 151–182.

(Graf & Richter et al. 2018)

Graf, J.; Richter, C. & Reinhart, G. (2018), „Automated handling of high-temperature thermoplastic Carbon Fiber material for a large-scale production“ in *Tagungsband des 2. Kongresses Montage Handhabung Industrieroboter*, Editors: T. Schüppstuhl, K. Tracht & J. Franke, Springer, Berlin, Germany, Heidelberg, Germany, p. 188–196.

(Grimme & Bossek 2018)

Grimme, C. & Bossek, J. (2018), *Einführung in die Optimierung. Konzepte, Methoden und Anwendungen*, Springer Vieweg, Wiesbaden, Germany.
<http://dx.doi.org/10.1007/978-3-658-21151-6>. ISBN: 978-3-658-21150-9.

(Gupta & Bourne et al. 1998)

Gupta, S. K.; Bourne, D. A.; Kim, K. H. & Krishnan, S. S. (1998), „Automated process planning for sheet metal bending operations“, *Journal of Manufacturing Systems*, 17 (5), p. 338–360, DOI:10.1016/S0278-6125(98)80002-2.

(Habla & Kropka et al. 2019)

Habla, F.; Kropka, M.; Muehlbacher, M.; Neumeyer, T. & Altstädt, V. (2019), „Tailor Made Hybrid Laminates Based on UD-Tapes - A Way to Efficient Thermoplastic Components“, *Key Engineering Materials*, 809 , p. 41–46, DOI:10.4028/www.scientific.net/KEM.809.41.

(Henning & Moeller 2011)

Henning, F. & Moeller, E. (2011), *Handbuch Leichtbau. Methoden, Werkstoffe, Fertigung*, Hanser, Munich, Germany. ISBN: 978-3-446-42267-4.

(Heuss & Müller et al. 2012)

Heuss, R.; Müller, N.; van Sintern, W.; Starke, A. & Tschiesner, A. (2012), *Lightweight, heavy impact. How carbon fiber and other lightweight materials will develop across industries and specifically in automotive*, McKinsey & Company. https://www.mckinsey.com/~/media/mckinsey/dotcom/client_service/automotive%20and%20assembly/pdfs/lightweight_heavy_impact.ashx.

(Hirsch 2011)

Hirsch, J. (2011), „Aluminium in Innovative Light-Weight Car Design“, *Materials Transactions*, 52 (5), p. 818–824, DOI:10.2320/matertrans.L-MZ201132.

(Holmes 2014)

Holmes, M. (2014), „Continued growth for European GRP market“, *Reinforced Plastics*, 58 (6), p. 28–30, DOI:10.1016/S0034-3617(14)70247-4.

(Huang & Guo et al. 2020)

Huang, P.-Y.; Guo, Z.-S. & Feng, J.-M. (2020), „General Model of Temperature-dependent Modulus and Yield Strength of Thermoplastic Polymers“, *Chinese Journal of Polymer Science*, 38 (4), p. 382–393, DOI:10.1007/s10118-020-2360-7.

(Iman & Helton et al. 1981)

Iman, R. L.; Helton, J. C. & Campbell, J. E. (1981), „An Approach to Sensitivity Analysis of Computer Models: Part I—Introduction, Input Variable Selection and Preliminary Variable Assessment“, *Journal of Quality Technology*, 13 (3), p. 174–183, DOI:10.1080/00224065.1981.11978748.

(Joost 2012)

Joost, W. J. (2012), „Reducing Vehicle Weight and Improving U.S. Energy Efficiency Using Integrated Computational Materials Engineering“, *JOM*, 64 (9), p. 1032–1038, DOI:10.1007/s11837-012-0424-z.

(Joppich 2019)

Joppich, T. (2019), *Beitrag zum Umformverhalten von PA6/CF Gelegelaminaten im nicht-isothermen Stempelumformprozess*. Doctoral Dissertation, Karlsruhe Institute of Technology, Karlsruhe, Germany.

(Joppich & Doerr et al. 2016)

Joppich, T.; Doerr, D.; van der Meulen, L.; Link, T.; Hangs, B. & Henning, F. (2016), „Layup and process dependent wrinkling behavior of PPS/CF UD tape-

laminates during non-isothermal press forming into a complex component“. *ESA-FORM 2016*. Nantes, France, p. 27–29, DOI:10.1063/1.4963568.

(Joppich & Menrath et al. 2017)

Joppich, T.; Menrath, A. & Henning, F. (2017), „Advanced Molds and Methods for the Fundamental Analysis of Process Induced Interface Bonding Properties of Hybrid, Thermoplastic Composites“, *Procedia CIRP*, 66 , p. 137–142, DOI:10.1016/j.procir.2017.03.275.

(Kant & Joshi et al. 2013)

Kant, R.; Joshi, S. N. & Dixit, U. S. (2013), „State of the art and Experimental Investigation on Edge Effect in Laser Bending Process“. *Proceedings of National Conference on Recent Advancement in Mechanical Engineering (NCRAME-2013)*. Pauri, India, p. 189–197.

(Kim & Yarlagadda et al. 2002)

Kim, H.; Yarlagadda, S.; Gillespie, J. W.; Shevchenko, N. B. & Fink, B. K. (2002), „A study on the induction heating of carbon fiber reinforced thermoplastic composites“, *Advanced Composite Materials*, 11 (1), p. 71–80, DOI:10.1163/156855102753613309.

(Kordi & Hüsing et al. 2007)

Kordi, M. T.; Hüsing, M. & Corves, B. (2007), „Development of a Multifunctional Robot Endeffector System for Automated Manufacture of Textile Preforms“. *IEEE/ASME international conference on advanced intelligent mechatronics*. Zurich, Switzerland. ISBN: 9781424412631. <http://ieeexplore.ieee.org/servlet/opac?punumber=4412397>.

(Kropka & Muehlbacher et al. 2017)

Kropka, M.; Muehlbacher, M.; Neumeyer, T. & Altstaedt, V. (2017), „From UD-tape to Final Part – A Comprehensive Approach Towards Thermoplastic Composites“, *Procedia CIRP*, 66 , p. 96–100, DOI:10.1016/j.procir.2017.03.371.

(Kühnel & Schuster et al. 2014)

Kühnel, M.; Schuster, A.; Buchheim, A.; Kießig, M.; Gerngroß, T. & Kupke, M. (2014), „Automatisiertes endkonturnahes Preforming Carbonfaser-Verstärkter Thermoplaste mittels robotischer Halbzeugablage“ in 63. *Deutscher Luft- und Raumfahrtkongress*, Augsburg, Germany. [https://publikationen.dglr.de/?tx_dglr-publications_pi1\[document_id\]=340052](https://publikationen.dglr.de/?tx_dglr-publications_pi1[document_id]=340052).

(Kunz & Raatz et al. 2013)

Kunz, H.; Raatz, A.; Dilger, K.; Dietrich, F.; Schnurr, R. & Dröder, K. (2013), „Form-flexible Handling Technology for Automated Preforming“. *Proceedings of the 19th International Conference on Composite Materials*. Montréal, Canada. <http://www.iccm-central.org/Proceedings/ICCM19proceedings/>.

(Kunze & Böhm et al. 2019)

Kunze, E.; Böhm, R.; Geller, S. & Gude, M. (2019), „Experimental analysis of process induced draping effects in textile preforms. AIP Conference Proceedings 2113“. *PROCEEDINGS OF THE 22ND INTERNATIONAL ESAFORM CONFERENCE ON MATERIAL FORMING*. Vitoria-Gasteiz, Spain, AIP Publishing, p. 20012, DOI:10.1063/1.5112517.

(Kupzik & Bachtin et al. 2021)

Kupzik, D.; Bachtin, A.; Coutandin, S. & Fleischer, J. (2021), „EXPERIMENTAL PARAMETER IDENTIFICATION FOR THE BENDING BASED PREFORMING OF THERMOPLASTIC UD-TAPE“. *Technologies for economic and functional light-weight design. Conference proceedings 2020*, Editors: K. Dröder & T. Vietor, Springer Vieweg, Berlin. ISBN: 978-3-662-62924-6.

(Kupzik & Biergans et al. 2019)

Kupzik, D.; Biergans, L.; Coutandin, S. & Fleischer, J. (2019), „Kinematic Description and Shape Optimization of UD-Tape Reinforcements Manufactured with a Novel Preforming Process“, *Procedia CIRP*, 85 , p. 78–83, DOI:10.1016/j.procir.2019.09.016.

(Kupzik & Ding et al. 2020)

Kupzik, D.; Ding, J.; Coutandin, S. & Fleischer, J. (2020), „Digital Process Management for the Integrated Bending of Thermoplastic CFRP Tapes“, *Procedia CIRP*, 93 , p. 514–519, DOI:10.1016/j.procir.2020.04.061.

(Lamontia & Funck et al. 2003)

Lamontia, M.; Funck, S. B.; Gruber, M. B.; Cope, R. D. & Waibel, Brian J., Gopez, Nanette M. (2003), „MANUFACTURING FLAT AND CYLINDRICAL LAMINATES AND BUILT UP STRUCTURE USING AUTOMATED THERMOPLASTIC TAPE LAYING, FIBER PLACEMENT, AND FILAMENT WINDING“, *Sampe Journal*, 39 (2), p. 30–43.

(Lang 1989)

Lang, R. J. (1989), *TreeMaker*. <http://www.langorigami.com/article/treemaker>.

(Lascelles & Brown et al. 2020)

Lascelles, P.; Brown, M. & Williams, D. (2020), *hum3 - Our Journey to Industrialisation*, Heraeus, Webinar. https://www.heraeus.com/en/hng/uv_ir_flash_academy/webinars/hum3_our_journey_to_industrialisation.html.

(Le Louët & Rousseau et al. 2017)

Le Louët, V.; Rousseau, B.; Le Corre, S.; Boyard, N.; Tardif, X.; Delmas, J. & De-launay, D. (2017), „Study of the reflective behaviour of carbon fibres reinforced polymer composite up to 450°C“. *Proceedings of the 20th International ESAFORM Conference on Material Forming. ESAFORM 2017 : Dublin, Ireland, 26-28 April 2017*, Editors: D. Brabazon, S. Naher & I. U. Ahad, AIP Publishing, Melville, New York, p. 120011. ISBN: 978-0-7354-1580-5, DOI:10.1063/1.5008149.

(Lee & Yang et al. 2014)

Lee, E.-H.; Yang, D.-Y. & Yang, W.-H. (2014), „Numerical modeling and experimental validation of focused surface heating using near-infrared rays with an elliptical reflector“, *International Journal of Heat and Mass Transfer*, 78 , p. 240–250, DOI:10.1016/j.ijheatmasstransfer.2014.06.073.

(Liao & Wang 2003)

Liao, X. & Wang, G.G. (2003), „Evolutionary path planning for robot assisted part handling in sheet metal bending“, *Robotics and Computer-Integrated Manufacturing*, 19 (5), p. 425–430, DOI:10.1016/S0736-5845(03)00053-X.

(Lienhard & Lienhard 2020)

Lienhard, J. H. [I.] & Lienhard, J. H. [V.] (2020), *A Heat Transfer Textbook*, Phlogiston Press, Cambridge, Massachusetts, USA. <http://ahtt.mit.edu>.

(Lightfoot & Wisnom et al. 2013)

Lightfoot, J. S.; Wisnom, M. R. & Potter, K. (2013), „Defects in woven preforms: Formation mechanisms and the effects of laminate design and layup protocol“, *Composites Part A: Applied Science and Manufacturing*, 51 (4), p. 99–107, DOI:10.1016/j.compositesa.2013.04.004.

(Löchte & Kunz et al. 2014)

Löchte, C.; Kunz, H.; Schnurr, R.; Langhorst, S.; Dietrich, F.; Raatz, A.; Dilger, K.

& Dröder, K. (2014), „Form-Flexible Handling and Joining Technology (FormHand) for the Forming and Assembly of Limp Materials“, *Procedia CIRP*, 23, p. 206–211, DOI:10.1016/j.procir.2014.10.086.

(Lüderwald & Merz 1978)

Lüderwald, I. & Merz, F. (1978), „Über den thermischen Abbau von Polyamiden der Nylon-Reihe“, *Angewandte Makromolekulare Chemie*, 74 (1), p. 165–185, DOI:10.1002/apmc.1978.050740112.

(Luersen & Le Riche 2004)

Luersen, M. A. & Le Riche, R. (2004), „Globalized Nelder–Mead method for engineering optimization“, *Computers & Structures*, 82 (23-26), p. 2251–2260, DOI:10.1016/j.compstruc.2004.03.072.

(Lukaszewicz & Ward et al. 2012)

Lukaszewicz, D. H.-J.A.; Ward, C. & Potter, K. D. (2012), „The engineering aspects of automated prepreg layup. History, present and future“, *Composites Part B: Engineering*, 43 (3), p. 997–1009, DOI:10.1016/j.compositesb.2011.12.003.

(Malhan & Kabir et al. 2018)

Malhan, R. K.; Kabir, A. M.; Shembekar, A. V.; Shah, B.; Gupta, S. K. & Centea, T. (2018), „Hybrid Cells for Multi-Layer Prepreg Composite Sheet Layup“. *2018 IEEE 14th International Conference on Automation Science and Engineering (CASE)*. Munich, Germany, IEEE, p. 1466–1472. ISBN: 978-1-5386-3593-3, DOI:10.1109/COASE.2018.8560586.

(Mascarin & Hannibal et al. 2016)

Mascarin, A.; Hannibal, T.; Raghunthan, A.; Ivanic, Z. & Clark, M. (03/2016), *Vehicle Lightweighting: Mass Reduction Spectrum Analysis and Process Cost Modeling*, Idaho National Laboratory, Idaho Falls, Idaho, USA.

(Matsuo & Hojo et al. 2017)

Matsuo, T.; Hojo, M. & Kageyama, K. (2017), „INFLUENCE OF GRIPPING CONDITION AND MATRIX TYPE ON TENSILE PROPERTIES OF UNIDIRECTIONAL CARBON FIBER REINFORCED THERMOPLASTIC COMPOSITES“. *Proceedings of 21st International Conference on Composite Materials*. Xi'an, China. <https://iccm-central.org/Proceedings/ICCM21proceedings/>.

(McGuinness & Brádaigh 1995)

McGuinness, G. B. & Brádaigh, C.M.Ó. (1995), „Effect of preform shape on buckling of quasi-isotropic thermoplastic composite laminates during sheet forming“, *Composites Manufacturing*, 6 (3-4), p. 269–280, DOI:10.1016/0956-7143(95)95020-Y.

(McGuinness & O Bradaigh 1997)

McGuinness, G. B. & O Bradaigh, C. M. (1997), „Characterisation of thermoplastic composite melts in rhombus-shear: the picture frame experiment“, *Composites Part A: Applied Science and Manufacturing*, 29 (1-2), p. 115–132, DOI:10.1016/S1359-835X(97)00061-4.

(McKay & Beckman et al. 1979)

McKay, M. D.; Beckman, R. J. & Conover, W. J. (1979), „Comparison of Three Methods for Selecting Values of Input Variables in the Analysis of Output from a Computer Code“, *Technometrics*, 21 (2), p. 239–245, DOI:10.1080/00401706.1979.10489755.

(Mennig & Stoeckhert 2013)

Editors: Mennig, G. & Stoeckhert, K. (2013), *Mold-Making Handbook*, Hanser, München, Germany. <http://www.sciencedirect.com/science/book/9781569904466>. ISBN: 978-1-56990-446-6.

(Ministry of Natural Resources Canada 2014)

Ministry of Natural Resources Canada (2014), *Learn the facts: Weight affects fuel consumption*, Ministry of Natural Resources Canada.

(Moeller 2014)

Editor: Moeller, E. (2014), *Handbuch Konstruktionswerkstoffe. Auswahl, Eigenschaften, Anwendung*, Hanser, München. ISBN: 978-3-446-43169-0.

(Moll & Ohlberg et al. 2019)

Moll, P.; Ohlberg, L.; Salzer, S.; Coutandin, S. & Fleischer, J. (2019), „Integrated Gripping-system for Heating and Preforming of Thermoplastic Unidirectional Tape Laminates“, *Procedia CIRP*, 85 , p. 266–271, DOI:10.1016/j.procir.2019.10.006.

(Monnot & Williams et al. 2018)

Monnot, P.; Williams, D. & Di Francesco, M. (2018), „POWER CONTROL OF A FLASHLAMP-BASED HEATING SOLUTION FOR AUTOMATED DRY FIBRE

PLACEMENT“. *Proceedings of ECCM18 - 18th European Conference on Composite Materials*. Athens, Greece. ISBN: 9781510896932. <https://iccm-central.org/Proceedings/ICCM18proceedings/>.

(Morii & Jumonji 2009)

Morii, T. & Jumonji, N. (2009), „EFFECTS OF FIBER LENGTH ON TENSILE AND AE PROPERTIES OF GLASS FIBER/POLYPROPYLENE INJECTION MOLDINGS“. *Proceedings of ICCM17*. Edinburgh. <http://iccm-central.org/Proceedings/ICCM17proceedings/>.

(Morris 1991)

Morris, M. D. (1991), „Factorial Sampling Plans for Preliminary Computational Experiments“, *Technometrics*, 33 (2), p. 161–174.

(Mueller & Kruck et al. 2013)

Mueller, S.; Kruck, B. & Baudisch, P. (2013), „LaserOrigami“. *Proceedings of the SIGCHI Conference on Human Factors in Computing Systems*. Paris, France, Editors: W. E. Mackay, S. Brewster & S. Bødker, ACM, New York, NY, USA, p. 2585–2592. ISBN: 9781450318990, DOI:10.1145/2470654.2481358.

(Mühlbacher 2012)

Mühlbacher, M. (2012), „Großserientauglicher Hochleistungsleichtbau. Ultralitec-Verfahren“, *Kunststoffe* (5), p. 53–58.

(Nagabandi & Wang et al. 2016)

Nagabandi, A.; Wang, L. & Fearing, R. S. (2016), „A Path Planning Algorithm for Single-Ended Continuous Planar Robotic Ribbon Folding“. *Proceedings of 2016 IEEE/RSJ International Conference on Intelligent Robots and Systems*. Daejeon, Korea, DOI:10.1109/IROS.2016.7759500.

(Neitzel & Mitschang et al. 2014)

Neitzel, M.; Mitschang, P. & Breuer, U. (2014), *Handbuch Verbundwerkstoffe. Werkstoffe, Verarbeitung, Anwendung*, Carl Hanser Fachbuchverlag, München, Germany. ISBN: 978-3-446-43696-1.

(Pangboonyanon & Zaiß et al. 2016)

Pangboonyanon, W.; Zaiß, M.; Fleischer, J. & Lanza, G. (2016), „Optimization of Process Chain for continuous-discontinuous long fiber reinforced polymer structures“. *Proceedings of the 17th European Conference on Composite Materials*.

Munich, Germany, MAI Carbon Cluster Management GmbH, Augsburg, Germany.
ISBN: 978-3-00-053387-7.

(Park 1994)

Park, J.-S. (1994), „Optimal Latin-hypercube design for computer experiments“, *Journal of Statistical Planning and Inference*, 39 , p. 95–111.

(Peraza Hernandez & Hartl et al. 2016)

Peraza Hernandez, E. A.; Hartl, D. J.; Akleman, E. & Lagoudas, D. C. (2016), „Modeling and analysis of origami structures with smooth folds“, *Computer-Aided Design*, 78 , p. 93–106, DOI:10.1016/j.cad.2016.05.010.

(Pourboghrat & Chu 1995)

Pourboghrat, F. & Chu, E. (1995), „Prediction of spring-back and side-wall curl in 2-D draw bending“, *Journal of Materials Processing Technology*, 50 (1-4), p. 361–374, DOI:10.1016/0924-0136(94)01398-K.

(Qin & Su et al. 2003)

Qin, H.; Su, Q.; Zhang, S.; Zhao, B. & Yang, M. (2003), „Thermal stability and flammability of polyamide 66/montmorillonite nanocomposites“, *Polymer*, 44 (24), p. 7533–7538, DOI:10.1016/j.polymer.2003.09.014.

(Reese & Vorhof et al. 2020)

Reese, J.; Vorhof, M.; Hoffmann, G.; Böhme, K. & Cherif, C. (2020), „Joule heating of dry textiles made of recycled carbon fibers and PA6 for the series production of thermoplastic composites“, *Journal of Engineered Fibers and Fabrics*, 15 (1-13), DOI:10.1177/1558925020905828.

(Rudolf & Mitschang et al. 2000)

Rudolf, R.; Mitschang, P. & Neitzel, M. (2000), „Induction heating of continuous carbon-fibre-reinforced thermoplastics“, *Composites Part A: Applied Science and Manufacturing*, 31 (11), p. 1191–1202, DOI:10.1016/S1359-835X(00)00094-4.

(Sachs & Akkerman et al. 2014)

Sachs, U.; Akkerman, R. & Haanappel, S. P. (2014), „Bending Characterization of UD Composites“, *Key Engineering Materials*, 611-612 , p. 399–406, DOI:10.4028/www.scientific.net/KEM.611-612.399.

(Schäferling 2019)

Schäferling, M. (2019), *Development of a Data Fusion-Based Multi-Sensor System*

for Hybrid Sheet Molding Compound. Doctoral Dissertation, Shaker, Düren, Germany. ISBN: 978-3-8440-6759-0.

(Schaler & Ruffatto et al. 2018)

Schaler, E. W.; Ruffatto, D.; Glick, P.; White, V. & Parness, A. (2018), „An Electrostatic Gripper for Flexible Objects“. *IEEE/RSJ International Conference on Intelligent Robots and Systems.*, Vancouver, British Columbia, Canada, p. 1172–1179.

(Schmidt-Rohr 2015)

Schmidt-Rohr, K. (2015), „Why Combustions Are Always Exothermic, Yielding About 418 kJ per Mole of O₂“, *Journal of Chemical Education*, 92 (12), p. 2094–2099, DOI:10.1021/acs.jchemed.5b00333.

(Schmoeckel & Beth 1993)

Schmoeckel, D. & Beth, M. (1993), „Springback Reduction in Draw-Bending Process of Sheet Metals“, *CIRP Annals*, 42 (1), p. 339–342, DOI:10.1016/S0007-8506(07)62457-3.

(Schröder 2010)

Schröder, D. (2010), *Intelligente Verfahren. Identifikation und Regelung nichtlinearer Systeme*, Springer, Berlin, Germany, Heidelberg, Germany. <http://dx.doi.org/10.1007/978-3-642-11398-7>. ISBN: 978-3-642-11397-0.

(Siebertz & van Bebber et al. 2017)

Siebertz, K.; van Bebber, D. & Hochkirchen, T. (2017), *Statistische Versuchsplannung. Design of Experiments (DoE)*, Vieweg, Berlin, Heidelberg. <https://ebookcentral.proquest.com/lib/gbv/detail.action?docID=5143216>. ISBN: 978-3-662-55742-6.

(Steinbuch & Gekeler 2016)

Editors: Steinbuch, R. & Gekeler, S. (2016), *Bionic Optimization in Structural Design. Stochastically Based Methods to Improve the Performance of Parts and Assemblies*, Springer, Berlin, Germany, Heidelberg, Germany. <http://search.ebsco-host.com/login.aspx?direct=true&scope=site&db=nlebk&AN=1092001>. ISBN: 978-3-662-46595-0.

(Stokes-Griffin & Compston 2015)

Stokes-Griffin, C. M. & Compston, P. (2015), „Optical characterisation and modelling for oblique near-infrared laser heating of carbon fibre reinforced thermoplastic

composites“, *Optics and Lasers in Engineering*, 72 , p. 1–11, DOI:10.1016/j.optlas-eng.2015.03.016.

(Strano 2005)

Strano, M. (2005), „Automatic tooling design for rotary draw bending of tubes“, *The International Journal of Advanced Manufacturing Technology*, 26 (7-8), p. 733–740, DOI:10.1007/s00170-003-2055-6.

(Sun & Wen et al. 2020)

Sun, Z.; Wen, Z.; Zhao, X.; Yang, Y. & Li, S. (2020), „Real-World Driving Cycles Adaptability of Electric Vehicles“, *World Electric Vehicle Journal*, 11 (1), p. 19, DOI:10.3390/wevj11010019.

(Takagi & Ichihara 2004)

Takagi, H. & Ichihara, Y. (2004), „Effect of Fiber Length on Mechanical Properties of "Green" Composites Using a Starch-Based Resin and Short Bamboo Fibers“, *JSME International Journal*, 47 (4), p. 551–555.

(Toray Advanced Composites 2020)

Toray Advanced Composites (2020), *HIGH PERFORMANCE INDUSTRIAL Advanced Composite Materials Selector Guide* . <https://www.toraytac.com/resources/selector-guides>.

(Utsumi & Sakaki 2002)

Utsumi, N. & Sakaki, S. (2002), „Countermeasures against undesirable phenomena in the draw-bending process for extruded square tubes“, *Journal of Materials Processing Technology*, 123 (2), p. 264–269, DOI:10.1016/S0924-0136(01)01230-4.

(Vaidya & Chawla 2008)

Vaidya, U. K. & Chawla, K. K. (2008), „Processing of fibre reinforced thermoplastic composites“, *International Materials Reviews*, 53 (4), p. 185–218, DOI:10.1179/174328008X325223.

(VDI 2221)

Verein Deutscher Ingenieure 2221 (1993), *Methodik zum Entwickeln und Konstruieren technischer Systeme und Produkte*.

(VDI 2860)

Verein Deutscher Ingenieure 2860 (1990), *Montage- und Handhabungstechnik -*

Handhabungsfunktionen. Handhabungseinrichtungen; Begriffe, Definitionen, Symbole.

(Verlinden & Cattrysse et al. 2007)

Verlinden, B.; Cattrysse, D.; Duflou, J. R. & van Oudheusden, D. (2007), „Modeling Sheet Metal Integrated Production Planning for Laser Cutting and Air Bending“, *Key Engineering Materials*, 344 , p. 913–920, DOI:10.4028/www.scientific.net/KEM.344.913.

(Verrey & Wakeman et al. 2006)

Verrey, J.; Wakeman, M. D.; Michaud, V. & Månson, J.-A.E. (2006), „Manufacturing cost comparison of thermoplastic and thermoset RTM for an automotive floor pan“, *Composites Part A: Applied Science and Manufacturing*, 37 (1), p. 9–22, DOI:10.1016/j.compositesa.2005.05.048.

(Vikhar 2016)

Vikhar, P. A. (2016), „Evolutionary algorithms: A critical review and its future prospects“. *International Conference on Global Trends in Signal Processing, Information Computing and Communication*. Jalgaon, India, IEEE, Piscataway, New Jersey, USA, p. 261–265. ISBN: 978-1-5090-0467-6, DOI:10.1109/ICGTSPICC.2016.7955308.

(Vorkov & Arola et al. 2018)

Vorkov, V.; Arola, A.-M.; Larkiola, J.; Vandepitte, D. & Duflou, J. R. (2018), „Influence of radiant heating on air bending“, *The International Journal of Advanced Manufacturing Technology*, 97 (1-4), p. 1421–1429, DOI:10.1007/s00170-018-2036-4.

(Wang & Plecnik et al. 2016)

Wang, L.; Plecnik, M. M. & Fearing, R. S. (2016), „Robotic folding of 2D and 3D structures from a ribbon“. *2016 IEEE International Conference on Robotics and Automation*. Stockholm, Sweden, p. 3655–3660, DOI:10.1109/ICRA.2016.7487550.

(Wang & Tu et al. 2013)

Wang, N.; Tu, R.; Ma, X.; Xie, Q. & Jiang, X. (2013), „Melting behavior of typical thermoplastic materials – An experimental and chemical kinetics study“, *Journal of Hazardous Materials*, 262 , p. 9–15, DOI:10.1016/j.jhazmat.2013.08.024.

(Weiland & Weimer et al. 2013)

Weiland, F.; Weimer, C.; Dumont, F.; Katsiropoulos, C. V.; Pantelakis, S. G.; Sitaras, I.; Skordos, A. A.; Berthé, E. & Luca, P. de (2013), „Process and cost modeling applied to manufacture of complex aerospace composite part“, *Plastics, Rubber and Composites*, 42 (10), p. 427–436, DOI:10.1179/1743289812Y.0000000047.

(Wulfsberg & Herrmann et al. 2014)

Wulfsberg, J.; Herrmann, A.; Ziegmann, G.; Lonsdorfer, G.; Stöß, N. & Fette, M. (2014), „Combination of Carbon Fibre Sheet Moulding Compound and Prepreg Compression Moulding in Aerospace Industry“, *Procedia Engineering*, 81 , p. 1601–1607, DOI:10.1016/j.proeng.2014.10.197.

(Xu & Hu et al. 2015)

Xu, H.; Hu, J. & Yu, Z. (2015), „Absorption behavior analysis of Carbon Fiber Reinforced Polymer in laser processing“, *Optical Materials Express*, 5 (10), p. 2330–2336, DOI:10.1364/OME.5.002330.

(Yu & Potter et al. 2014)

Yu, H.; Potter, K. D. & Wisnom, M. R. (2014), „A novel manufacturing method for aligned discontinuous fibre composites (High Performance-Discontinuous Fibre method)“, *Composites Part A: Applied Science and Manufacturing*, 65 , p. 175–185, DOI:10.1016/j.compositesa.2014.06.005.

(Zhang & Jones et al. 2005)

Zhang, W.; Jones, M.; Graham, M.; Farrell, B.; Azer, M.; Erikson, C.; Zhang, J. & Yao, Y. L. (2005), „Large diameter and thin wall laser tube bending“. *International Congress on Applications of Lasers & Electro-Optics*. Miami, Florida, USA, Laser Institute of America, p. 107. ISBN: 978-0-912035-82-6, DOI:10.2351/1.5060413.

List of Figures

Figure 2-1: Manufacturing of LFT pellets and manufactured pellet (a) and direct LFT extrusion (b) (Neitzel & Mitschang et al. 2014)	7
Figure 2-2: LFT is processed by directly molding the material	8
Figure 2-3: Manufacturing monolithic components from UD-tape requires the stacking of numerous material parts and the preforming of the stack for a reliable insertion and molding.	9
Figure 2-4: Process route for the manufacturing of hybrid LFT – UD-tape components. This thesis focuses on the preforming of the reinforcements.	12
Figure 2-5: Barrel End Effector (based on (Ehinger 2012))	15
Figure 2-6: Working principle of the Form Hand (based on (Löchte & Kunz et al. 2014))	16
Figure 2-7: Movement of the gripping units (based on (Moll & Ohlberg et al. 2019))	17
Figure 2-8: Function of the Octopus End Effector (based on (Brecher & Kukla et al. 2015))	17
Figure 2-9: Grasping and placement of the organo sheet using the Vortex End Effector (based on (Bruns & Raatz 2017))	18
Figure 2-10: Function of the Pixel End Effector (based on (Förster & Ballier et al. 2017))	19
Figure 2-11: Representation of shear by lines of constant length: For parallel fibers, shear only leads to a longitudinal displacement of the fibers (simple-shear) (a). Two layers of fibers require a shear in at least two directions (pure shear) (b). Three directions of fibers require slippage between the fibers, or the shear is locked (c).	23
Figure 3-1: Single tape strips can be formed into complex geometries without changing the angle between its fibers. The forming of stacks as required for monolithic components causes angular changes between the fibers and a linked displacement of the outer contour.	28

Figure 3-2: Derivation of the challenges for conducting the bending process.	29
Figure 3-3: The tape strip can be brought into a complex shape with only local deformation	30
Figure 3-4: Sequential forming of a tape strip	30
Figure 3-5: Steps of bending: Supplying a tape strip (1), gripping the free end (2), heating the bending area (3), bending (4), cooling (5), releasing (6)	31
Figure 3-6: Fiber deformation on the inner and outer sides of the bend. (A_Penev 2019)	31
Figure 3-7: Bending of a heated area by gravitational forces	32
Figure 3-8: Ishikawa diagram of the expected influencing parameters	33
Figure 3-9: Possible preform geometry with straight and askew bends. (Figure by Alexej Bachtin)	34
Figure 3-10: Approximation of a reinforcement shape without preforming (a), with one bend (b) or with three bends (c)	34
Figure 3-11: Work packages within the thesis	35
Figure 4-1: Research questions of this thesis	36
Figure 4-2: Function chart representation of the sequential bending process with tape supply in green, heating in red, and bending and movement of the specimen in blue	37
Figure 4-3: Function charts with highlighted bending and handling system	38
Figure 4-4: Function charts with highlighted heating and cooling	41
Figure 4-5: Parameters of the radiation heater with aperture	45
Figure 4-6: Circle, ellipse, and parabola are sections of a cone with the circle being normal to the symmetry axis of the cone and the parabola being parallel to a line on the cone surface. The ellipse is a stretched circle along one axis, and is between the circle and parabola shape.	46
Figure 4-7: Reflection of a beam from one ellipse focus point to the other	46

Figure 4-8: Reflector comparison setup	47
Figure 4-9: Forming of the molten area by gravity after a settling time at 140°C (a), 165°C (b), 186°C (c) and 222°C (d) jaw temperature. (Image: re-enacted experimentation on the final test rig)	50
Figure 4-10: Bending end effector with both heating devices	51
Figure 4-11: The radiation heating (a) melts a larger area of the tape than the contact heating (b) in the final implementation at the optimized heating settings.	52
Figure 4-12: Function chart with highlighted process steps connected to the tape supply	52
Figure 4-13: Cutting parameters	53
Figure 4-14: The tape is moving through the supply unit from left to right	54
Figure 4-15: Control architecture of the experimental cell	55
Figure 4-16: Frontal view of the bending setup	56
Figure 4-17: Radiation heater (a) and contact heater (b)	57
Figure 5-1: Research questions of this thesis	58
Figure 5-2: It can be proven that a rotation around a fixed TCP is not a sufficient description of the bending as the required rotational center of the real kinematic movement is moving along the red line depending on the angle β . The dark green line represents the result of a pure rotational around the dark green cross.	60
Figure 5-3: Qualitative example of the influence of tension. By moving the gripper horizontally, the position of the bent zone can be influenced: a) compression, b) correct length, and c) tension in the tape.	61
Figure 5-4: Deformation resulting from too much tape length between supply unit and end effector	61
Figure 5-5: Definition of the coordinate systems a (position of the bend), b (system of the rotated bending edge), c (initial position of the gripper), and d (final position of the gripper) (Figure based on Alexej Bachtin)	62

Figure 5-6: Kinematic description of a bending zone (figure based on (A_Bachtin 2020))	63
Figure 5-7: Overview over the swing folding process	65
Figure 5-8: Detailed chart of the swing folding process	66
Figure 5-9: Sharpness of the bend for $b_0=1$ mm (a) and $b_0=5$ mm (b)	70
Figure 5-10: Bending motion of the tape without (a) and with sufficient (b) preheating. The created arc in (a) causes tension in the tape, which may pull more tape into the area between supply unit and end effector.	70
Figure 5-11: Airflow-induced deformation of the bend with the single nozzle cooling. The bending zone is bent in an S-shape instead of an even arc by the force that pushes the tape down. (Image source: (A_Bachtin 2020))	71
Figure 5-12: Adjustment of the low power level by comparing the size of the molten area after 30 seconds recognizable by the variation in surface reflectivity. Too weak heating power (a), small molten area (b), overheating and minor smoke development (c)	72
Figure 5-13: Type, goal, varied parameters, and output of the experimental series with radiation heating	72
Figure 5-14: Results of the experimental series R01	74
Figure 5-15: Results of the experimental series R01	75
Figure 5-16: Variation of the bend shape depending on t_0 and b_0 . (Image source: (A_Bachtin 2020))	76
Figure 5-17: Angular deviations $\Delta\alpha$ and $\Delta\beta$ depending on α and β	78
Figure 5-18: Measurement of the bending angles using the GOM System (Image source: (A_Bachtin 2020))	79
Figure 5-19: Angular error along the tape.	79
Figure 5-20: Mean Average Error in β and selected heating parameters	80
Figure 5-21: Regression for t_0 , b_0 and t_{ph} (translated figure from (A_Steidle-Sailer 2021))	83
Figure 5-22: Regression for t_0 and b_0 (translated figure from (A_Steidle-Sailer 2021))	83

Figure 5-23: Heat Map of the predicted α and β error depending on the input angle (PP) (translated figure from (A_Steidle-Sailer 2021))	84
Figure 5-24: Heat Map of the predicted α and β error depending on the input angle (PA) (translated figure from (A_Steidle-Sailer 2021))	84
Figure 5-25: Correction gripper position to ensure even contact force between the heated jaws	86
Figure 5-26: When setting $t_0=0$, overbending might occur due to the movement changing the tape orientation between supply and end effector	86
Figure 5-27: Pulling of threads resulting from the adhesion (a) and squeeze out of the matrix (b)	87
Figure 5-28: Type, goal, varied parameters, and output of the experimental series with contact heating	88
Figure 5-29: Results of C01 PP	90
Figure 5-30: Results of C01 PA	92
Figure 5-31: $\Delta\beta$ depending on the tensioning for PP and PA	93
Figure 5-32: Comparison of the dependency between L and $\Delta\beta$ (a) and β and $\Delta\beta$ (b) with each specimen represented in a different color	95
Figure 5-33: Placement of the same pair of tapes next to each other. The way they were manufactured (a) or one tape rotated (b)	95
Figure 5-34: Remaining bending error after improving the used cooling nozzle	97
Figure 5-35: Regression for b_0 and t_0 (translated figure from (A_Steidle-Sailer 2021))	99
Figure 5-36: Regression for T, t_{cph} , and t_c (translated figure from (A_Steidle-Sailer 2021))	99
Figure 5-37: Heat Map of the predicted α and β error depending on the input angle (PP) (translated figure from (A_Steidle-Sailer 2021))	100
Figure 5-38: Heat Map of the predicted α and β error depending on the input angle (PA) (translated figure from (A_Steidle-Sailer 2021))	100

Figure 5-39: Comparison between single-layer radiation (a), single-layer contact (b), and double-layer radiation (c) from outside (small letters) and inside (capital letters) the bend.	102
Figure 6-1: Research questions of this thesis	104
Figure 6-2: These component geometries will be used to explain the algorithm in this thesis.	106
Figure 6-3: Optimization methods are used for the finding of maxima or minima of a function. One challenge is that the method can converge to local optima close to the starting point instead of the globally best point. (Figure by Alexej Bachtin)	107
Figure 6-4: The steps of an evolutionary generation. Own representation based on (Grimme & Bossek 2018; Steinbuch & Gekeler 2016)	109
Figure 6-5: Steps of iterative optimization	111
Figure 6-6: The tape centerline is described by its longitudinal vectors (a). The bend line can be described depending on those vectors, the normal vectors, and the bending angle α (b). (Figure based on Alexej Bachtin)	112
Figure 6-7: The longitudinal and normal vector of the next segment can be calculated by rotation around the bend line (a). For the calculation of the tape's sides, the length values are adjusted according to the width w and α (b) (Figure based on Alexej Bachtin)	112
Figure 6-8: Constant number of evaluation points per segment (a) vs. Equidistant evaluation points (b) (Figure based on Alexej Bachtin)	114
Figure 6-9: The tape can be represented symmetrically by moving P_{start} to P'_{start} and describing the two halves with two separate kinematic descriptions.	114
Figure 6-10: Overview of the comparison between real component and kinematic description of the tape.	116
Figure 6-11: Randomly initialized solution (a), after 300 generations with 300 individuals of optimization (b) and 2D preprocessor solution (c)	120
Figure 6-12: Coordinate System placement	121
Figure 6-13: Height profile (a) and resulting 2D solution (b)	122

Figure 6-14: Adaption to a skew surface by the evolutionary optimization. 2D preprocessor solution (a) and 100 generations with 100 individuals of evolutionary optimization (b)	123
Figure 6-15: 2D Edge detection on a geometry with clear edges (translated figure from (A_Wenzel 2020))	123
Figure 6-16: Fitness value depending on the distance from the optimum with the examined functions.	127
Figure 6-17: No change in only a single bend does improve the fitness although combined changes of multiple bends can improve the fitness.	131
Figure 6-18: Comparison of the evolutionary algorithm and the pseudo-gradient approach. Initial solution (a), fitness graph of the evolutionary optimization (300 Generations, 300 Individuals (b)), result of the evolutionary optimization (c), result of the adapted pseudo-gradient evolutionary optimization (d)	132
Figure 6-19: Optimization Workflow	133
Figure 6-20: Preprocessor parameters in GUI Window 1	134
Figure 6-21: Presentation of the geometry in GUI Window 2	134
Figure 6-22: GUI Window 3: Confirmation of the preprocessor results	135
Figure 6-23: Optimization control in GUI Window 4	136
Figure 6-24: GUI Window 5 and 6: Confirmation and Export of a solution	136
Figure 6-25: Results for four example geometries	137
Figure 7-1: Outline (a) and implementation (b) of the assembly station	143
Figure 7-2: UD-reinforced specimen	143

List of Tables

Table 2-1: Material Characteristics	11
Table 2-2: Comparison of Barrel End Effector (A), Form Hand (B), MoPaHyb End Effector (C), Octopus End Effector (D), Vortex End Effector (E), Pixel End Effector (F), Tape Laying (G), and Sequential Draping (H)	21
Table 3-1: Material properties of the used UD-tapes	33
Table 4-1: Morphological box of the function principles for the individual functions	37
Table 4-2: Available gripper types (Fantoni & Santochi et al. 2014)	40
Table 4-3: Concepts for limiting the heat-affected area using radiation heating	44
Table 4-4: Melting time and width depending on the geometric parameters	45
Table 4-5: Heating time with various reflector geometries. An x indicates that the tape could not be molten.	48
Table 4-6: Heating time with a reflector and various aperture sizes	48
Table 4-7: Effects of the contact heating depending on the jaw temperature	49
Table 4-8: Comparison of contact and radiation heating	51
Table 5-1: Influence parameters of the swing folding process	68
Table 5-2: Angle combinations per parameter set	69
Table 5-3: Parameter set of experimental series R01	73
Table 5-4: Significance level of the effects	75
Table 5-5: Parameters used in the experimental series R02	77
Table 5-6: Bends of the specimens	78
Table 5-7: Set of Experiments for the LHS	82
Table 5-8: Experimental plan of C01 PP	89
Table 5-9: Significance levels in C01 PP	89

Table 5-10: Significance levels in C01 PA	91
Table 5-11: Used process parameters and average results of experimental series C02 PP and C02 PA	92
Table 5-12: $\Delta\beta$ results of the experimental series C02 PP measured with GOM ATOS	93
Table 5-13: Results of C03 depending on the length:	94
Table 5-14: Result of C03 PP measured with GOM ATOS	94
Table 5-15: Result C03 PA measured with GOM ATOS	94
Table 5-16: Examination of the bending error with the improved cooling nozzle	97
Table 5-17: Set of Experiments for the LHS	98
Table 6-1: Example for the chromosome of three individuals with five genes each	109
Table 6-2: Coding of the tape geometry in the genome	115
Table 6-3: Comparison of the behavior of different weight combinations after an optimization run with 30 Generations of 50 Individuals	129
Table 6-4: Extreme weighting of a certain subfitness function can cause small changes in this function to override important improvement in other functions and thereby optimize only for the one goal.	129

Forschungsberichte aus dem wbk
Institut für Produktionstechnik
Karlsruher Institut für Technologie (KIT)

Bisher erschienene Bände:

Band 0

Dr.-Ing. Wu Hong-qi

Adaptive Volumenstromregelung mit Hilfe von drehzahlgeregelten Elektroantrieben

Band 1

Dr.-Ing. Heinrich Weiß

**Fräsen mit Schneidkeramik - Verhalten des System
Werkzeugmaschine-Werkzeug-Werkstück und Prozessanalyse**

Band 2

Dr.-Ing. Hans-Jürgen Stierle

Entwicklung und Untersuchung hydrostatischer Lager für die Axialkolbenmaschine

Band 3

Dr.-Ing. Herbert Hörner

Untersuchung des Geräuschverhaltens druckgeregelter Axialkolbenpumpen

Band 4

Dr.-Ing. Rolf-Dieter Brückbauer

Digitale Drehzahlregelung unter der besonderen Berücksichtigung von Quantisierungseffekten

Band 5

Dr.-Ing. Gerhard Staiger

Graphisch interaktive NC-Programmierung von Drehteilen im Werkstattbereich

Band 6

Dr.-Ing. Karl Peters

Ein Beitrag zur Berechnung und Kompensation von Positionierfehlern an Industrierobotern

Band 7

Dr.-Ing. Paul Stauss

Automatisierte Inbetriebnahme und Sicherung der Zuverlässigkeit und Verfügbarkeit numerisch gesteuerter Fertigungseinrichtungen

Band 8

Dr.-Ing. Günter Möckesch

Konzeption und Realisierung eines strategischen, integrierten Gesamtplanungs- und -bearbeitungssystems zur Optimierung der Drehteilorganisation für auftragsbezogene Drehereien

Band 9

Dr.-Ing. Thomas Oestreicher

Rechnergestützte Projektierung von Steuerungen

Band 10

Dr.-Ing. Thomas Selinger

Teilautomatisierte werkstattnahe NC-Programmerstellung im Umfeld einer integrierten Informationsverarbeitung

Band 11

Dr.-Ing. Thomas Buchholz

Prozessmodell Fräsen, Rechnerunterstützte Analyse, Optimierung und Überwachung

Band 12

Dr.-Ing. Bernhard Reichling

Lasergestützte Positions- und Bahnvermessung von Industrierobotern

Band 13

Dr.-Ing. Hans-Jürgen Lesser

Rechnergestützte Methoden zur Auswahl anforderungsgerechter Verbindungselemente

Band 14

Dr.-Ing. Hans-Jürgen Lauffer

Einsatz von Prozessmodellen zur rechnerunterstützten Auslegung von Räumwerkzeugen

Band 15

Dr.-Ing. Michael C. Wilhelm

Rechnergestützte Prüfplanung im Informationsverbund moderner Produktionssysteme

Band 16
Dr.-Ing. Martin Ochs

Entwurf eines Programmsystems zur wissensbasierten Planung und Konfigurierung

Band 17
Dr.-Ing. Heinz-Joachim Schneider

Erhöhung der Verfügbarkeit von hochautomatisierten Produktionseinrichtungen mit Hilfe der Fertigungsleittechnik

Band 18
Dr.-Ing. Hans-Reiner Ludwig

Beanspruchungsanalyse der Werkzeugschneiden beim Stirnplanfräsen

Band 19
Dr.-Ing. Rudolf Wieser

Methoden zur rechnergestützten Konfigurierung von Fertigungsanlagen

Band 20
Dr.-Ing. Edgar Schmitt

Werkstattsteuerung bei wechselnder Auftragsstruktur

Band 21
Dr.-Ing. Wilhelm Enderle

Verfügbarkeitssteigerung automatisierter Montagesysteme durch selbsttätige Behebung prozessbedingter Störungen

Band 22
Dr.-Ing. Dieter Buchberger

Rechnergestützte Strukturplanung von Produktionssystemen

Band 23
Prof. Dr.-Ing. Jürgen Fleischer

Rechnerunterstützte Technologieplanung für die flexibel automatisierte Fertigung von Abkantteilen

Band 24
Dr.-Ing. Lukas Loeffler

Adaptierbare und adaptive Benutzerschnittstellen

Band 25
Dr.-Ing. Thomas Friedmann

Integration von Produktentwicklung und Montageplanung durch neue rechnergestützte Verfahren

Band 26

Dr.-Ing. Robert Zurrin

Variables Formhonen durch rechnergestützte Hornprozesssteuerung

Band 27

Dr.-Ing. Karl-Heinz Bergen

Langhub-Innenrundhonen von Grauguss und Stahl mit einem elektromechanischem Vorschubsystem

Band 28

Dr.-Ing. Andreas Liebisch

Einflüsse des Festwalzens auf die Eigenspannungsverteilung und die Dauerfestigkeit einsatzgehärteter Zahnräder

Band 29

Dr.-Ing. Rolf Ziegler

Auslegung und Optimierung schneller Servopumpen

Band 30

Dr.-Ing. Rainer Bartl

Datenmodellgestützte Wissensverarbeitung zur Diagnose und Informationsunterstützung in technischen Systemen

Band 31

Dr.-Ing. Ulrich Golz

Analyse, Modellbildung und Optimierung des Betriebsverhaltens von Kugelgewindetrieben

Band 32

Dr.-Ing. Stephan Timmermann

Automatisierung der Feinbearbeitung in der Fertigung von Hohlformwerkzeugen

Band 33

Dr.-Ing. Thomas Noe

Rechnergestützter Wissenserwerb zur Erstellung von Überwachungs- und Diagnoseexpertensystemen für hydraulische Anlagen

Band 34

Dr.-Ing. Ralf Lenschow

Rechnerintegrierte Erstellung und Verifikation von Steuerungsprogrammen als Komponente einer durchgängigen Planungsmethodik

Band 35

Dr.-Ing. Matthias Kallabis

Räumen gehärteter Werkstoffe mit kristallinen Hartstoffen

Band 36

Dr.-Ing. Heiner-Michael Honeck

Rückführung von Fertigungsdaten zur Unterstützung einer fertigungsgerechten Konstruktion

Band 37

Dr.-Ing. Manfred Rohr

Automatisierte Technologieplanung am Beispiel der Komplettbearbeitung auf Dreh-/Fräszellen

Band 38

Dr.-Ing. Martin Steuer

Entwicklung von Softwarewerkzeugen zur wissensbasierten Inbetriebnahme von komplexen Serienmaschinen

Band 39

Dr.-Ing. Siegfried Beichter

Rechnergestützte technische Problemlösung bei der Angebotserstellung von flexiblen Drehzellen

Band 40

Dr.-Ing. Thomas Steitz

Methodik zur marktorientierten Entwicklung von Werkzeugmaschinen mit Integration von funktionsbasierter Strukturierung und Kostenschätzung

Band 41

Dr.-Ing. Michael Richter

Wissensbasierte Projektierung elektrohydraulischer Regelungen

Band 42

Dr.-Ing. Roman Kuhn

Technologieplanungssystem Fräsen. Wissensbasierte Auswahl von Werkzeugen, Schneidkörpern und Schnittbedingungen für das Fertigungsverfahren Fräsen

Band 43

Dr.-Ing. Hubert Klein

Rechnerunterstützte Qualitätssicherung bei der Produktion von Bauteilen mit frei geformten Oberflächen

Band 44

Dr.-Ing. Christian Hoffmann

Konzeption und Realisierung eines fertigungsintegrierten Koordinatenmessgerätes

Band 45

Dr.-Ing. Volker Frey

Planung der Leittechnik für flexible Fertigungsanlagen

Band 46

Dr.-Ing. Achim Feller

Kalkulation in der Angebotsphase mit dem selbsttätig abgeleiteten Erfahrungswissen der Arbeitsplanung

Band 47

Dr.-Ing. Markus Klaiber

Produktivitätssteigerung durch rechnerunterstütztes Einfahren von NC-Programmen

Band 48

Dr.-Ing. Roland Minges

Verbesserung der Genauigkeit beim fünfachsigem Fräsen von Freiformflächen

Band 49

Dr.-Ing. Wolfgang Bernhart

Beitrag zur Bewertung von Montagevarianten: Rechnergestützte Hilfsmittel zur kostenorientierten, parallelen Entwicklung von Produkt und Montagesystem

Band 50

Dr.-Ing. Peter Ganghoff

Wissensbasierte Unterstützung der Planung technischer Systeme: Konzeption eines Planungswerkzeuges und exemplarische Anwendung im Bereich der Montagesystemplanung

Band 51

Dr.-Ing. Frank Maier

Rechnergestützte Prozessregelung beim flexiblen Gesenkbiegen durch Rückführung von Qualitätsinformationen

Band 52

Dr.-Ing. Frank Debus

Ansatz eines rechnerunterstützten Planungsmanagements für die Planung in verteilten Strukturen

Band 53

Dr.-Ing. Joachim Weinbrecht

Ein Verfahren zur zielorientierten Reaktion auf Planabweichungen in der Werkstattregelung

Band 54

Dr.-Ing. Gerd Herrmann

Reduzierung des Entwicklungsaufwandes für anwendungsspezifische Zellenrechnersoftware durch Rechnerunterstützung

Band 55

Dr.-Ing. Robert Wassmer

Verschleissentwicklung im tribologischen System Fräsen: Beiträge zur Methodik der Prozessmodellierung auf der Basis tribologischer Untersuchungen beim Fräsen

Band 56

Dr.-Ing. Peter Uebelhoer

Inprocess-Geometriemessung beim Honen

Band 57

Dr.-Ing. Hans-Joachim Schelberg

Objektorientierte Projektierung von SPS-Software

Band 58

Dr.-Ing. Klaus Boes

Integration der Qualitätsentwicklung in featurebasierte CAD/CAM-Prozessketten

Band 59

Dr.-Ing. Martin Schreiber

Wirtschaftliche Investitionsbewertung komplexer Produktionssysteme unter Berücksichtigung von Unsicherheit

Band 60

Dr.-Ing. Ralf Steuernagel

Offenes adaptives Engineering-Werkzeug zur automatisierten Erstellung von entscheidungsunterstützenden Informationssystemen

Band 62

Dr.-Ing. Uwe Schauer

Qualitätsorientierte Feinbearbeitung mit Industrierobotern: Regelungsansatz für die Freiformflächenfertigung des Werkzeug- und Formenbaus

Band 63

Dr.-Ing. Simone Loeper

Kennzahlengestütztes Beratungssystem zur Verbesserung der Logistikleistung in der Werkstattfertigung

Band 64

Dr.-Ing. Achim Raab

Räumen mit hartstoffbeschichteten HSS-Werkzeugen

Band 65,

Dr.-Ing. Jan Erik Burghardt

Unterstützung der NC-Verfahrenskette durch ein bearbeitungs-elementorientiertes, lernfähiges Technologieplanungssystem

Band 66

Dr.-Ing. Christian Tritsch

Flexible Demontage technischer Gebrauchsgüter: Ansatz zur Planung und (teil-)automatisierten Durchführung industrieller Demontageprozesse

Band 67

Dr.-Ing. Oliver Eitrich

Prozessorientiertes Kostenmodell für die entwicklungsbegleitende Vorkalkulation

Band 68

Dr.-Ing. Oliver Wilke

Optimierte Antriebskonzepte für Räummaschinen - Potentiale zur Leistungssteigerung

Band 69

Dr.-Ing. Thilo Sieth

Rechnergestützte Modellierungsmethodik zerspantechnologischer Prozesse

Band 70

Dr.-Ing. Jan Linnenbuerger

Entwicklung neuer Verfahren zur automatisierten Erfassung der geometrischen Abweichungen an Linearachsen und Drehschwenkköpfen

Band 71

Dr.-Ing. Mathias Klimmek

Fraktionierung technischer Produkte mittels eines frei beweglichen Wasserstrahlwerkzeuges

Band 72

Dr.-Ing. Marko Hartel

Kennzahlenbasiertes Bewertungssystem zur Beurteilung der Demontage- und Recyclingeignung von Produkten

Band 73

Dr.-Ing. Jörg Schaupp

Wechselwirkung zwischen der Maschinen- und Hauptspindeltriebsdynamik und dem Zerspanprozess beim Fräsen

Band 74

Dr.-Ing. Bernhard Neisius

Konzeption und Realisierung eines experimentellen Telemanipulators für die Laparoskopie

Band 75

Dr.-Ing. Wolfgang Walter

Erfolgsversprechende Muster für betriebliche Ideenfindungsprozesse. Ein Beitrag zur Steigerung der Innovationsfähigkeit

Band 76

Dr.-Ing. Julian Weber

Ein Ansatz zur Bewertung von Entwicklungsergebnissen in virtuellen Szenarien

Band 77

Dr.-Ing. Dipl. Wirtsch.-Ing. Markus Posur

Unterstützung der Auftragsdurchsetzung in der Fertigung durch Kommunikation über mobile Rechner

Band 78

Dr.-Ing. Frank Fleissner

Prozessorientierte Prüfplanung auf Basis von Bearbeitungsobjekten für die Kleinserienfertigung am Beispiel der Bohr- und Fräsbearbeitung

Band 79

Dr.-Ing. Anton Haberkern

Leistungsfähigere Kugelgewindetriebe durch Beschichtung

Band 80

Dr.-Ing. Dominik Matt

Objektorientierte Prozess- und Strukturinnovation (OPUS)

Band 81

Dr.-Ing. Jürgen Andres

Robotersysteme für den Wohnungsbau: Beitrag zur Automatisierung des Mauerwerkbaus und der Elektroinstallation auf Baustellen

Band 82

Dr.-Ing. Dipl.Wirtschaftsing. Simone Riedmiller

Der Prozesskalender - Eine Methodik zur marktorientierten Entwicklung von Prozessen

Band 83

Dr.-Ing. Dietmar Tilch

Analyse der Geometrieparameter von Präzisionsgewinden auf der Basis einer Least-Squares-Estimation

Band 84

Dr.-Ing. Dipl.-Kfm. Oliver Stiefbold

Konzeption eines reaktionsschnellen Planungssystems für Logistikketten auf Basis von Software-Agenten

Band 85

Dr.-Ing. Ulrich Walter

Einfluss von Kühlschmierstoff auf den Zerspansprozess beim Fräsen: Beitrag zum Prozessverständnis auf Basis von zerspantechnischen Untersuchungen

Band 86

Dr.-Ing. Bernd Werner

Konzeption von teilautonomer Gruppenarbeit unter Berücksichtigung kultureller Einflüsse

Band 87

Dr.-Ing. Ulf Osmers

Projektieren Speicherprogrammierbarer Steuerungen mit Virtual Reality

Band 88

Dr.-Ing. Oliver Doerfel

Optimierung der Zerspantechnik beim Fertigungsverfahren Wälzstossen: Analyse des Potentials zur Trockenbearbeitung

Band 89

Dr.-Ing. Peter Baumgartner

Stufenmethode zur Schnittstellengestaltung in der internationalen Produktion

Band 90
Dr.-Ing. Dirk Vossmann

Wissensmanagement in der Produktentwicklung durch Qualitätsmethodenverbund und Qualitätsmethodenintegration

Band 91
Dr.-Ing. Martin Plass

Beitrag zur Optimierung des Honprozesses durch den Aufbau einer Honprozessregelung

Band 92
Dr.-Ing. Titus Konold

Optimierung der Fünffachsfräsbearbeitung durch eine kennzahlenunterstützte CAM-Umgebung

Band 93
Dr.-Ing. Jürgen Brath

Unterstützung der Produktionsplanung in der Halbleiterfertigung durch risikoberücksichtigende Betriebskennlinien

Band 94
Dr.-Ing. Dirk Geisinger

Ein Konzept zur marktorientierten Produktentwicklung

Band 95
Dr.-Ing. Marco Lanza

Entwurf der Systemunterstützung des verteilten Engineering mit Axiomatic Design

Band 96
Dr.-Ing. Volker Hüntrup

Untersuchungen zur Mikrostrukturierbarkeit von Stählen durch das Fertigungsverfahren Fräsen

Band 97
Dr.-Ing. Frank Reinboth

Interne Stützung zur Genauigkeitsverbesserung in der Inertialmesstechnik: Beitrag zur Senkung der Anforderungen an Inertialsensoren

Band 98
Dr.-Ing. Lutz Trender

Entwicklungintegrierte Kalkulation von Produktlebenszykluskosten auf Basis der ressourcenorientierten Prozesskostenrechnung

Band 99

Dr.-Ing. Cornelia Kafka

Konzeption und Umsetzung eines Leitfadens zum industriellen Einsatz von Data-Mining

Band 100

Dr.-Ing. Gebhard Selinger

Rechnerunterstützung der informellen Kommunikation in verteilten Unternehmensstrukturen

Band 101

Dr.-Ing. Thomas Windmüller

Verbesserung bestehender Geschäftsprozesse durch eine mitarbeiterorientierte Informationsversorgung

Band 102

Dr.-Ing. Knud Lembke

Theoretische und experimentelle Untersuchung eines bistabilen elektrohydraulischen Linearantriebs

Band 103

Dr.-Ing. Ulrich Thies

Methode zur Unterstützung der variantengerechten Konstruktion von industriell eingesetzten Kleingeräten

Band 104

Dr.-Ing. Andreas Schmälzle

Bewertungssystem für die Generalüberholung von Montageanlagen –Ein Beitrag zur wirtschaftlichen Gestaltung geschlossener Facility- Management- Systeme im Anlagenbau

Band 105

Dr.-Ing. Thorsten Frank

Vergleichende Untersuchungen schneller elektromechanischer Vorschubachsen mit Kugelgewindetrieb

Band 106

Dr.-Ing. Achim Agostini

Reihenfolgeplanung unter Berücksichtigung von Interaktionen: Beitrag zur ganzheitlichen Strukturierung und Verarbeitung von Interaktionen von Bearbeitungsobjekten

Band 107

Dr.-Ing. Thomas Barrho

Flexible, zeitfenstergesteuerte Auftragseinplanung in segmentierten Fertigungsstrukturen

Band 108

Dr.-Ing. Michael Scharer

Quality Gate-Ansatz mit integriertem Risikomanagement

Band 109

Dr.-Ing. Ulrich Suchy

Entwicklung und Untersuchung eines neuartigen Mischkopfes für das Wasser Abrasivstrahlschneiden

Band 110

Dr.-Ing. Sellal Mussa

Aktive Korrektur von Verlagerungsfehlern in Werkzeugmaschinen

Band 111

Dr.-Ing. Andreas Hühsam

Modellbildung und experimentelle Untersuchung des Wälzschälprozesses

Band 112

Dr.-Ing. Axel Plutowsky

Charakterisierung eines optischen Messsystems und den Bedingungen des Arbeitsraums einer Werkzeugmaschine

Band 113

Dr.-Ing. Robert Landwehr

Konsequent dezentralisierte Steuerung mit Industrial Ethernet und offenen Applikationsprotokollen

Band 114

Dr.-Ing. Christoph Dill

Turbulenzreaktionsprozesse

Band 115

Dr.-Ing. Michael Baumeister

Fabrikplanung im turbulenten Umfeld

Band 116

Dr.-Ing. Christoph Gönninger

Konzept zur Verbesserung der Elektromagnetischen Verträglichkeit (EMV) in Produktionssystemen durch intelligente Sensor/Aktor-Anbindung

Band 117

Dr.-Ing. Lutz Demuß

Ein Reifemodell für die Bewertung und Entwicklung von Dienstleistungsorganisationen: Das Service Management Maturity Modell (SMMM)

Band 118

Dr.-Ing. Jörg Söhner

Beitrag zur Simulation zerspanungstechnologischer Vorgänge mit Hilfe der Finite-Element-Methode

Band 119

Dr.-Ing. Judith Elsner

Informationsmanagement für mehrstufige Mikro-Fertigungsprozesse

Band 120

Dr.-Ing. Lijing Xie

Estimation Of Two-dimension Tool Wear Based On Finite Element Method

Band 121

Dr.-Ing. Ansgar Blessing

Geometrischer Entwurf mikromechatronischer Systeme

Band 122

Dr.-Ing. Rainer Ebner

Steigerung der Effizienz mehrachsiger Fräsprozesse durch neue Planungsmethoden mit hoher Benutzerunterstützung

Band 123

Dr.-Ing. Silja Klinkel

Multikriterielle Feinplanung in teilautonomen Produktionsbereichen – Ein Beitrag zur produkt- und prozessorientierten Planung und Steuerung

Band 124

Dr.-Ing. Wolfgang Neithardt

Methodik zur Simulation und Optimierung von Werkzeugmaschinen in der Konzept- und Entwurfsphase auf Basis der Mehrkörpersimulation

Band 125

Dr.-Ing. Andreas Mehr

Hartfeinbearbeitung von Verzahnungen mit kristallinen diamantbeschichteten Werkzeugen beim Fertigungsverfahren Wälzstoßen

Band 126

Dr.-Ing. Martin Gutmann

Entwicklung einer methodischen Vorgehensweise zur Diagnose von hydraulischen Produktionsmaschinen

Band 127

Dr.-Ing. Gisela Lanza

Simulative Anlaufunterstützung auf Basis der Qualitätsfähigkeiten von Produktionsprozessen

Band 128

Dr.-Ing. Ulf Dambacher

Kugelgewindetrieb mit hohem Druckwinkel

Band 129

Dr.-Ing. Carsten Buchholz

Systematische Konzeption und Aufbau einer automatisierten Produktionszelle für pulverspritzgegossene Mikroteile

Band 130

Dr.-Ing. Heiner Lang

Trocken-Räumen mit hohen Schnittgeschwindigkeiten

Band 131

Dr.-Ing. Daniel Nesges

Prognose operationeller Verfügbarkeiten von Werkzeugmaschinen unter Berücksichtigung von Serviceleistungen

Im Shaker Verlag erschienene Bände:

Band 132

Dr.-Ing. Andreas Bechle

Beitrag zur prozesssicheren Bearbeitung beim Hochleistungsfertigungsverfahren Wälzschälen

Band 133

Dr.-Ing. Markus Herm

Konfiguration globaler Wertschöpfungsnetzwerke auf Basis von Business Capabilities

Band 134

Dr.-Ing. Hanno Tritschler

**Werkzeug- und Zerspanprozessoptimierung beim Hartfräsen
von Mikrostrukturen in Stahl**

Band 135

Dr.-Ing. Christian Munzinger

**Adaptronische Strebe zur Steifigkeitssteigerung
von Werkzeugmaschinen**

Band 136

Dr.-Ing. Andreas Stepping

**Fabrikplanung im Umfeld von Wertschöpfungsnetzwerken und
ganzheitlichen Produktionssystemen**

Band 137

Dr.-Ing. Martin Dyck

**Beitrag zur Analyse thermische bedingter Werkstückdeformationen
in Trockenbearbeitungsprozessen**

Band 138

Dr.-Ing. Siegfried Schmalzried

**Dreidimensionales optisches Messsystem für eine effizientere
geometrische Maschinenbeurteilung**

Band 139

Dr.-Ing. Marc Wawerla

Risikomanagement von Garantieleistungen

Band 140

Dr.-Ing. Ivesa Buchholz

**Strategien zur Qualitätssicherung mikromechanischer Bauteile
mittels multisensorieller Koordinatenmesstechnik**

Band 141

Dr.-Ing. Jan Kotschenreuther

**Empirische Erweiterung von Modellen der Makrozerspanung
auf den Bereich der Mikrobearbeitung**

Band 142

Dr.-Ing. Andreas Knödel

Adaptronische hydrostatische Drucktascheneinheit

Band 143

Dr.-Ing. Gregor Stengel

Fliegendes Abtrennen räumlich gekrümmter Strangpressprofile mittels Industrierobotern

Band 144

Dr.-Ing. Udo Weismann

Lebenszyklusorientiertes interorganisationelles Anlagencontrolling

Band 145

Dr.-Ing. Rüdiger Pabst

Mathematische Modellierung der Wärmestromdichte zur Simulation des thermischen Bauteilverhaltens bei der Trockenbearbeitung

Band 146

Dr.-Ing. Jan Wieser

Intelligente Instandhaltung zur Verfügbarkeitssteigerung von Werkzeugmaschinen

Band 147

Dr.-Ing. Sebastian Haupt

Effiziente und kostenoptimale Herstellung von Mikrostrukturen durch eine Verfahrenskombination von Bahnerosion und Laserablation

Band 148

Dr.-Ing. Matthias Schlipf

Statistische Prozessregelung von Fertigungs- und Messprozess zur Erreichung einer variabilitätsarmen Produktion mikromechanischer Bauteile

Band 149

Dr.-Ing. Jan Philipp Schmidt-Ewig

Methodische Erarbeitung und Umsetzung eines neuartigen Maschinenkonzeptes zur produktflexiblen Bearbeitung räumlich gekrümmter Strangpressprofile

Band 150

Dr.-Ing. Thomas Ender

Prognose von Personalbedarfen im Produktionsanlauf unter Berücksichtigung dynamischer Planungsgrößen

Band 151

Dr.-Ing. Kathrin Peter

**Bewertung und Optimierung der Effektivität von Lean Methoden
in der Kleinserienproduktion**

Band 152

Dr.-Ing. Matthias Schopp

Sensorbasierte Zustandsdiagnose und -prognose von Kugelgewindetrieben

Band 153

Dr.-Ing. Martin Kipfmüller

Aufwandsoptimierte Simulation von Werkzeugmaschinen

Band 154

Dr.-Ing. Carsten Schmidt

**Development of a database to consider multi wear mechanisms
within chip forming simulation**

Band 155

Dr.-Ing. Stephan Niggeschmidt

**Ausfallgerechte Ersatzteilbereitstellung im Maschinen- und Anlagenbau
mittels lastabhängiger Lebensdauerprognose**

Band 156

Dr.-Ing. Jochen Conrad Peters

**Bewertung des Einflusses von Formabweichungen in der
Mikro-Koordinatenmesstechnik**

Band 157

Dr.-Ing. Jörg Ude

**Entscheidungsunterstützung für die Konfiguration
globaler Wertschöpfungsnetzwerke**

Band 158

Dr.-Ing. Stefan Weiler

Strategien zur wirtschaftlichen Gestaltung der globalen Beschaffung

Band 159

Dr.-Ing. Jan Rühl

Monetäre Flexibilitäts- und Risikobewertung

Band 160

Dr.-Ing. Daniel Ruch

Positions- und Konturerfassung räumlich gekrümmter Profile auf Basis bauteilimmanenter Markierungen

Band 161

Dr.-Ing. Manuel Tröndle

Flexible Zuführung von Mikrobauteilen mit piezoelektrischen Schwingförderern

Band 162

Dr.-Ing. Benjamin Viering

Mikroverzahnungsnormal

Band 163

Dr.-Ing. Chris Becke

Prozesskrafttrichtungsangepasste Frässtrategien zur schädigungsarmen Bohrungsbearbeitung an faserverstärkten Kunststoffen

Band 164

Dr.-Ing. Patrick Werner

Dynamische Optimierung und Unsicherheitsbewertung der lastabhängigen präventiven Instandhaltung von Maschinenkomponenten

Band 165

Dr.-Ing. Martin Weis

Kompensation systematischer Fehler bei Werkzeugmaschinen durch self-sensing Aktoren

Band 166

Dr.-Ing. Markus Schneider

Kompensation von Konturabweichungen bei gerundeten Strangpressprofilen durch robotergestützte Führungswerkzeuge

Band 167

Dr.-Ing. Ester M. R. Ruprecht

Prozesskette zur Herstellung schichtbasierter Systeme mit integrierten Kavitäten

Band 168

Dr.-Ing. Alexander Broos

Simulationsgestützte Ermittlung der Komponentenbelastung für die Lebensdauerprognose an Werkzeugmaschinen

Band 169

Dr.-Ing. Frederik Zanger

Segmentspanbildung, Werkzeugverschleiß, Randschichtzustand und Bauteileigenschaften: Numerische Analysen zur Optimierung des Zerspanungsprozesses am Beispiel von Ti-6Al-4V

Band 170

Dr.-Ing. Benjamin Behmann

Servicefähigkeit

Band 171

Dr.-Ing. Annabel Gabriele Jondral

Simulationsgestützte Optimierung und Wirtschaftlichkeitsbewertung des Lean-Methodeneinsatzes

Band 172

Dr.-Ing. Christoph Ruhs

Automatisierte Prozessabfolge zur qualitätssicheren Herstellung von Kavitäten mittels Mikrobahnerosion

Band 173

Dr.-Ing. Steven Peters

Markoffsche Entscheidungsprozesse zur Kapazitäts- und Investitionsplanung von Produktionssystemen

Band 174

Dr.-Ing. Christoph Kühlewein

Untersuchung und Optimierung des Wälzschälverfahrens mit Hilfe von 3D-FEM-Simulation – 3D-FEM Kinematik- und Spanbildungssimulation

Band 175

Dr.-Ing. Adam-Mwanga Dieckmann

Auslegung und Fertigungsprozessgestaltung sintergefügter Verbindungen für μ MIM-Bauteile

Band 176

Dr.-Ing. Heiko Hennrich

Aufbau eines kombinierten belastungs- und zustandsorientierten Diagnose- und Prognosesystems für Kugelgewindetriebe

Band 177

Dr.-Ing. Stefan Herder

Piezoelektrischer Self-Sensing-Aktor zur Vorspannungsregelung in adaptiven Kugelgewindetrieben

Band 178

Dr.-Ing. Alexander Ochs

Ultraschall-Strömungsgreifer für die Handhabung textiler Halbzeuge bei der automatisierten Fertigung von RTM-Bauteilen

Band 179

Dr.-Ing. Jürgen Michna

Numerische und experimentelle Untersuchung zerspanungsbedingter Gefügeumwandlungen und Modellierung des thermo-mechanischen Lastkollektivs beim Bohren von 42CrMo4

Band 180

Dr.-Ing. Jörg Elser

Vorrichtungsfreie räumliche Anordnung von Fügepartnern auf Basis von Bauteilmarkierungen

Band 181

Dr.-Ing. Katharina Klimscha

Einfluss des Fügespalts auf die erreichbare Verbindungsqualität beim Sinterfügen

Band 182

Dr.-Ing. Patricia Weber

Steigerung der Prozesswiederholbarkeit mittels Analyse akustischer Emissionen bei der Mikrolaserablation mit UV-Pikosekundenlasern

Band 183

Dr.-Ing. Jochen Schädel

Automatisiertes Fügen von Tragprofilen mittels Faserwickeln

Band 184

Dr.-Ing. Martin Krauße

Aufwandsoptimierte Simulation von Produktionsanlagen durch Vergrößerung der Geltungsbereiche von Teilmodellen

Band 185

Dr.-Ing. Raphael Moser

Strategische Planung globaler Produktionsnetzwerke

Bestimmung von Wandlungsbedarf und Wandlungszeitpunkt mittels multikriterieller Optimierung

Band 186

Dr.-Ing. Martin Otter

Methode zur Kompensation fertigungsbedingter Gestaltabweichungen für die Montage von Aluminium Space-Frame-Strukturen

Band 187

Dr.-Ing. Urs Leberle

Produktive und flexible Gleitförderung kleiner Bauteile auf phasenflexiblen Schwingförderern mit piezoelektrischen 2D-Antriebs-elementen

Band 188

Dr.-Ing. Johannes Book

Modellierung und Bewertung von Qualitätsmanagementstrategien in globalen Wertschöpfungsnetzwerken

Band 189

Dr.-Ing. Florian Ambrosy

Optimierung von Zerspanungsprozessen zur prozesssicheren Fertigung nanokristalliner Randschichten am Beispiel von 42CrMo4

Band 190

Dr.-Ing. Adrian Kölmel

Integrierte Messtechnik für Prozessketten unreifer Technologien am Beispiel der Batterieproduktion für Elektrofahrzeuge

Band 191

Dr.-Ing. Henning Wagner

Featurebasierte Technologieplanung zum Preforming von textilen Halbzeugen

Band 192

Dr.-Ing. Johannes Gebhardt

Strukturoptimierung von in FVK eingebetteten metallischen Lasteinleitungselementen

Band 193

Dr.-Ing. Jörg Bauer

Hochintegriertes hydraulisches Vorschubsystem für die Bearbeitung kleiner Werkstücke mit hohen Fertigungsanforderungen

Band 194

Dr.-Ing. Nicole Stricker

Robustheit verketteter Produktionssysteme

Robustheitsevaluation und Selektion des Kennzahlensystems der Robustheit

Band 195

Dr.-Ing. Anna Sauer

Konfiguration von Montagelinien unreifer Produkttechnologien am Beispiel der Batteriemontage für Elektrofahrzeuge

Band 196

Dr.-Ing. Florian Sell-Le Blanc

Prozessmodell für das Linearwickeln unrunder Zahnspulen

Ein Beitrag zur orthozyklischen Spulenwickeltechnik

Band 197

Dr.-Ing. Frederic Förster

Geregeltes Handhabungssystem zum zuverlässigen und energieeffizienten Handling textiler Kohlenstofffaserzuschnitte

Band 198

Dr.-Ing. Nikolay Boev

Numerische Beschreibung von Wechselwirkungen zwischen Zerspanprozess und Maschine am Beispiel Räumen

Band 199

Dr.-Ing. Sebastian Greinacher

Simulationsgestützte Mehrzieloptimierung schlanker und ressourceneffizienter Produktionssysteme

Band 200

Dr.-Ing. Benjamin Häfner

Lebensdauerprognose in Abhängigkeit der Fertigungsabweichungen bei Mikroverzahnungen

Band 201

Dr.-Ing. Stefan Klotz

Dynamische Parameteranpassung bei der Bohrungsherstellung in faserverstärkten Kunststoffen unter zusätzlicher Berücksichtigung der Einspannsituation

Band 202

Dr.-Ing. Johannes Stoll

Bewertung konkurrierender Fertigungsfolgen mittels Kostensimulation und stochastischer Mehrzieloptimierung

Anwendung am Beispiel der Blechpaketfertigung für automobiler Elektromotoren

Band 203

Dr.-Ing. Simon-Frederik Koch

Fügen von Metall-Faserverbund-Hybridwellen im Schleuderverfahren
ein Beitrag zur fertigungsgerechten intrinsischen Hybridisierung

Band 204

Dr.-Ing. Julius Ficht

Numerische Untersuchung der Eigenspannungsentwicklung für sequenzielle Zerspanungsprozesse

Band 205

Dr.-Ing. Manuel Baumeister

Automatisierte Fertigung von Einzelblattstapeln in der Lithium-Ionen-Zellproduktion

Band 206

Dr.-Ing. Daniel Bertsch

Optimierung der Werkzeug- und Prozessauslegung für das Wälzschälen von Innenverzahnungen

Band 207

Dr.-Ing. Kyle James Kippenbrock

Deconvolution of Industrial Measurement and Manufacturing Processes for Improved Process Capability Assessments

Band 208

Dr.-Ing. Farboud Bejnoud

Experimentelle Prozesskettenbetrachtung für Räumbauteile am Beispiel einer einsatzgehärteten PKW-Schiebemuffe

Band 209

Dr.-Ing. Steffen Dosch

Herstellungsübergreifende Informationsübertragung zur effizienten Produktion von Werkzeugmaschinen am Beispiel von Kugelgewindetrieben

Band 210

Dr.-Ing. Emanuel Moser

Migrationsplanung globaler Produktionsnetzwerke

Bestimmung robuster Migrationspfade und risiko-effizienter Wandlungsbefähiger

Band 211

Dr.-Ing. Jan Hochdörffer

Integrierte Produktallokationsstrategie und Konfigurationssequenz in globalen Produktionsnetzwerken

Band 212

Dr.-Ing. Tobias Arndt

Bewertung und Steigerung der Prozessqualität in globalen Produktionsnetzwerken

Band 213

Dr.-Ing. Manuel Peter

Unwuchtminimale Montage von Permanentmagnetrotoren durch modellbasierte Online-Optimierung

Band 214

Dr.-Ing. Robin Kopf

Kostenorientierte Planung von Fertigungsfolgen additiver Technologien

Band 215

Dr.-Ing. Harald Meier

**Einfluss des Räumens auf den Bauteilzustand in der Prozesskette
Weichbearbeitung – Wärmebehandlung – Hartbearbeitung**

Band 216

Dr.-Ing. Daniel Brabandt

**Qualitätssicherung von textilen Kohlenstofffaser-Preforms mittels
optischer Messtechnik**

Band 217

Dr.-Ing. Alexandra Schabunow

**Einstellung von Aufnahmeparametern mittels projektionsbasierter Qualitäts-
kenngrößen in der industriellen Röntgen-Computertomographie**

Band 218

Dr.-Ing. Jens Bürgin

Robuste Auftragsplanung in Produktionsnetzwerken

Mittelfristige Planung der variantenreichen Serienproduktion unter Unsicherheit
der Kundenauftragskonfigurationen

Band 219

Dr.-Ing. Michael Gerstenmeyer

**Entwicklung und Analyse eines mechanischen Oberflächenbehandlungs-
verfahrens unter Verwendung des Zerspanungswerkzeuges**

Band 220

Dr.-Ing. Jacques Burtscher

**Erhöhung der Bearbeitungsstabilität von Werkzeugmaschinen durch
semi-passive masseneinstellbare Dämpfungssysteme**

Band 221

Dr.-Ing. Dietrich Berger

**Qualitätssicherung von textilen Kohlenstofffaser-Preforms mittels prozess-
integrierter Wirbelstromsensor-Arrays**

Band 222

Dr.-Ing. Fabian Johannes Ballier

Systematic gripper arrangement for a handling device in lightweight production processes

Band 223

Dr.-Ing. Marielouise Schäferling, geb. Zaiß

Development of a Data Fusion-Based Multi-Sensor System for Hybrid Sheet Molding Compound

Band 224

Dr.-Ing. Quirin Spiller

Additive Herstellung von Metallbauteilen mit dem ARBURG Kunststoff-Freiformen

Band 225

Dr.-Ing. Andreas Spohrer

Steigerung der Ressourceneffizienz und Verfügbarkeit von Kugelgewindetrieben durch adaptive Schmierung

Band 226

Dr.-Ing. Johannes Fisel

Veränderungsfähigkeit getakteter Fließmontagesysteme

Planung der Fließbandabstimmung am Beispiel der Automobilmontage

Band 227

Dr.-Ing. Patrick Bollig

Numerische Entwicklung von Strategien zur Kompensation thermisch bedingter Verzüge beim Bohren von 42CrMo4

Band 228

Dr.-Ing. Ramona Pfeiffer, geb. Singer

Untersuchung der prozessbestimmenden Größen für die anforderungsgerechte Gestaltung von Pouchzellen-Verpackungen

Band 229

Dr.-Ing. Florian Baumann

Additive Fertigung von endlosfaserverstärkten Kunststoffen mit dem ARBURG Kunststoff-Freiform Verfahren

Band 230

Dr.-Ing. Tom Stähr

Methodik zur Planung und Konfigurationsauswahl skalierbarer Montagesysteme – Ein Beitrag zur skalierbaren Automatisierung

Band 231

Dr.-Ing. Jan Schwennen

Einbringung und Gestaltung von Lasteinleitungsstrukturen für im RTM-Verfahren hergestellte FVK-Sandwichbauteile

Band 232

Dr.-Ing. Sven Coutandin

Prozessstrategien für das automatisierte Preforming von bebinderten textilen Halbzeugen mit einem segmentierten Werkzeugsystem

Band 233

Dr.-Ing. Christoph Liebrecht

Entscheidungsunterstützung für den Industrie 4.0-Methodeneinsatz
Strukturierung, Bewertung und Ableitung von Implementierungsreihenfolgen

Band 234

Dr.-Ing. Stefan Treber

Transparenzsteigerung in Produktionsnetzwerken
Verbesserung des Störungsmanagements durch verstärkten Informationsaustausch

Band 235

Dr.-Ing. Marius Dackweiler

Modellierung des Fügewickelprozesses zur Herstellung von leichten Fachwerkstrukturen

Band 236

Dr.-Ing. Fabio Echsler Minguillon

Prädiktiv-reaktives Scheduling zur Steigerung der Robustheit in der Matrix-Produktion

Band 237

Dr.-Ing. Sebastian Haag

Entwicklung eines Verfahrensablaufes zur Herstellung von Batteriezellstapeln mit großformatigem, rechteckigem Stapelformat und kontinuierlichen Materialbahnen

Band 238

Dr.-Ing. Raphael Wagner

Strategien zur funktionsorientierten Qualitätsregelung in der Serienproduktion

Band 239

Dr.-Ing. Christopher Ehrmann

Ausfallfrüherkennung von Ritzel-Zahnstangen- Trieben mittels Acoustic Emission

Band 240

Dr.-Ing. Janna Hofmann

Prozessmodellierung des Fünf-Achs-Nadelwickelns zur Implementierung einer trajektoriebasierten Drahtzugkraftregelung

Band 241

Dr.-Ing. Andreas Kuhnle

**Adaptive Order Dispatching based on Reinforcement Learning
Application in a Complex Job Shop in the Semiconductor Industry**

Band 242

Dr.-Ing. Andreas Greiber

**Fertigung optimierter technischer Oberflächen durch eine Verfahrenskombination aus Fliehkraft-Tauchgleitschleifen und Laserablation
Prozesseinflüsse und Prozessauslegung**

Band 243

Dr.-Ing. Jan Niclas Eschner

Entwicklung einer akustischen Prozessüberwachung zur Porenbestimmung im Laserstrahlschmelzen

Band 244

Dr.-Ing. Sven Roth

Schädigungsfreie Anbindung von hybriden FVK/Metall-Bauteilen an metallische Tragstrukturen durch Widerstandspunktschweißen

Band 245

Dr.-Ing. Sina Kathrin Peukert

Robustheitssteigerung in Produktionsnetzwerken mithilfe eines integrierten Störungsmanagements

Band 246

Dr.-Ing. Alexander Jacob

Hochiterative Technologieplanung

Rekursive Optimierung produkt- und fertigungsbezogener
Freiheitsgrade am Beispiel der hybrid-additiven Fertigung

Band 247

Dr.-Ing. Patrick Moll

**Ressourceneffiziente Herstellung von Langfaser-Preforms
im Faserblasverfahren**

Band 248

Dr.-Ing. Eric Thore Segebade

**Erhöhung der Verschleißbeständigkeit von Bauteilen aus Ti-6Al-4V mittels
simulationsgestützter Zerspanung und mechanischer Mikrotextrurierung**

Band 249

Dr.-Ing. Shun Yang

**Regionalized implementation strategy of smart
automation within assembly systems in China**

Band 250

Dr.-Ing. Constantin Carl Hofmann

**Vorausschauende und reaktive Mehrzieloptimierung
für die Produktionssteuerung einer Matrixproduktion**

Band 251

Dr.-Ing. Paul Ruhland

Prozesskette zur Herstellung von hybriden Faser-Metall-Preforms

Modellbildung und Optimierung des Binderauftrags und
der Drapierung für stabförmige Bauteile

Band 252

Dr.-Ing. Leonard Schild

**Erzeugung und Verwendung von Anwendungswissen in der industriellen
Computertomographie**

Band 253

Dr.-Ing. Benedikt Klee

**Analyse von Phaseninformationen in Videodaten zur Identifikation
von Schwingungen in Werkzeugmaschinen**

Band 254

Dr.-Ing. Bruno Vargas

Wälzschälern mit kleinen Achskreuzwinkeln

Prozessgrenzen und Umsetzbarkeit

Band 255

Dr.-Ing. Lucas Bretz

Function-oriented in-line quality assurance of hybrid sheet molding compound

Band 256

Dr.-Ing. Bastian Rothaupt

Dämpfung von Bauteilschwingungen durch einstellbare Werkstückdirektspannung mit Hydrodehnspanntechnik

Band 257

Dr.-Ing. Daniel Kupzik

Robotic Swing Folding of three-dimensional UD-tape-based Reinforcement Structures

wbk Institut für Produktionstechnik Karlsruher Institut für Technologie (KIT)

Zum Buch

Hybrid fiber-reinforced components made of Long-Fiber-reinforced Thermoplastic (LFT) and unidirectional continuous fiber reinforced tapes (UD-tape) offer great opportunity to reduce weight while saving manufacturing cost compared to monolithic UD-tape components. In such a combination, the excellent formability of LFT is used for filling corners, ribs, and other geometrically complex areas of the component while the UD-tape increases strength and stiffness. Preforming continuous fiber materials, like UD-tape, is a costly step in manufacturing fiber-reinforced polymer (FRP) components. The effort for preforming should be minimized to further improve the competitiveness of the hybrid design. Current preforming processes do not fit the requirements of reinforcement structures. Therefore, they require additional handling steps for positioning the material and costly tooling for controlling the forming of the material. At the same time, the existing processes offer high capability for workpiece complexity, which is not needed as the complex areas in hybrid components are formed by LFT.

In this thesis, a process for the flexible preforming of linear reinforcements from UD-tape strips is designed, commissioned, and optimized. An algorithm for adjusting the preform shape to the preforming process restrictions while maintaining the general shape is presented. Using the novel preforming process, cost for component specific preforming tools can be avoided and deviations in subsequent process steps can be compensated for during running manufacturing.

ISBN 978-3-8440-8716-1



9

SHAKER
VERLAG